THE FATE OF DINITROPYRENES IN *SALMONELLA TYPHIMURIUM*:

METABOLISM AND DNA-ADDUCT FORMATION.

By

ⓒ   Paul Andrews, M.Sc.

A Thesis

Submitted to the School of Graduate Studies

in Partial Fulfillment of the Requirements

for the Degree

Doctor of Philosophy

McMaster University

August, 1988

THE FATE OF DINITROPYRENES IN *SALMONELLA TYPHIMURIUM*

DOCTOR OF PHILOSOPHY (1988)   McMASTER UNIVERSITY

                                     Hamilton, Ontario

TITLE: The Fate of Dinitropyrenes in Salmonella

       Typhimurium: Metabolism and DNA-Adduct Formation.

AUTHOR: Paul John Andrews, B.Sc. (McMaster University)

                          M.Sc. (Queen's University)

Supervisors: Dr. M. Quilliam and Dr. D. McCalla

Number of pages: xviii,208

ABSTRACT

The nitro substituted polycyclic aromatic hydrocarbons (nitro-PAH) are a class of environmental contaminants which are potent mutagens in a number of biological test systems. The three dinitropyrene (DNP) isomers are of special interest because of their extremely high mutagenicity in the Ames *Salmonella typhimurium* reversion assay.

Metabolic studies in *S. typhimurium* using both tritium labelled and unlabelled DNP demonstrated that the DNPs undergo nitro reduction and N-acetylation. Mutagenicity studies of DNP metabolites in *S. typhimurium* strains demonstrated that the reactive metabolite responsible for the mutagenic activity of the DNPs is at the oxidation state intermediate between nitroso-nitropyrene and amino-nitropyrene and both nitro reduction and acetylation are required for expression of mutagenicity.

Efforts were directed toward synthesis of hydroxylamino-nitropyrenes (HANP) derivatives as they appeared to be likely candidates for the reactive metabolite and could be easily synthesized. The 1,8-HANP derivative was shown to produce the same covalently DNA bound adduct as that produced *in vivo* by the bacterial metabolism of 1,8-DNP. The 1,3- and 1,6- substituted HANP derivatives were also shown to produce covalently bound DNA adducts *in vitro*.

Based upon the known structures of other DNA-adducts, it was postulated that these *in vitro* adducts were the result of bond formation between the exocyclic amino nitrogen of an amino-nitropyrene moiety and

iii

C-8 of 2'-deoxyguanosine. However, the characterization of these adducts presented many difficulties.

Acquisition of UV-visible spectra of these DNP-DNA adducts was aided by coupling reverse phase high pressure liquid chromatography (RPLC) with diode array detection. The RPLC analyses of these adducts also demonstrated that they undergo extensive degradation under both acidic and basic conditions. Interpretation of their NMR spectra was difficult because of line broadening effects due to stacking of the adducts in solution.

The acquisition of mass spectra of these in vitro was difficult because of their low volatility and pH instability. A number of "soft" ionization techniques such as "in-beam" ionization, fast atom bombardment (FAB), field desorption (FD), and coupled LCFAB-MS were evaluated, but only poor quality spectra were obtained. These difficulties were overcome by producing the trimethylsilyl and t-butyldimethylsilyl derivatives. MS analysis of these derivatives using desorption electron ionization (DEI) mass spectrometry produced mass spectra that were rich in fragmentation ions allowing final characterization of the adducts.

Finally the interaction between calf thymus-DNA and aminonitropyrene (ANP) or diaminopyrene (DAP) metabolites was studied because these metabolites were structurally similar to known DNA intercalators. The interaction of these metabolites was shown to be different than the structurally similar intercalators.

ACKNOWLEDGEMENTS

Table of Contents

LIST OF TABLES

x

LIST OF FIGURES

List of Abbreviations

AP	Aminopyrene
ANP	Aminonitropyrene
AcAAP	N-Acetylaminopyrene
BSTFA	N,O-bis-(trimethylsilyl)-trifluoroacetamide
COSY	Correlation spectroscopy
CT	Calf thymus
DAP	Diaminopyrene
DAcAAP	N,N'-Diacetylaminopyrene
DCI	Desorption chemical ionization
DCM	Dichloromethane
dA	Deoxyadenosine
dG	Deoxyguanosine
dI	Deoxyinosine
DNA	Deoxyribonucleic acid
DNP	Dinitropyrene
DEI	Desorption electron ionization
DMF	Dimethylformamide
DMSO	Dimethylsulfoxide
ESR	Electron spin resonance
FAB	Fast atom bombardment
HANP	N-Hydroxylamino-nitropyrene
HPLC	High pressure liquid chromatography
LUMO	Lowest unoccupied molecular orbital
MCPBA	m-Chloro perbenzoic acid

MTBSTFA	N-methyl-N-(t-butyldimethylsilyl)-trifluoroacetamide
NANP	Nitroso-amino-nitropyrene
NOP	Nitrosopyrene
NP	Nitropyrene
NMR	Nuclear magnetic resonance
NOAP	Nitroso-amino-pyrene
NOE	Nuclear overhauser effect
NANP	N-Acetylamino-nitropyrene
NONP	Nitroso-nitropyrene
NPLC	Normal phase high pressure liquid chromatography
PAH	Polyaromatic hydrocarbon.
ppm	Parts per million
RPLC	Reverse phase high pressure liquid chromatography
SCTASi	Sterically crowded tri-alkyl silyl
TBDMS	t-butyldimethylsilyl
TFA	Trifluoroacetamide
TLC	Thin layer chromatography
TMS	Trimethylsilyl
UV-VIS	Ultraviolet-visible

I. INTRODUCTION

I.1 Polycyclic Aromatic Hydrocarbons

The link between cancer in humans and exposure to hazardous chemicals in the environment was first demonstrated by Sir Percivil Potts when he pointed out that cancer of the scrotum was an occupational disease peculiar to chimney sweeps (1). Since then, a class of fused aromatic compounds known as polycyclic aromatic hydrocarbons (PAH) has been implicated in the etiology of cancers and other health risks (2). These PAH are widespread in the environment and have been the subject of much scientific investigation.

PAH are an extremely diverse class of compounds that contain some of the most extensively studied carcinogens (Figure 1). They are produced mainly by the burning of carbonaceous materials. Estimates as high as 121 metric tons a year of benzo[a]pyrene 5, an extremely potent carcinogen, have been reported to be emitted each year in the United States (3). PAH also occur naturally as major constituents of coals, crude oil, oil shales and sediments resulting from the degradation of plant materials (4,5). Because of concern over their potential health hazard, a wide variety of environmental and manufactured materials have been analysed for these compounds. PAH have been detected in diesel exhaust particulate (6), cigarette smoke (7), urban airborne particulate (8-11), food (12,13), and soil (14).

In complex environmental samples, not only are the parent PAH present, but also the analogous sulphur, nitrogen and oxygen

1
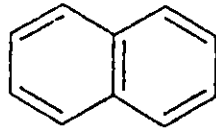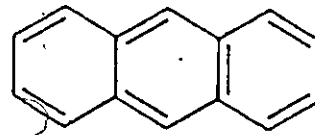
Naphthalene 1   Anthracene 2
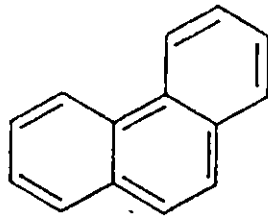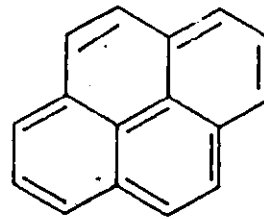
Phenanthrene 3   Pyrene 4
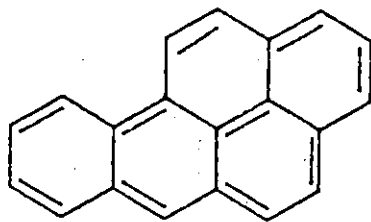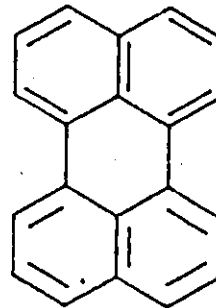
Benzo[a]pyrene 5   Perylene 6

Figure 1: Typical PAH structures.

heterocyclics, and alkyl, amino, nitro, phenol and quinone derivatives. Data from the synthesis and biological testing of many of these PAH derivatives has shown that the nature and extent of substitution has a direct bearing on their biological activity (15).

The biological activity of the parent PAH can be considerably enhanced by alkyl or bridged alkyl substitution at selected positions which is thought to hinder certain detoxification processes (16). The increased potency of other substituted PAH derivatives is derived from the metabolic transformation of the substituent into a reactive species. The aromatic amino- and nitro-PAH are of particular interest because they are not only produced by natural processes but are the intermediates in the production of many manufactured products. The 1- and 2-aminonaphthalenes were once routinely used as dyestuff intermediates and as anti-oxidants in the rubber industry, but were abandoned when a high incidence of bladder cancer was noted in workers routinely exposed to their vapours (17). The majority of the nitroaromatic compounds used in industry are the single-ringed benzene and toluene derivatives. These explosive and dyestuff intermediates along with many of the amino-PAH, are potent inducers of methemoglobinemia (18,19).

The nitro-PAH (Figure 2) became the focus of attention in 1978 when extracts of certain xerographic toners were shown to have extraordinary mutagenicity in bacterial test systems (20). Analysis of these toners showed that mono-, di- and tri-nitropyrenes were responsible for the majority of the activity, the dinitropyrenes being the most mutagenic (21). By altering the manufacturing process for the carbon black constituent of toners, these nitro-substituted pyrenes were eliminated.
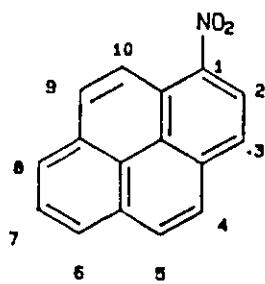
1-Nitropyrene 7
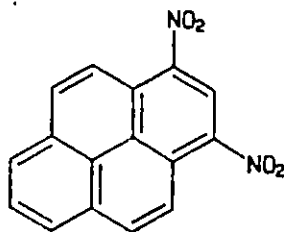
1,3-Dinitropyrene 8
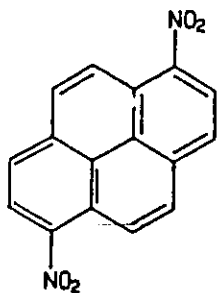
1,6-Dinitropyrene 9
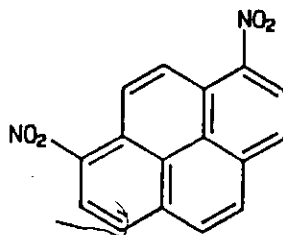
1,8-Dinitropyrene 10
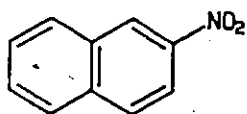
2-Nitronaphthalene 11
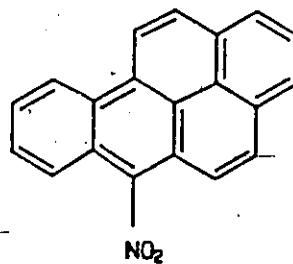
6-Nitrobenzo[a]pyrene 12

Figure 2: Typical nitro-PAH: names, structures and numbering.

As a result of these findings, 2,7,7-trinitrofluoren-9-one, a photosensitizer in another photocopying process was shown to be mutagenic and was withdrawn from the market (22,23).

Because of the concern over the potential health risks due to these nitro-PAH, samples from a variety of environmental sources have been analyzed. Nitro-PAH were found to be widespread environmental contaminants with over 200 compounds detected to date (24). Diesel engine exhaust particulate (25), fly ash (26) and urban airborne particulate (27) have all have been shown to contain a variety of nitro-PAH such as 1-NP 7, 3-nitrofluoranthene 21, and 6-nitrobenzo[a]pyrene 12. Wood and coal burning stoves and kerosene heaters appear to be major contributors of nitro-PAH in the urban environment in certain areas (28).

The nitro-PAH are formed under conditions in which incomplete combustion of fossil fuel takes place in the presence of water, nitrogen oxides and/or nitric acid. They have also been shown to be produced by the gas phase nitration of PAH (29). The nitro-substitution pattern is often dependent on whether the nitro-PAH is produced during combustion or by an atmospheric photochemical reaction. Concern has been expressed that some of the environmental nitro-PAH detected could have been the result of direct nitration of PAH in the sampling apparatus by NO_2 (30).

I.2 Genotoxicity of the Nitroaromatics

A wide variety of bacterial and mammalian cell systems are available for the testing of mutagenic and genotoxic activity of test compounds. The Ames bacterial reversion assay is often chosen because it

not only provides information on mutagenic potency but also on mutagenic specificity. This assay can be used for the rapid screening of large numbers of test compounds or environmental samples for mutagenicity (31).

The Ames test is based on special mutated strains of *Salmonella typhimurium* that are deficient in one of the enzymes required for the synthesis of histidine, an essential amino acid. These mutants do not grow in media that does not contain histidine. However, when incubated in the presence of a test mutagen, these mutated bacteria can undergo a back mutation or "reversion" to their original state and can then grow in the absence of histidine. The mutagenic potential of test compounds can be gauged by counting the number of "revertant" colonies obtained. The number of revertants obtained is dependent on both the intrinsic activity of the compound, and on the concentration of the compound in the test media. As the concentration of the test compound is increased, the number of revertants observed also increases until cell toxicity and/or solubility problems of the test compound start to occur. From this dose/response information the mutagenicity is usually expressed as revertants/nmole or revertants/μg.

Compounds that show activity in the Ames test are classed as either direct- or indirect-acting. Indirect-acting compounds require the presence of an S-9 activating system in order for their mutagenicity to be expressed. S-9 is a soluble fraction isolated from liver and contains many of the oxidative enzymes required for the metabolic activation of PAH and many other compounds. Direct acting compounds, which do not require S-9, may be classed as those that are chemically reactive in their own right; or those that require the presence of endogenous

bacterial enzymes for activation. Typical of chemically reactive, direct acting compounds are alkylimines, alkylene epoxides, sulphate esters, and nitrogen mustards, all of which are potent alkylating agents. The mutagenicity data for the nitropyrenes 7-10 and some other nitro-PAH are shown in Table 1. Note that many of the nitro-PAH are more active without S-9 and hence have been classed as "direct-acting". However, the nitro-PAH require metabolic activation by endogenous bacterial reductases, and hence do not act in the same fashion as the alkylating agents.

The nitro-PAH have also been tested for mutagenicity in mammalian cell lines, activity in neoplastic cell transformation assays and for carcinogenicity in whole animals. As in the mutagenicity studies, the dinitropyrenes (DNPs) 8-10 appeared to be very active. 1,8-DNP 10, and 1,6-dinitropyrene (1,6-DNP) 9, were potent inducers of resistance to 6-thioguanine (33) and diphtheria toxin in CH lung cells (34), caused sister chromatid exchange in CHO cells (35,36) and DNA strand breakage (37). 1,3-Dinitropyrene (1,3-DNP) 8 was also active but not as potent. The DNPs 8-10 also induce lung carcinomas, fibrosarcomas, as well as other tumours in a number of animals (24,38,39).

I.3 Metabolism and Adduct Formation

Although many events must occur in a cellular system before mutagenicity or carcinogenicity is expressed, the initial step is often the interaction of a carcinogen (or a reactive species derived from it) and DNA. This interaction may be non-covalent in nature such as the intercalation of proflavine dyes between base pairs of DNA (40) or

Table 1: Mutagenicity of nitro-PAH in the Ames assay (32)

Compound No.	Name	Mutagenic Activity (revertants/nmole)	
		-S9[a]	+S9[a]
7	1-nitropyrene	453	35
8	1,3-dinitropyrene	144760	4900
9	1,6-dinitropyrene	183570	37850
10	1,8-dinitropyrene	254000	75500
13	1,3,6-trinitropyrene	40700	28330
14	1,3,6,8-tetranitropyrene	15600	5200
15	1-nitronaphthalene	0	0.05
16	1,3-dinitronaphthalene	0	0.89
17	1,3,6,8-tetranitronaphthalene	1	0.20
12	6-nitrobenzo[a]pyrene	31	141
18	3-nitrobenzo[a]pyrene	67	1011

[a] -S9,+S9 = activity without and with the presence of S9

covalent binding of a nucleophilic species to electrophilic sites on
nucleotides (41). The consequence of either of these interactions is
alterations in DNA structure and misreading of biological information.

Nitroreduction is a vital step in the bioactivation of many
nitro-PAH (42,43). Nitroreduction in *S.typhimurium* is catalyzed by a
family of nitroreductases that vary in substrate specificity (44).
Furthermore, it has been shown that the mutagenicity of some nitro-PAH,
such as 1-NP *1*, is much reduced in *S.typhimurium* strains that are
deficient in functional nitroreductase (45). Although the ultimate
genotoxic metabolite has not been isolated, the nitro group is known to
be reduced to the nitroso, hydroxylamino and amino oxidation states
(Figure 3). The putative ultimate mutagen, the aryl nitrenium cation,
can be produced by direct decomposition of either the hydroxylamine or
its O-acetyl derivative. This reduction sequence is, in a sense, the
reverse of the P_{450} mediated oxidation of aromatic amines which also
leads to the aryl nitrenium cation (46).

Mutagenicity data obtained using various *S.typhimurium* strains has
indicated that nitro-PAH induce frame shift mutations which are caused by
the formation of covalently bound adducts as opposed to intercalation
(47). Structures of some of the adducts resulting from the reaction of
compounds that generate reactive nitrenium cations and DNA are described
in Table 2 (50-53).

In the majority of adducts, bond formation occurred between the aryl
nitrogen and the electrophilic site at position C-8 of 2'-deoxyguanosine
(2'-dG) *20* (Figure 4a). During the course of this work, other
investigators showed that the mutagenicity in *S.typhimurium* of aryl
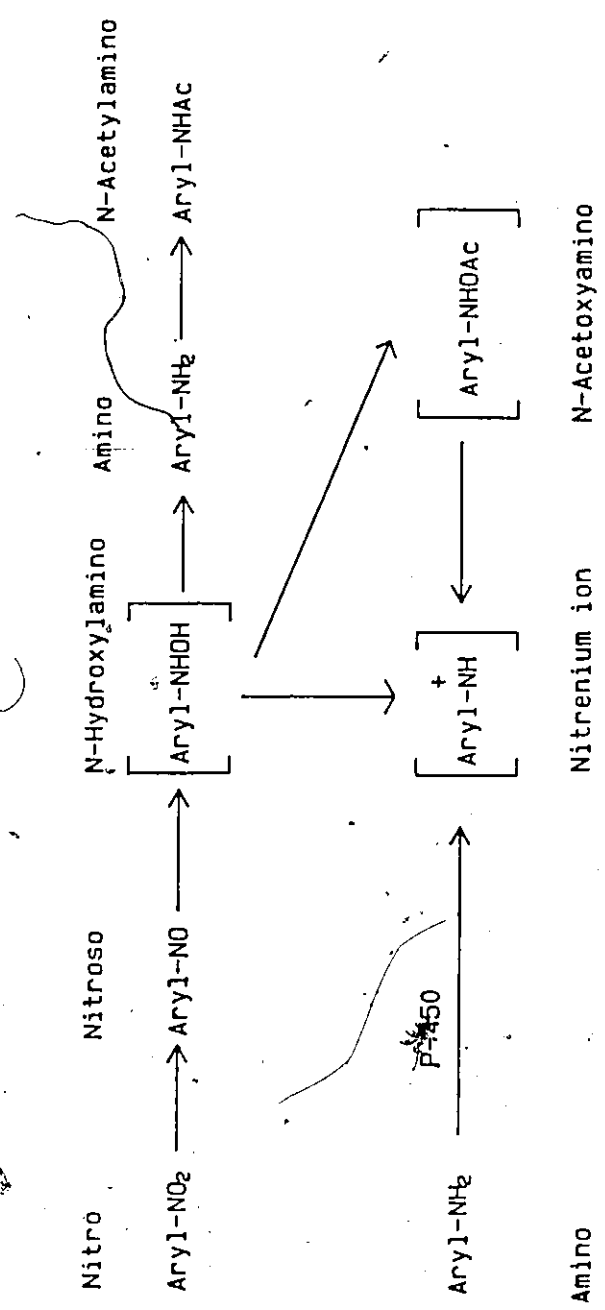
Figure 3: Reductive pathways for a nitroaromatic.

Table 2: Adducts formed from the *in vivo* and *in vitro* reaction of N-hydroxylamines and DNA

Hydroxylamine	Adduct	Reference
N-Hydroxyl-2-aminonaphthalene	N-(deoxyguanosin-8-yl)-2-aminonaphthalene	48
	1-(deoxyguanosin-N^2-yl)-2-aminonaphthalene	
	1-(deoxyadenosin-N^6-yl)-2-aminonaphthalene	
N-hydroxyl-1-aminonaphthalene	N-(deoxyguanosin-O^6-yl)-1-aminonaphthalene	49
	2-(deoxyguanosin-O^6-yl)-1-aminonaphthalene	
N-hydroxyl-1-aminopyrene	N-(deoxyguanosin-8-yl)-1-aminopyrene	50
N-hydroxyl-DMABP*	N-(deoxyguanosin-8-yl)-DMABP	51
	5-(deoxyguanosin-N^2-yl)-DMABP	

* dimethylaminobiphenyl

a) C-8 bond formation

(b) O^6 bond formation

(c) Bamberger rearrangement
N^2 bond formation
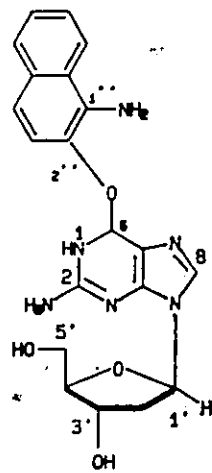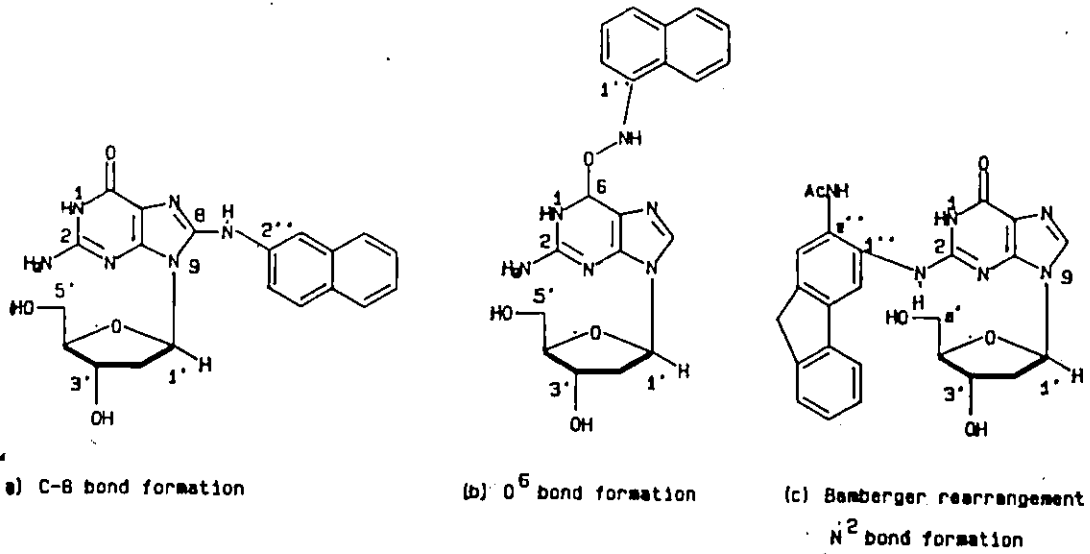
(d) Bamberger rearrangement
O^6 bond formation
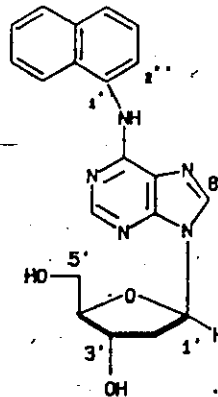
(e) Bamberger rearrangement
N^6 bond formation

Figure 4: Structures of nucleoside-nitro-PAH adducts formed via the
in vivo and in vitro reaction of N-hydroxylamino-PAH
and DNA.

hydroxylamine intermediates of 1,8-DNP 10 and 1-NP 7, were directly related to the extent of substitution at C-8 of 2'-dG 20 (52). Adduct formation occurs to a lesser extent at O^6 of 2'-dG 20 through the aryl nitrogen (Figure 4b) or through the ortho carbon via a Bamberger rearrangement (Figure 4c,4d). Adduct formation with 2'-deoxyadenosine (2'-dA) 21 has only rarely been observed and then only in in vitro reactions (Figure 4d).

I.4 Adduct Isolation and Characterization

There are many experimental difficulties in the isolation and spectroscopic characterization of DNA adducts produced in vivo. After hydrolysis of modified DNA by either chemical or enzymatic methods, the vast majority of the resulting DNA hydrolysate is comprised of unmodified nucleotides, nucleosides, or bases. Because the degree of in vivo modification is usually quite low, isolation and detailed spectroscopic characterization of in vivo adducts is often not possible. Instead, in vivo adducts are usually detected by incubating cellular test systems with tritium or carbon-14 labelled mutagen (48-51). Their chromatographic behaviour is then compared to that of adducts produced in vitro by the reaction of a postulated reactive species with either nucleosides (53,54) or DNA (49,50,55) and characterization of the in vitro adduct is then undertaken.

In addition to the problem of the low levels of adduct formed, the adduct usually must be separated from a vast excess of unmodified nucleosides and nucleotides before further characterization can take place. As the adduct is often more lipophilic than the unmodified

components of the DNA hydrolysate, organic extraction (52) or ion pairing separation steps (56) have been used to act as simple concentration techniques. Various chromatographic techniques such as thin layer chromatography (TLC) (56), high performance liquid chromatography (HPLC) (48-51), and size exclusion chromatography (57) have also been used not only as crude separation methods but in conjunction with spectroscopic analysis techniques to obtain molecular weight and structural information on the separated adduct.

A host of spectroscopic techniques can be used for characterization of an adduct. Ultraviolet-visible (UV-VIS) absorbance spectroscopy has been useful in determining both the site of bond formation and nature of mutagen moiety bound to the nucleoside (50,57,59). The functionality of adduct chromophores can be determined from their fluorescence spectra (60). Other specialized techniques such as circular dichroism and electric linear dichroism have been used to determine conformational properties of species covalently bound to DNA (61,62). The interpretation of proton NMR spectra has been greatly facilitated by such recent advances as correlation spectroscopy (COSY) and the nuclear overhauser effect (NOE) (63).

I.5 Mass Spectrometry

Perhaps the greatest advances in the area of adduct characterization have been in the field of mass spectrometry (MS). MS is an ideal technique for analysis of DNA adducts and other high molecular weight polar biomolecules because of its high sensitivity and the unique information provided, i.e., molecular weight, elemental composition, and

structure. The crucial step in any MS analysis is the production of gaseous ions. The most common method is thermal vapourization of the analyte from a direct insertion probe followed by bombardment with electrons to produce positively charged species. This process is termed electron ionization (EI). A common alternative to EI is chemical ionization (CI). In CI, a reagent gas is introduced into the source in relatively high concentrations relative to the analyte. Vigorous electron bombardment of the gas results in production of reactive ion species which in turn react with the analyte. Typical charged analyte species result from protonation, hydride extraction and charge transfer. Both EI and CI require that the analyte have an appreciable vapour pressure in the ion source. High molecular weight polar molecules are often extensively hydrogen bonded which reduces their volatility and increases their thermal lability. MS analysis of these compounds requires different strategies.

Chemical derivatization is a common method for converting target compounds to more volatile, thermally stable derivatives, which can also provide important fragment information. Most derivatization schemes aim to replace the reactive hydrogens of hydroxyl, thiol and amino groups with less polar alkyl, acyl or silyl groups (64). Silyl derivatives are of special interest because of their volatility, thermal stability and ease of formation. Trimethylsilylation is now the method of choice for the MS analysis of many DNA adducts (50,51,57,65). Sterically crowded trialkylsilyl (SCTASi) derivatives such as t-butyldimethylsilyl (TBDMS) have the added advantage of being stable to hydrolysis and hence can be used in combination with HPLC separation methods (68).

Until recently, the major factor which has limited the analysis of underivatized polar biomolecules has been their low volatility and thermal lability. Because of this, the "soft" ionization methods have been developed whereby a labile sample is desorbed or ionized, often without going through a thermal vapourization step (69). These soft ionization methods can be coupled with derivatization techniques for increased volatility and stability of the analyte. Table 3 lists some of these methods.

Field desorption (FD) is one of the original "soft" ionization methods, and has been used for the analysis of many polar biomolecules (71). An "activated" emitter made of a metal having very high surface area, is dipped into a solution of the analyte and placed in the source where it is heated in the presence of a high electric field gradient. Electrons are removed from the analyte by the process of quantum tunneling which requires less energy than normal electron ionization. The analyte ions usually appear as the protonated molecular ion, $[M+H]^+$, or as the cationized $[M+Na]^+$ and $[M+K]^+$ ions. This technique is very sensitive to the presence of alkali earth cations which often suppress the analyte signal.

Fast atom bombardment (FAB) is one of the newer particle sputtering techniques developed for analysis of thermally labile nonvolatile compounds (72-74). A neutral atom beam (usually xenon or argon) is directed onto a liquid matrix on an insertion probe in the source. The sample, dissolved or dispersed in the matrix, is sputtered from the surface or the bulk of the matrix as a charged species and mass analysed. The resulting FAB mass spectrum of the analyte is superimposed on the FAB

Table 3: Soft ionization techniques used for the mass spectrometry of biological compounds (70)

Technique	Example Applications
Field Desorption (FD)	proteins, nucleosides
Desorption Chemical Ionization (DCI)	peptides, sugars
Laser Desorption (LD)	nucleotides, oligosacharides, cardiac glycosides
Laser Desorption Chemical Ionization (LDCI)	androsterone glucuronide
Plasma Desorption (PD)	marine toxins, oligonucleotides
Secondary Ion (SI)	alkaloids, nucleosides, vitamins
Electrohydrodynamic Desorption (EHD)	amino acids, peptides, nucleosides
Fast Atom Bombardment (FAB)	sugars, oligonucleotides,
Thermospray (TLC)	sugars, nucleosides, peptides

mass spectrum of the supporting matrix. The matrix plays a very important role in FAB-MS analyses. The matrix should dissolve the analyte allowing fast replenishment of the surface analyte that has been discharged by the atom beam. The matrix should have low volatility under MS vacuum conditions and should not react chemically with the sample. The nature of the charged analyte species is also dependent on the matrix and/or matrix additives. Typical charged species are $[M+H]^+$, $[M+Na]^+$, and $[M+K]^+$ and $[M+A+H]^+$ where A is a loosely bound species of analyte and matrix or coadditive molecule. Typical negatively charged species are $[M-H]^-$ and $[M+A-H]^-$. Acids or bases are often added to the matrix to aid in the production of charged species by protonating or deprotonating the analyte. Other matrices such as p-nitrobenzyl alcohol and nitrophenyl-octylether have been reported to prevent decomposition of the sample during analysis (75).

Direct beam insertion or "in-beam" ionization is a technique first described by Baldwin et al (76). This method differs from normal EI in that ion production is much more gentle. A sample is deposited on the surface of an extended tip of a conventional probe and inserted directly into the ion source volume very near the electron beam in the source. The source temperature is raised until analyte spectra are observed. A variety of probe tip surfaces such as SE-30 coated glass (77), vespel (78), and quartz (79) have been used in the vapourization and analysis of sugars (79), and steroidal glycosides (80).

Direct chemical ionization (DCI) is a method related to both "in beam" and chemical ionization methods whereby analyte is "distilled" off a rapidly heated filament into a source filled with reagent gas. During

this rapid heating, volatilization processes occur faster than thermal decomposition processes (78).

Coupled high performance liquid chromatography-mass spectrometry has been the subject of much interest in recent years (81). As polar biomolecules are often separated and isolated by HPLC this coupled technique affords direct analysis of compounds without further sample handling (82). The major difficulties with HPLC-MS are the interfacing of the chromatographic equipment with the ionization source, and the large volumes of solvent which must be removed before the sample enters the high vacuum region of the source.

Belt interfaces utilize a moving polyimide belt onto which the eluant from the chromatography column is dripped or sprayed (83). The analyte and mobile phase on the belt are transported through a series of vacuum locks and infrared heaters where the excess mobile phase is evaporated, and analyte is carried into the source where it is vapourized and ionized by EI or CI. Because analyte thermal stability and volatility are still required, SCTASi derivatives are useful as they are stable under chromatographic conditions (84). An alternative to EI or CI is FAB whereby a particle beam is directed onto the belt in the source (85).

Thermospray is another coupled LC-MS technique in which the eluent from the column is pumped through a line embedded in a block heater before entering the source. The eluant is superheated in the block and emerges as a supersonic jet of fine droplets. The formation of charged analyte species requires the presence of volatile buffer salts such as ammonium acetate, or ammonium formate (86).

I.6 Research Objectives

The findings that nitro-PAH in general, and the DNPs 8-10 specifically, are widespread environmental contaminants and genotoxic in many test systems raises many questions. Given that DNPs must be metabolized in order for their mutagenicity to be expressed and that this mutagenicity is the result of DNA adduct formation, six research objectives discussed below were set. These objectives are summarized in Figure 5.

(1) Elucidate the metabolism of the DNPs in *Salmonella typhimurium*, the organism used in bacterial test systems.

(2) Postulate the nature of reactive DNP metabolites that might react with DNA and chemically synthesize both radioactively labelled and unlabelled precursors.

(3) Devise methods for the production of DNP-DNA adducts in *Salmonella typhimurium* and in chemical systems and compare these two products.

(4) Isolate and characterize the DNP-nucleoside adduct formed chemically.

(5) Evaluate the application of soft ionization methods for the MS of the DNP-nucleoside adducts.

(6) Investigate if any DNP metabolites interact with DNA in a non-covalent manner.
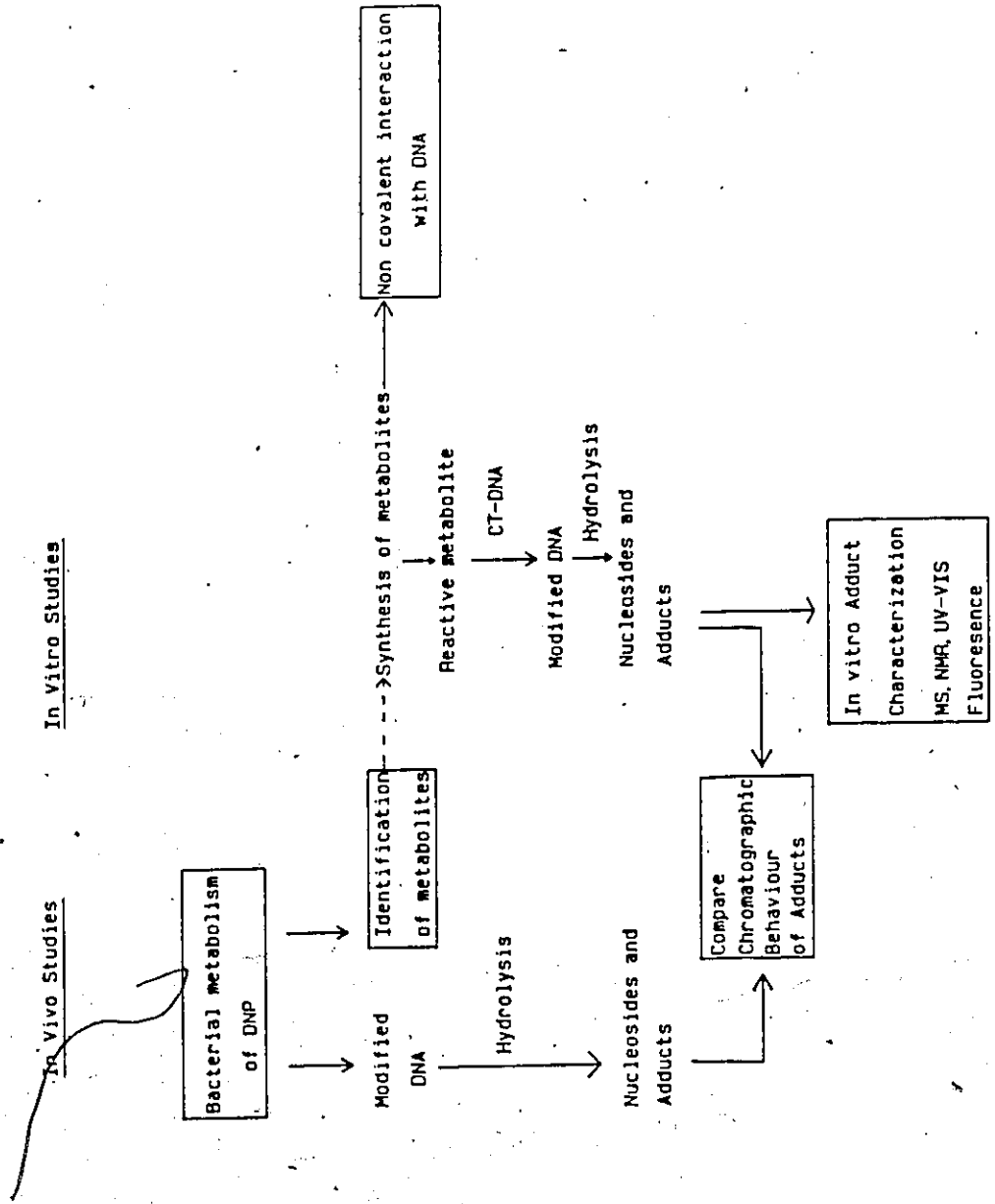
Figure 5: Summary of Research Objectives.

II RESULTS AND DISCUSSION

II.1 Characterization and Mutagenicity of Metabolites of 1,8-DNP 10 and 1-NP 7

This section describes the results of studies which were undertaken to answer some fundamental questions regarding the biological activity of DNPs 8-10 and 1-NP 7. The first part of this section describes the isolation and identification of metabolites of 1,8-DNP 10 from bacterial culture media. The second part of this section presents the results of mutagenicity testing of these metabolites and a proposed metabolic pathway of the DNPs 8-10 in S.typhimurium. Finally the relative rates of metabolism of 1,8-DNP 10 and 1-NP 7 are discussed.

II.1.1 Metabolism of 1,8-Dinitropyrene

As discussed in Section I.3, the metabolism of nitro-PAH occurs in a stepwise fashion from nitro through nitroso to N-hydroxylamino and amino derivatives, of which the latter two may be subsequently be acetylated. The metabolic pathway for 1,8-DNP 10 was therefore expected to be complex as there are two nitro groups which could undergo metabolic transformation. However, as Figure 6 illustrates, because 1,8-DNP 10 has a plane of symmetry, positions one and eight are equivalent. Therefore, the total possible number of metabolites is reduced. 1,3-DNP 8 and 1,6-DNP 9 also exhibit similar symmetry.

22
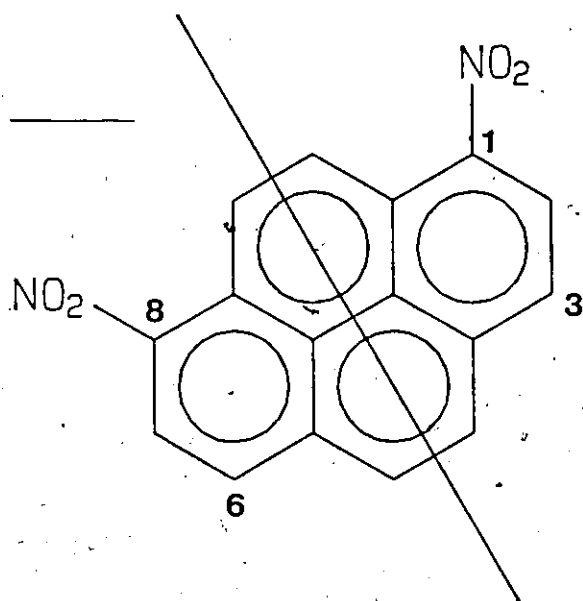
Figure 6: 1,8-Dinitropyrene 10.

The results of a reverse phase liquid chromatography (RPLC) analysis of a dichloromethane (DCM) extract of growth medium containing S.typhimurium TA98 and 1,8-DNP 10 are shown in Figure 7. [3H]-1,8-DNP was added to the incubation mixture as a marker to aid in determining which of the chromatographic peaks were due to metabolites of 1,8-DNP 10. In addition to unmetabolized 1,8-DNP 10 at 22.4 minutes, a compound which was both UV absorbing and radioactive eluted at 16.9 minutes. Co-chromatography with authentic material and MS analysis (Figure 8) proved it to be 1-amino-8-nitropyrene (1,8-ANP) 22. The radioactive peak at 13.5 minutes was an impurity present in the starting material. Further studies by co-workers using crude enzyme extracts from S.typhimurium TA98 revealed three more metabolites: 1,8-diaminopyrene (1,8-DAP) 23, 1-N-acetylamino-8-aminopyrene (1,8-AcAAP) 24, and 1,8-N,N'-diacetylaminopyrene (1,8-DAcAP) 25 (Figure 9). Under the chromatographic conditions described in Figure 7, these polar compounds would have eluted very early in the analysis. In fact, 1,8-AcAAP 24 was shown to co-elute with the radioactive peak at 4.5 minutes.

II.1.2 Mutagenicity of Metabolites of 1,8-DNP 10 and 1-NP 7.

To determine which metabolic reduction step resulted in the formation of reactive metabolites, the mutagenicity of identified and postulated metabolites of 1,8-DNP 10 was studied in four strains of S.typhimurium (Table 4). Mutagenicity testing was carried out by L. Davidson, Department of Biochemistry, McMaster University. TA98NR is a mutant of the wild type (TA98) which was selected for resistance to niridazole (88) and appeared to be deficient in a nitroreductase. Strain DNP$_6$ was

Figure 7: RPLC analysis of dichloromethane extracts of growth medium
containing *S.typhimurium* TA98 and [^{3}H]-1,8-DNP. The eluent was
monitored (a) for radioactivity by liquid scintillation counting of
collected fractions and (b) for UV absorbance at 254 nm. HPLC
conditions: 10μm Altex ODS-2, 250 x 4.6mm, 1 mL/min gradient elution
from 60% aqueous methanol to 100 % methanol in 20 min.
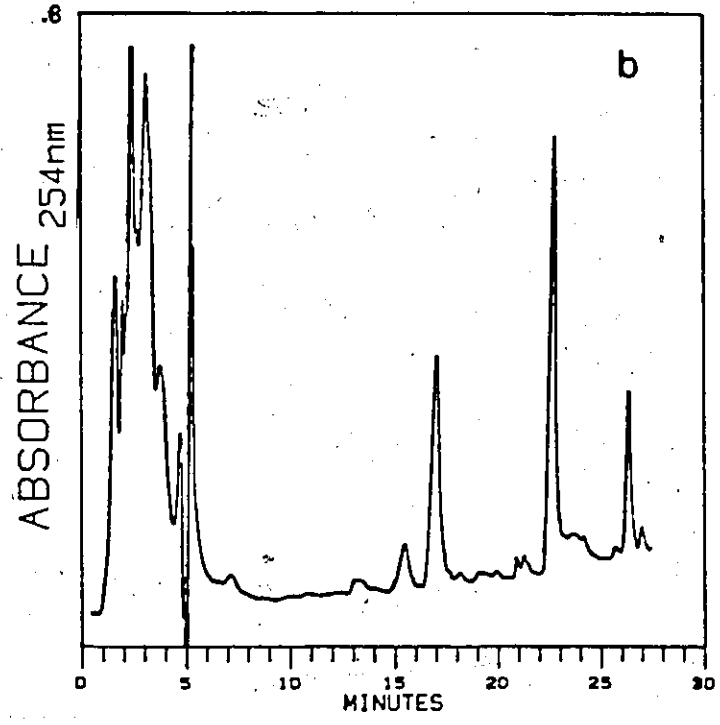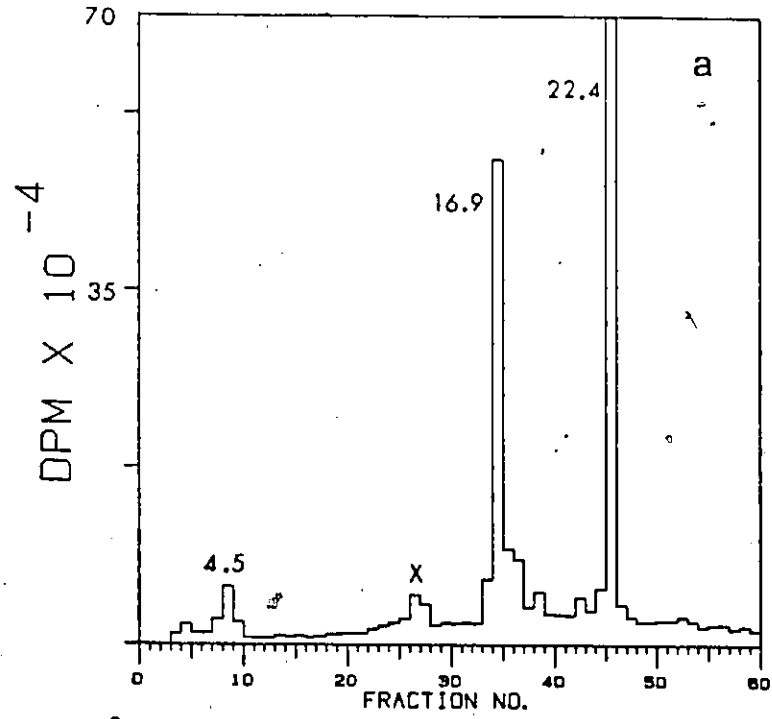
Figure 7.
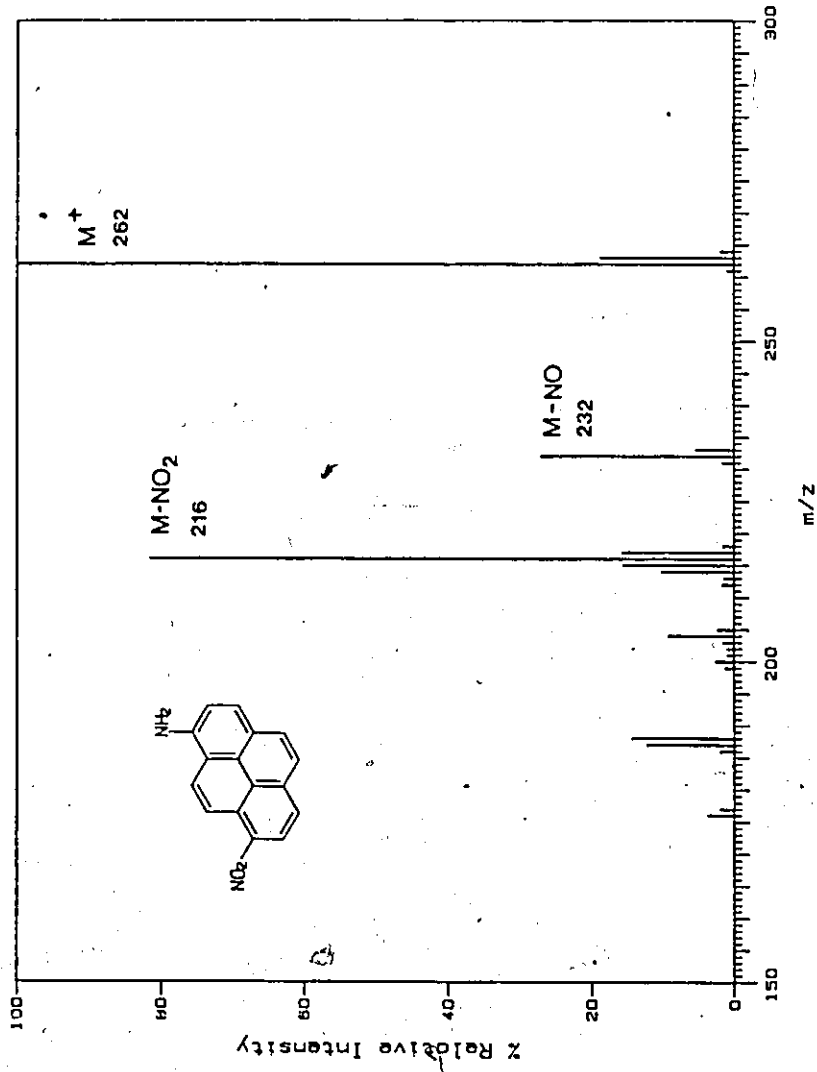
Figure 8: Mass spectrum of 1,8-ANP 22.
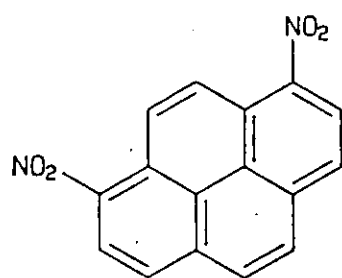
1,8-DNP <u>10</u>
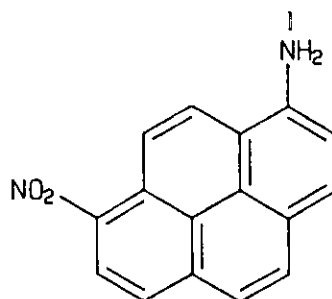
1,8-ANP <u>22</u>
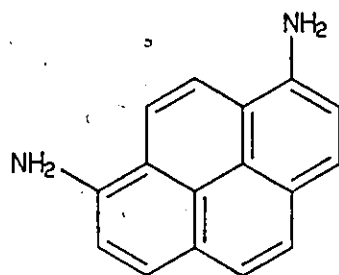
1,8-DAP <u>23</u>
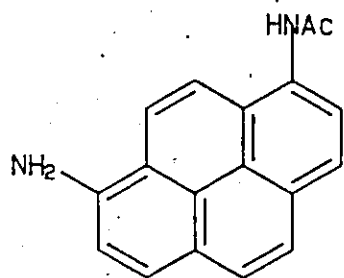
1,8-AcAAP <u>24</u>
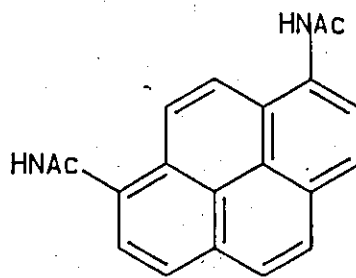
1,8-DAcAAP <u>25</u>

Figure 9: The structures of metabolites of 1,8-DNP <u>10</u>.

Table 4: Mutagenicity of 1,8-Dinitropyrene and Derivatives and 1-Nitropyrene in Salmonella Typhimurium Strains (88).

Compound no.	Compound	Mutagenic Activity in revertants/nmole			
		TA98	TA98NR	DNP_6	$TA98NR/DNP_6$
10	1,8-dinitropyrene	171200 ± 5500^a	106000 ± 7000	2400 ± 100	1251 ± 114
26	1-nitroso-8-nitropyrene	6000 ± 600	3000 ± 300	119 ± 6	60 ± 5
22	1-amino-8-nitropyrene	120 ± 5	102 ± 5	1.9 ± 0.1	1.7 ± 0.1
23	1,8-diaminopyrene	$0.01\pm0.$	0	0	0
24	1-N-acetylamino-8-aminopyrene	0.16 ± 0.1	0	0	0
25	1,8-N-N'-diacetylaminopyrene	0.01 ± 0	0	0	0
7	1-nitropyrene	157 ± 6	16 ± 3	129 ± 4	$3\pm.5$

a   standard deviation

selected for resistance to 1,8-DNP 10 and still retains the wild type reductase. This strain is deficient in the enzyme responsible for the acetylation of N-hydroxylamines to reactive N-acetoxy derivatives (89). The double mutant TA98NR/DNP$_6$ lacked both the acetylase and reductase activity. Mutagenicity of 1-NP 7 in these strains is shown for comparison. The mutagenicity data presented in Table 4 are somewhat different than that reported by Fifer et al (90) although the basic conclusions are the same.

From the results described in Table 4 it is apparent that both acetylase and reductase enzymes must be present for the full mutagenic activity of 1,8-DNP 10 to be expressed. 1-NP 7 required only nitroreductase activity to be present in order for its mutagenicity to be expressed and was one thousand times less active than 1,8-DNP 10 in TA98. However, it is not readily apparent which metabolite is responsible for the mutagenic activity of 1,8-DNP 10. There is a large drop in the mutagenic activity of both 1,8-nitroso-nitropyrene (1,8-NONP) 26 and 1,8-ANP 22 compared to 1,8-DNP 10. Although the reason for this discrepancy is not clear, the chemically reactive N-hydroxylamino derivative can be postulated to be the metabolite responsible for the mutagenic activity of 1,8-DNP 10. This postulated metabolite is at an oxidation state intermediate of 1,8-NONP 26 and 1,8-ANP 22.

Based on these results a hypothetical pathway for the metabolism of 1,8-DNP 10 was proposed (Figure 10). The N-acetoxy species 28 was postulated to be very unstable and would be difficult to synthesize; however derivatives analogous to the N-hydroxylamine 27 have been well characterized (48,49). Since both of these compounds non-enzymatically

Figure 10: Proposed pathway for the metabolism of 1,8-DNP 10 in
S.typhimurium TA98. Compounds in brackets were not detected in the
incubation media.

decompose to the ultimate mutagen, the nitrenium ion 29, synthetic

efforts were directed toward the latter for use as a precursor in the *in*

vitro production of DNA adducts.

II.1.3 Rates of Metabolism of 1,8-DNP 10 and 1-NP 7.

One feature of the data presented in Table 4 is the large

difference in the mutagenicity of 1,8-DNP 10 and 1-NP 7 in *S.typhimurium*

TA98. To determine if the difference in mutagenic activity of 1-NP 7 and

1,8-DNP 10 was due to different rates of nitroreduction, the time course

of their metabolism by *S.typhimurium* TA98 was followed (Figure 11).

Earlier studies in this laboratory demonstrated that, like 1,8-DNP 10,

1-NP 7 was reduced to 1-aminopyrene (1-AP) 30 and acetylated to

1-N-acetylaminopyrene (1-AcAP) 31. The rate of metabolism of 1,8-DNP 10

($t_{1/2}$ =60 min) and the appearance of its reduced metabolites in whole

cells were approximately three times faster than that of 1-NP 7. Studies

by co-workers of the time course for metabolism of 1,8-DNP 10 by crude

enzyme extracted from TA98, showed that the rate of metabolism of 1-NP 7

in this system was even greater than that of 1,8-DNP 10. The difference

in the rates of reduction may have been due to differences in

bioavalaibility or enzyme specificity.

II.2 Synthesis and UV-Visible Characterization of Disubstituted Pyrenes.

This section describes the synthesis, isolation, and UV-VIS

characterization of pure isomers of disubstituted pyrenes. The first

part of this section describes the small scale (μ-mg) syntheses and

normal phase liquid chromatography (NPLC) separation of pure isomers of
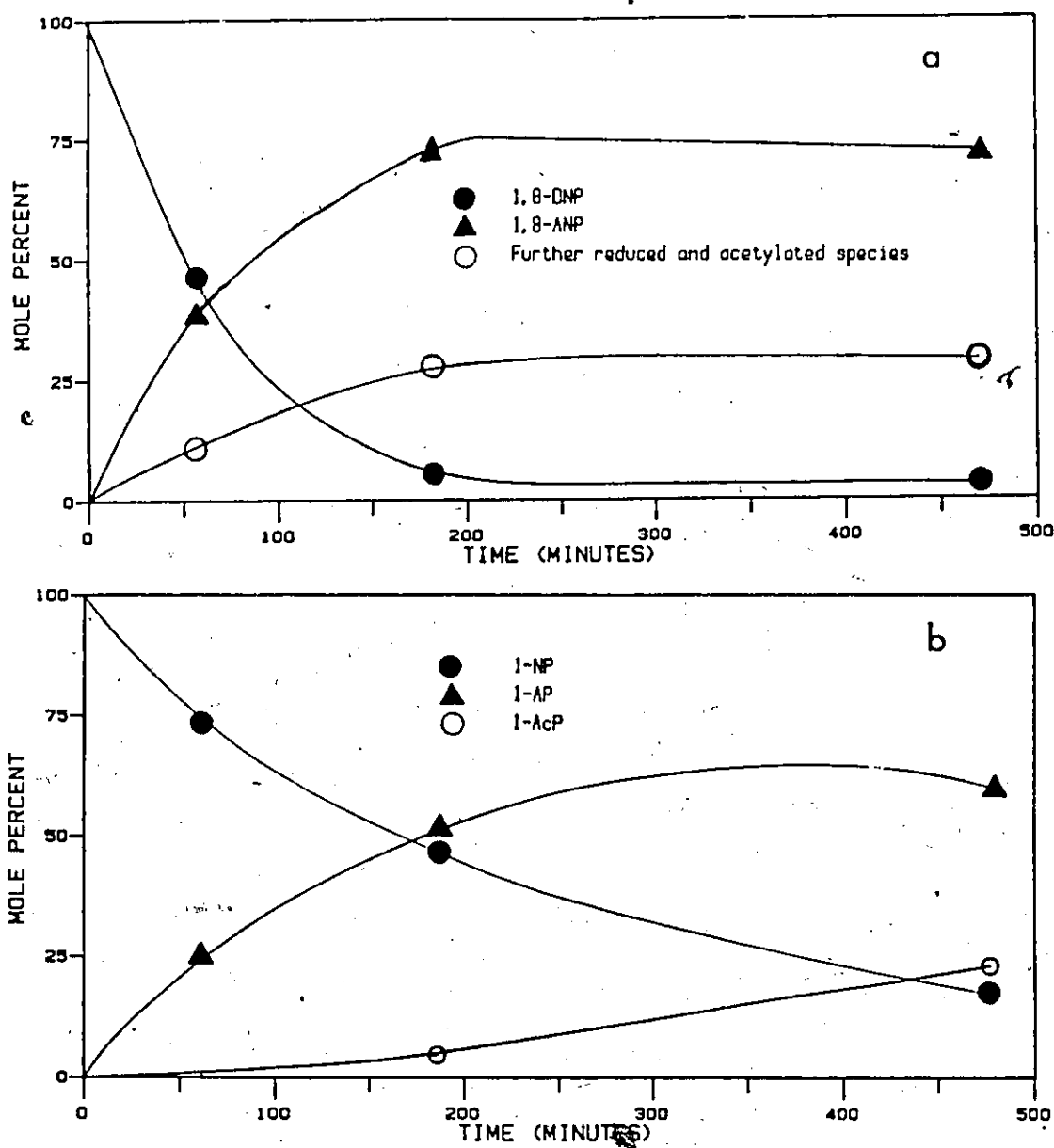
Figure 11: Time course of metabolism of 1,8-DNP 10 and 1-NP 7. The time course of metabolism by *S. typhimurium* TA98 of (a) [³H]-1,8-DNP, (b) [³H]-1-NP , and appearance of metabolites was followed by RPLC analysis of dichloromethane extracts of incubation media. The open circles (O) represent the sum of the mole per cent of 1,8-DAP 23, 1,8-AcAAP 24, and 1,8-DAcAAP 25 which co-eluted under the chromatographic conditions used. Per cent metabolism at each time point was calculated by liquid scintillation counting of eluent fractions. Each time point represents a separate incubation.

the DNPs 8-10, their tritium labelled analogues, 1,3-ANP 32, 1,6-ANP 33, and 1,8-ANP 22 for use as chromatographic and mass spectrometric standards. The tritium labelled analogues were used as tracers in the metabolism studies.

The second part of this section describes the larger scale (50mg-100mg) syntheses and isolation of pure isomers of various disubstituted pyrenes used in the *in vitro* production of DNP-nucleoside adducts. In addition, many of these pyrene derivatives were tested for mutagenicity in the Ames bacterial reversion assay as described in II.1. The overall routes are summarized in Figure 12.

II.2.1 Synthesis of Unlabelled and Tritium Labelled DNPs 8-10.

Pyrene was used as starting starting material for the synthesis of the DNP and ANP derivatives. Using the method of Streitweiser and Fahey (91), the nitration of pyrene in a solution of acetic anhydride and fuming nitric acid at room temperature proceeded smoothly yielding a mixture of 1,3-DNP 8, 1,6-DNP 9, 1,8-DNP 10, and 1-NP 7 in a 1:3:4:1 ratio (Scheme 1). The dinitropyrene isomers 8-10 were easily separated by semi-preparative NPLC (Figure 13a).

Nitration of [^{3}H]-pyrene (38 Ci/mmole, custom synthesized by Amersham Corp.) also yielded the analogous tritiated derivatives. During RPLC cleanup of this mixture, polar decomposition products eluted early in the analysis allowing collection of crude DNP and 1-NP 7 fractions. The tritium labelled derivatives were then purified by NPLC as described for the unlabelled DNPs 8-10 described above. Typical activities for 1-NP 7 and DNPS 8-10 were 14-18 Ci/mmole, and 2-4 Ci/mmole respectively.

Isomer mixture   Chromatographic   Separated Pure Isomers
                  Separation

Pyrene ──────→ DNPs
        Zinin
        Reduction

DAPs ──────┤ Silica Gel ├──────→ 1,3-, 1,6-, or 1,8-DAP
                                              │ Excess MCPBA
                                              ↓
DNPs ──────┤ Semi-preparative NPLC ├──────→ 1,3-, 1,6- or 1,8-DNP
           │ Solvent Extraction   │   │ Zinin Reduction
                                              ↓
ANPs ──────┤ Semi-preparative NPLC ├──────→ 1,3-, 1,6- or 1,8-ANP
                                              │ 2 eq. MCPBA
                                              ↓
                                           1,3-, 1,6-, or 1,8-NONP
                                              │ 5 eq. ascorbate
                                              ↓
                                           1,3-, 1,6-, or 1,8-HANP

DAPs ←────── DNPs ──────→ ANPs
   Hydrogenation   Zinin
                    Reduction
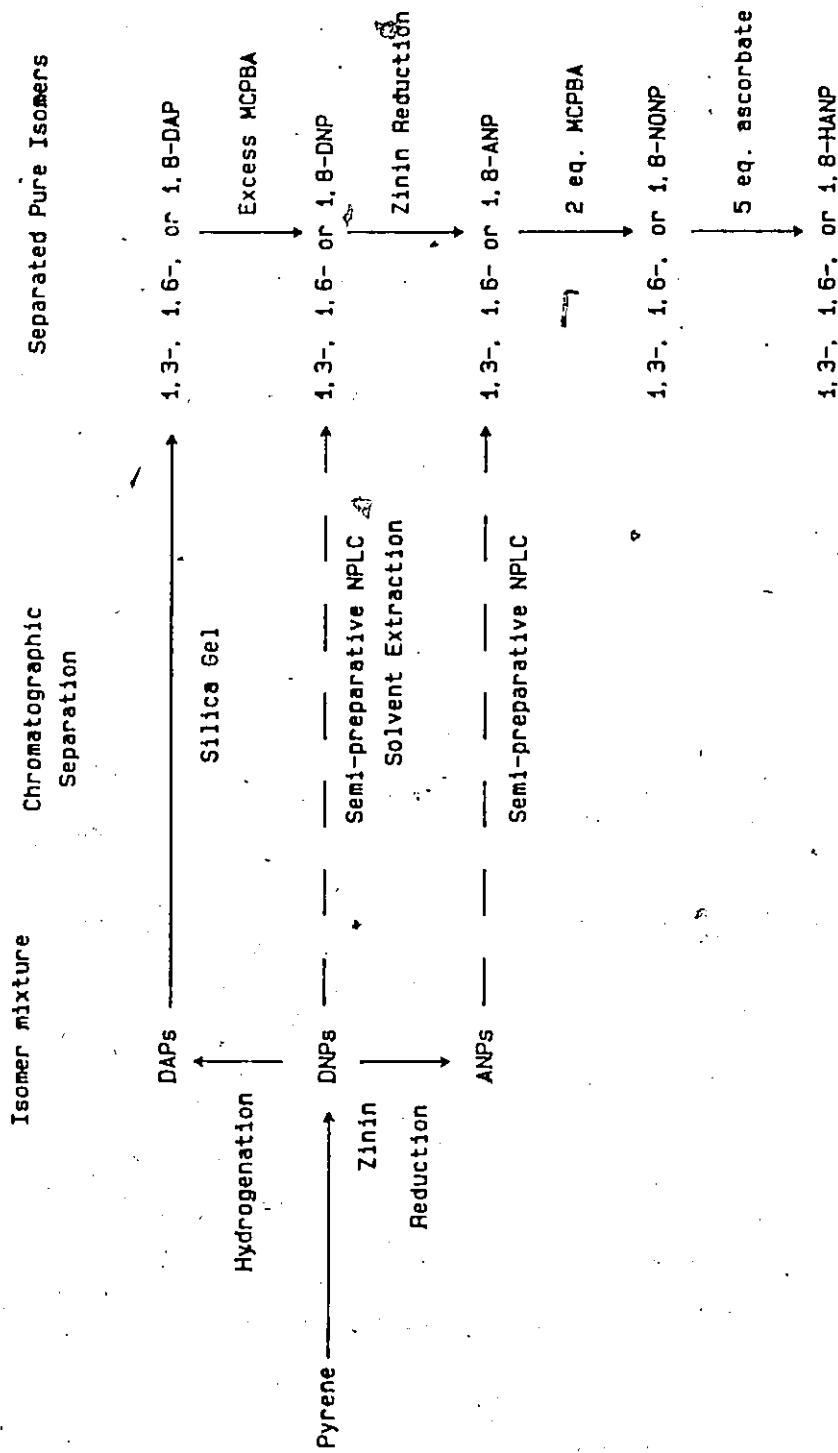
Figure 12: Summary of synthetic steps and chromatographic separations used in the isolation of pure isomers of disubstituted pyrenes. Solid arrows represent pathways for large scale syntheses, dotted arrows represent routes for small scale syntheses and isolation.

Pyrene 4

Fuming HNO₃

Acetic anhydride

1-NP 7

1,3-DNP 8
1,6-DNP 9
1,8-DNP 10
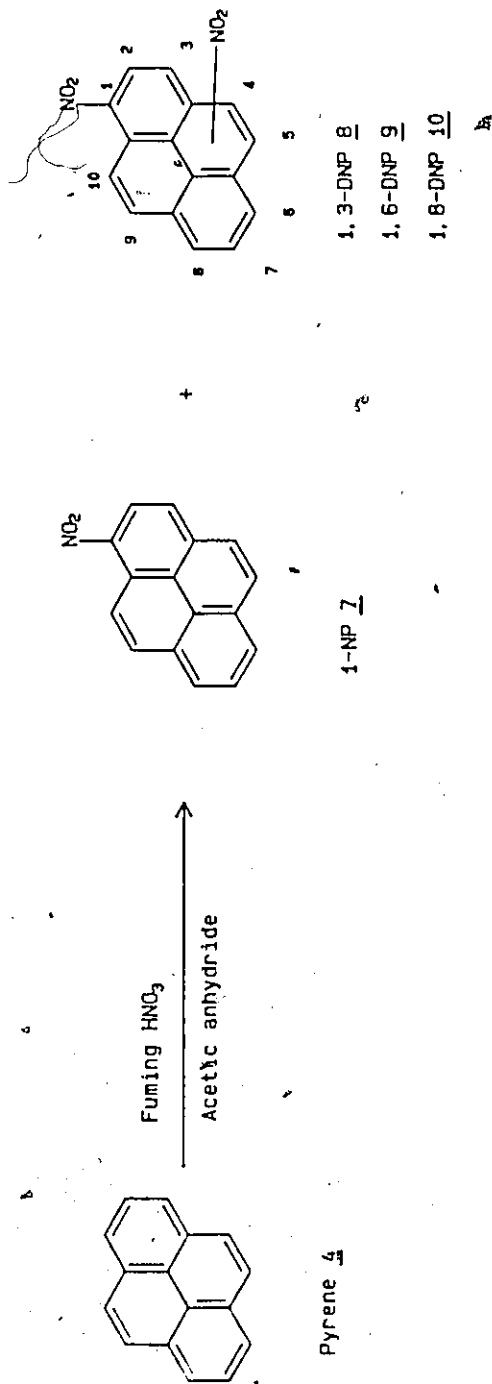
Scheme 1. Nitration of pyrene to 1-NP 7 and DNPs 8-10.
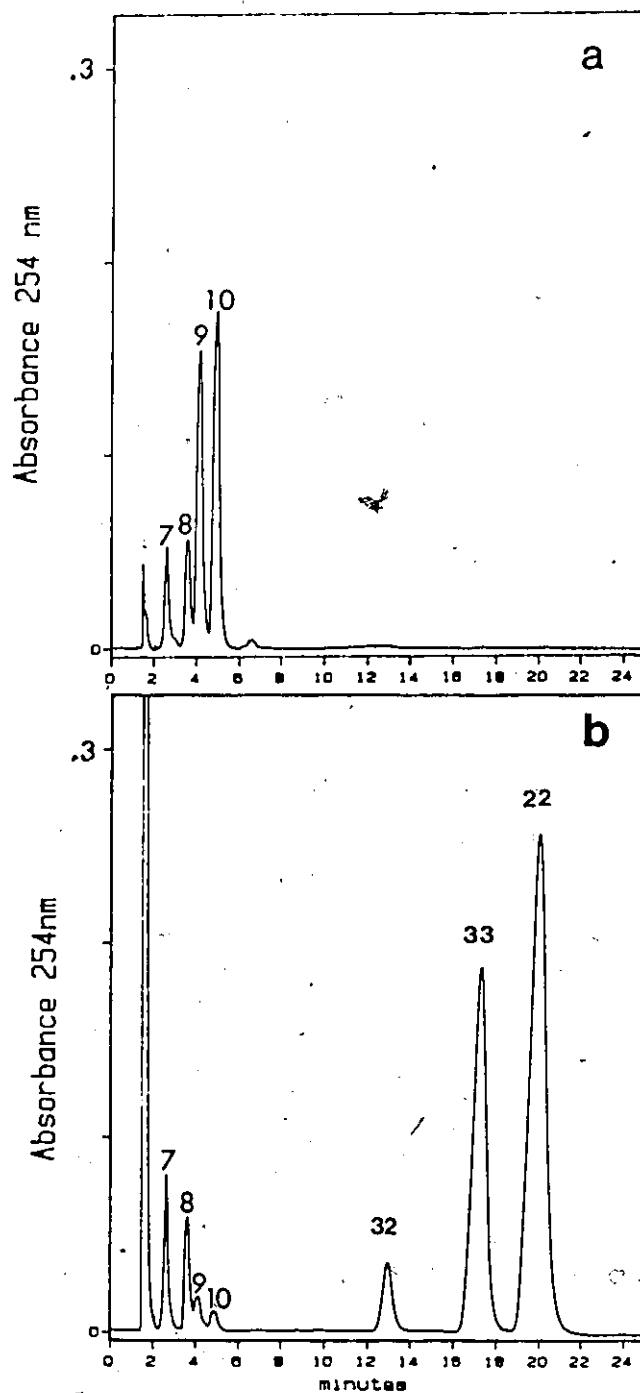
Figure 13: NPLC chromatograms of a mixture of 1-NP 7 and DNP isomers 8-10
(a) before and (b) after addition of polysulphide. Compounds: 1-NP 7,
1,3-DNP 8, 1,6-DNP 9, 1,8-DNP 10, 1,3-ANP 32, 1,6-ANP 33, 1,8-ANP 22. HPLC
conditions: 5μm Altex Ultrasphere Cyano, 250x4.6 mm, 1 mL/min.
90% hexane/isopropanol.

II.2.2 Zinin Polysulphide Reduction of DNPs 8-10 to ANPs 32, 33 and 22.

In initial studies by co-workers, ANP isomer mixtures were prepared by nitration and hydrolysis of 1-N-acetyl-aminopyrene 31. However, subsequent RPLC analysis of the hydrolysis products revealed that only 1,8-ANP 22 and 1,6-ANP 33 were present. As these two derivatives were easily separated by chromatography on alumina, this procedure initially served as a ready source of 1,8-ANP 22 and 1,6-ANP 33 for use in metabolism studies.

A second more direct route to the ANPs 32, 33 and 22 used the Zinin polysulphide reduction (Scheme 2). First used by Zinin in 1842 to prepare aniline from nitrobenzene, this procedure is a procedure for the mono-nitroreduction of polynitroarenes by negative divalent sulphur. The polysulphide reducing reagent, produced by dissolving $Na_2S \cdot H_2O$ in an aqueous solution of sulphur, contains the paramagnetic S_3^{2-}, S_4^{2-}, and S_6^{2-} species (93). A review of the procedure described the use of a variety of reducing agents such as ammonium, sodium, and potassium sulphides, hydrosulphides, and polysulphides (94). Methods using HS^{2-} as reducing species were much less effective.

In initial studies, the Zinin reduction of a mixture of the DNP isomers, produced as in Scheme 1, was studied. By varying the conditions described by Porter et al. (93), such as choice of organic solvent, concentration of base, presence of oxygen, and reaction temperature, maximal reduction of the DNPs to the corresponding ANPs was achieved. Ethanol:chloroform (1:1) was chosen as the solvent because of its high refluxing temperature, and was of the correct polarity for the solution

39
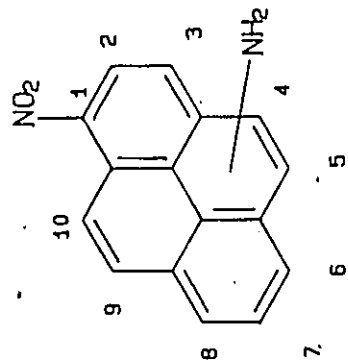
Polysulphide/NaOH
—————————————→
Ethanol/Chloroform
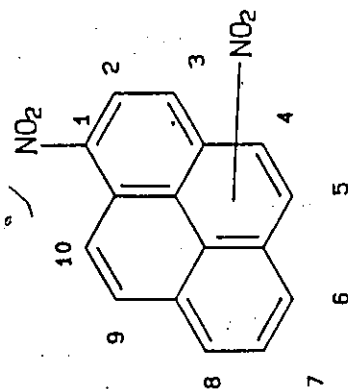
1,3-DNP 8

1,6-DNP 9

1,8-DNP 10

1,3-ANP 32

1,6-ANP 33

1,8-ANP 22

Scheme 2. Zinin polysulphide reduction of DNPs 8-10 to ANPs
32, 33 and 22.

of starting materials, product, polysulphide and base. The amount of base added was crucial as excess base resulted in large production of a purple coloured water soluble side product. Rigorous exclusion of oxygen from the reaction prevented oxidation of the reducing reagent. The NPLC analysis of the starting DNP mixture and ANP reduction products is shown in Figure 13. Note that 1-NP 7 was not reduced and the extent of reduction of 1,3-DNP 8 appeared to be less than the other DNPs.

Although there may be other explanations, the differences in extent of nitroreduction of the DNPs may be due to differences in their reduction potentials. During studies on the relationship between polarographic reduction potential, calculated LUMO energies and mutagenicities of a number of nitroarenes, Klopman et al (95) showed that the $E_{1/2}$ for 1,8-DNP 10 (-0.505 V) and 1,6-DNP 9 (-0.493 V) was much lower than that of 1-NP 7 (-.750 V) and hence the former would be more easily reduced. The $E_{1/2}$ for 1,3-DNP 10 (-0.523 V) is slightly higher than those of the DNPs 9, and 10 and therefore it would also undergo reduction but not as easily. Tallec et al reported a similar pattern of reduction potentials for nitro substituted benzenes (96,97).

II.2.3 Large Scale Synthesis of Disubstituted Pyrenes.

This section describes the synthesis of the target compounds 1-N-hydroxylamino-3-nitropyrene (1,3-HANP) 34, 1-N-hydroxylamino-6-nitropyrene (1,6-HANP) 35, and 1-N-hydroxylamino-8-nitropyrene (1,8-HANP) 27. As described in II.1, these HANPs were postulated to be reactive metabolites of DNPs and were prepared for in vitro syntheses of DNP-nucleoside adducts. As the m-chloroperbenzoic acid (MCPBA) oxidation

of 1-aminopyrene (1-AP) 30 to 1-nitrosopyrene (1-NOP) 36 and subsequent ascorbate reduction to 1-N-hydroxylaminopyrene 37 was well characterized (50,98), efforts were directed to the three ANP isomers.

The most direct route to the ANPs 32, 33, and 22 was by Zinin reduction of a DNP isomer mixture to a mixture of the corresponding ANPs. Although this was a facile route to synthesis of ANP isomer mixtures in high yield, all attempts to separate the isomers on a preparative scale failed. Semi-preparative NPLC using conditions described in Figure 13 was tedious and limited by the solubility of the compounds in the mobile phase. Chromatography on alumina or silica resulted in separation of only the 1,6-ANP 33, from the co-eluting 1,8-ANP 22 and 1,3-ANP 32. Altering solvent polarities and reaction temperature during the reduction in an attempt to reduce 1,6-DNP 9 and 1,8-DNP 10 preferentially also failed. Amide and carbamate derivatives of the ANPs also could not be resolved chromatographically using a number of eluting solvents and chromatographic supports.

Because of the problems with separation of the ANP derivatives, methods of separating the DNP isomers which could then be used in this reduction procedure were investigated. However, all attempts at preparative scale separation and isolation of the DNP isomers 8-10 in an acceptable time frame were unsuccessful. As with the ANPs, NPLC separation of the DNPs 8-10 was useful only on an analytical scale as column loading was very limited due to low solubility. Similar results were obtained with chromatography on alumina in a modified soxhlet extractor according to the method of Bodin et al (99). As alumina separation of 1,8-ANP 24 and 1,6-ANP 35 was demonstrated by co-workers,

solvent extraction of 1,3-DNP 8 according to the method of Kaplan *et al* (100) was attempted. The DNP isomer mixture, produced as in Scheme 1, was stirred in acetonitrile for 12 hours and the soluble residue analysed by NPLC. However, NPLC analysis demonstrated that the extraction of 1,3-DNP 8 into acetonitrile was not very selective.

As the separation of DNP or ANP isomer mixtures was tedious, reduction of a DNP isomer mixture to a mixture of 1,3-DAP 38, 1,6-DAP 39 and 1,8-DAP 23 was attempted. The high solubility of these DAPs allowed higher column loadings, and the reduction of the mixture of the DNPs 8-10 in methanol by hydrogen and Pt(IV) oxide was achieved in virtually 100 % yield (Scheme 3). The resulting solution of DAP isomers was very fluorescent and easily oxidized. Separation of the three DAP isomers was achieved by preparative silica gel flash chromatography. This chromatography was carried out in a column specially constructed to withstand high pressures generated due to high flow rates required (98 mL/min). The DAP mixture was coated on deactivated silica and loaded onto the top of the column. This procedure allowed the DAP mixture to be swept by the mobile phase onto the activated silica in a narrow band. Although there appeared to be some on-column decomposition after a separation, replacement of the top 1 cm of packing material with fresh silica allowed the column to be used for multiple separations without costly replacement of packing material.

After chromatography, the separated diamines 38, 39, and 23 were oxidized for 16 hours with excess MCPBA in DCM, affording an orange solution containing a mixture of the corresponding DNPs 8, 9, or 10 and NONP derivatives 40, 41, or 26 (Scheme 4). The ratio of DNP to NONP

43

1,3-DNP 8
1,6-DNP 9
1,8-DNP 10

Pt(IV) Oxide/H₂
Methanol

1,3-DAP 38
1,6-DAP 39
1,8-DAP 23

Silica gel
Chromatography

1,3-DAP 38

1,6-DAP 39

1,8-DAP 23
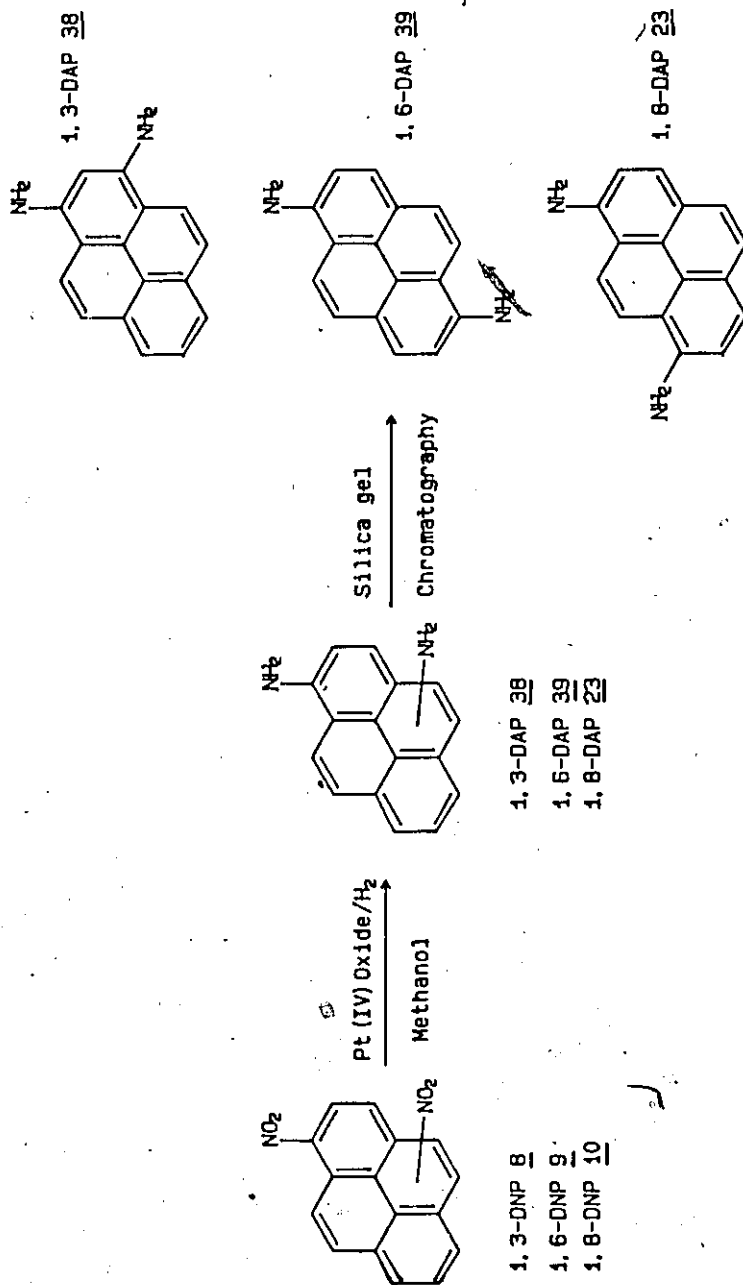
Scheme 3. Reduction of DNPs 8-10 to DAPs 38, 39 and 23.

1,3-DAP 38
1,6-DAP 39
or
1,8-DAP 23

Excess MCPBA
Methanol

+

Polysulphide
NaOH

1,3 ANP 32
1,6-ANP 33
or
1,8-ANP 22
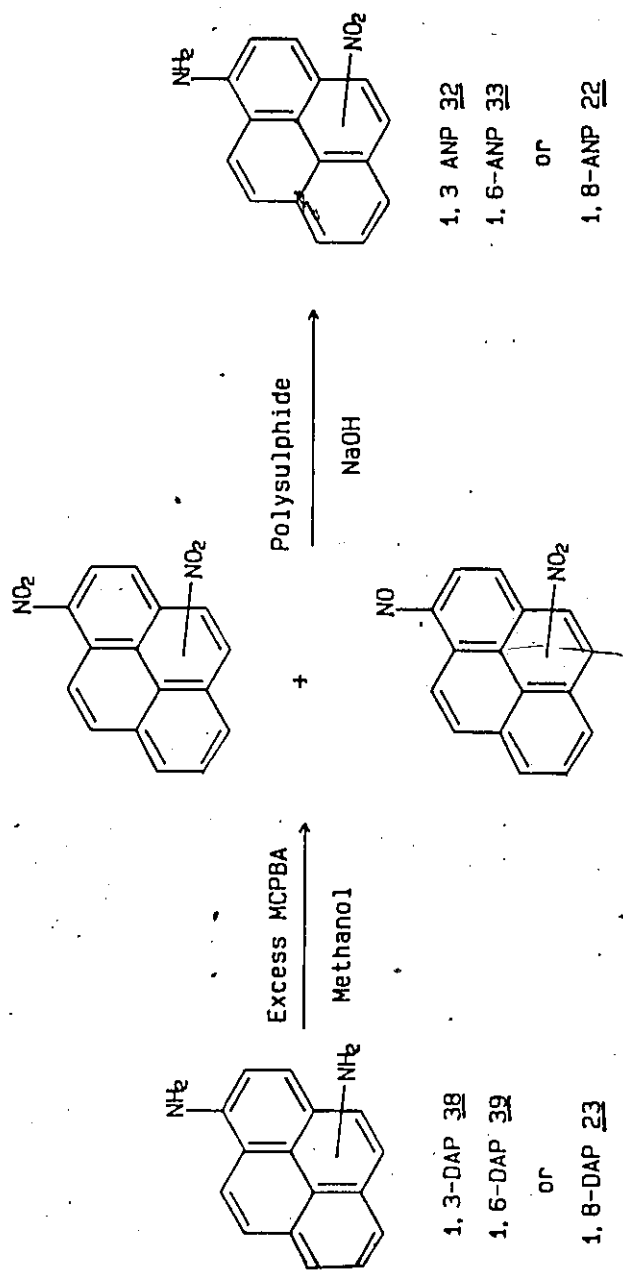
Scheme 4. The MCPBA oxidation of DAPS 38, 39 and 23 to DNPs 8-10 and NONPS 40, 41 and 26 and subsequent Zinin reduction to ANPs 32, 33 and 22.

44

concentrations in this mixture depended on the DAP and MCPBA
concentrations, and reaction time. Interestingly, attempts at the
partial oxidation of 1,3-DAP 38 to 1,3-ANP 32 yielded a product which by
MS analysis proved to be 1-nitroso-3-aminopyrene (1,3-NOAP). However,
the oxidation of 1,6-DAP 39 and 1,8-DAP 23 resulted in mixtures
containing the ANP, NONP, and DNP derivatives.

There was no need to separate these DNP and NONP derivatives as
they were cleanly reduced to the corresponding ANPs via the Zinin
reduction. These separated ANP derivatives were then oxidized in DCM to
orange NONP derivatives with 2 equivalents of MCPBA according to the
method of Howard et al (50) (Scheme 5). Final reduction of the NONP to
the unstable N-hydroxylamino-nitropyrene was effected with 5 equivalents
of ascorbic acid. This reduction was not performed until the reaction of
the HANP and CT-DNA was about to take place.

II.2.4 UV-Visible Characterization.

Characterization of the HANPs and their synthetic precursors by
UV-VIS spectrophotometry was hampered by the fact that these compounds
were produced in complex mixtures or were unstable and decomposed during
isolation and purification. These difficulties were overcome by coupling
HPLC with diode array detection for chromatographic separation and UV-VIS
spectrum acquisition.

Diode array detectors, such as the HP-1040A used in this work,
allow very rapid (10 ms) spectrum acquisition while simultaneously
monitoring several wavelengths. Polychromatic light from a deuterium
lamp is focussed through the flow cell and onto a holographic grating.

2 eq. MCPBA

5 eq. Ascorbate

DMF

1,3-ANP 32
1,6-ANP 33
or
1,8-ANP 22

1,3-NONP 40
1,6-NONP 41
or
1,8-NONP 26
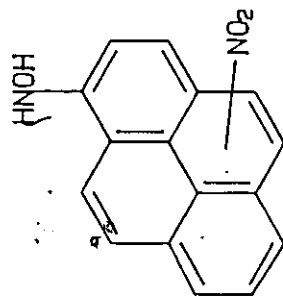
1,3-HANP 34
1,6-HANP 35
or
1,8-HANP 27
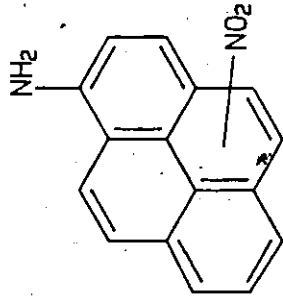
Scheme 5. MCPBA oxidation of ANPs 32, 33 and 22 to NONPs 40, 41 and 26 and subsequent reduction to HANPs 34, 35, and 27.

The light is then dispersed onto a 211 element diode array where light intensities are simultaneously measured from 190 nm to 600 nm. By repetitive measurements and calculating the log ratio to a reference energy spectrum, a 3-D matrix of absorbance as a function of time and wavelength is acquired. By monitoring absorbance at selected wavelengths, one can suppress signals from interfering compounds and enhance signals from compounds of interest. In addition, by monitoring the UV-VIS spectra as a function of time, peak purity and chemical identity can be confirmed.

The UV-VIS spectra of various disubstituted pyrenes acquired during their RPLC analysis are summarized in Table 5. As depicted in Figure 14, the spectra of these compounds were very susceptible to electron density changes in the pyrene system. As the nitro group of 1,8-DNP 10 was reduced through nitroso and hydroxylamino to amino, the nitrogen became more electron donating and the absorption bands were shifted to longer wavelength. The pattern of substitution of the compounds may also be deduced from their spectra. In the ANP and HANP derivatives, the position of the absorbance maxima appeared in the order of 1,3-,1,6- and 1,8- substitution, the 1,8-isomer being shifted furthest to longer wavelength. For example, in Figure 15, the absorbance maxima of 1,3- , 1,6- and 1,8-HANP isomers appeared at 444, 457 and 464 nm respectively. As will be discussed in Section II.3, the position of UV-VIS absorbance maxima were useful in determining both site of bond formation and isomer identification of adducts formed between HANP species and nucleosides.

PAH and their derivatives are known to form dimers and higher aggregates in solution (101). By monitoring their UV-VIS and

Table 5: UV-Visible absorbance maxima (nm) of various substituted pyrenes. Spectra were acquired during RPLC using diode array detection. Mobile phase composition during acquisition was approximately 65/35 acetonitrile/water.

First Substituent:	NO_2	NO	NHOH	NH_2	NO_2	NO_2	NO_2	NO_2	NO	NH_2
Second Substituent:	H	H	H	H	NO_2	NO	HNOH	NH_2	NH_2	NH_2
Abbreviation	NP	NOP	HAP	AP	DNP	NONP	HANP	ANP	NOAP	DAP
Substituent positions										
1&3	394	438	350	358	419	446	444	466	524	382
1&6					412	445	457	488		390
1&8					399	440	464	498		390

49
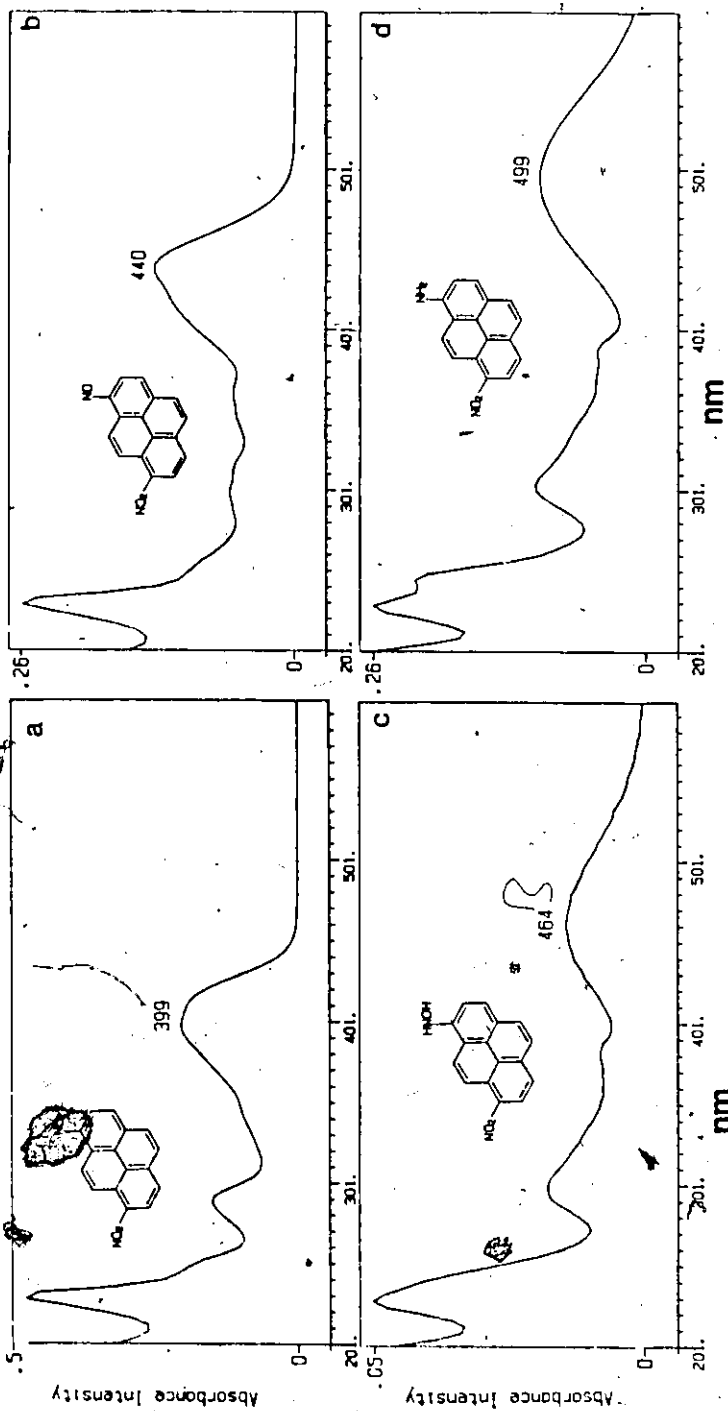
Figure 14: UV-VIS spectra of (a) 1,8-DNP 10, (b) 1,8-NONP 26, (c) 1,8-HANP 27, and (d) 1,8-ANP 22. Spectra were acquired during RPLC analyses using an acetonitrile/water gradient. Spectral acquisition conditions: range, 200 to 600 nm in increments of 4 nm.
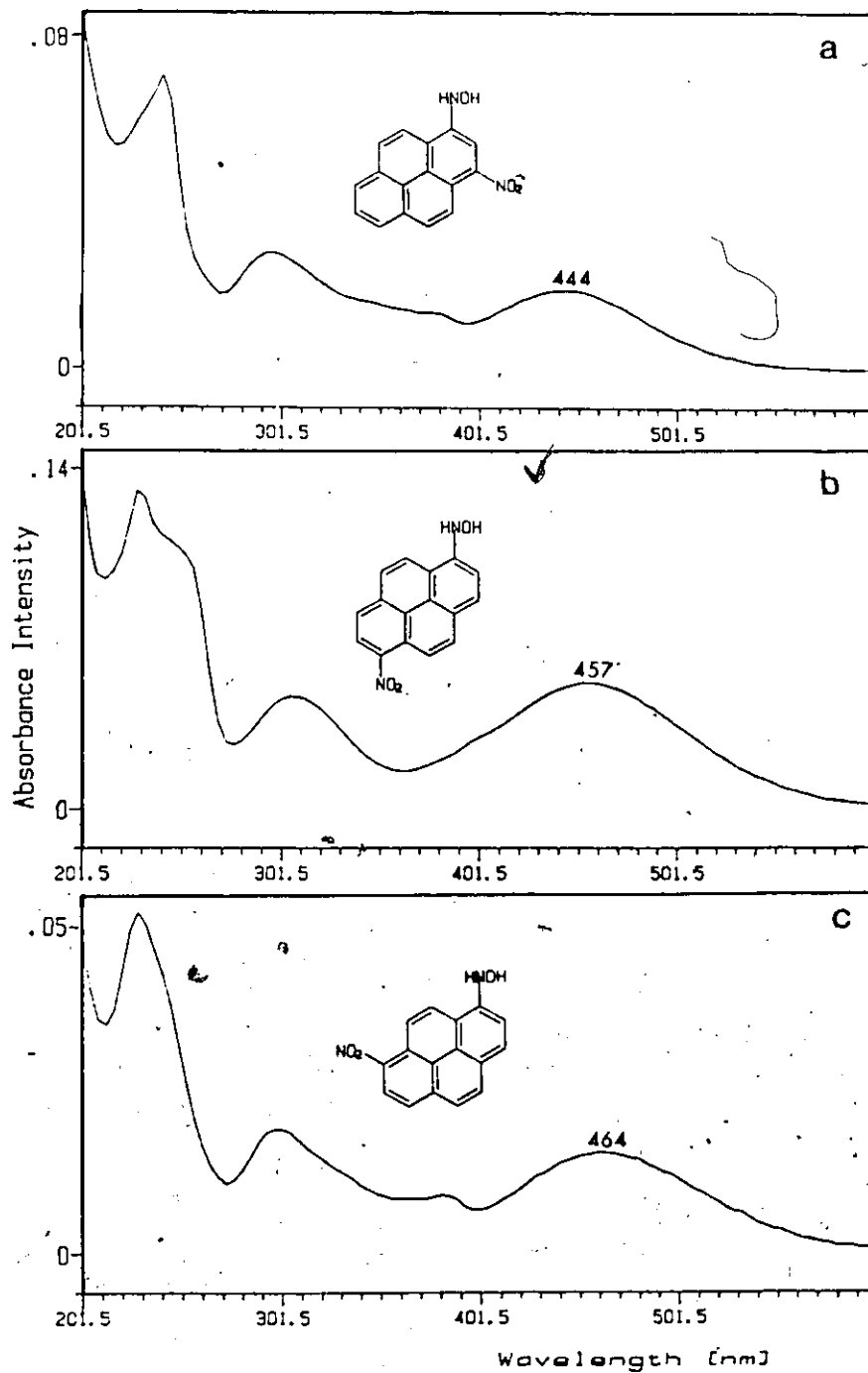
Figure 15: UV-VIS spectra of (a) 1,3-HANP 34, (b) 1,6-HANP 35, and (c) 1,8-HANP 27. Spectral acquisition conditions were as described in Figure 14.

fluorescence spectra, the concentration at which stacking behaviour begins may be determined. This information is useful as the stacked species often have different extinction coefficients, fluorescence spectra, exhibit broad NMR signals, and may have different biological properties than the free species. The UV absorbance and fluorescence intensity of 1,8-ANP 22 as a function of concentration are shown in Figure 16. Significant deviations from Beer's law indicate that stacking occurs at low concentrations (2×10^{-5}M). Therefore any quantitative measurements should be made below this concentration. Fluorescence measurements by co-workers showed that 1,8-DAP 23 stacks at 6×10^{-9}M (data not shown).

II.3 DNP-Nucleoside Adduct Formation, Isolation and Characterization.

The key intermediates in the bacterial metabolism of the DNPs 8-10, described in II.1, were postulated to be the hydroxylamino-nitropyrenes (HANPs) 34, 35 and 27. These hydroxylamines could then be transformed to a reactive nitrenium ion directly by a nonenzymatic hydrolysis, or enzymatically via an N-acetoxy derivative. This section, as summarized in Figure 17, describes the procedures for the production of DNA modified in vivo by 1,8-DNP 10, and in vitro by HANPs 34,35, and 27, the enzymatic hydrolysis of this modified DNA, and the isolation and spectroscopic characterization of DNP-nucleoside adducts.
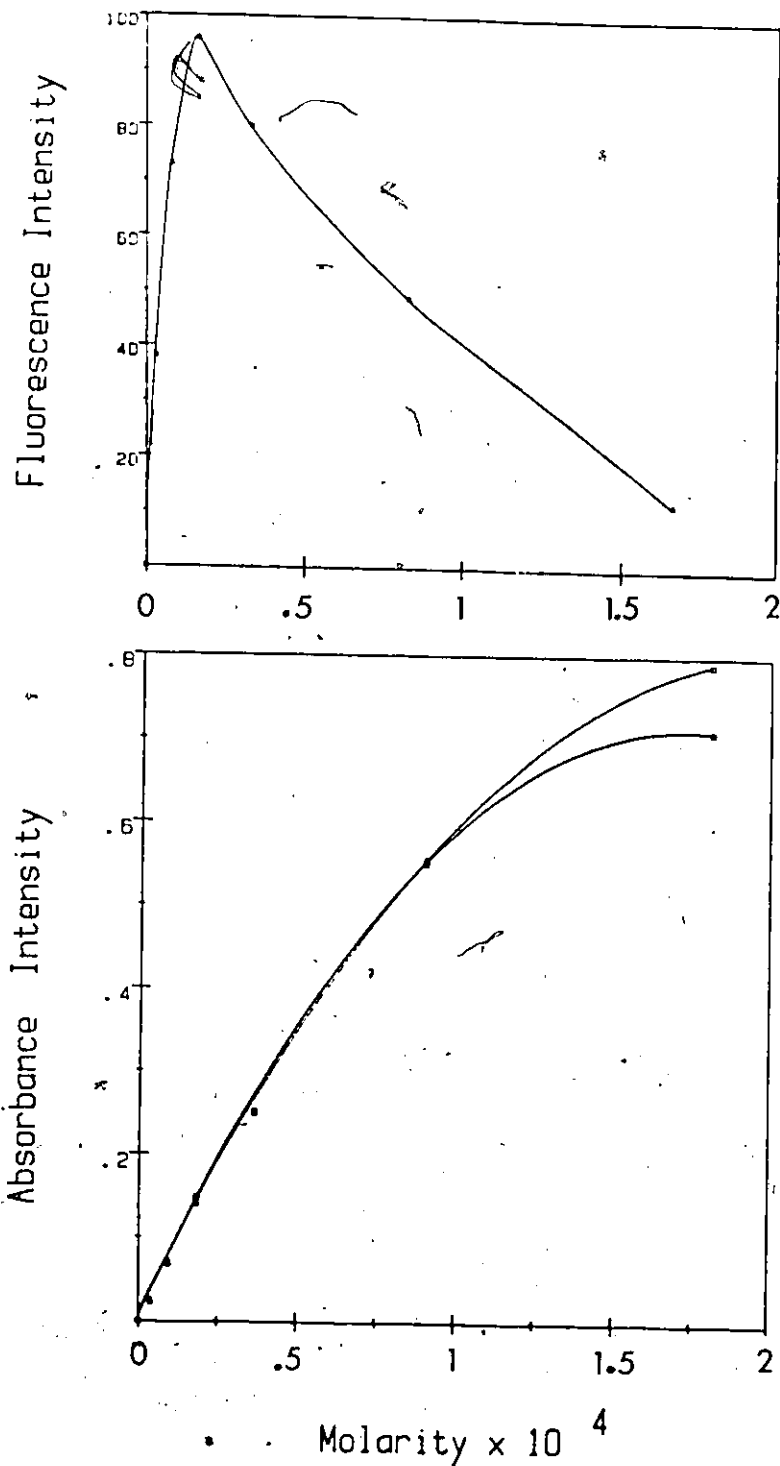
Figure 16: The dependence of (a) fluorescence intensity at 443 nm and (b) absorbance at 498 nm, on concentration of 1,8-ANP 22 in acetonitrile solutions. The two curves in (b) are the result of two different experiments.

In Vivo Studies   In Vitro Studies

```
┌─────────────────────┐
│ Bacterial metabolism │
│      of DNP          │
└─────────────────────┘
     │           │
     ▼           ▼
Modified    ┌──────────────┐
            │Identification│- - - -> Synthesis of metabolites
DNA         │of metabolites│                    │
            └──────────────┘                    ▼
                                        Reactive metabolite
  │ Hydrolysis                                   │ CT-DNA
  │                                              ▼
  ▼                                       Modified DNA
Nucleosides and                                 │ Hydrolysis
Adducts                                          ▼
                                         Nucleosides and
                                         Adducts
     │        ┌──────────────┐                  │ │
     │        │Compare       │                  │ │
     └───────>│Chromatographic│<────────────────┘ │
              │Behaviour,    │                     │
              │of Adducts    │                     ▼
              └──────────────┘            ┌──────────────┐
                                          │In vitro Adduct│
                                          │Characterization│
                                          │MS, NMR, UV-VIS │
                                          │Fluoresence     │
                                          └──────────────┘
```
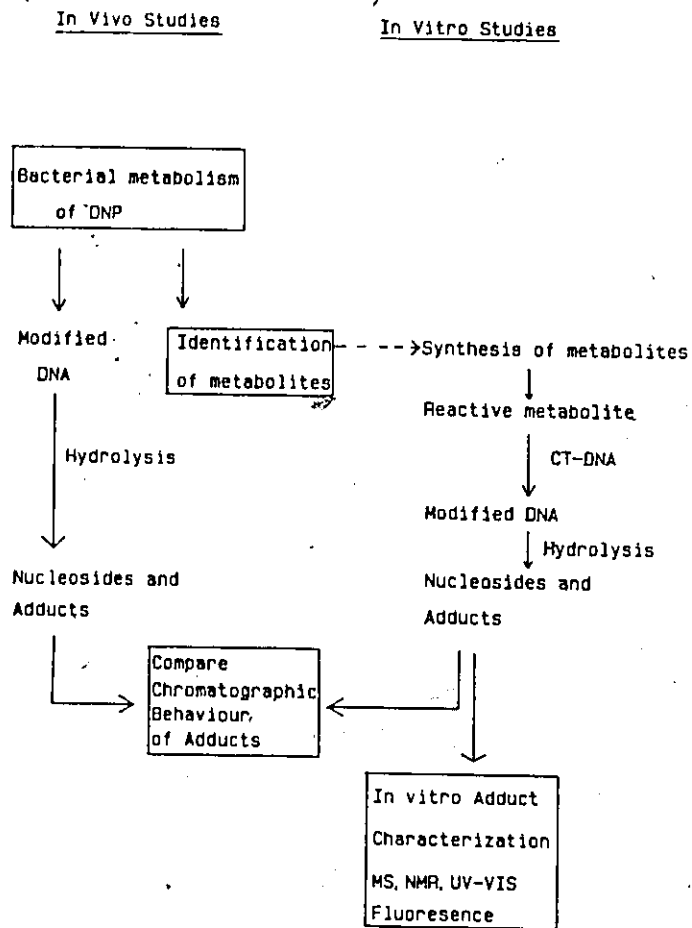
Figure 17: Summary of steps for the production of in vitro
and in vivo modified DNA, and the isolation and characterization of DNA
adducts.

II.3.1 Covalent DNP-DNA Adduct Formation, Modified DNA hydrolysis and Isolation of Nucleotide Adducts.

The results of *in vivo* DNA binding experiments in which [^{3}H]-1,8-DNP 10 was incubated with *S.typhimurium* TA98 are shown in Table 6. The results for binding of [^{3}H]-1-NP 7 under similar conditions are shown for comparison. Bacteria were allowed to grow in the presence of labelled compound, cells collected at three time points, and the bacterial DNA isolated and counted for tritium. The concentration of both labelled compounds was 1.5×10^{-5} M. The binding of metabolites of [^{3}H]-1,8-DNP 10 appeared to be time dependent. Binding of 26 adducts/10^7 nucleotides was observed after 6 hours. This was approximately 10 times the DNA binding observed with [^{3}H]-1-NP 7. Covalent binding was also observed for [^{3}H]-1,3-DNP 8, and [^{3}H]-1,6-DNP 9, (measured under different experimental conditions; data not shown).

The results of *in vitro* binding experiments with 1,3-HANP 34, 1,6-HANP 35, and 1,8-HANP 27 and calf thymus (CT)-DNA are shown in Table 7. The HANPs were generated from the corresponding NONPs by reduction with ascorbate, and allowed to react with CT-DNA in a 1:3 solution of DMF:pH 5 citrate buffer. The DNA solution was then exhaustively extracted with phenol until no color was observed in the phenol layer. Initial studies showed that the extent of adduct formation, as evidenced by intensity of orange colour of the DNA, was maximal at this pH. This pH maximum was also shown by co-workers to correspond to the pH of maximum stability of 1,8-HANP 27 (102). The positions of the UV-VIS absorbance maxima of the modified DNA appeared in the same order as the absorbance maxima of the HANPs used in the reaction, ie, 1,3-HANP modified DNA had

Table 6: Binding of metabolites of $[^3H]$-1,8-DNP and $[^3H]$-1-NP to DNA in
S typhimurium TA98. The concentration of $[^3H]$-1,8-DNP 10 and
$[^3H]$-1-NP 7 was 1.5 x 10^{-5} M. For experimental details see Figure 11.
Each time point represents one experiment and standard deviation for all
values is 15%.

Incubation Time (hr)	Adducts/10^7 Nucleotides	
	1,8-DNP 10	1-NP 7
1	5.8	0.1
3	25	1.1
6	26	3.7

56

Table 7: UV-visible absorbance maxima of some disubstituted pyrenes and CT-DNA after reaction with HANPs 34,35 and 27, and estimates of *in vitro* binding. All spectra were acquired in 65/35 acetonitrile/water. CT-DNA (1 mg/mL) and HANP (0.15 mg/mL) were reacted for 15 hours in 250 mL 30/70 DMF/20 mM pH 5 citrate buffer. Results are from one experiment.

Compound	Absorbance maximum(nm)	No. Adducts/10^4 Nucleotides*
1,3-HANP 34	444	
1,6-HANP 35	457	
1,8-HANP 27	464	
1,3-HANP+DNA	453	2.3
1,6-HANP+DNA	468	4.5
1,8-HANP+DNA	474	6.5
1,3-ANP 32	466	
1,6-ANP 33	488	
1,8-ANP 22	498	

* estimated by assuming the extinction coefficient of the adduct was the same as the corresponding ANP derivative.

the shortest wavelength and 1,8-HANP modified DNA the longest wavelength. In addition, the absorbance maxima of the HANP modified DNA were closer to the analogous HANP absorbance maxima than ANP maxima. These data suggest that although the ANP moiety was present, it was bonded to an electron withdrawing portion of a nucleoside.

The extent of binding was estimated by assuming that the adduct species would have extinction coefficients similar to those of the corresponding ANP species. As will be discussed in II.3.2, this turned out to be a valid assumption. The level of binding appeared to be greatest for 1,8-HANP 27, and was approximately 4×10^3 times that observed in the in vivo studies.

The hydrolysis of modified DNA was a very important step in the isolation of DNP-nucleoside adducts. Classically, DNA was readily hydrolysed by strong base or by acids such as trifluoroacetic acid (103). Although this would have been a rapid and inexpensive procedure for the degradation of modified DNA generated in this study, it would have subjected any adduct present to extremely vigorous pH conditions. As will be shown, the adducts generated in this study were sensitive to extremes of pH.

Enzymatic hydrolysis of modified DNA is a much gentler method for DNA degradation. In the first step of the hydrolysis, DNA is cleaved into long oligomer fragments with a DNAse. The length of the fragments will depend on incubation time, the nature of DNA adducts present, and often on degree of interstrand crosslinking (104). The phosphodiester linkages are then cleaved either from the 3' or 5' end by a phosphodiesterase and the phosphates of the resulting nucleotides removed with a phosphatase.

Initial experiments used a hydrolysis procedure in which the DNA was
treated with DNAse, snake venom phosphodiesterase, and alkaline
phosphatase over a period of 3 days at neutral and basic pH. However,
this method was time consuming, and appeared to result in extensive
decomposition of modified nucleoside. As a result, the method of Martin
et al (105) was used in all subsequent hydrolyses. This method differed
in that a micrococcal nuclease P_1 and a mixture of acid and alkaline
phosphatases at neutral pH were used over a period of 18 hours.

The RPLC analysis of a typical DNA hydrolysis solution is shown in
Figure 18. Instead of the expected pattern of the four standard
2'-deoxyribonucleosides, 2'-deoxyinosine (2'-dI) 42 was detected instead
of 2'-deoxyadenosine (2'-dA) 21. The presence of 2'-dI 42 may be due to
a deaminase activity which is present in certain preparations of alkaline
phosphatase (Figure 19) (106). Subsequently, the activity of this
deaminase was greatly diminished by heat treating the phosphatase before
use.

Chromatography of the DNA hydrolysates on Biogel P-2 and Sephadex
LH-20 were evaluated as possible methods for separating the DNP-nucle-
oside adducts from the bulk of the unmodified nucleosides and
nucleotides. This separation was necessary before any spectroscopic
characterization of the adducts could take place. However, because of
concerns over adduct decomposition, and the large fraction volumes
collected, other separation techniques which involved a minimum of sample
handling were investigated. Preconcentration of adducts on C_{18} solid
phase cartridges (Waters Sep-Paks) was useful only for small volumes of
hydrolysate. A simple procedure for the concentration of the adduct from
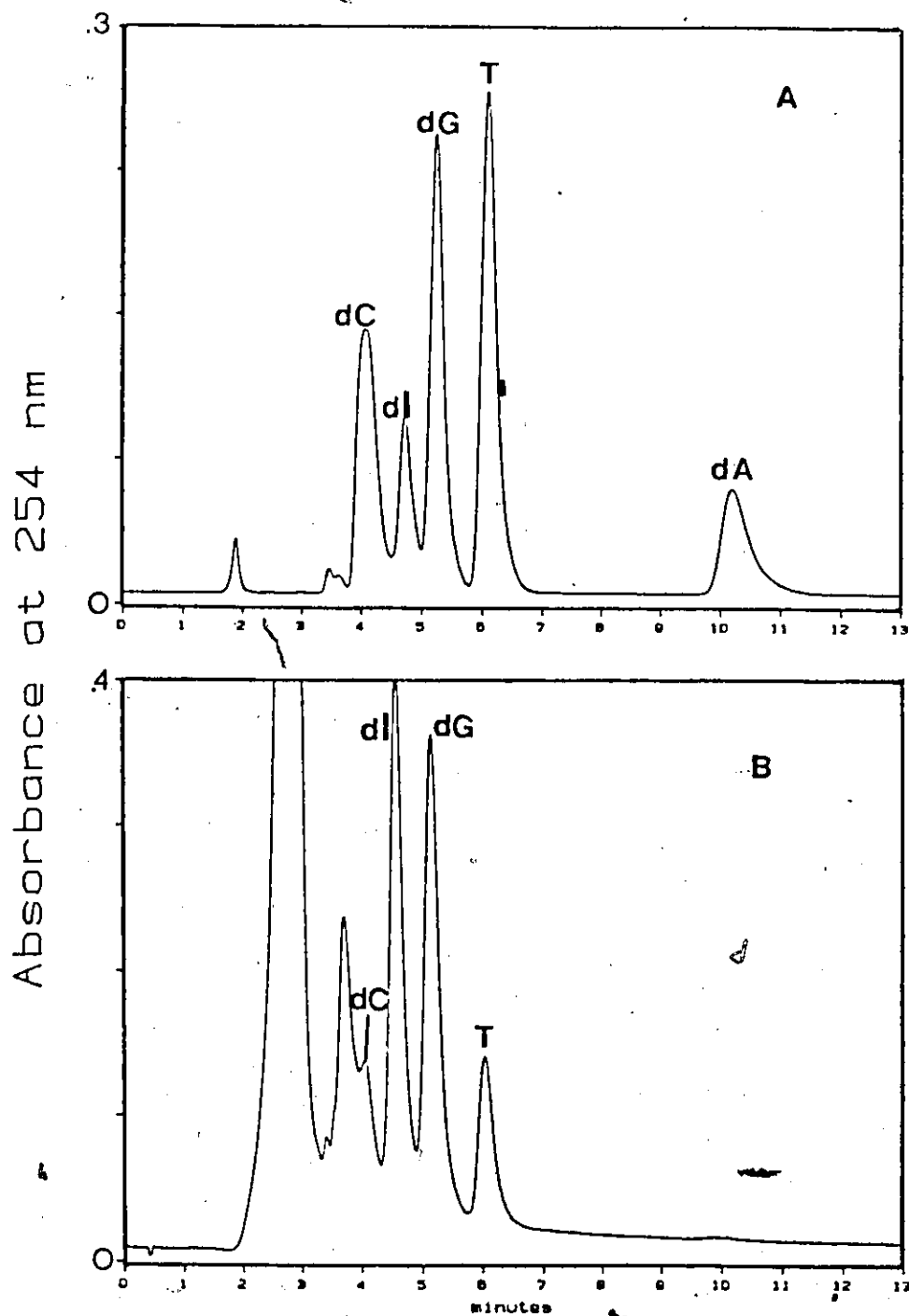
Figure 18: RPLC analyses of (a) standard 2'-deoxynucleosides and (b) DNA hydrolysate. Compounds:dG: 2'-deoxyguanosine 20, dI: 2'deoxyinosine 42, dC: 2'-deoxycytosine 43, T: thymidine 44, dA: 2'-deoxyadenosine 21. Conditions:10μm Alltech Lichrosorb RP-18, 250 x 4.6 mm, 1 mL/min, 20% methanol/water.

2'-Deoxyadenosine 21
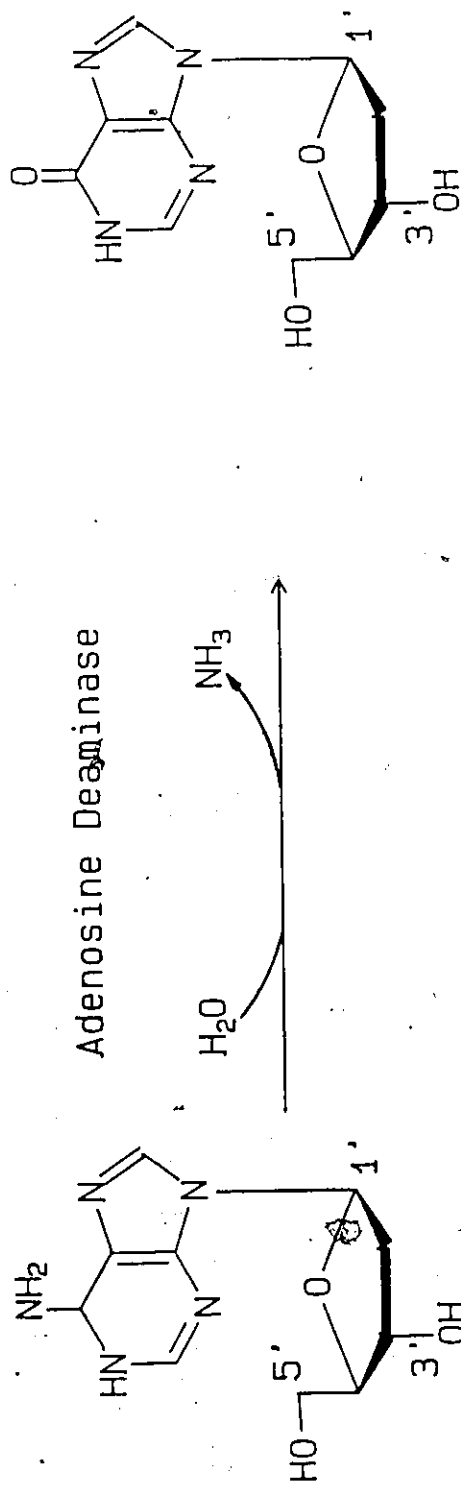
Adenosine Deaminase

2'-Deoxyinosine 42

Figure 19: Conversion of 2'-deoxyadenosine 21 to 2'-deoxyinosine 42 by adenosine deaminase.

the bulk of the unmodified nucleosides was extraction with water saturated n-butanol according to the method of Howard *et al* (50). For the DNA hydrolysates obtained from *in vivo* experiments, extraction efficiencies greater than 85% were achieved as measured by extractable radioactivity. Presumably, residual radioactivity remaining in the aqueous phase was due to partially hydrolysed DNA. Also, all material absorbing at 440 nm was extracted from DNA hydrolysates produced in *in vitro* experiments.

II.3.2   *In vivo* and *In vitro* Adduct Formation, Isolation, and
Characterization.

During the course of this work, Howard *et al.* (50) showed that the adduct formed in the bacterial metabolism of 1-NP 7 was 2'-deoxy-8-(1-pyrenylamino)-guanosine 45. Based upon this evidence, as well as the observation that DNA which had been reacted with the HANPs 34,35 and 27 was of similar colour to the analogous ANP derivatives, structures for the adducts were postulated (Figure 20).

After demonstrating that covalent binding had taken place (Section II.3.1), the second step in the characterization of the DNP-nucleosides adducts was to determine if the adducts formed *in vivo* were the same as those produced *in vitro*. Figures 21a and 21b show the RPLC chromatograms of n-butanol extracts from the hydrolysis of DNA extracted from *S. typhimurium* TA98NR which had been exposed to [^{3}H]-1,8-DNP 10, and CT-DNA which had been reacted with 1,8-HANP 27. A single major peak with retention time of 14.8 min was detected at both 254 nm and 440 nm. The 440 nm wavelength was chosen as it was expected
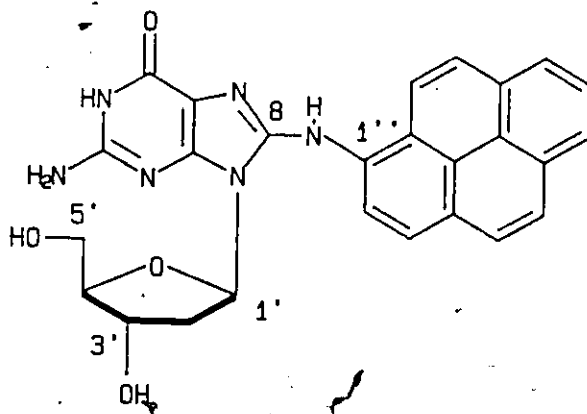
2'-deoxy-(8-pyrenylamino)-guanosine   45
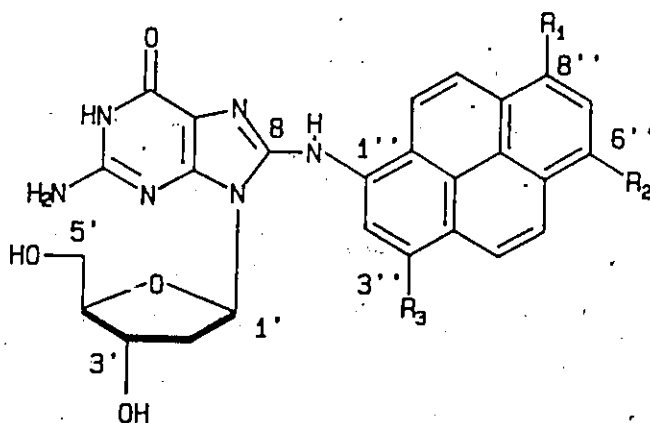
R₁	R₂	R₃	Compound Name	No.
H	H	NO₂	2'-deoxy-(3-nitro-8-pyrenylamino)-guanosine	46
H	NO₂	H	2'-deoxy-(6-nitro-8-pyrenylamino)-guanosine	47
NO₂	H	H	2'-deoxy-(8-nitro-8-pyrenylamino)-guanosine	48

Figure 20: Structures of DNA adducts formed by the reaction of DNA and (a) 1-N-hydroxylaminopyrene 37 and (b) 1,3-HANP 34, 1,6-HANP 35, and 1,8-HANP 27.

Figure 21: RPLC analyses of butanol extracts of nucleoside mixtures following extensive DNA hydrolyses. The crude *in vitro* 1,8-adduct <u>48</u> was chromatographed and eluent monitored at (a) 254 nm and (b) 440 nm. The *in vivo* adduct, derived from the incubation of [^{3}H]-1,8-DNP <u>10</u> with *S.typhimurium* TA98NR was analyzed under identical conditions and and the eluent monitored by (c) liquid scintillation counting of collected fractions. Conditions: 10μm Alltech Lichrosorb RP-18, 250 x 4.6 mm, 1 mL/min gradient elution from 50% methanol/water to 100% methanol in 20 min.
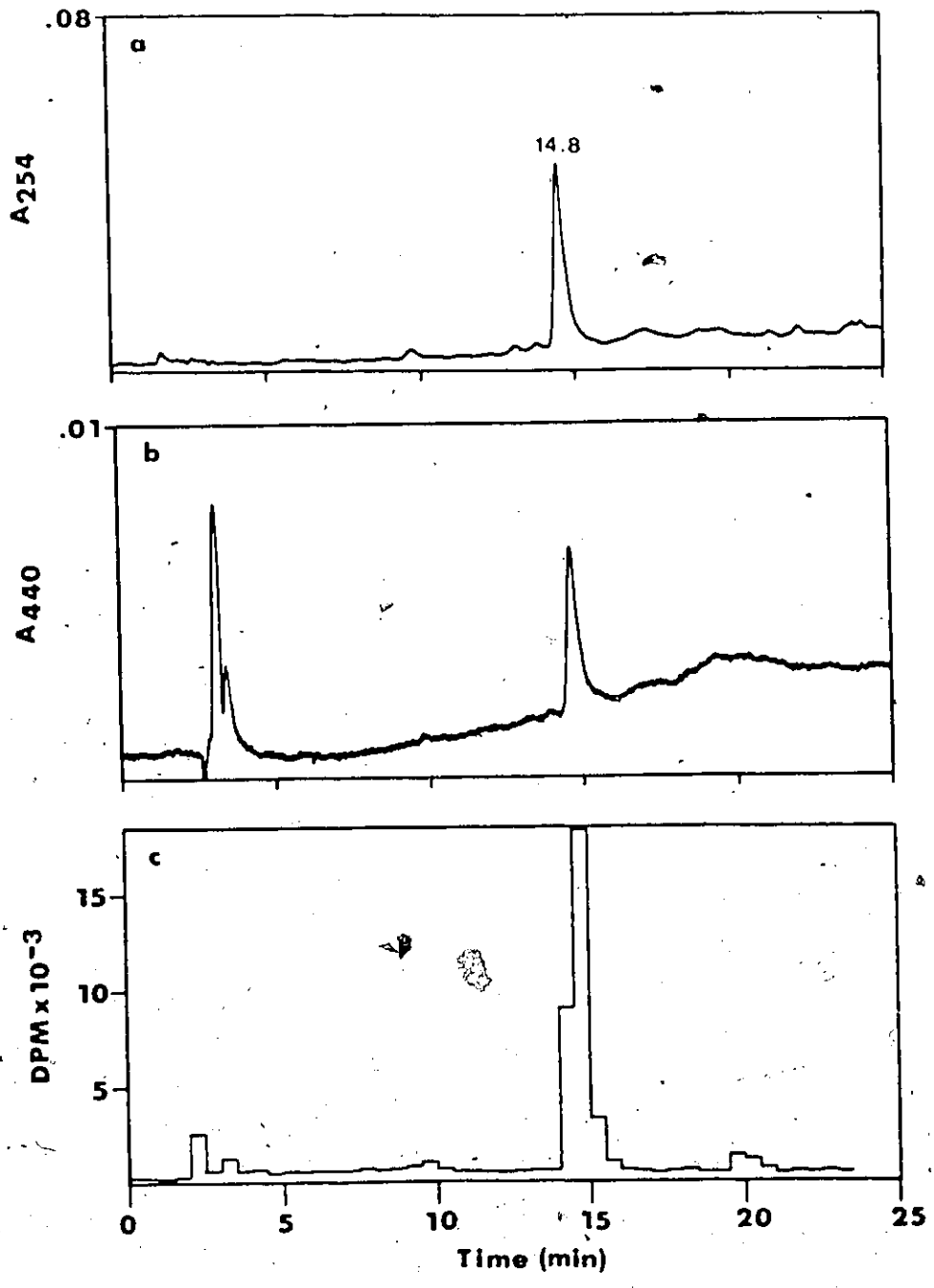
Figure 21

that only the adducts and their decomposition products would absorb at this wavelength. The major radioactive component (Figure 21c), obtained by hydrolysis of DNA isolated from *S.typhimurium* TA98NR which had been exposed to [^{3}H]-1,8-DNP 10, had a retention time identical to that of the *in vitro* material. Treatment of the RPLC purified *in vitro* or *in vivo* adduct with 0.1 N NaOH resulted in the appearance of a single new product which eluted at 9.5 min (Figure 22). On the other hand, treatment of the *in vitro* or *in vivo* compounds with 0.1 N HCl resulted in the formation of two new components, eluting at 17.7 and 19.3 min (Figure 23). The 19.3 min peak had a retention time identical to that of 1,8-ANP 22. The further characterization of these decomposition products will be discussed later.

The coincidence of RPLC retention times of compounds formed in intact bacteria, and material produced *in vitro*, together with the identical chromatographic and chemical behaviour of the breakdown products formed from these compounds, provided compelling evidence that the *in vivo* and *in vitro* adducts had the same structure. Therefore, spectroscopic characterization was carried out on the *in vitro* adducts. The amount of *in vivo* adduct produced was too small for analysis by NMR or MS.

Butanol extracts of hydrolysates from the *in vitro* reaction of HANPs and CT-DNA still contained nucleosides as well as nucleoside adducts. Therefore, before spectroscopic characterization of the adducts could be undertaken, these interferences were removed by RPLC. Initial procedures utilized isocratic semi-preparative RPLC separation of the adduct from the more polar nucleosides and enzyme debris using a
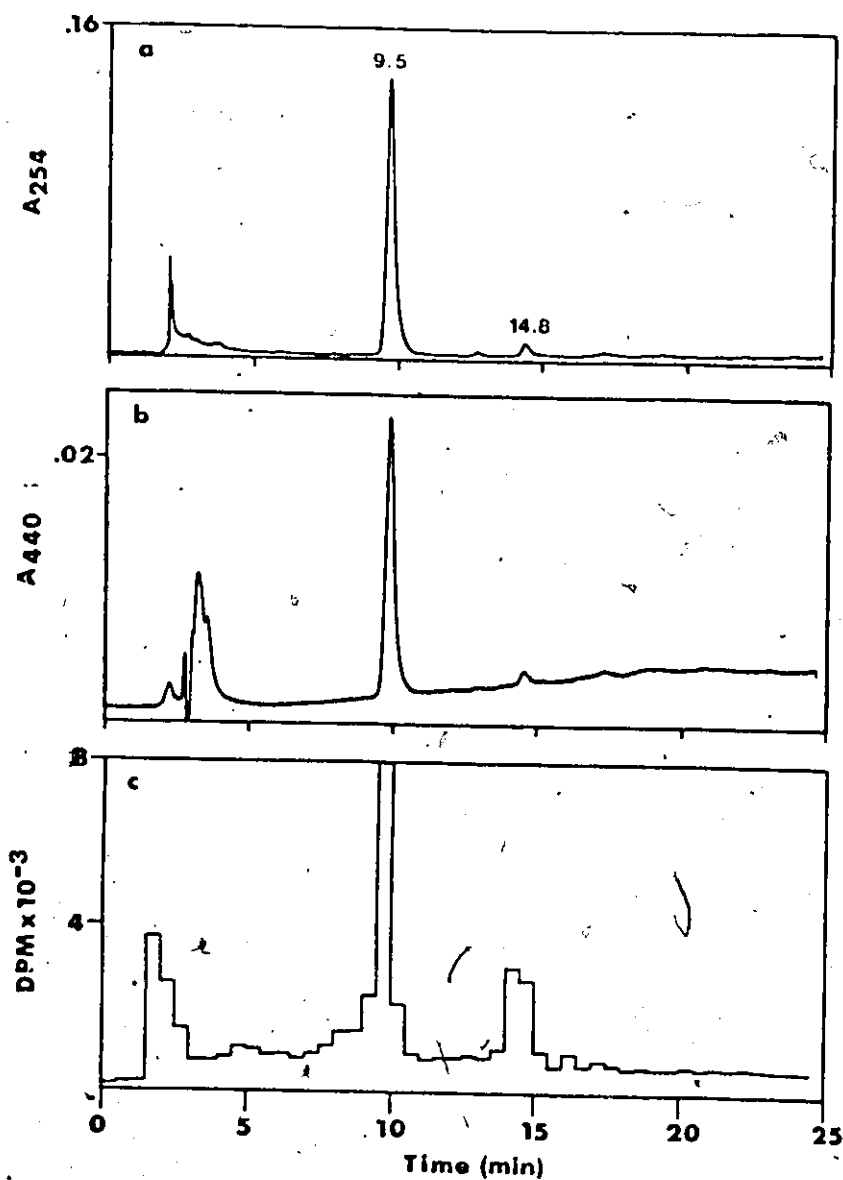
Figure 22: RPLC analyses following treatment of the purified *in vitro*
1,8-adduct <u>48</u> (a,b) and *in vivo* adduct (c) with 0.1 N NaOH for 6 h at room
temperature. Chromatographic conditions were the same as those in Figure
21.
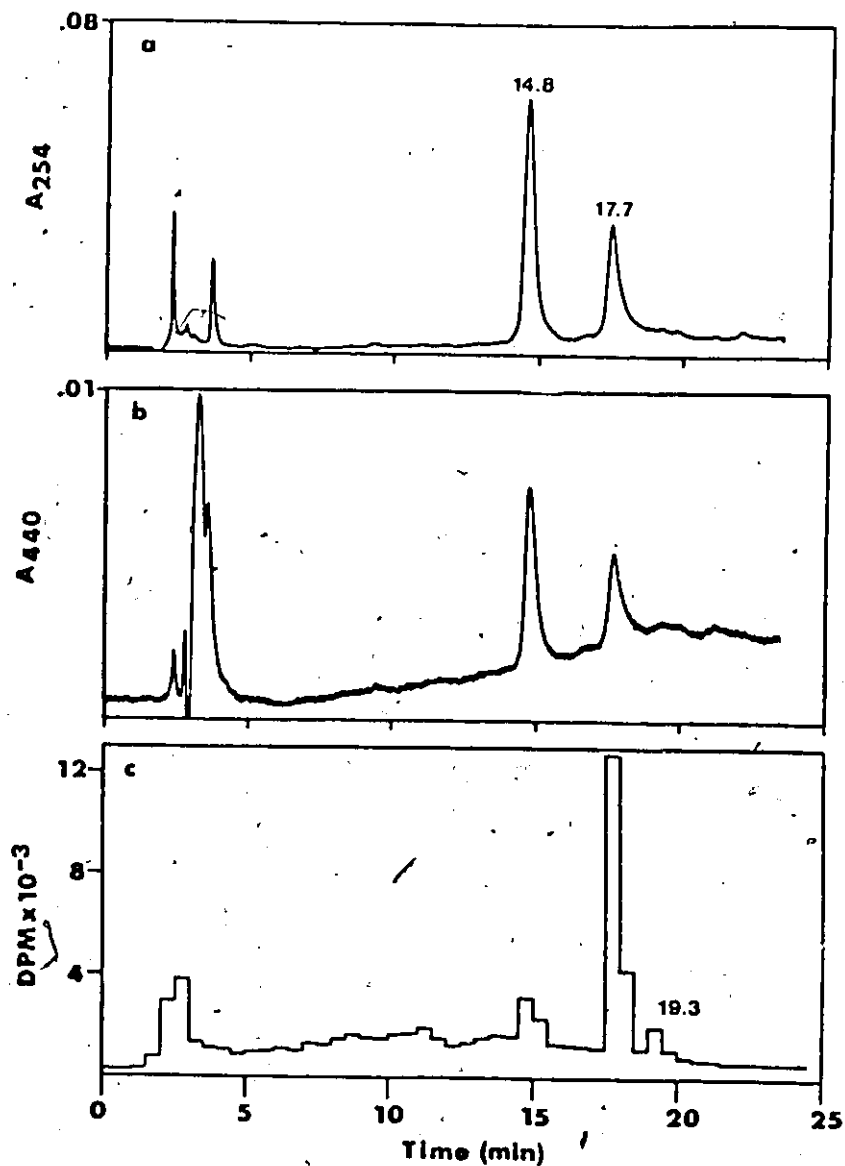
Figure 23: RPLC analyses following treatment of the purified *in vitro* 1,8-adduct <u>48</u> (a,b) and *in vivo* adduct (c) with 0.1 N HCl for 6 h at room temperature. Chromatographic conditions were the same as those in Figure 21.

methanol/water mobile phase. Although this procedure was successful it was time consuming as column loading was limited to 100-150 μl of sample. An alternate procedure was developed using column pre-concentration techniques (Figure 24). An aliquot (0.5-1.5 mL) of n-butanol was loaded on the column using 60% methanol/water as a mobile phase. After the UV signal from the nucleosides appeared and returned to baseline, the mobile phase was stepped to 100% methanol and flow rate to 10 mL/min. The adduct appeared as a sharp peak 4.2 min after appearance of the methanol solvent front. The compounds eluting at 14 minutes were nonpolar components of the incubation medium and were not other adducts. The adduct was collected and rechromatographed until pure by gradient analytical RPLC. This product was analysed by NMR and MS as described in II.3.4.

The interpretation of the results of RPLC analysis of adducts generated from the *in vitro* reaction of HANPs 34,35, and 27 and CT-DNA was greatly aided by the use of diode array detection (DAD). Not only were the individual adducts easily identified by their UV-VIS spectra but also their acid and base decomposition products. As discussed in Section II.2 the wavelengths of absorbance maxima indicated the presence of nitro functionality.

Figure 25 shows the results of RPLC analysis of an n-butanol extract containing a mixture of adducts generated by reacting a mixture of the three HANPs 34, 35, and 27 with CT-DNA. The three adduct isomers 47,48 and 46 are clearly resolved at 9.8, 10.3 and 11 minutes respectively. In order to verify the identity of each of the adduct isomers, adducts formed by reaction of each of the HANP isomers and CT-DNA were analysed
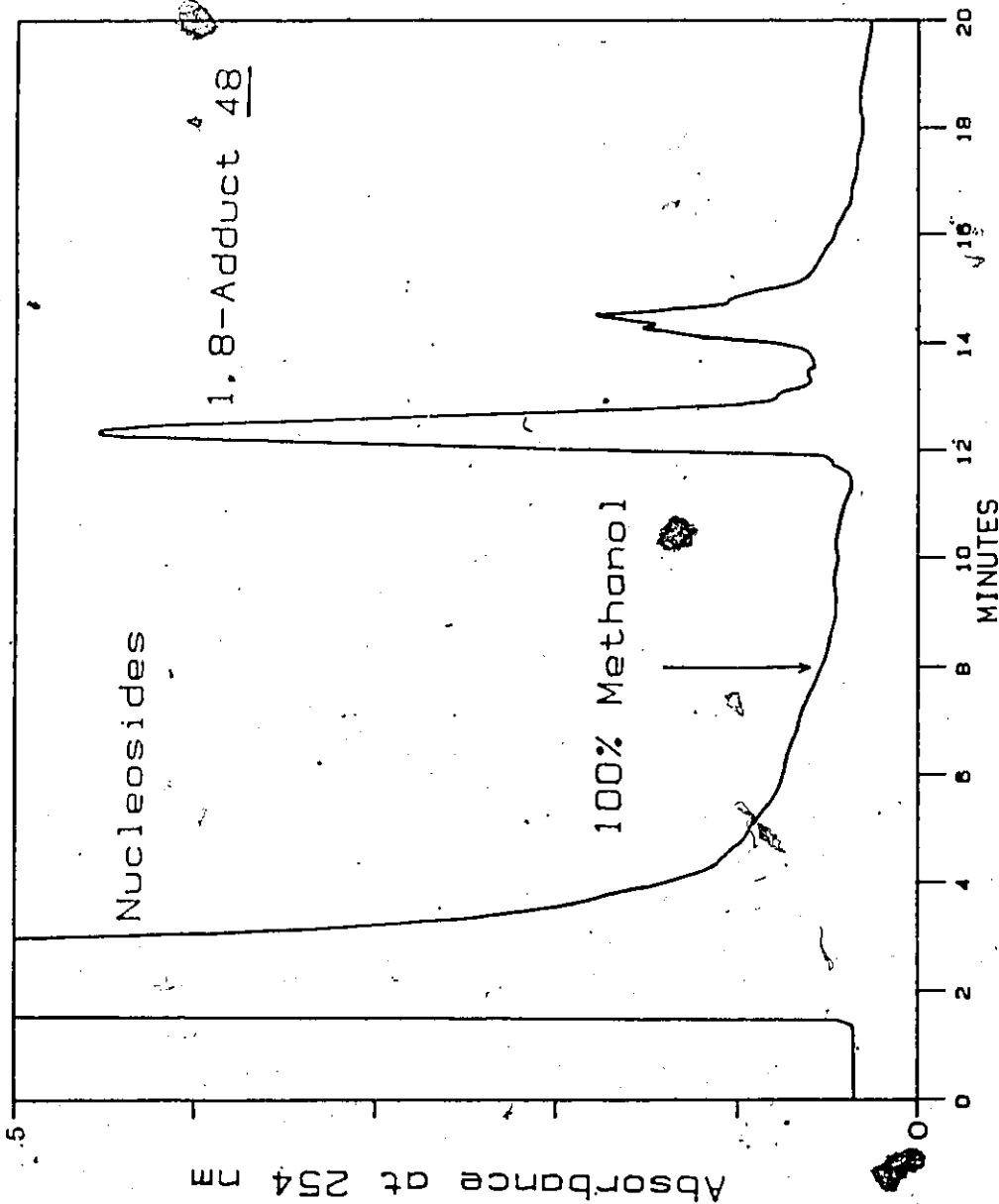
Figure 24: Semi-preparative RPLC of an n-butanol extract of CT-DNA hydrolysate. The DNA had been reacted with 1,8-HANP 27. Conditions: 10μm : Whatman ODS-2, 50cmX9.4mm, 60% methanol/water at 4 mL/min for 8 min, then stepped to 100% methanol at 30 mL/min.
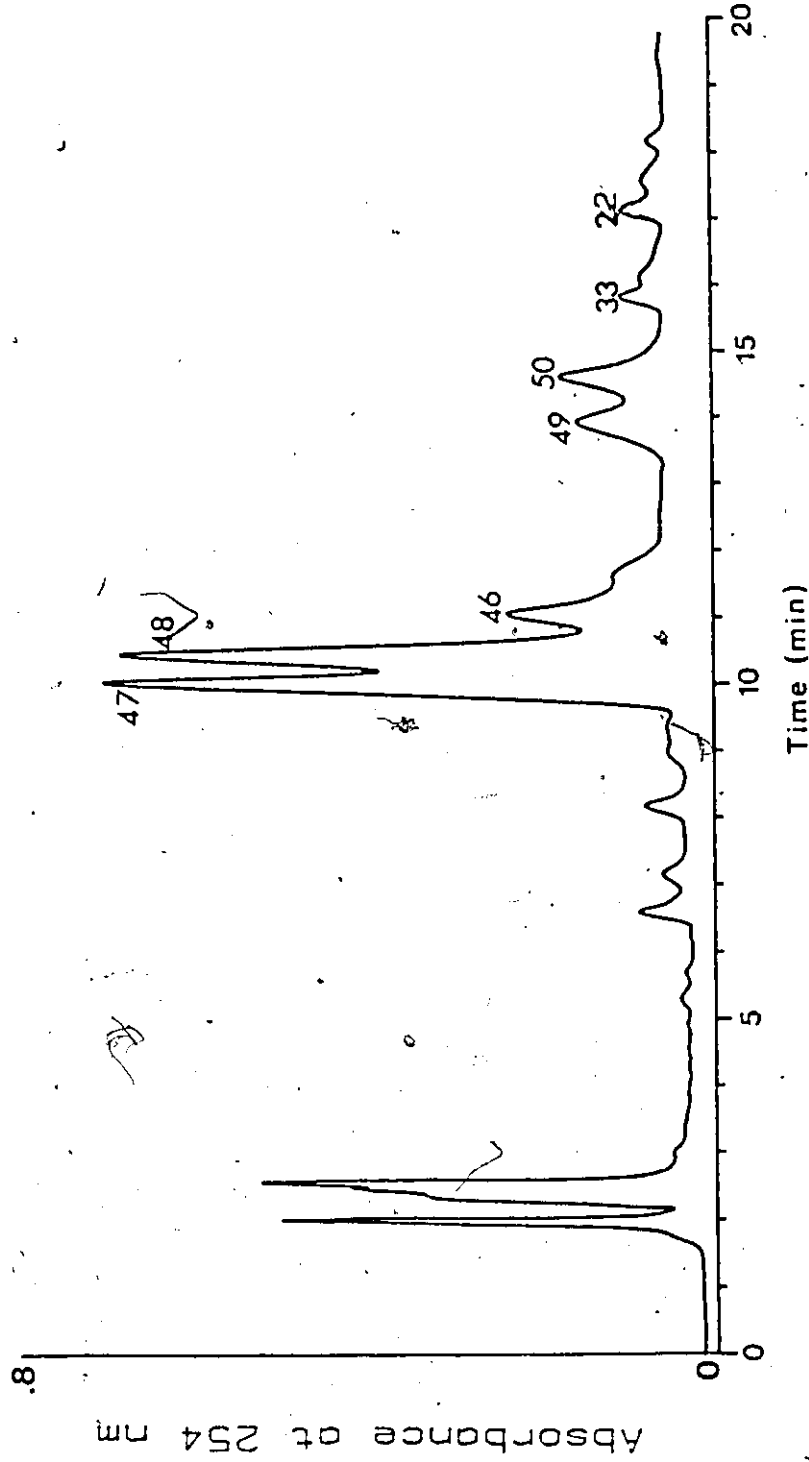
Figure 25: RPLC analysis of an n-butanol extract of CT-DNA hydrolysate. The CT DNA had been reacted with a mixture of 1,3-HANP 34, 1,6-HANP 35, and 1,8-HANP 27. Compounds: 1,6-adduct 47, 1,8-adduct 48, 1,3-adduct 46, 1,6-adduct acid decomposition product 49, 1,8-adduct acid decomposition product 50, 1,6-ANP 33, 1,8-ANP 22. Conditions: 5μm Altex ODS-3, 60% methanol/water gradient to 100% methanol in 30 min.

individually by RPLC. Acid decomposition products 49 and 50, eluted at 13.6 min and 14.6 min respectively and had UV-VIS spectra similar to the parent adduct. 1,6-ANP 33, and 1,8-ANP 22 eluted at 15.7 and 17.2 minutes. The 1,3 acid decomposition product and 1,3 ANP-32 were not observed as they were probably below the detection level.

The UV-VIS spectra of the adducts and their corresponding ANP isomers are shown in Figure 26. The UV-VIS spectra of the adducts were all shifted to shorter wavelength relative to the absorbance maxima of the corresponding ANP isomer, illustrating the electron withdrawing effect of the purine nucleus on the aminonitropyrene system. The relative position of the absorbance maxima for each of the adducts was also found to be the same as in the ANPs, i.e., 1,8- maxima farthest in the red, then 1,6-, and 1,3- isomer farthest in the blue.

The fluorescence emission spectra of the 1,8-adduct 48 before and after reduction with sodium borohydride are shown in Figure 27, together with 1,8-DAP 23 for comparison. While the adduct was only weakly fluorescent, reduction of the adduct with sodium borohydride rapidly generated a 3000-fold increase in fluorescence. In addition, the fluorescence emission spectra of the "reduced adduct" 51 and 1,8-DAP 23 were identical, indicating that the reduced adduct contained a 1,8-DAP moiety.

The acid and base decomposition products of aromatic amine-nucleoside adducts have been well characterized (50,107,108). Kriek and co-workers have shown that treatment of C-8 substituted 2'-dG adducts with alkali resulted in opening of the imidazole ring to the
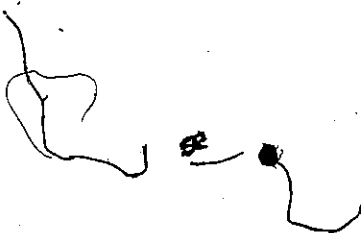
Figure 26: UV-visible spectra of (a) 1,8-ANP $\underline{22}$ and 1,8-adduct $\underline{48}$,
(b) 1,6-ANP $\underline{33}$ and 1,6-adduct $\underline{47}$ and (c) 1,3-ANP $\underline{32}$ and 1,3-adduct $\underline{46}$.
Spectra were acquired during RPLC analysis by DAD using a
water/methanol gradient. Spectral acquisition conditions: range, 200
to 600 nm, in increments of 4 nm.
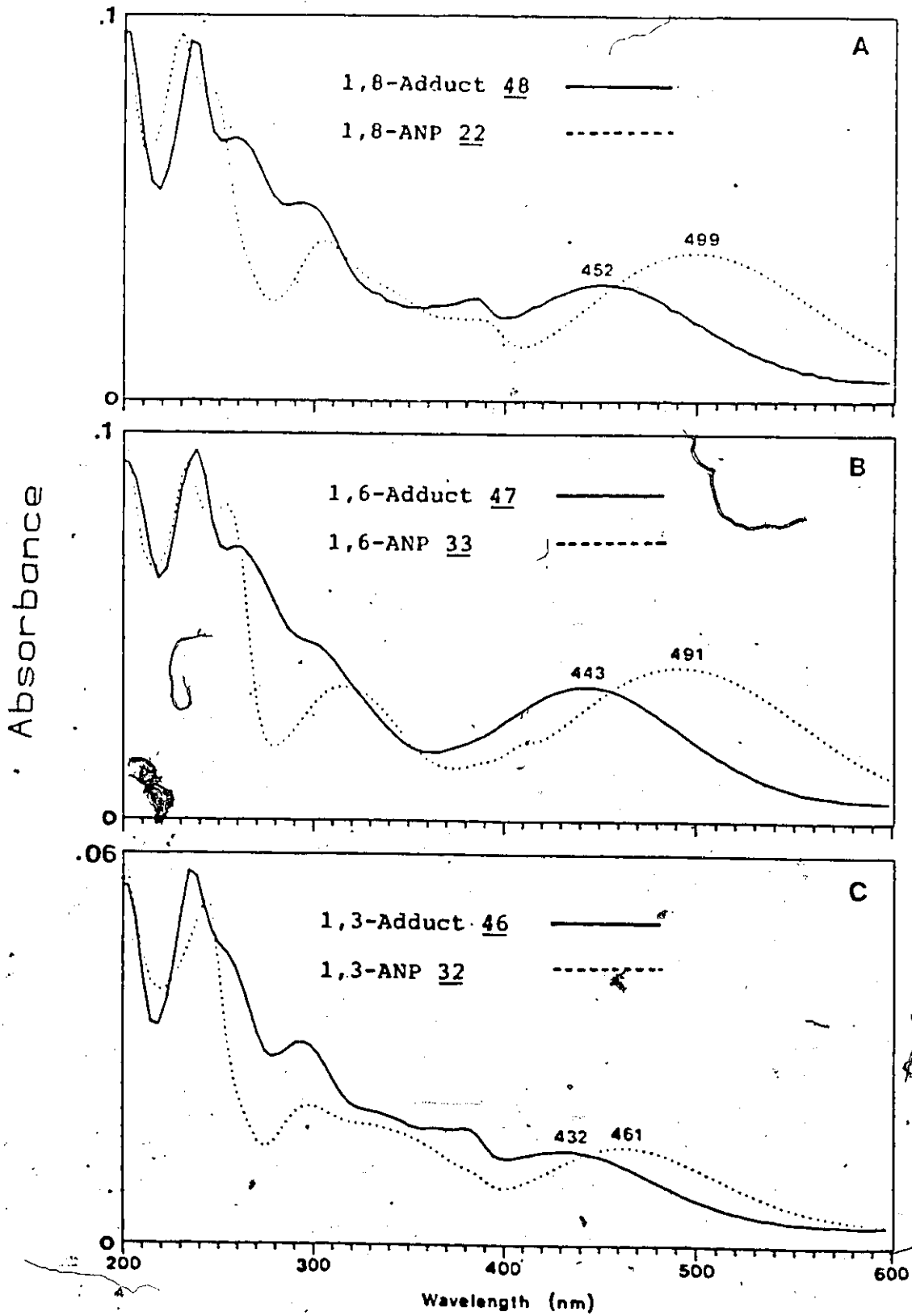
Figure 26
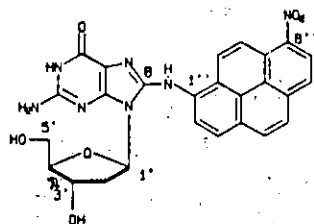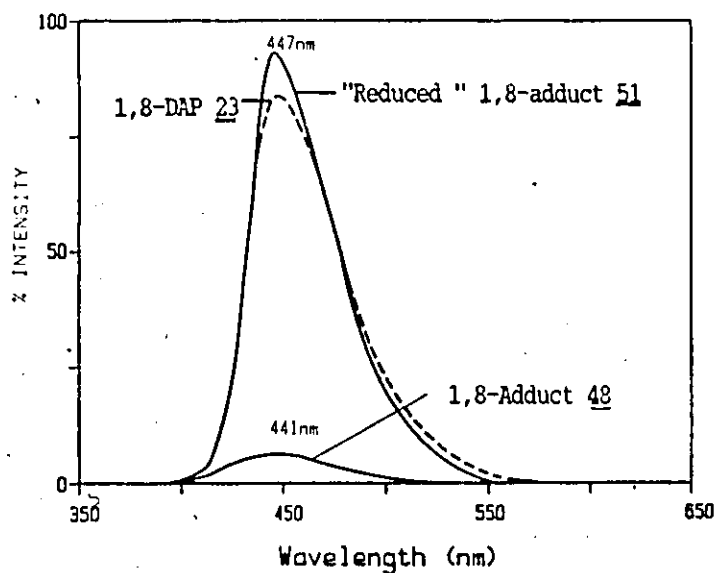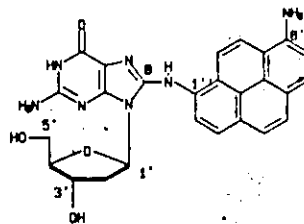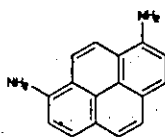
Figure 27: The fluorescence emission spectra of the 1,8-adduct 48, the NaBH$_4$ reduction product of this adduct, 51 (after a 200-fold dilution), and 1,8-DAP 23. Excitation was at 254 nm.

amide (107). In addition, Kriek and co-workers also showed that reaction of these C-8 substituted 2'-dG compounds with acid resulted in loss of 2'-deoxyribose.

The UV-VIS spectra and structure of the 1,6-adduct 47, its proposed base decomposition product 52, and a model compound, 1-N-acetylamino-6-nitropyrene (1,6-NANP) 53, are shown in Figure 28. The postulated structure of the base decomposition product was based upon the work by Kriek et al (107). The absorbance maximum of the proposed ring opened base decomposition product was shifted to shorter wavelength due to the electron withdrawing effect of the amide group. As expected, the spectrum of this base decomposition product 52 was similar to that of 1,6-NANP 53.

The UV-VIS spectra of the acid decomposition product of the 1,6-adduct 49 and 1,6-adduct 47 were almost identical, as loss of the deoxyribose had little effect on the electron density of the base and ANP moiety (data not shown). As will be discussed in II.3.5, field desorption MS confirmed the identity of the acid decomposition product as the deribosylated compound (Figure 29).

The chromatographic behavior of these decomposition products agrees with the postulated structures. Due to the loss of the sugar, the acid decomposition product would be less polar and should therefore elute after the adduct during RPLC, while the base decomposition product would be much more polar and elute before the parent adduct. This chromatographic behaviour is observed for the adducts generated in vivo (Figures 22,23) and in vitro (Figure 25).
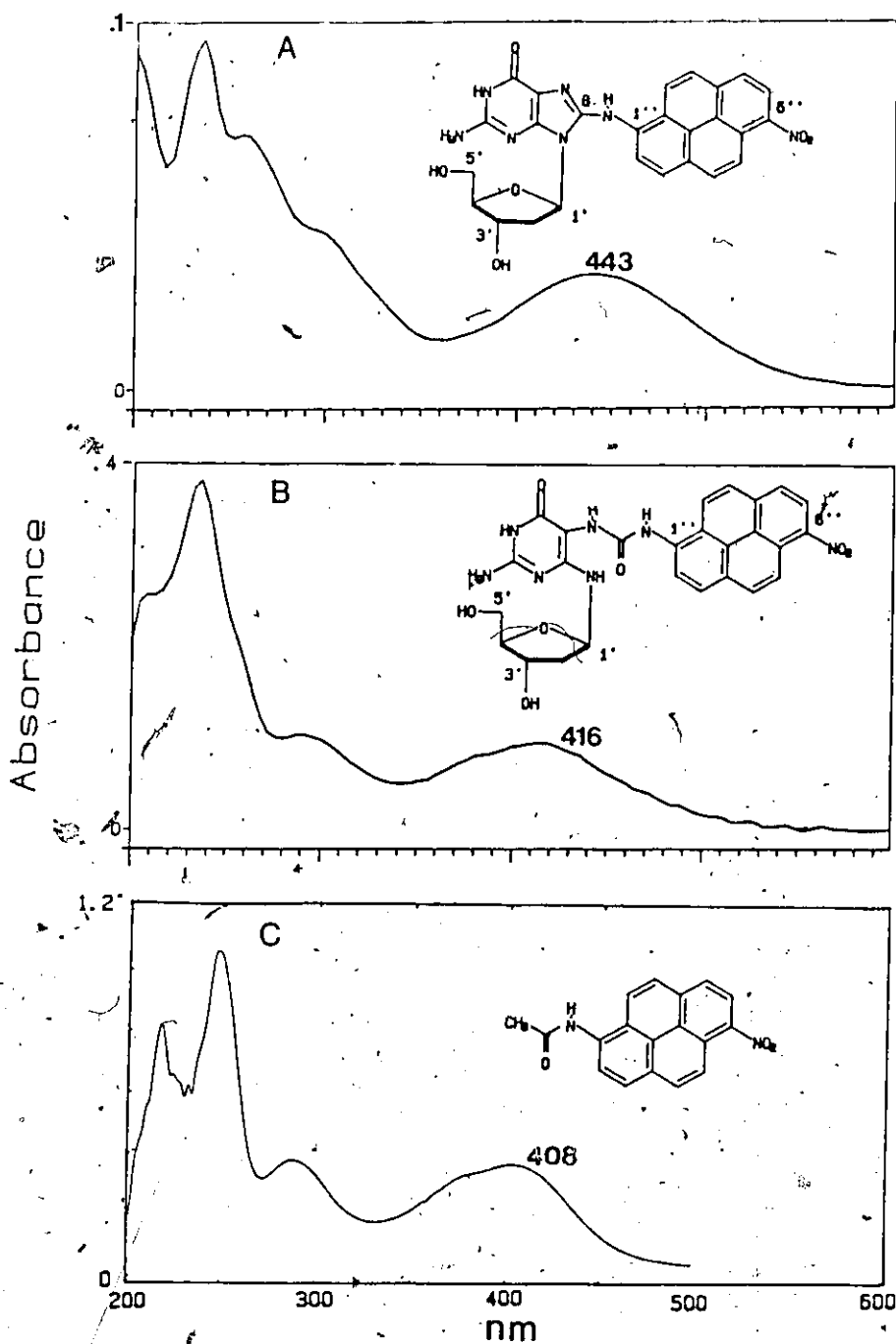
Figure 28: UV-visible spectra of (a) 1,6-adduct 46 (b) 1,6-adduct base decomposition product 52 and (c) 1-N-acetylamino-6-nitropyrene 53. Spectral acquisition conditions were described in Figure 26.
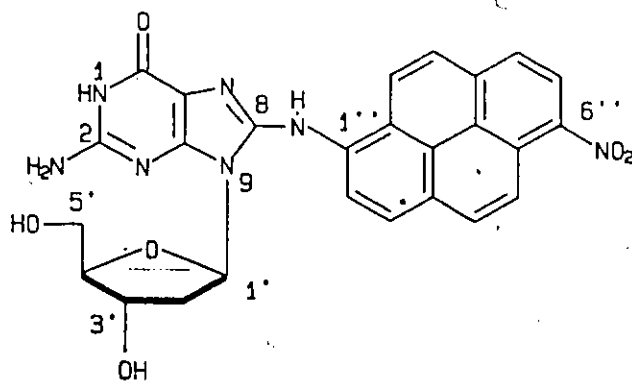
1,6-Adduct 47
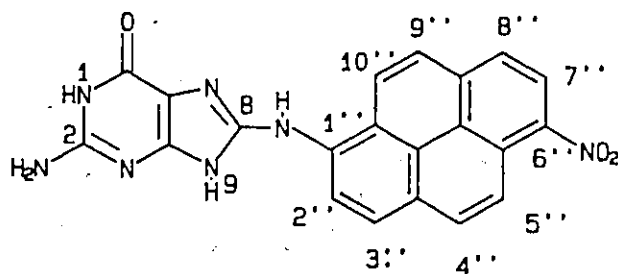
1,6-Adduct acid decomposition product 49

Figure 29: Structure of (a) the 1,6-adduct 47 and (b) the proposed structure of its acid decomposition product 49.

II.3.3 NMR Studies

The 500 MHz and 250 MHz spectral data of the *in vitro* 1,8 adduct 48, and 1,8-ANP 22, are summarized in Table 8. The numbering scheme for these compounds is shown in Figure 30. In the NMR of both the 1,8-adduct 48 and 1,6-adduct 47, most of the signals from the 2'-deoxyribose protons were obscured by interfering signals and therefore are not shown. The origin of these interferences, which appear to be aliphatic in nature, was probably from column packing degeneration during the RPLC cleanup of these samples.

The proton NMR spectra of the 1,8-adduct 42, 1,8-ANP 22, and 2'-dG 20 at 250 mHz are shown in Figure 30. In DMSO-d_6, the spectrum of the 1,8-adduct 48 (Figure 30a) showed 3 broad singlets whose signal disappeared when the spectrum was acquired in methanol-d_4. These exchangeable protons were assigned as the N-1-H amide proton at 10.35 ppm, the bridging $N^{1''}$-H proton at 9.35 and the two exocyclic amino N^2-H_2 protons at 6.45 ppm. The signal at 7.07 ppm (Figure 31a) may be due to an impurity or acid decomposition of the adduct during spectrum acquisition. The signal of the bridging $N^{1''}$-H proton appeared at 9.35 ppm and integrated to one proton, (Figure 30a), while the amino protons of 1,8-ANP 22 appeared at 7.2 ppm and integrated to two protons (Figure 30b). The C-8 proton of 2'-dG 21 (Figure 30c) normally present at 7.93 ppm, was absent in the spectrum of the 1,8-adduct 48. Also, the aromatic protons of the ANP nucleus of the adduct appeared between 8 and 9 ppm while those of 1,8-ANP 24 appeared between 7.5 and 8.8 ppm. This downfield shift is analogous to the hypsochromic shift observed in the

Table 8: Proton NMR data for 1,8-ANP 22 and the *in vitro* 1,8-adduct 48 isolated from hydrolysate of DNA reacted with 1,8-HANP 27. See Figure 30 for numbering.

1-Amino-8-nitropyrene 22				1,8-Adduct 48			
Assig.[a]	Mult.	δ	J_{HH}	Assig.	Mult.	δ	J_{HH}
NH_2	s	7.14		N^2-H_2	s	6.58	
2	d	7.52	8.70	5"[b]	d	8.26	9.08
5[b]	d	7.92	8.73	3"	d	8.30	8.48
6	d	8.10	8.56	6"	d	8.41	9.01
4[b]	d	8.22	8.73	4"[b]	d	8.45	9.08
3	d	8.26	8.70	2"	d	8.52	8.48
7	d	8.65	8.56	10"	d	8.68	9.81
9,10	d	8.74		7"	d	8.78	9.01
				9"	d	8.82	9.81
				$N^{1"}$-H	s	9.35	
				N-1-H	s	10.65	

[a] Assig.-assignment

Mult.-multiplicity: s, singlet; d, doublet

δ -chemical shift in ppm relative to TMS internal standard

J_{HH}-$^3J_{HH}$ in Hz .

[b] Assignments may be reversed
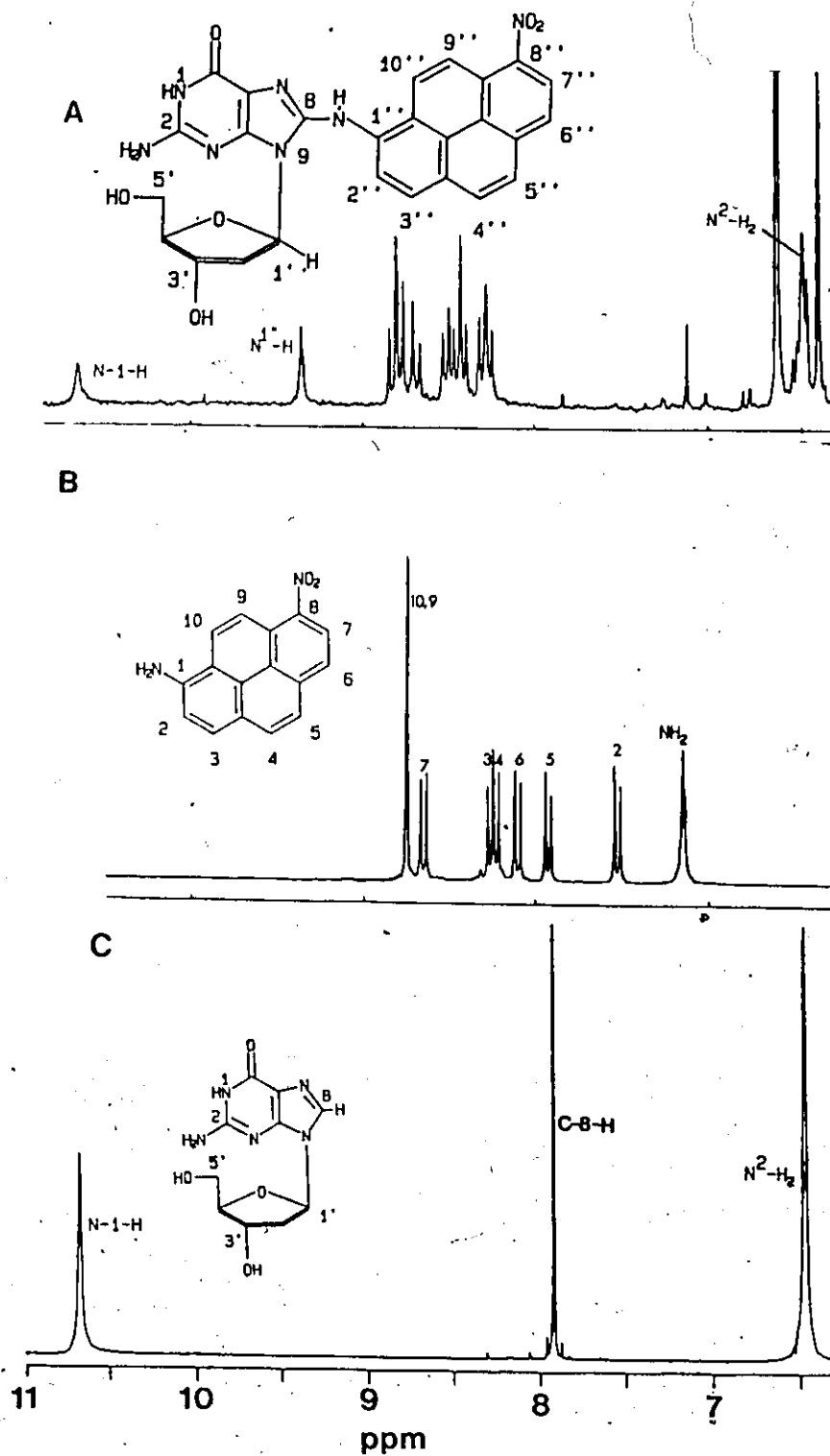
Figure 30: Proton NMR spectra of (a) 1,8-adduct 48 (b) 1,8-ANP 22 and (c) 2'-dG 20. All spectra were acquired at room temperature in DMSO-d$_6$ at 250 MHz. Concentrations:1,8-adduct:32μm, 1,8-ANP:6 mg/mL, and 2'-dG:15 mg/mL.

UV-VIS spectra of the adduct (Figure 26). All these observations indicated that the 1,8-ANP moiety of the adduct 48 was bonded through its amino group to C-8 of 2'-dG 21.

Assignment of protons of the 1,8-adduct 48 in the region from 8.0 ppm to 9.0 ppm was based on work by Kaplan et al. (100). During NMR studies of the DNPs 8-10, he observed that the coupling constants of proton pairs 5,4 and 9,10 were larger than the other protons in 1,3-DNP 8 and 1,6-DNP 9 (Figure 31). Also, the protons ortho and peri to the nitro group in these compounds were shifted the farthest downfield.

The 500 MHz spectrum of the 1,8 adduct 48 showed 8 aromatic protons of the ANP nucleus as AB doublets between 8.0 and 9.0 ppm (Figure 32). Based on the above discussion, the doublets farthest downfield were assigned to the 9" and 7" protons respectively, 9" assigned to the doublet further downfield because of its larger coupling constant. By comparing coupling constants, these doublets were determined to be coupled to protons 10" and 6" at 8.68 and 8.41 ppm respectively. The remaining protons were assigned based on the magnitude of their coupling constants. The doublets with the larger coupling constants at 8.45 and 8.26 ppm were 4" and 5" and the remaining protons are 2" and 3" at 8.52 and 8.30 ppm.

Proton chemical shift data for 1,6-ANP 33 and the 1,6-adduct 47 are listed in Table 9. and their proton NMR spectra are shown in Figure 33. Again, the downfield shift of the $N^{1"}$-H and aromatic pyrene protons, and lack of 2'-dG C-8 proton was observed. Unlike the 1,8-adduct 48 spectrum, the two exocyclic N^2-H protons and the 2'-deoxyribose 1'-H proton are now well resolved. The 500 MHz spectra of the aromatic region
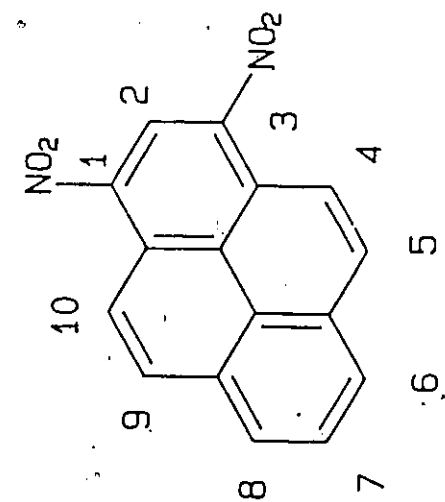
1,6-DNP **9**
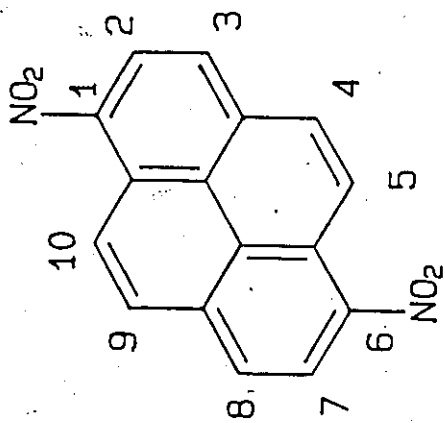
1,3- DNP **8**

Figure 31: Structures of 1,6-DNP **9** and 1,3-DNP **8**.
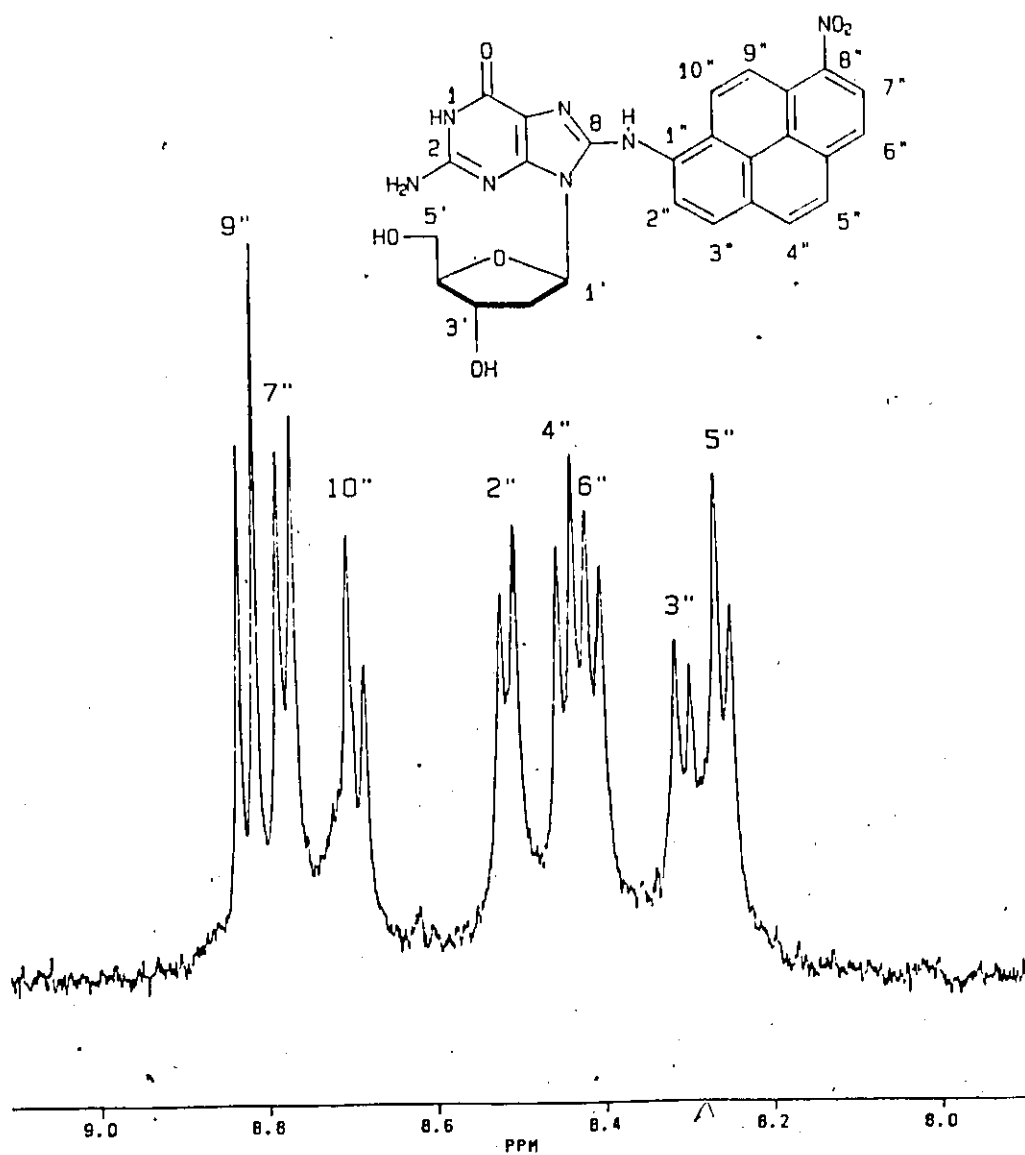
Figure 32: Proton NMR spectrum of 1,8-adduct 48 between 8.0 ppm and 9.0. ppm. Spectral acquisition conditions were described in Figure 30.

Table 9: Proton NMR data for 1,6-ANP 33, and the *in vitro* 1,6-adduct 47 isolated from hydrolysate of DNA reacted with 1,6-HANP 35. See Figure 33 for numbering.

1-Amino-6-nitropyrene 33				1,6-Adduct 47			
Assig.[a]	Mult.	δ	J_{HH}	Assig.	Mult.	δ	J_{HH}
NH_2	s	7.10		N^2-H_2	s	6.41	
2	d	7.46	8.54	3"	d	8.27	8.42
8	d	8.04	8.47	4"[b]	d	8.34	9.35
4[b]	d	8.05	8.37	8"	d	8.41	8.57
3	d	8.18	8.54	2"	d	8.45	8.42
9	d	8.25	9.06	9"	d	8.52	9.44
10	d	8.51	9.06	10"	d	8.61	9.44
5[b]	d	8.60	9.37	5"[b]	d	8.71	9.35
7	d	8.62	8.47	7"	d	8.77	8.57
				$N^{1"}$-H	s	9.32	
				N-1-H	s	10.63	

[a]Assig.—assignment

Mult.—multiplicity: s, singlet; d, doublet

δ —chemical shift in ppm relative to TMS internal standard

J_{HH}—$^3J_{HH}$ in Hz

[b]Assignments may be reversed
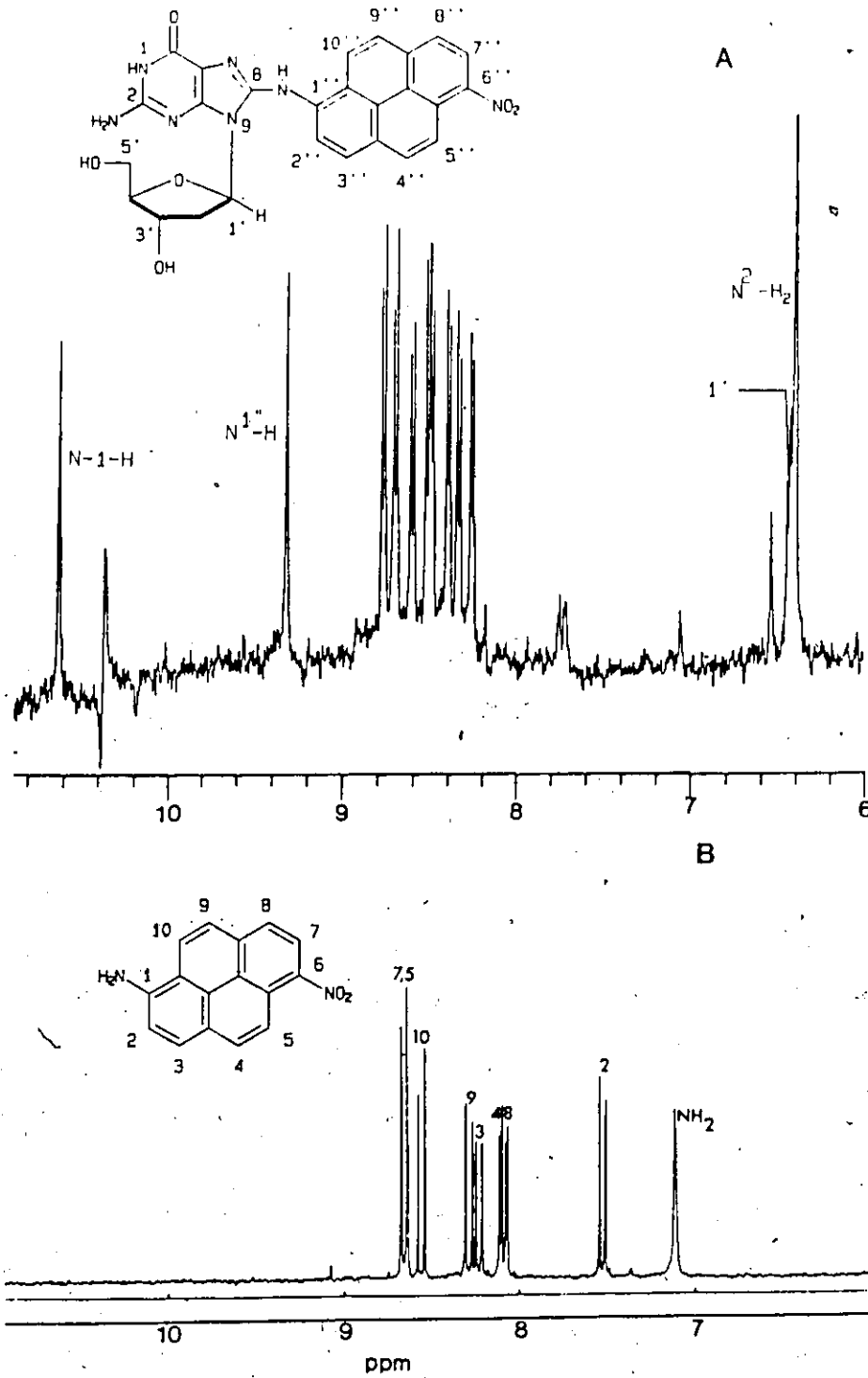
Figure 33: Proton NMR spectra of (a) 1,6-adduct <u>47</u> at 500 MHz and (b) 1,6-ANP <u>33</u> at 250 MHz. Spectra were acquired at room temperature in DMSO-d$_6$, at concentrations of 9μM and 5 mg/mL respectively.

between 8.0 and 9.0 ppm is shown in Figure 34. Chemical shifts were assigned as discussed for the 1,8-adduct 48. Examination of this region however, revealed another set of less intense signals at slightly higher field. These signals may be due to the deribosylated acid decomposition product which may have been produced during the spectrum acquisition. This derivative, which would now have a proton at position 9, may account for signal at 6.58 ppm, slightly downfield of the N^2-H_2 protons (Figure 33).

As can be seen in Figures 33 and 34, the peak widths of NMR signals from the adducts were very concentration dependent. The NMR spectrum of the 1,8-adduct 48 was acquired at a concentration of $32\mu M$, which was approximately 4 times that of the 1,6-adduct 47. Above concentrations of $60\mu M$, the peak widths quickly broadened and soon were indistinguishable from background. Because of this, repeated dilution and long acquisition times were required to obtain signals with narrow peak widths. An explanation may be that the adduct molecules stack in solution and tumble more slowly in solution causing a decrease in spin relaxation time. Therefore, the peak width becomes wider because it is inversely proportional to relaxation time. The effect of stacking on the UV-VIS and fluorescence spectra was also described in Section II.2. The 1,3-adduct 46 appeared to be especially susceptible to this phenomena as no spectra could be obtained even upon repeated dilution.
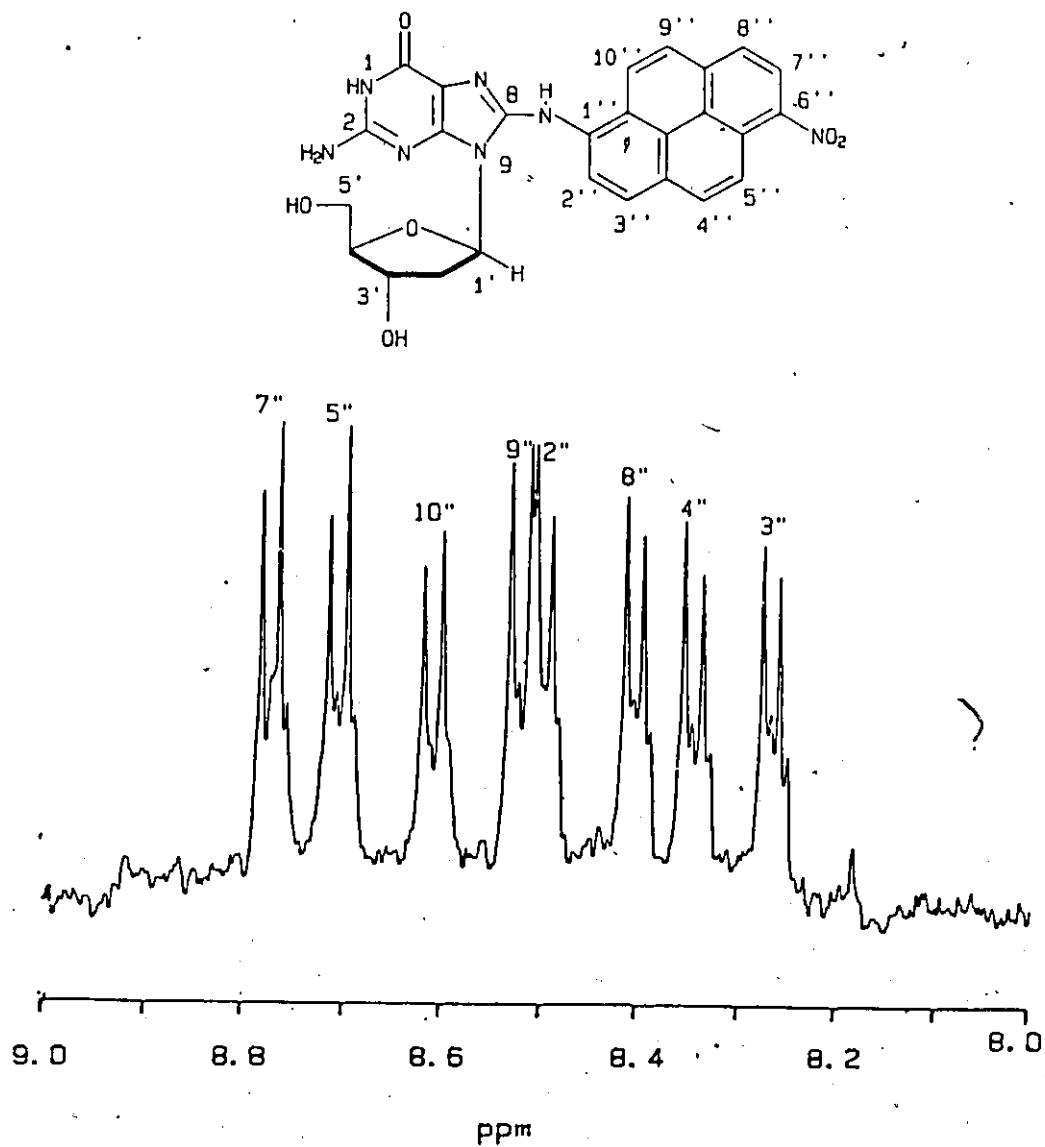
Figure 34: Proton NMR spectrum of 1,6-adduct 47 between 8.0 ppm and 9.0 ppm. Spectral acquisition conditions were described in Figure 31.

II.3.4 Mass Spectrometry Studies of DNP-Nucleoside Adducts

This section describes the MS characterization of the adducts 46-48

using "soft" ionization techniques and direct electron ionization with

chemical derivatization. These techniques are summarized in Table 10. MS

conditions were optimized using 2'-dG 20, 1,6-ANP 33, 1,8-ANP 22, or a

mixture of the three adducts 46-48 as test compounds. MS analyses by FD

and LC-FABMS were carried out by Dr. M. Quilliam, McMaster University.

II.3.4.1 Ionization of Underivatized Adducts on Extended Probes and by

LC-MS.

Volatilization from extended solids probe tips is a simple

technique for the EI and CI ionization of non-volatile compounds

(76,78,80,109,). Volatilization and ionization from conventional and

extended probes is illustrated in Figure 35. Compounds undergo a process

of volatilization and condensation in the sample delivery capillary of a

conventional probe. It is during this distillation that thermal

degradation occurs. However, by coating compounds on an extended probe

tip, less pyrolysis of the sample occurs. This extended probe tip can be

inserted directly into the heated source, close to the electron beam.

This technique is also termed "in-beam" ionization because of the

proximity of the probe tip to the electron beam.

Many attempts were made to obtain spectra by EI or ammonia CI using

probes constructed of SE-30 coated silica, silylated silica glass,

Vespel, Teflon, and polyimide coated fused silica. These inert materials

were selected to reduce possible catalytic decomposition reactions, and

adsorption processes. Despite all efforts at optimizing conditions for

Table 10: A summary of techniques used for the MS analyses of
adducts <u>46-48</u>

(A) PROBE METHODS: UNDERIVATIZED ADDUCTS

(a) "In Beam" Ionization:

(i)   Extended solids probes (Vespel, Silica, Teflon)
(ii) Desorption Chemical Ionization (DCI)
(iii) Desorption Electron Ionization (DEI)

(b) Fast Atom Bombardment (FAB)

(c) Field Desorption (FD)

(B) COUPLED LIQUID CHROMATOGRAPHY-MASS SPECTROMETRY (LC-MS)

(a) LC-CIMS

(b) LC-FABMS

(C) PROBE METHODS ON DERIVATIZED ADDUCTS

(a) DEI

(b) DCI
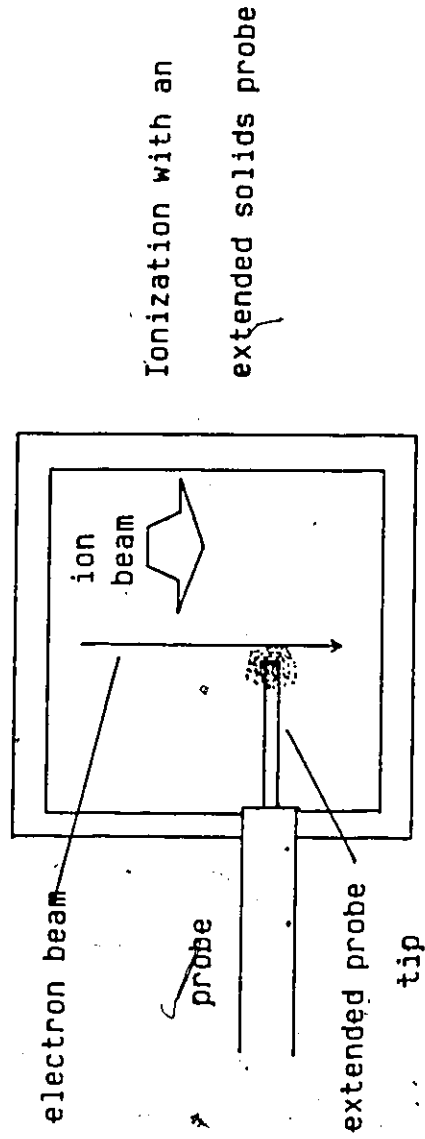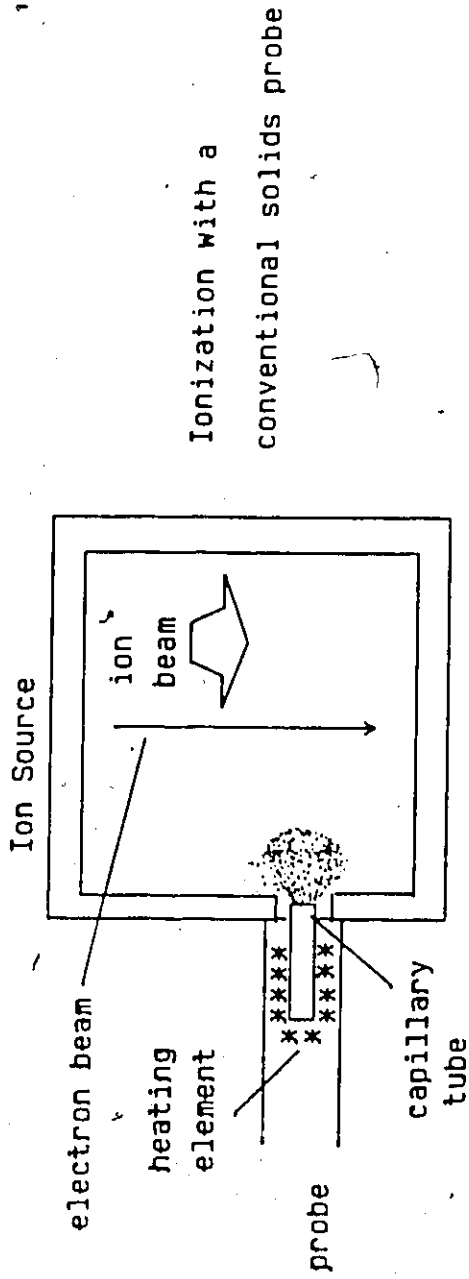
Figure 35: Volatilization from a conventional solids probe and an extended solids probe.

ionization, only weak EI spectra of 2'-dG 20, and no spectra of the

1,8-adduct 48 were obtained. Although these results imply that the

volatility of the adduct was too low at the source temperatures used,

other factors may play a role. Hanson and co-workers showed that the

intensity of $[M]^{+}$ and total ion current (TIC) is very dependent on the

distance between the end of probe tip and the electron beam axis (109).

Because of the design of the vacuum lock system on the VG 7070F mass

spectrometer on which these analyses were carried out, it was difficult

to determine if the probe tip was close enough to the electron beam.

Other "in-beam" ionization methods were investigated using a probe

designed for use in a VG ZAB-E mass spectrometer delivered near the end

of this study. This probe was constructed of a platinum filament

suspended between two metal posts fitted in an insulating ceramic tip.

The filament, which was connected to a variable power supply through

contacts in the source block, could be heated at a controlled rate. The

filament of this probe extended well into the the source approximately

2mm from the electron beam (Figure 36).

In a typical experiment, sample was loaded onto the filament which

was heated rapidly leading to desorption and ionization of the compound.

When used in the CI mode this process is termed desorption chemical

ionization (DCI). When ionization takes place under EI conditions, the

term desorption electron ionization (DEI) is used. The difference

between this technique and the other "in-beam" technique discussed

previously, is that volalization occurs in a more rapid and controlled

fashion. Although "thermal desorption" has been used to describe the

process taking place, it appears that during heating, simple thermal

Ion Source

electron beam

ion
beam

probe

ceramic post

metal post   filament
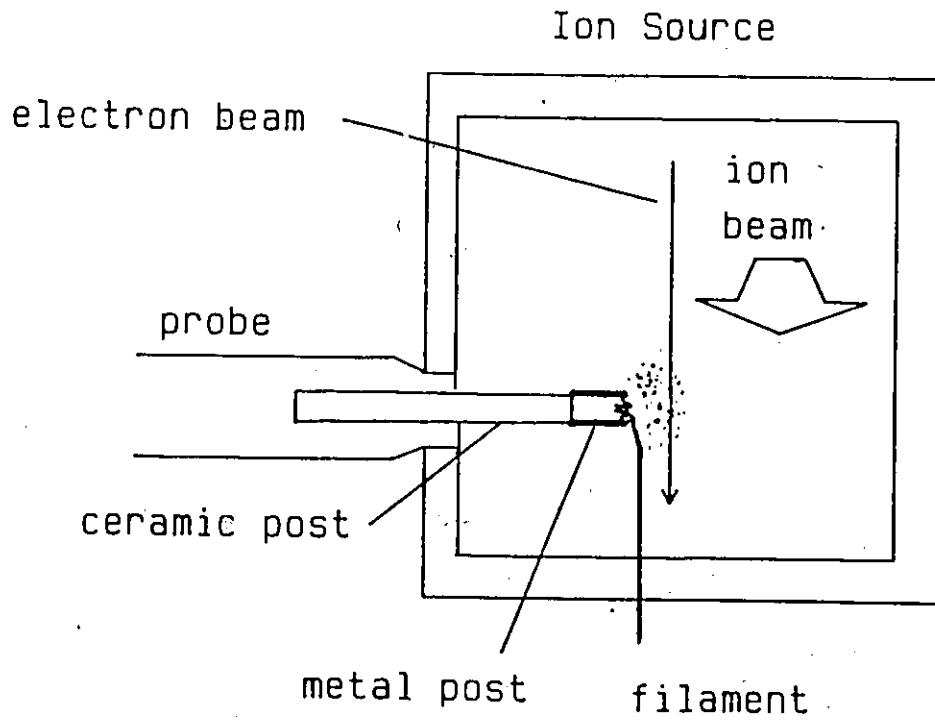
Figure 36: Volatilization from a DEI/DCI probe.

volatilization of neutrals occurs. Daves *et al* (110) showed that during volatilization, no molecular ions were observed if the electron beam was turned off.

Conditions for ionization of 2'-dG $\underline{20}$ were optimized by varying the filament heating rate until the molecular ion appeared as a sharp pulse. However, in spite of the reported success of DCI and DEI in the ionization of compounds such as disaccharides and steroid glycosides (80,111), only thermal decomposition ions were observed for the 1,8-adduct $\underline{48}$.

Attempts at obtaining FD spectra of a mixture of the three adduct isomers, and the 1,8-adduct acid decomposition product $\underline{50}$, met with limited success. The FD spectrum of the adduct isomer mixture was dominated by Na^+ and K^+ ions. In the FD spectrum of $\underline{50}$ (Figure 37) a molecular ion ($[M+H]^+$, m/z 412) and cationized molecular ions with sodium ($[M+Na]^+$, m/z 434) and potassium ($[M+K]^+$, m/z 450) were observed.

Fast atom bombardment (FAB) is one of the newer "soft" ionization techniques used for the MS analysis of a wide variety polar biological molecules. Generally, FAB is better suited to formally charged compounds, or those which can act as proton donors or acceptors. Therefore, the nature of the matrix in which the analyte is dissolved plays an important role in the ionization process. Many reactions such as protonation, deprotonation, cationization, and cluster formation of analyte and matrix molecules and/or co-additive molecules can occur. By appropriate choice of matrix and co-additives, the positive or negative ionization of the target compound can be optimized.
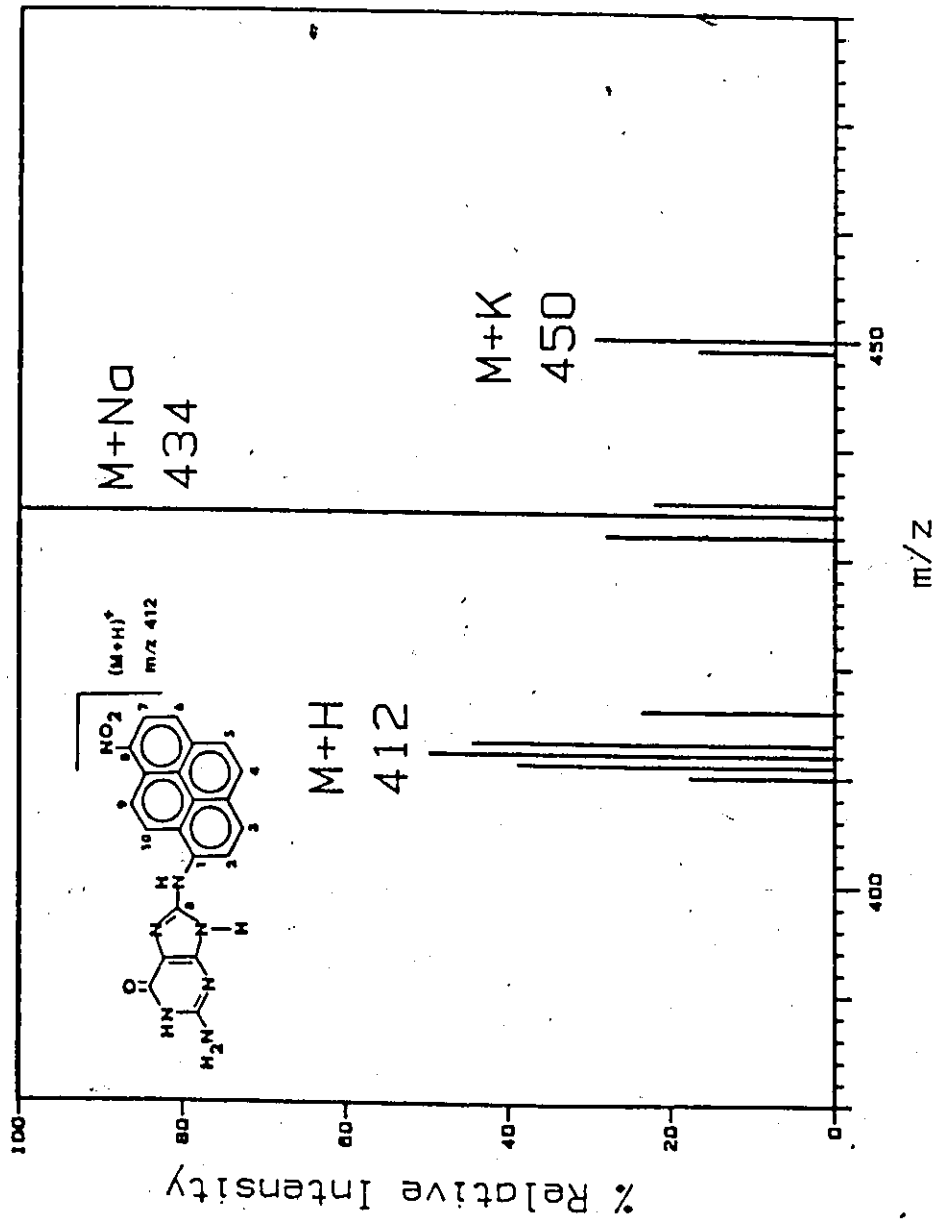
Figure 37: Field desorption (FD) spectrum of the 1,8-adduct acid decomposition product 50.

Table 11 lists some of the matrices used in attempts to obtain FAB

spectra of 1,6-ANP 33, 2'-dG 20, and the 1,6-adduct 47. Glycerol gives a

background spectrum of ion clusters at m/z $[93+(92)_x]^+$ which are used for

calibration purposes. Thioglycerol, the sulphur analogue of glycerol, is

used for compounds that are less soluble in glycerol. Since no spectra

of the 1,6-adduct 47 were obtained using these two matrices, a number of

matrix modifiers were added. Acids such as trifluoroacetic acid (TFA) and

oxalic acid were added in an attempt to produce a protonated species.

Methanol, water and DMF were added to alter the solubility of the

1,6-adduct 46 in these matrices.

Other matrices were also evaluated in an attempt to obtain FAB

spectra of the test compounds. The two nitro containing matrices,

3-nitrobenzyl alcohol (3-NBA) and 2-nitrophenyl-octylether (3-NPOE) are

useful for relatively non polar compounds and are thought to enhance

formation of M $^+$ as opposed to $[M+H]^+$ (75). A mixture of 5:1

dithiothreitol:dithioerithretol, also known as Magic Bullet, is often

used for compounds that do not give good spectra in glycerol or

thioglycerol. Many of these matrices were also used for FAB MS analysis

in the negative ion mode. Triethanolamine is a matrix which is most

commonly used for negative ion FAB because it enhances the production of

$[M-H]^-$.

A mass spectrum of the 1,6-DNP adduct 47 was observed only in a

matrix of glycerol saturated with ammonium chloride (Figure 38). This

spectrum was of low quality and the peaks appeared only at the beginning

of the atom bombardment. Although most of the analyte ions were of low

intensity, they appeared reproducibly. A protonated molecular ion $[M+H]^+$

Table 11: Matrices evaluated for the FAB MS analyses of 1,6-ANP 33, 2'-dG 20 , and 1,6-DNP adduct 47. Approximately 50-100 ng of sample in 2μL DMF was mixed with 100μL of matrix. All analyses were performed on a VG-ZABE mass spectrometer using an 8kV Xe beam. No spectra were observed with 1,6-ANP 33.

Matrix	Ion Mode[a]	Results	
		2'-dG 20	1,6-Adduct 47
Glycerol	+/-	c	b
+TFA	+	c	c
+NH$_4$Cl	+	c	b
+TFA+NH$_4$Cl	+	c	b
+MeOH/H$_2$O/TFA	+	b	b
+DMF	+	b	b
+oxalic acid	+	b	b
+MeOH/H$_2$O/TFA/oxalic acid	+	c	b
+DMF/oxalic acid	+	c	b
+Triethanolamine (TEA)	-	d	b
Thioglycerol	+/-	c	b
+NH$_4$Cl	+/-	c	b
5:1 Dithiothreitol:dithioerithritol	+	b	b
DMF	+/-	b	b
3-Nitrobenzyl alcohol (3-NBA)	+	b	b
2-Nitrophenyl-octylether (2-NPOE)	+	b	b
Triethanolamine (TEA)	-	c	b

[a] Ion mode: + - positive ions detected
    : - - negative ions detected
    :+/- - positive or negative ions detected

[b] matrix background ions only

[c] spectra with two analyte ions of low abundance
    2'-dG 20 : [M+H]$^+$ m/z 268, [B+2H]$^+$ m/z 152
    1,6-adduct 47 : [M+H]$^+$ m/z 528, [B+2H]$^+$ m/z 412

[d] spectra with two analyte ions of low abundance
    2'-dG 20: [M-H]$^-$ m/z 266, [B-H]$^-$ m/z 150
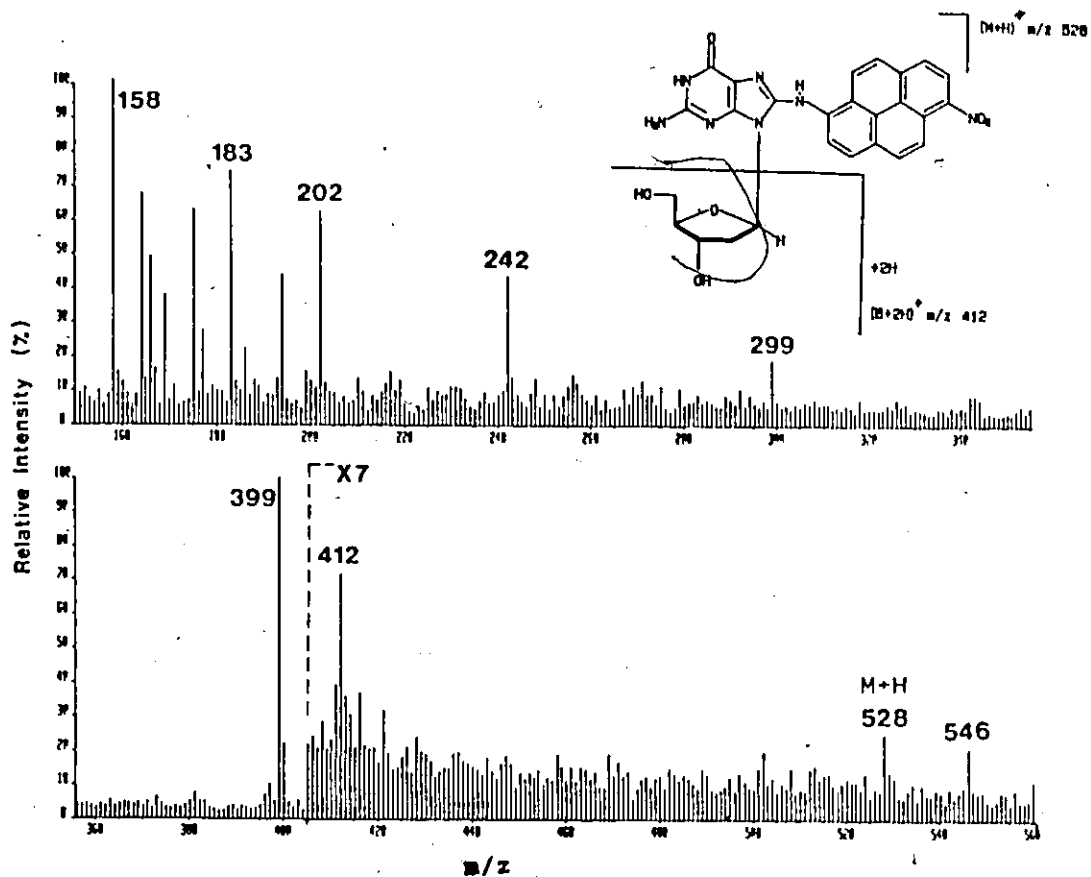
Figure 38: FAB spectrum of the 1,6-adduct 47 acquired from a matrix of glycerol saturated with ammonium chloride.

at m/z 528 was observed. The addition of water to the 1,6-adduct 47

before or during FABMS resulted in the formation of the base decompostion

product 51 at m/z 546. A more abundant ion was observed at m/z 412.

This species, ([B+2H]$^{+}$), would result from protonation of the base

fragment, abstraction of a proton from the sugar and loss the

2'-deoxyribose. This ion may also have arisen from decomposition of the

adduct in the matrix. The ions at m/z 399 and 299 were present in the

glycerol and were not due to the adduct. The ions at lower mass

(m/z 242,202,183,158), were glycerol or glycerol/ammonium ion clusters.

Coupled LC-MS is a useful method for the simultaneous separation

and MS analysis of polar biological compounds. A VG-7070F LC belt

interface was used to introduce the sample into the ion source. In this

system, eluent from the chromatography column is sprayed onto a polyimide

belt and carried through two vacuum locks into the source. For EI,

volatilization of the analyte from the belt is achieved by a heater at

the tip of the belt assembly which protruded into the source. Ionization

can also be accomplished by directing the atom beam from a FAB gun onto

the belt. As the analyte elutes from the column and is mass analysed, a

three dimensional array of ion intensities, m/z values and scan numbers

(or elution times) can be acquired by a data system.

In initial studies, only thermal decomposition products were

observed in the LC-EIMS analysis of the 1,8-adduct 48. Figure 39 shows

the results of LC-FABMS of the 1,8-adduct 48. The total ion current

(TIC) (Figure 39a) and mass chromatogram at m/z 412 (Figure 39b)

illustrated that two components were present at scans 113 and 160 (4.4

min and 6.0 min). These two components were postulated to be the
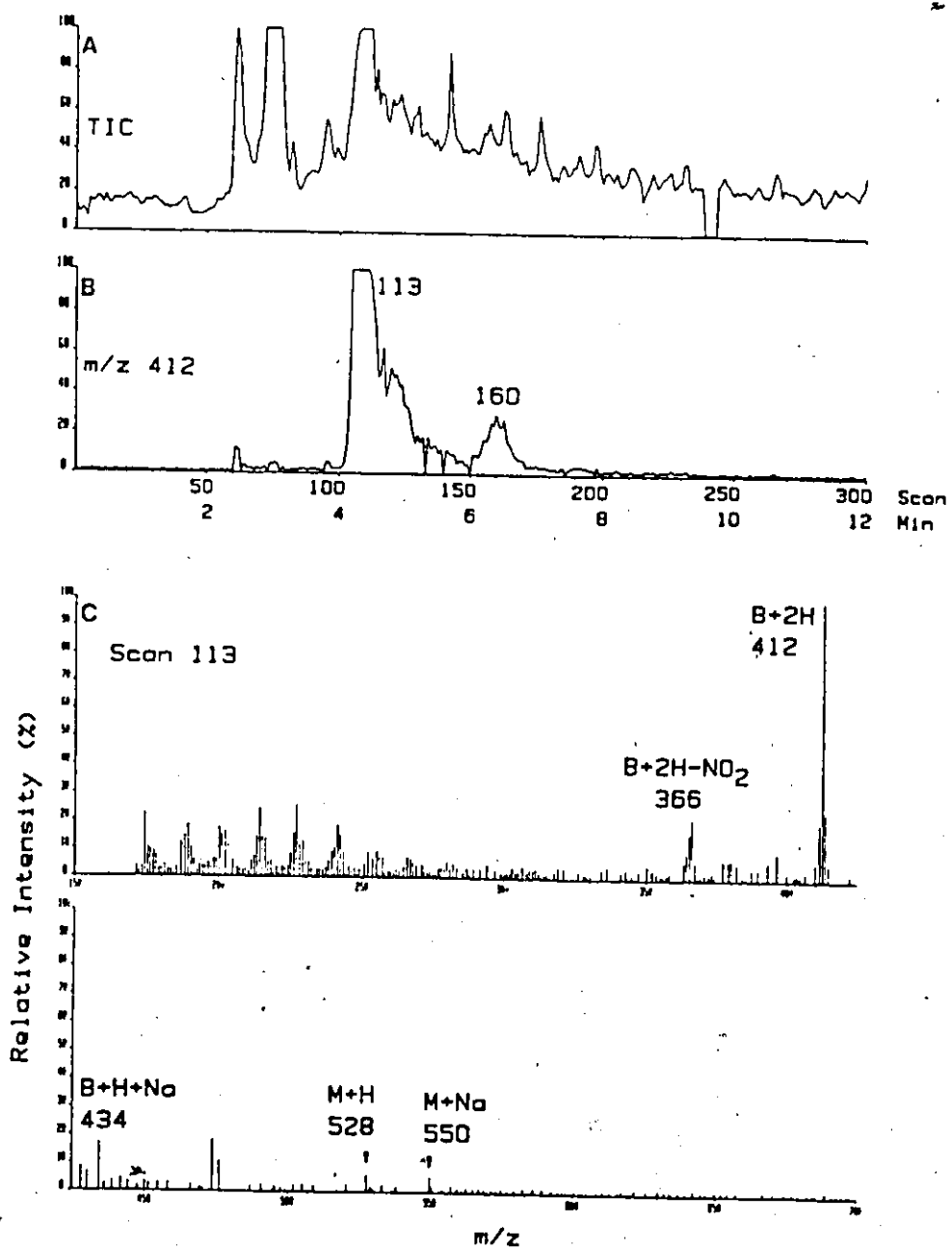
Figure 39: The results of LC-FABMS of the 1,8-adduct 48. Chromatograms of (a) total ion current (TIC), and (b) m/z 412, and mass spectrum of scan 113 (c). HPLC and MS conditions are described on page 142.

1,8-adduct <u>48</u>, and its acid decomposition product <u>50</u>, based on their

chromatographic behaviour discussed in II.3.1. The spectrum of scan 113

and postulated fragmentation pattern are shown in Figures 39c and 40

respectively. A low abundance adduct molecular ion $[M+H]^+$ (m/z 528) and

cationized ion $[M+Na]^+$ (m/z 550) were observed. Charge retention on the

base fragment and loss of the 2'-deoxyribose with a proton rearrangement

resulted in ions at $[B+2H]^+$ (m/z 412) and $[B+H+Na]^+$ (m/z 434). The ion

at m/z 366, $[B+H-NO_2]^+$, resulted from loss of a nitro group from the base

fragment. This spectrum was similar to that of the 1,6-adduct <u>47</u> obtained

in a matrix of glycerol and ammonium chloride (Figure 37). The spectrum

at scan 160 showed ions consistent with the structure of the 1,8-adduct

acid decomposition product <u>50</u>. The spectrum was similar to that of the

adduct except that ions at m/z greater than 412 were not observed (data

not shown).

II.3.4.2 Ionization of Derivatized Adducts on Extended Probes.

One strategy to increase the volatility of compounds for EI and CI

is chemical derivatization. Trialkylsilyl derivatives such as

trimethylsilyl (TMS) and sterically crowded trialkylsilyl derivatives

such as t-butyldimethylsilyl (TBDMS) have been used to aid in the MS

analyses of many polar biological compounds (85,112,113). These

derivatizing reagents greatly facilitated the MS analysis of small

quantities of modified nucleosides generated in this work.

The silylating reagent chosen for the formation of TMS derivatives

of test compound 2'-dG <u>20</u> and the adducts 46-48 was

N,O-bis-(trimethylsilyl)-trifluoroacetamide (BSTFA) (Figure 41). In DMF,

$(M+H)^+$ m/z 528

$(M+H+Na)^+$ m/z 550

$(B+2H-NO_2)^+$ m/z 366

+2H

NO_2

$(B+2H)^+$ m/z 412

+2H

$(B+H+Na)^+$ m/z 434

+H + Na
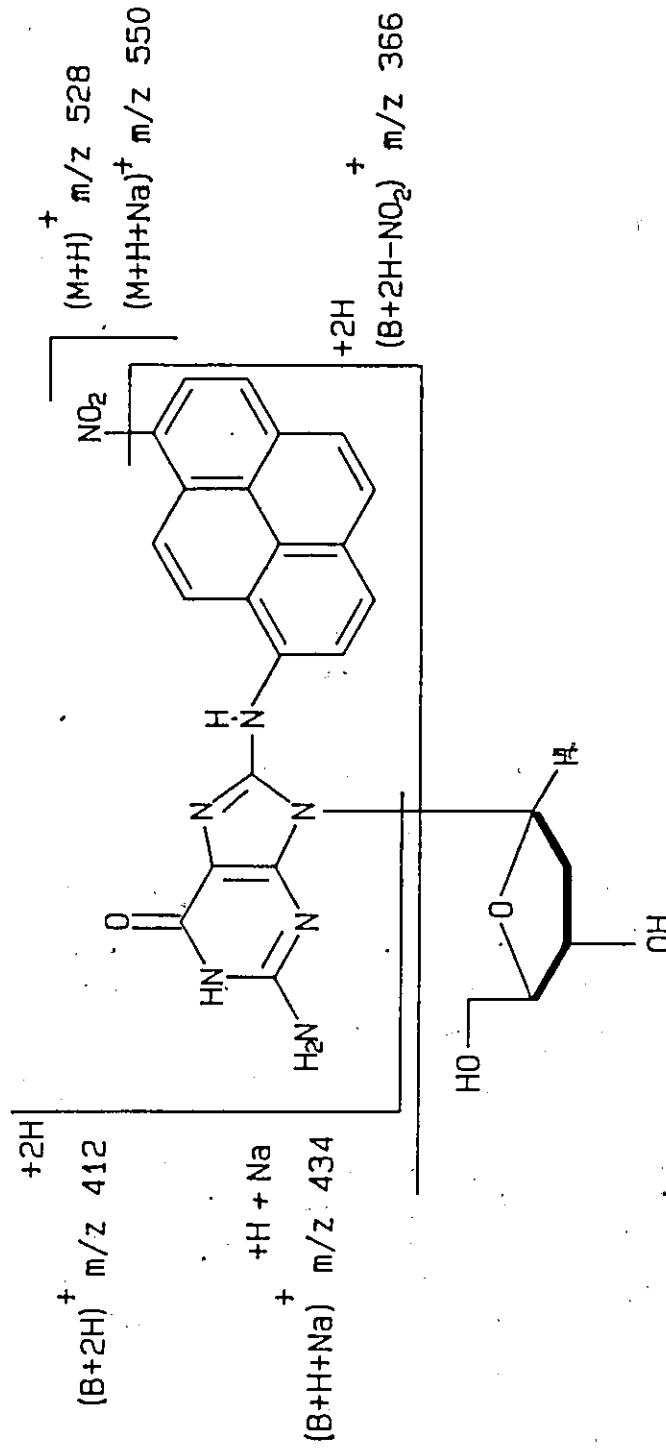
1,8-adduct 48

Figure 40: Assignment of ions observed in the mass spectrum of the 1,8-adduct 48 acquired during LC-FABMS analysis.

this powerful TMS donor rapidly forms derivatives with alcohols, amines, phenols, and carboxylic acids (64). A formulation of BSTFA with 1% trimethylchlorosilane was used because the adducts 46-48 contained amino and amide groups which are difficult to silylate. This formulation catalyzes the formation of N-TMS derivatives. Another advantage of BSTFA over other reagents is the high volatility of its side products.

N-methyl-N-(t-butyldimethylsilyl)-trifluoroacetamide (MTBSTFA) is a recently developed reagent which is useful for the production of TBDMS derivatives of nucleosides (114) (Figure 41). The nucleoside TBDMS ethers formed are more than 10^4 times more stable than TMS ethers. One advantage of this stability is that TBDMS derivatives of nucleosides can be studied by LC-MS techniques. Both TMS and TBDMS derivatives give rise to mass spectra that are rich in structurally important fragmentation patterns.

All MS analyses of silylated derivatives were performed using the DCI/DEI probe. No spectra were obtained in ammonia DCI MS analyses of TBDMS derivatives of a mixture of the three adducts 46-48. However, with DEI a strong spectrum rich in structurally important ions was observed. Spectra of the TBDMS derivatives of the individual 1,3-,1,6-,and 1,8-adducts 46-48, and the TMS derivative of the 1,8-adduct 48 were then recorded. The DEI probe, containing 10-100 ng of derivative, was inserted into the source, and volatile derivatization reaction byproducts allowed to distill off the probe before the filament was heated.

CF₃—C≡N—Si(CH₃)₃

BSTFA

CF₃—C≡N—Si—C(CH₃)₃
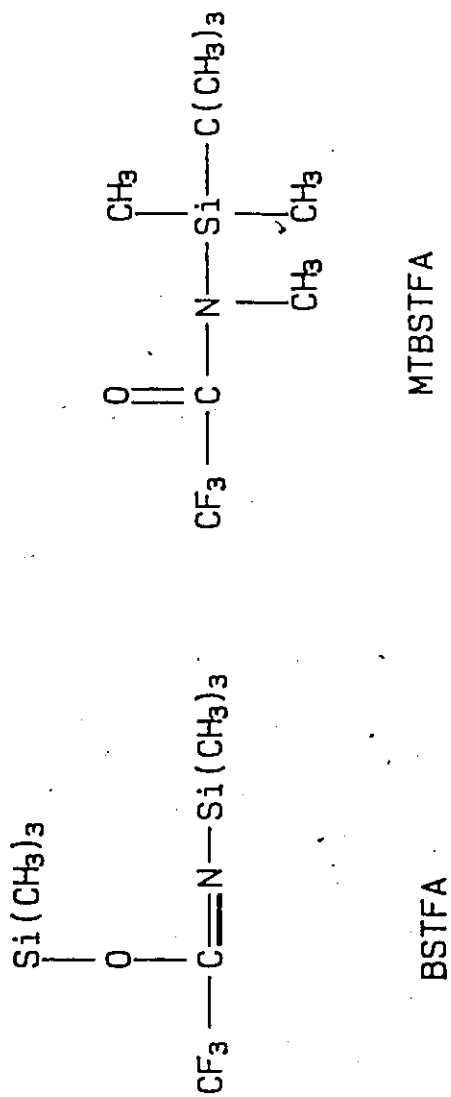
MTBSTFA

Figure 41: The structures of derivatizing reagents BSTFA and MTBSTFA.

II.3.4.2.1 TBDMS Derivatives

The DEI mass spectrum of a mixture of the tris-, and tetrakis-TBDMS derivatives of the 1,8-adduct 48 is shown in Figure 42. The fragmentation of the tetrakis derivative will be discussed as it was the most abundant species. Fragmentation of the tris derivative occurred in a similar fashion. An interpretation of some of the important ions of the TBDMS derivative is presented in Table 12. The partial fragmentation pathway and numbering scheme for the fragment ions used in the following discussion are shown in Schemes 6-8. A full table of m/z and ion . abundance for the three TBDMS adduct derivatives may be found in Appendix B. The spectra of the TBDMS derivatives of the 1,3-adduct 46 and 1,6-adduct 47 did not vary significantly from that of the 1,8-adduct 48, although the intensity of ions assigned to the pentakis derivatives were higher. The following discussion of the interpretation of the spectra is based upon previous published studies on TBDMS derivatives of nucleosides (112).

(A) Ions Resulting in Initial Siliconium Ion Formation (Scheme 6).

$[M]^+$ m/z 983

$[M-Me)^{+-}$ m/z 968, 6a

$[M-tBu]^+$,   m/z 926, 6b

$[M-tBu-tBuMe_2SiOH]^+$ m/z 794, 6c

$[M-30]^+$.   m/z 953, 6d

High resolution data on the molecular ion M^+, confirmed the empirical formula of the tetrakis derivative as $C_{50}H_{77}N_7O_6Si_4$ (predicted m/z 983.501, found m/z 983.500). Charge retention adjacent to a silicon
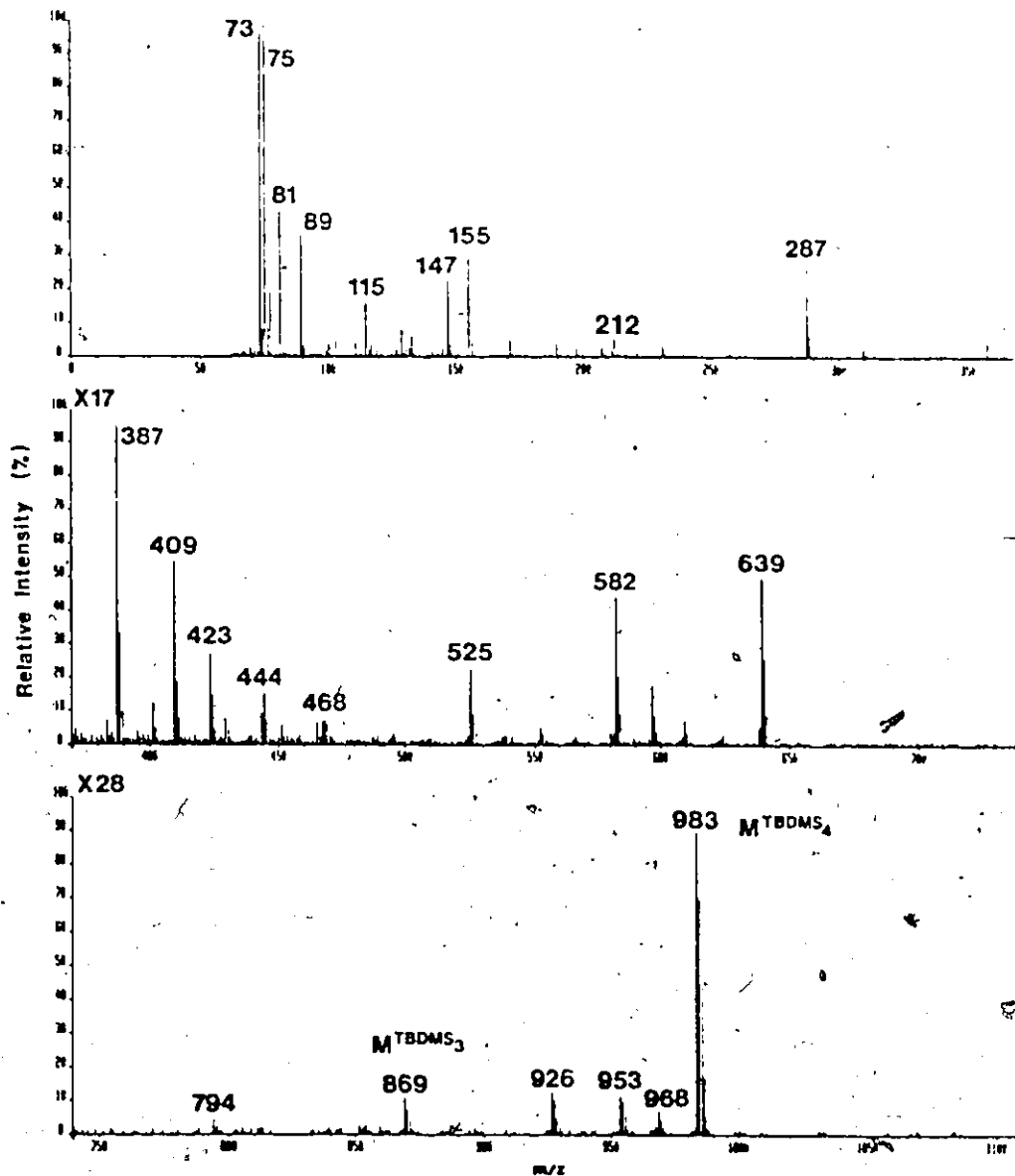
Figure 42: DEI mass spectrum of TBDMS derivatives of the 1,8-adduct 48.

Table 12: Ions observed in the DEI spectra of TBDMS
derivatives of DNP-nucleoside adducts 46-48. Incomplete
N-silylation resulted in a mixture of tris-, and tetrakis-
and pentakis t-butyldimethylsilyl (TBDMS$_3$,TBDMS$_4$ and
TBDMS$_5$) derivatives. See Figure 43 for representative
spectrum.

		m/z	
Assignment[b]	TBDMS$_3$	TBDMS$_4$[a]	TBDMS$_5$
M	869	983[d]	1097
M-Me	854	968	(1062)
M-tBu	812	926	1040
M-30[c]	839	953	(1067)
M-tBuMe$_2$SiOH	(737)	(851)	(965)
M-Me-tBuMe$_2$SiOH	(722)	(836)	(950)
M-tBu-tBuMe$_2$SiOH	(680)	794	(908)
B+H	525	639[d]	753
B+H-Me	510	624	(738)
B+H-tBu	468	582	696
M-BH-tBu		287	
M-BH-tBuMe$_2$SiOH		212	
M-BH-tBu-tBuMe$_2$SiOH		155	
Me$_2$SiOSiMe$_3$		147	
tBuMe$_2$Si		115	
Me$_2$SiOH		75	
Me$_3$Si		73	

a: major derivative
b: Me=CH$_3$, tBu=t-Butyl, B=nucleoside base unit
c: reduced compound
d: confirmed by high resolution MS
( ): not detected

107
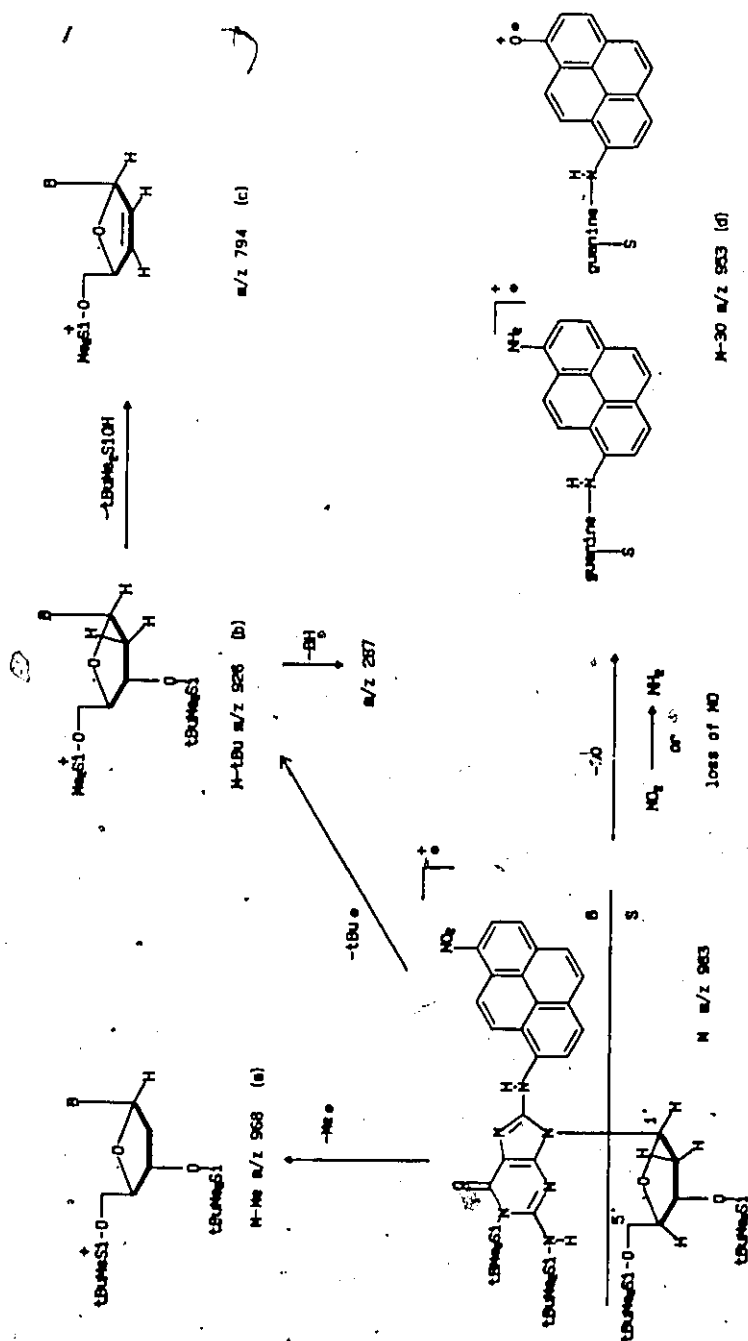
Scheme 6. Partial fragmentation pathway for the tetrakis TBDMS derivative of the 1,8-adduct 48.: Ions resulting in initial siliconium ion formation.

resulted in loss of either a methyl radical (M-15, m/z 968) 6a, or a
t-butyl radical (M-57, m/z 926) 6b. These losses could occur from the
any of the TBDMS groups. The [M-57]$^+$ ion is usually seen as a major ion
in the spectra of TBDMS-nucleoside derivatives, but was of much lower
abundance in these spectra. Loss of t-BuMe$_2$SiOH from 6b can occur by
abstraction of the 2' proton to form 6c (m/z 794). Loss of 30 from the
molecular ion to 6d (M-30, m/z 953) may occur via two pathways. In
parallel high resolution EI studies of 1,8-ANP 22, this nominal loss of
m/z 30 was shown to arise from both loss of NO (m/z 29.998) or reduction
of NO$_2$ to NH$_2$ (loss of 29.974) in the source prior to ionization. This
reduction was also observed by Quilliam et al (115) in MS studies of
[^{15}N]-nitro-PAH.

(B) Ions Resulting From Charge Retention on the Sugar (Scheme 7).

#[M-tBu-BH]$^+$ m/z 287, 7a #B-nucleoside base unit

[M-tBuMe$_2$SiOH-BH]$^+$ m/z 212, 7b

[M-tBu-tBuMe$_2$SiOH-BH]$^+$ m/z 155, 7c

Although [M-BH]$^+$ (m/z 344) was not observed, three ions which are
indicative of 2'-deoxyribose moiety were present. The ion at m/z 287,
7a, likely arises from loss of B+H from 6b (m/z 926) or possibly via a
sequential loss of B+H and tBu from M$^+$. The low abundance ion m/z 212,
7b, was formed in a similar fashion by loss of B+H and tBuMe$_2$SiOH from
the molecular ion. Both 7a and 7b could be precursors for m/z 155, 7c.
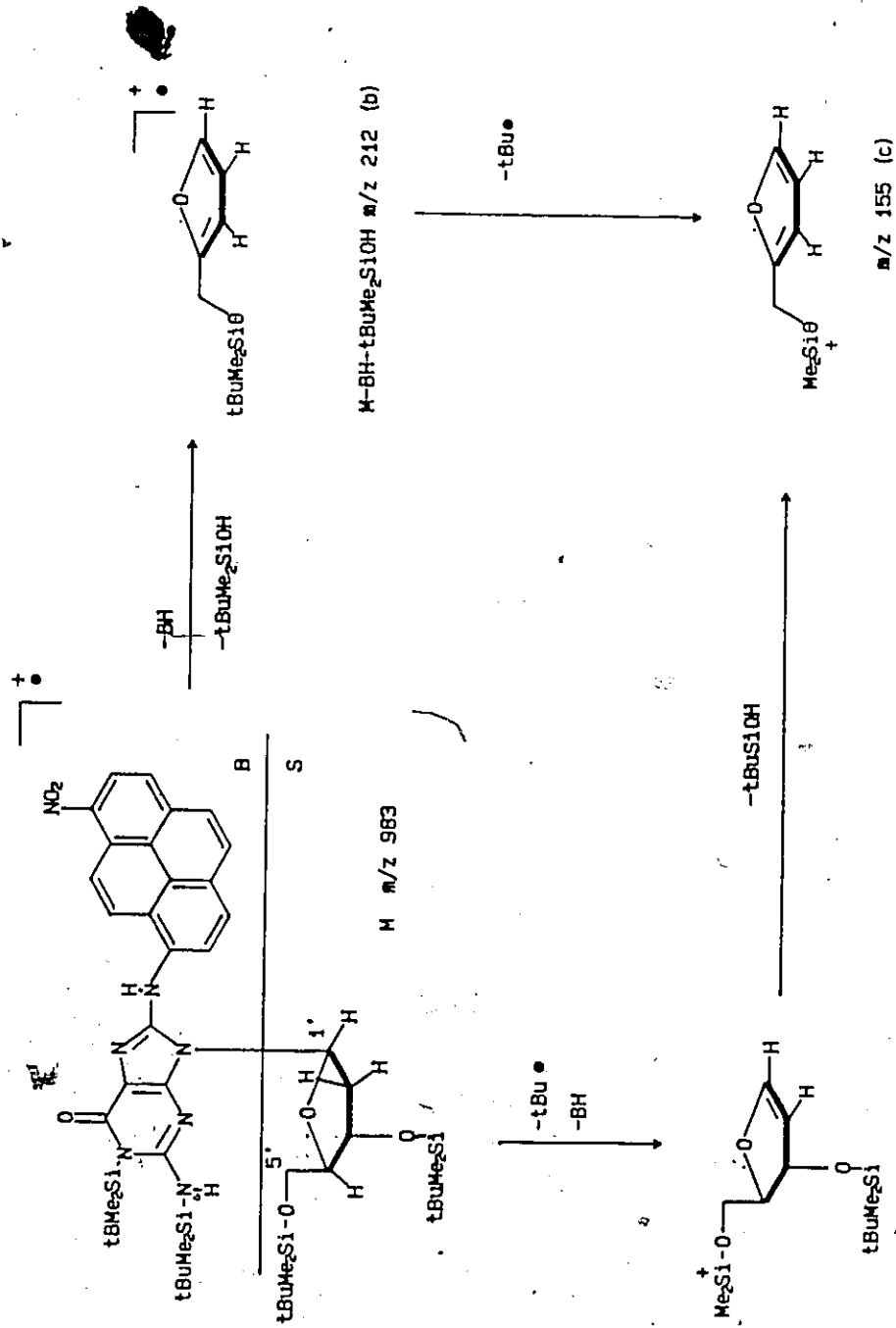
Scheme 7. Partial fragmentation pathway for the tetrakis TBDMS derivative of the 1,8-adduct 48.:Ions resulting from charge retention on the sugar (S).

(C) Ions Resulting from Charge Retention on Base (B) (Scheme 8).

$[B+H]^+$ m/z 639,   <u>8a</u>

$[B+H-Me]^+$ m/z 624,   <u>8b</u>

$[B+H-tBu]^+$ m/z 582,   <u>8c</u>

Charge retention on the guanine of the molecular ion, proton rearrangement from the sugar and cleavage of the glycosidic bond leads to $[B+H]^+$ (M-344), <u>8a</u>. High resolution MS analysis confirmed the empirical formula for this ion as $C_{33}H_{41}N_7Si_2O_3$ (predicted m/z 639.281, found 639.280). In the FAB spectra of the underivatized 1,8- and 1,6-adducts <u>47</u> and <u>48</u> (Figures 38,39), the diprotonated base fragment is also a predominant ion, attesting to the weakness of the glycosidic bond. The ions <u>8b</u> (m/z 624) and 8c (m/z 582) are formed from 8a by loss of methyl and t-butyl respectively.

The ions at m/z 147,115,89,81,75 and 73 were due to fragmentation associated with silicon groups. These ions, which are also observed in the spectrum of the 1,8-adduct TMS derivative, are usually of high abundance but offer little structural information. The ions at m/z 444, 423, 409, and 387 have not yet been assigned; most were observed in the spectra of the TBDMS derivatives of the other adducts.

II.3.4.2.2 TMS Derivatives

The DEI spectrum of a mixture of the tris-,tetrakis-, and pentakis-TMS derivatives of the 1,8-adduct <u>48</u> is shown in Figure 43. The fragmentation of the tetrakis derivative will be discussed as this was the most abundant species. Fragmentation of the tris- and pentakis- derivatives occurred in a similar fashion. An interpretation of some

B+H-Me m/z 624 (b)

-Me•

B+H m/z 639 (a)

-tBu•

B+H-tBu m/z 582 (c)

M m/z 983

-S
+H
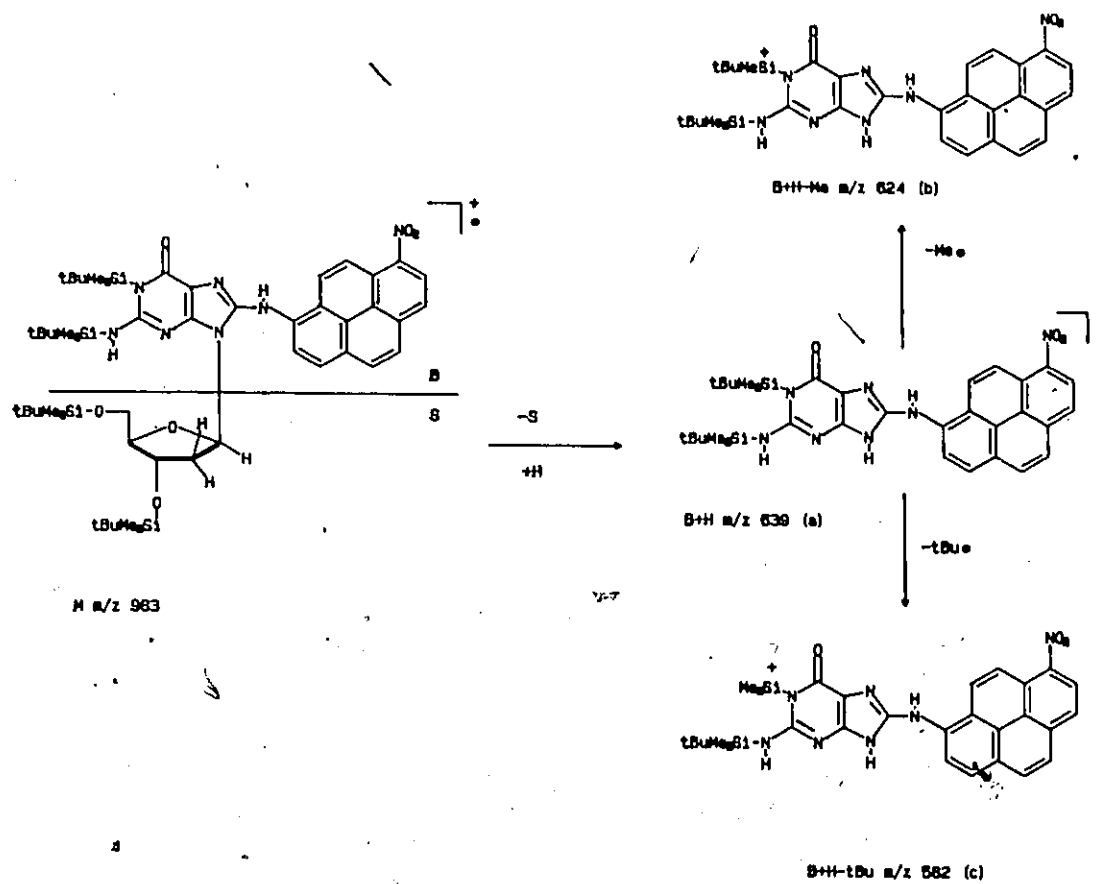
Scheme 8. Partial fragmentation pathway for the tetrakis TBDMS derivative of the 1,8-adduct 48.: Ions resulting from charge retention on the base (B).
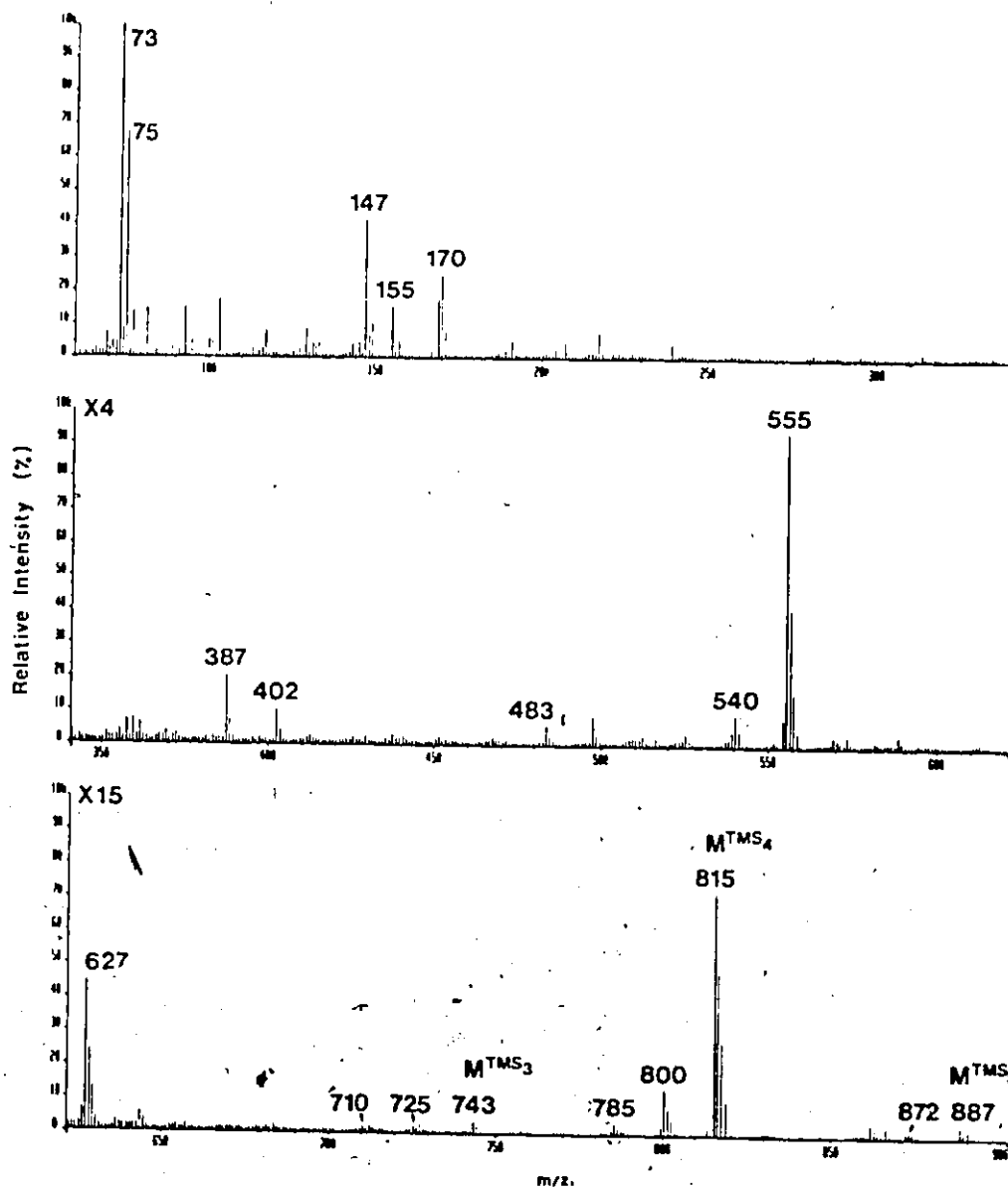
Figure 43: DEI mass spectrum of TMS derivatives of the
1,8-adduct 48.

important ions is summarized in Table 13. The partial fragmentation pathway and numbering scheme for the fragment ions used in the following discussion are shown in Schemes 9-11. A full table of m/z and ion abundance may be found in Appendix B. Spectra for the 1,3-adduct 46 and 1,6-adduct 47 TMS derivatives were not obtained.

(A) Ions Resulting In Initial Siliconium Ion Formation (Scheme 9).

$[M]^+$ m/z 815

$[M-Me]^+$ m/z 800,   9a

$[M-Me_3SiOH]^+$ m/z 725,   9b

$[M-Me-Me_3SiOH]^+$ m/z 710,   9c

$[M-30]^+$ m/z 785

The fragmentation behaviour of the tetrakis-TMS 1,8-adduct derivative was analogous to the tetrakis TBDMS derivative. Loss of a methyl radical from M^+ (m/z 815) leads to 9a (m/z 800), which then can then lose Me$_3$SiOH to 9c (m/z 725). Another pathway to 9c is via loss of Me$_3$SiOH to 9b (m/z 725). The (M-30)$^+$ (m/z 785) species was also observed, which as discussed above could be due to loss of NO from M^+ or chemical reduction in the source prior to ionization.

(B) Ions Resulting from Retention of Charge on the Sugar (Scheme 10).

$[M-BH-Me_3SiOH]^+$ m/z 170,   10a

$[M-BH-Me-Me_3SiOH]^+$ m/z 155,   10b

Unlike the TBDMS derivative, only two ions indicative of 2'-deoxyribose functionality were observed in the spectra of the TMS derivative. These ions at m/z 170, 10a, and m/z 155, 10b, were more

Table 13: Ions observed in·the DEI spectra of TMS derivatives of 1,8-adduct 48. Incomplete N-silylation resulted in a mixture of tris-, and tetrakis- and pentakis trimethylsilyl (TMS_3, TMS_4 and TMS_5) derivatives. See Figure 43 for representative spectrum.

	m/z		
Assignment[b]	TMS_3	TMS_4 [a]	TMS_5
M	743	815	887
M-Me	728	800	872
M-30[c]	713	785	857
M-Me$_3$SiOH	(653)	725	(787)
M-Me-Me$_3$SiOH	(638)	710	782
B+H	483	555	627
B+H-Me	468	540	612
M-BH-Me$_3$SiOH		170	
M-BH-Me-Me$_3$SiOH		155	
Me$_2$SiOSiMe$_3$		147	
Me$_2$SiOH		75	
Me$_3$Si		73	

a : major derivative
b : Me=CH$_3$, B=nucleoside base unit
c : reduced compound
( ): not detected

m/z 719 (c)

Me₃Si-O

−Me•

−Me₃SiOH

M−Me₃SiOH m/z 725 (b)

Me₃Si-O

−Me₃SiOH

−Me•

N−Me m/z 800 (a)

Me₃Si

Me₃Si-O

M m/z 815

B

S

NO₂

Me₃Si-N-H

Me₃Si-N-H

Me₃Si-O

Scheme 9. Partial fragmentation pathway for the tetrakis
TMS derivative of the 1,8-adduct 48.: Ions
resulting in initial siliconium ion formation.
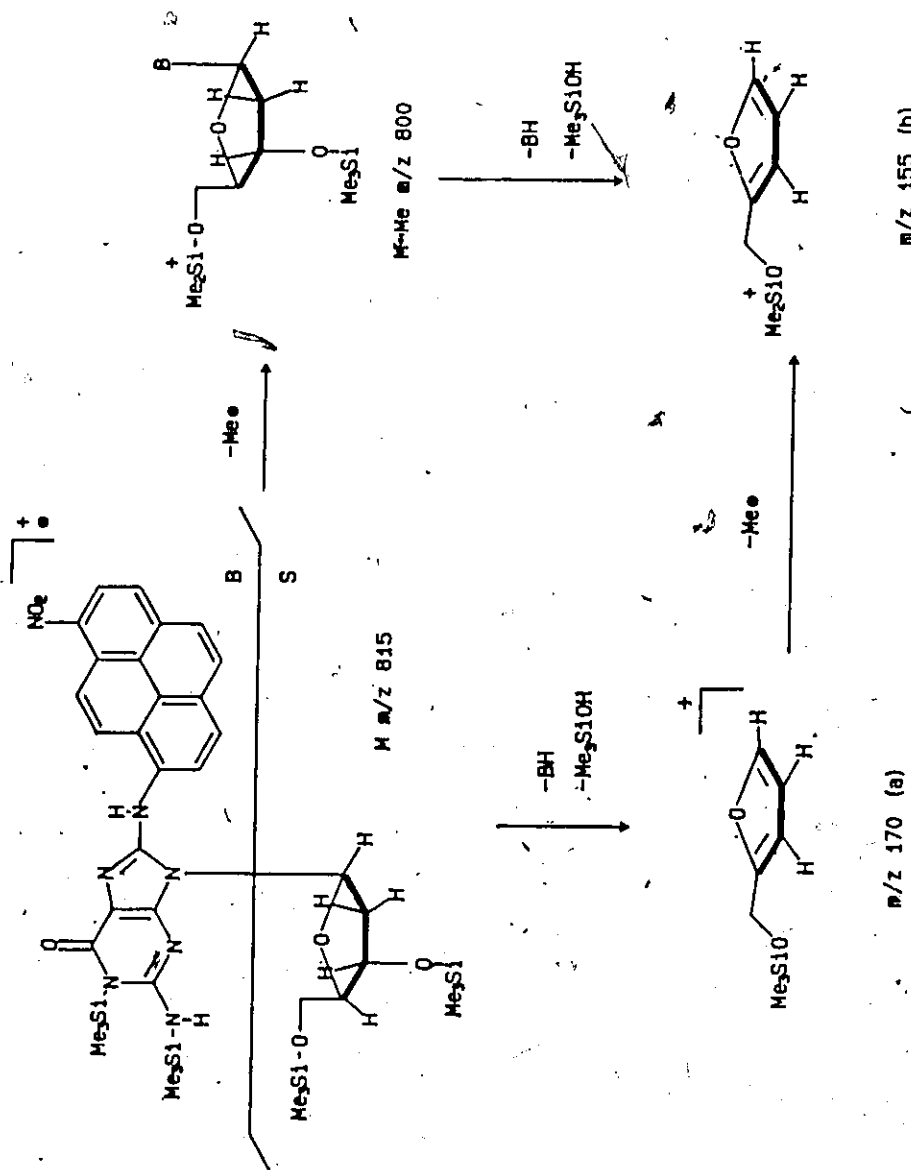
Scheme 10. Partial fragmentation pathway for the tetrakis
TMS derivative of the 1,8-adduct 48.:Ions
resulting from charge retention on the sugar (S)

abundant than the analogous TBDMS ions, 7b and 7c. The ion at m/z 155 could arise via loss of methyl from 10b or loss of B+H and Me_3SiOH from 9c.

(C) Ions Resulting from Retention of Charge on Base (B) (Scheme 11).

$[B+H]^+$ m/z 555,   11a

$[B+H-Me]^+$ m/z 540,   11b

Charge retention on the base, proton abstraction from the sugar and cleavage of the glycosidic bond, results in the ion at m/z 555, 11a. Loss of methyl radical from this species leads to 11b. Both 11a and 11b were more abundant than the analogous TBDMS ions 8a and 8b.

The major difficulty with the MS analysis of the underivatized adducts 46-48 appeared to be their high polarity and thermal instability. The "in-beam" volatilization and ionization techniques were simply not suited for these low volatility compounds. FAB ionization appeared promising, particularly LC-FABMS with belt interface, although it was not that sensitive and yielded little structural information. More structural information could possibly be obtained by combining tandem MS-MS with FAB ionization.

Trialkylsilyl derivatization appears to be the strategy of choice for the MS analysis of these compounds. This technique provides very high sensitivity and good molecular weight and structural information. DEI proved to be a simple sample introduction technique for the MS analysis of TMS and TBDMS adduct derivatives. TBDMS derivatization is especially promising because of the possibility of combined LC-MS directly on reaction mixtures.
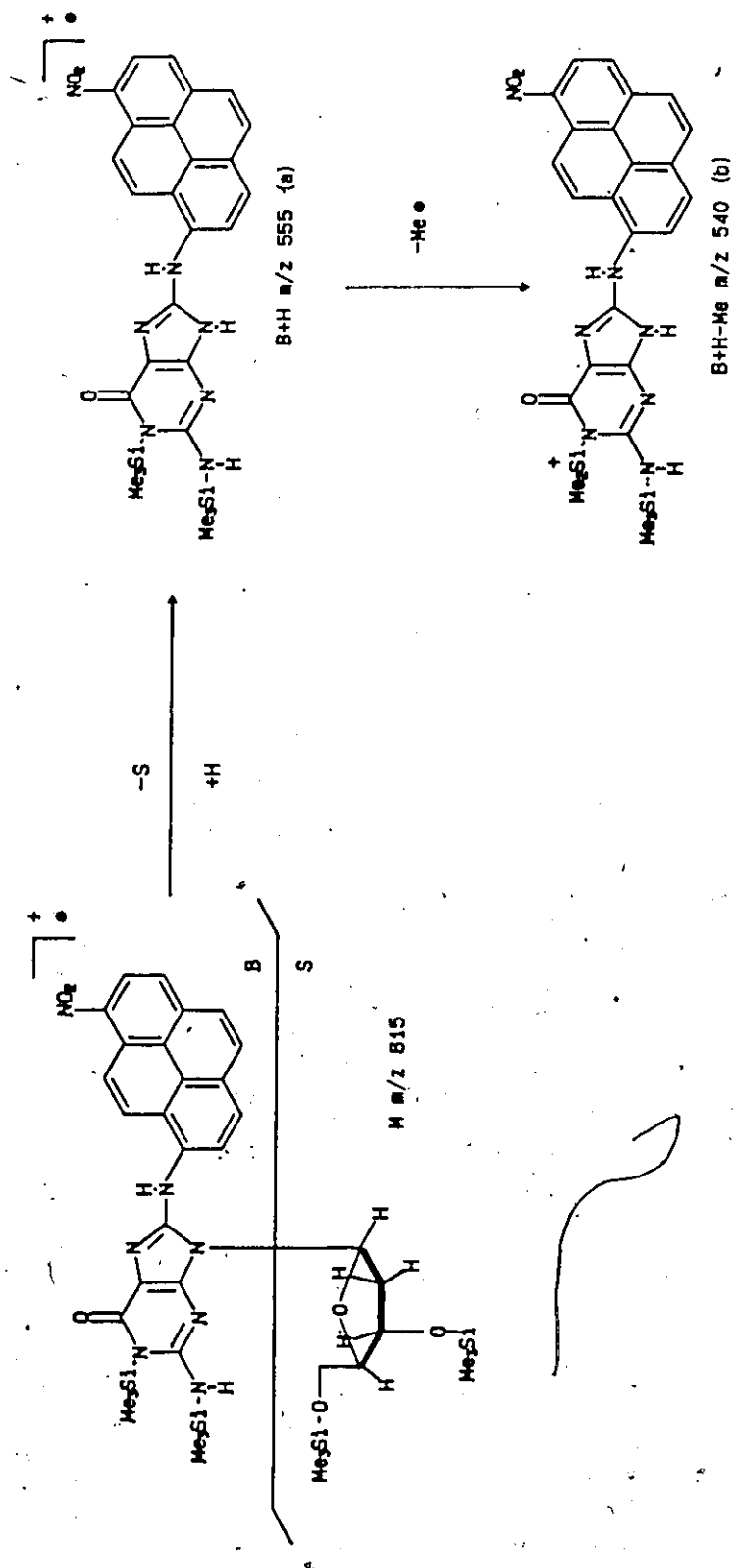
Scheme 11. Partial fragmentation pathway for the tetrakis—
TMS derivative of the 1,8-adduct 48.; Ions
resulting from charge retention on the base (B).

II.4   The Noncovalent Interaction of Disubstituted Pyrenes and CT-DNA.

In addition to covalent adduct formation, many compounds can interact with DNA in a noncovalent fashion. The most important of these compounds are characterized by their extended heterocyclic aromatic chromophores. By intercalating the planar aromatic portion of the molecule between adjacent nucleotide base pairs, they cause a partial unwinding of the DNA double helix. Some of these intercalators are widely used as antibiotics and as probes of DNA structure (116). Many of these compounds cause frame shift mutations.

Figure 44 illustrates that many intercalators are similar in structure to ANPs 32, 33 and 22 and DAPs 38, 39 and 23. Both classes of compounds have large, planar, aromatic rings. The DAPs are of special interest because the same diamino functionality is also present in proflavine 54 and ethidium 55. The bacterial mutagenicity of the DNPs 8-10 could be hypothesized to be the result of a combination of covalent adduct formation and noncovalent DNA interaction by key metabolites. The noncovalent interaction could occur by intercalation or by binding at some other site on DNA. This section discusses the results of spectroscopic and electrophoretic studies of CT-DNA, before and after reaction with these DNP metabolites.

II.4.1   UV-Visible Spectroscopy

The interaction of the test compounds and CT-DNA was easily followed by UV-VIS spectroscopy because it resulted in changes in the electron density of their extended chromophore systems. These electron density changes, as discussed in II.2.2, produced a shift in the UV-VIS
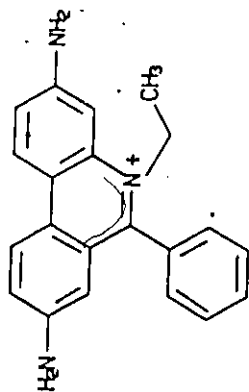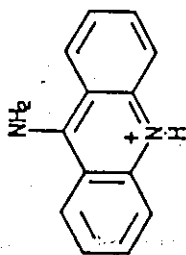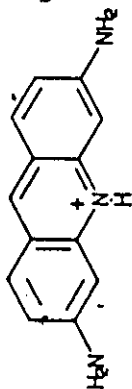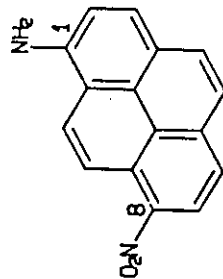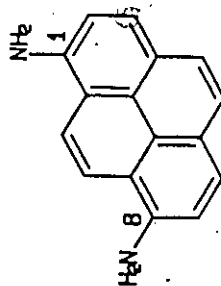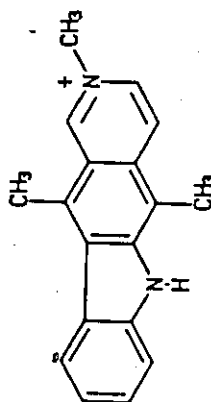
Figure 44: The structures of some intercalating dyes that form complexes with DNA, and disubstituted pyrenes 1,8-DAP 23 and 1,8-ANP 22.

absorbance maxima of the compound. Table 14 tabulates the absorbance maxima before and after interaction of test compound with CT-DNA.

The UV-VIS absorbance maximum of proflavine 54, a diamino substituted intercalator, shifted from 440 nm to 460 nm in the presence of CT-DNA. Because of their structural similarity, shifts of absorbance maxima of 1,8-DAP 23, and 1,6-DAP 39 were also expected to occur. After mixing solutions of 1,8-DAP 23 and CT-DNA, no immediate spectral changes were observed. However, after 1 hour a blue coloured species with an absorbance maximum of 612 nm had appeared. Reaction of 1,6-DAP 39 and DNA resulted in the appearance of a coloured species with an absorbance maximum of 590 nm and 432 nm (Figure 45a). The absorbance maximum at 372 nm, due to unreacted 1,6-DAP 39, decreased with time.

By treating the DAP/DNA with either Mg^{2+} or spermidine, these spectral changes were reversed. No spectral changes were observed in the proflavine/DNA solution after treatment with Mg^{2+} or spermidine. Spermidine, a long chain alkyl triamine, and divalent cations are both known to bind to sites on the outer surface of DNA. The disappearance of the blue species appeared to support the hypothesis that the interaction between the DAPs 23 and 39 and DNA took place on the outer surface of the DNA rather than by intercalation. Models showed that the distance between the two amino groups of the DAP was large enough to bridge two phosphate groups in the DNA.

A broad ESR signal, with no fine structure, also appeared in conjunction with the blue coloured species (Figure 45b). This species may have been a charge transfer complex formed between bound DAP species, or bound and free DAP species. Charge transfer may have occurred to such

Table 14: UV-Visible absorbance maxima of disubstituted pyrenes and proflavine before and after reaction with CT-DNA. Conditions: 1 mg/mL DNA (3 mM in nucleotide), all other compounds at 40-70 μM. Spectra were acquired on a HP-8451 DAD in 20 mM pH 7 phosphate buffer.

Compound	Absorbance Maximum (nm)	
	-DNA	+DNA
proflavine 54	442	460
1,8-DAP 23	386	612
1,6-DAP 39	372	590
1,8-ANP 22	492	534
1,6-ANP 33	482	470
1,3-ANP 32	452	490

Figure 45: The time dependent spectral changes followed by (a) UV-VIS and (b) ESR spectroscopy of the reaction of 1,6-DAP 33 and CT-DNA. UV-VIS conditions: CT-DNA, 1 mg/ml (3 mM in nucleotide), 1,6-DAP 33 11 mM, solvent 20 mM pH 7 buffer. Spectra acquired on a HB-8451A'DAD UV-VIS spectrometer. ESR conditions: spectra were acquired on a Bruker ER 100D ESR spectrometer in a glass capillary tube in a Tm 4103 cavity. Magnetic field:3368 G midrange, 100 G scan range, 100 sec scan time. Concentrations of 1,6-DAP 33 and DNA were as described above.
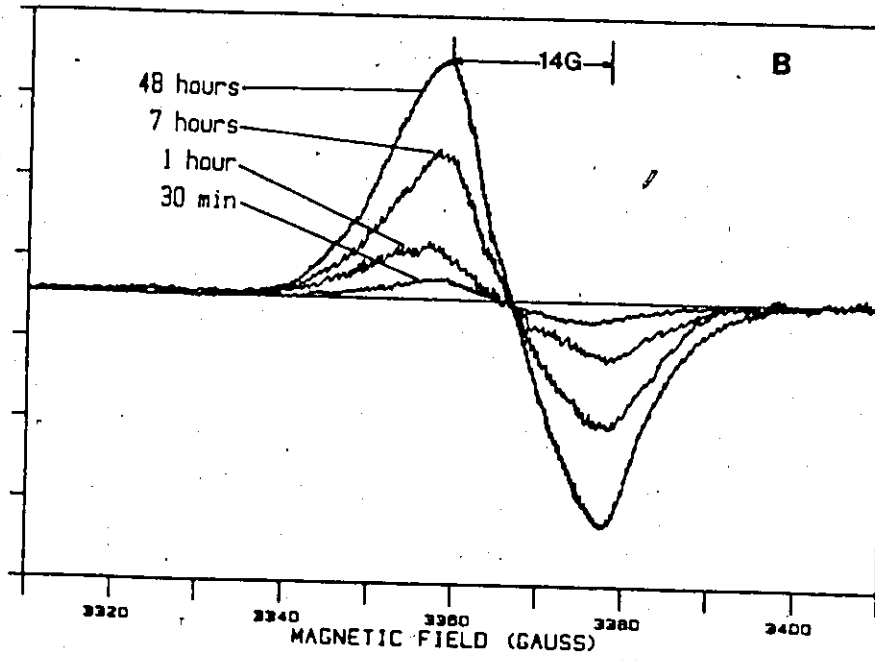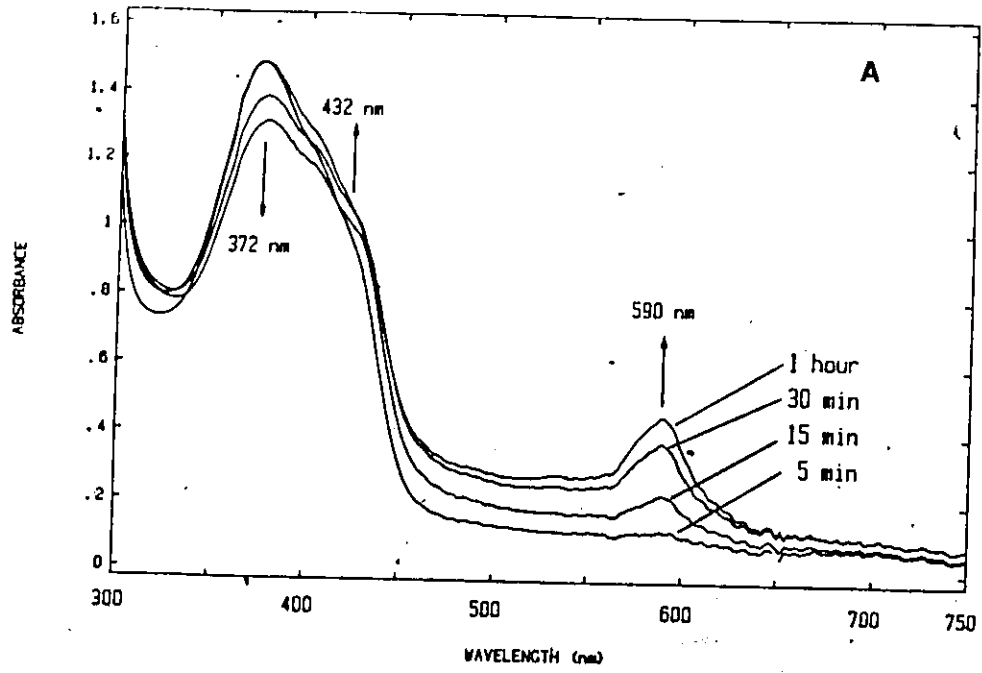
Figure 45

an extent that complete transfer of an electron may have taken place.
The slow appearance of the complex may have been due to slow breakup of
stacked DAP species in the aqueous media or because the concentration of
protonated DAP species was very low at pH 7. Co-workers showed that this
blue coloured species appeared instantaneously on addition of DNA if the
pH of the solution was close to the the pK_a (2.8 and 3.2) of the DAP
amino groups.

Instantaneous spectral changes were also observed when individual
solutions of the three ANPs 22, 33 and 32 were mixed with CT-DNA (Table
14). One explanation for these spectral changes is that the ANPs 22, 32,
and 33 can exist in a resonance form in which the amino nitrogen is
positively charged, and the nitro group is negatively charged. The
intimate contact between the ANPs and DNA could mean that the negative
charges on the phosphate groups favor the polarized canonical form. This
would lead to lowering of the excited state and hence the red shift.
This polarized canonical form is not possible for 1,8-DAP 23.
Interestingly, the shift in absorbance maximum observed with 1,6-ANP 33
was opposite to those observed with 1,3-ANP 32 and 1,8-ANP 22. This
suggested that the interaction of 1,6-ANP 33 and DNA was different than
the other ANPs, 32 and 22. These shifts were not accompanied by the
appearance of an ESR signal, and were reversed by addition of spermidine
or Mg^{2+}. From these data, the interaction between the ANPs 32, 33 and 22
and CT-DNA appeared to be different than observed with the DAPs 23, and
39.

II.4.2 Circular Dichroism

Circular dichroism (CD) spectroscopy is a technique which can be used to probe changes in the structure of compounds which contain asymmetric centers. A circular dichroism spectrum is a plot of the difference of extinction coefficients of left (ϵ_1) and right (ϵ_r) circularly polarized light as a function of wavelength. This difference in extinction coefficients is termed the Cotton effect. Chiral compounds, or compounds such as DNA which have an asymmetric secondary structure, will have a distinctive CD spectrum. Changes in this spectrum can indicate a change in conformation of the molecule. Compounds such as 1,8-ANP 22 and 1,8-DAP 23, do not have an asymmetric center and do not exhibit Cotton effects in dilute solutions.

The CD spectra of DNA, and DNA which had been interacted with proflavine, and 1,8-ANP 22 are shown in Figure 46a. The CD spectrum of CT-DNA alone showed that it was in the B configuration. This configuration is typical of DNA under the experimental conditions used (117). The CD spectrum of the DNA which had been interacted with proflavine showed slightly increased positive and negative Cotton effects at 219 nm and 272 nm respectively. These slight increases are consistent with the slight elongation of DNA which occurs during intercalation. The CD spectrum of DNA which had been interacted with 1,8-DAP 23 or 1,6-DAP 39 showed no changes (data not shown). However, the spectrum of DNA which had been interacted with 1,8-ANP 22 showed a large negative Cotton effect (Figure 46b). This change was approximately 10 times as great as the change observed with proflavine. Similar CD changes were observed with 1,6-ANP 33 and 1,3-ANP 32 (data not shown).
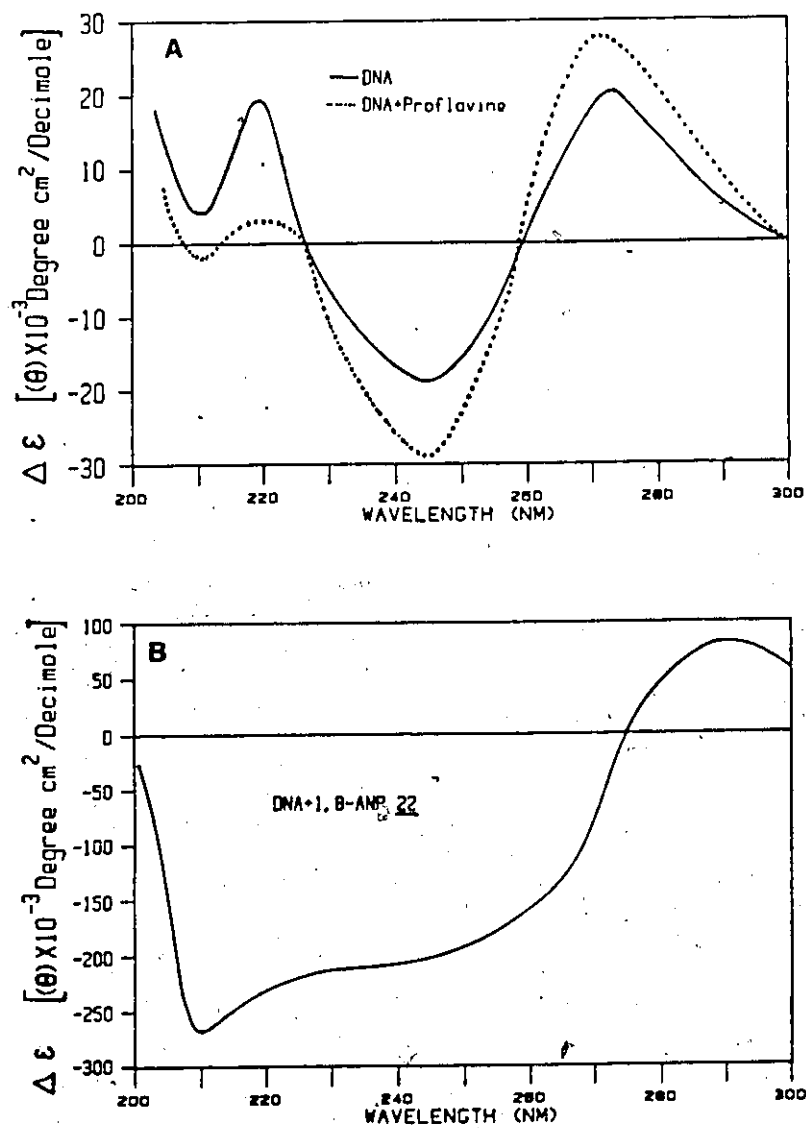
Figure 46: Circular dichroism spectra of (a) CT-DNA and CT-DNA after interaction with proflavine **54** and (B) CT-DNA after interaction with 1,8-ANP **22**. Spectra were acquired in 20 mM pH 7.2 phosphate buffer at a nucleotide concentration of 1.5×10^{-4} M, and compound concentration of 1.5×10^{-5} M (ratio of nucleotide:compound of 10:1)

Induced Cotton effects can be seen in the CD spectra of nonchiral compounds if they are closely bound in an asymmetric environment (118). The magnitude of the induced Cotton effect is a measure of the interaction between the bound species and the asymmetric environment (119). Therefore, the CD changes seen in the spectrum of DNA interacted with 1,8-ANP 22 may not arise from a conformational change in DNA, but from an induced Cotton effect in the 1,8-ANP 23 itself. The magnitude of the DNA CD spectral changes after interaction with intercalators (120,121), compounds which bind in the minor groove (122), and histones (123), were much smaller than those observed with 1,8-ANP 22.

The results of the CD spectroscopy indicate that the ANPs and the the DAPs interact with DNA in very different ways. 1,8-DAP 23 did not cause any changes in the CD spectrum of DNA which were typical of elongation of DNA. This is consistent with DAP binding to sites on the outer surface of the DNA. Reaction of 1,8-ANP 22 and DNA resulted in a CD spectra which was consistent with 1,8-ANP 22 closely bound in an asymmetric environment. Although the nature of this binding is unknown, it appeared to be very different from the 1,8-DAP 23-DNA binding.

II.4.3 Electrophoresis

Circular closed plasmid DNA can exist in a variety of forms which can be resolved by agarose gel electrophoresis. Compact, supercoiled DNA migrates fastest, followed by the more relaxed forms. The electrophoretic mobility of these different forms of plasmid DNA is also affected by compounds such as cis-platin which cause partial DNA uncoiling by intercalation (124). The results of agarose gel

electrophoresis of circularly coiled DNA which had been exposed to
increasing concentrations of 1,8-DAP 23 and 1,8-ANP 22 are shown in
Figure 47. The behaviour of control DNA and a positive control of DNA
interacted with cis-platin is shown for comparison.

The two bands observed in the control DNA lane were due to super
coiled, and relaxed DNA. The positive cis-platin control showed that as
the concentration of intercalator increased, the mobility of the altered
DNA increased and resulted in diffuse bands of DNA characteristic of
unwinding and rewinding effects (125). This type of behaviour was not
observed with either 1,8-DAP 23 or 1,8-ANP 22. As the concentration of
1,8-DAP 23 increased, more of the DNA precipitated in the well. The
electrophoretic mobility of DNA which had been interacted with 1,8-ANP 22
was identical to that of control DNA. These observations demonstrate
that 1,8-ANP 22 and 1,8-DAP 23 interacted with plasmid DNA, but in a
manner different than cis-platin.

The results of UV-VIS, ESR, and CD spectroscopy, and
electrophoresis of DNA which had been interacted with ANPS or DAPS
indicated that these compounds did interact with DNA in noncovalent
fashion. The ANPs and DAPs bound to different sites, or to the same site
in different ways. The DAPs appeared to bind on the outer surface of
DNA, possibly to the phosphate backbone. This binding resulted in the
formation of charge transfer complexes. The UV-VIS and CD results
demonstrated that the ANPs were closely bound to DNA in an asymmetric
environment.

DIRECTION OF MIGRATION

Lane   1   2   3   4   5   6   7   8   9   10
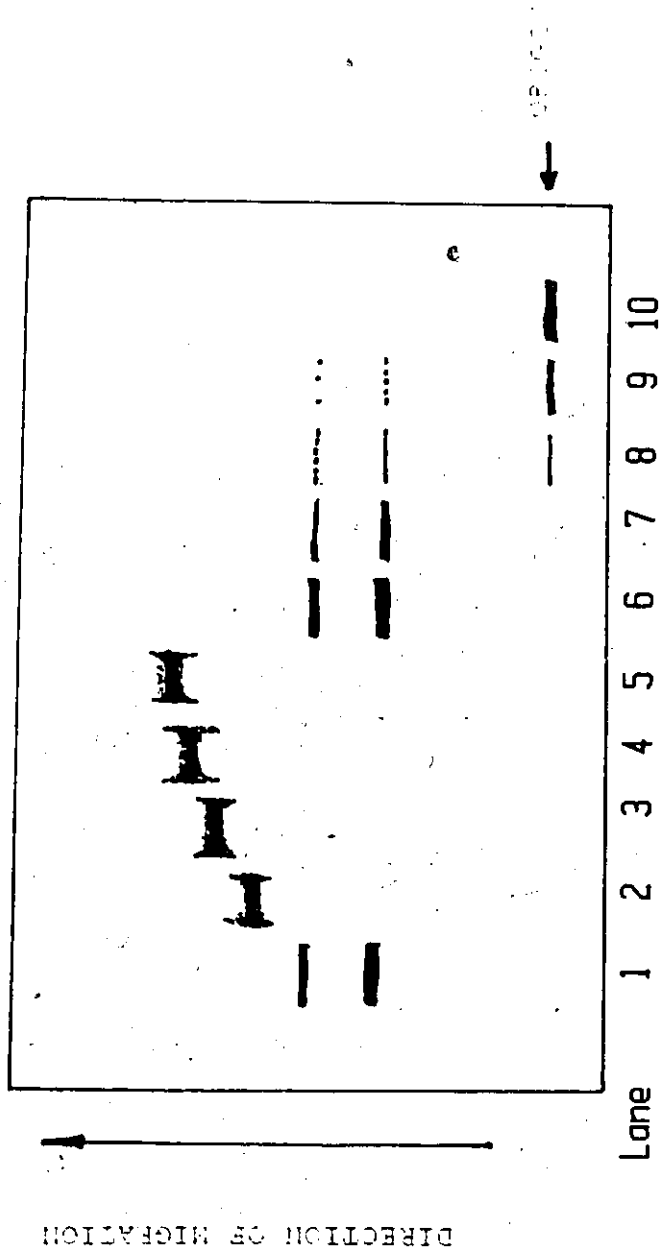
Figure 47: Electrophoresis of closed circular DNA, before and after interaction with cis-platin and 1,8-DAP 23. In all lanes DNA was at concentration of 100 μg/mL. Lane 1; control DNA. Lanes 2-5: cis-platin/DNA, cis-platin:nucleotide ratios were .1, 1, 3 and 8 respectively. Lanes 6-10:1,8-DAP 23/DNA, DAP:nucleotide concentrations were .1, .96, 1.93, 3.86, and 9.6 respectively.

These data indicate that although the DAPs and ANPs interacted with DNA, they did not intercalate. Therefore, it seems unlikely they contribute to the mutagenic activity of the DNPs by acting as intercalators.

II.5 Comments on the Formation of DNP-DNA Adducts.

The results discussed in Sections II.3 and II.4 clearly demonstrate that metabolism of 1,8-DNP 10 by *S.typhimurium* TA98NR resulted in covalent formation of a single adduct. This adduct was shown to be identical to the adduct formed *in vitro* by the reaction of 1,8-HANP 27 and CT-DNA. The structure of this adduct was shown by UV-VIS spectroscopy, NMR, and MS to be the result of bond formation between position 8 of 2'-dG 20, and the amino group of 1,8-ANP 22. Similar *in vitro* adducts were shown to be formed by the reaction of 1,3-HANP 34, and 1,6-HANP 35 with CT-DNA.

II.5.1 Adduct Formation at Sites Other Than C-8 of 2'-dG.

These observations raise many questions. Why was only one type of adduct observed in this study? Covalent adduct formation by other mutagens often resulted in formation of more than one type of adduct (Section I.4, Figure 4). Specifically, why were no adducts observed which resulted from electrophilic attack at other nucleophilic sites on 2'-dG 20 (N^2, O^6), or other nucleosides? Is there any evidence of formation of the analogous "reduced" adduct in which the nitro group has been reduced to an amino group?

A simple answer to these questions is that other adducts may have been formed, but at levels below the detection limit of the HPLC assay used in this study. Many of the smaller peaks in HPLC chromatograms of DNA hydrolysates (Figures 21, 22, 23 and 25) could have been due to other adducts. The detection of tritium labelled adducts was limited by the relative low counting efficiency associated with tritium.

During the course of this work, a more sensitive assay for the detection of modified nucleosides, based upon the method of Gupta *et al* (56), was evaluated. In the first step, modified DNA was hydrolysed enzymatically to the 3'-monophosphate nucleotides. Extraction of the modified nucleotides into n-butanol was aided by an ion pairing reagent, t-butyl ammonium chloride. Nucleotide adducts were then labelled in the 5'-position with γ-[^{32}P]-ATP, a process catalyzed by nucleotide kinase. After four dimensional thin layer chromatography (TLC), separated [^{32}P] labelled adducts were visualized by autoradiography.

Reaction of 1,8-HANP 27 with CT-DNA gave rise to 10 distinct spots after four dimensional TLC. One spot, which contained most of the radioactivity, was postulated to be the 1,8-adduct 48 described in this study. The behaviour of this labelled adduct in acid and base was consistent with that described in Section II.3.1. Treatment of the adduct with NaBH$_4$ resulted in a new spot which presumably was the "reduced" 1,8-adduct 51 . This spot did not correspond to any of those obtained from the hydrolysis of DNA modified *in vivo* by the bacterial metabolism of 1,8-DNP 10.

Alternating copolymer (dA-dT) was also reacted with 1,8-HANP and carried through the post-labelling procedure. Although adduct formation

appeared to be low, at least one product chromatographed with a product derived from reaction of 1,8-HANP 27 with CT-DNA This provides direct evidence that DNPs 8-10 may react with residues other than 2'-dG 20.

Why adduct formation occurred mainly at C-8 of 2'-dG 20 is a matter of conjecture. In studies of nitro-PAH, Rosenkranz et al (126) hypothesized that because of steric hinderances, nitro-PAH with more than two rings could not react with the electronicaly preferred N^2 and O^6 sites. Adduct formation therefore occurred at the more accessible C-8 position.

Kadlubar et al suggested that attack at exocyclic N^2 and O^6 centers was due to a reaction mechanism predominately S_n1 in character (48). Substitution at the ring positions, C-8 and N-7, were due to mechanisms which were more S_n2. 1,8-Adduct 48 formation at C-8 may be hypothesized to result from attack of 1,8-HANP 27 or the acetoxy derivative 28, rather than the nitrenium ion derived from these species.

II.5.2 The Relationship Between Mutagenicity and DNA-Adduct Formation.

Another question relating to adduct formation centers on the role the C-8 adduct plays in the expression of mutagenicity of the DNPs 8-10. Why are the DNPs 8-10 more active in bacterial test strains than other nitro-PAH? Heflich et al (52) have demonstrated that adduct for adduct, 1,8-DNP 10 and 1-NP 7 induce an equal number of mutations. The greater mutagenicity of 1,8-DNP must therefore be due to the fact that adducts are formed more readily.

While there is no direct proof that the C-8 adduct is responsible for the mutagenic effects of DNP, there is indirect evidence to suggest

that the C-8 adduct is important. Beland *et al* studied the carcinogenic activity, and nature and extent of adduct formation of a number of arylamines (54). The arylamines that produced predominantly, or in some cases, solely 2'-dG C-8 adducts, were more active bladder and liver carcinogens and produced more adducts.

The formation of DNP-DNA adducts may be more facile than other nitro-PAH adducts, such as 1-NP 7, because of the relative stability of the DNP-N-hydroxyl intermediate. The stability of this intermediate may result in an increased opportunity for acetylation of the N-hydroxyl derivative to the more reactive acetoxy derivative. This in turn may account for the greater number of DNP-DNA adducts formed per unit length of DNA, compared to 1-NP-DNA adducts.

The non-covalent interactions discussed in Section II.4 may also play a role in the facile formation of DNP-DNA adducts. By UV-VIS and CD spectroscopy, 1,8-ANP 22 was shown to rapidly form closely bound complexes with DNA. If 1,8-ANP 22 can act as a model for the N-hydroxyl 27 or N-acetoxy 28 derivatives, then this this interaction could raise the "local" concentration of these reactive species at the surface of DNA.

At present, little is known of the effect C-8-DNP or C-8-NP adducts have on the structure of DNA, or how persistent the adducts are in target tissues. These adducts probably do not result in the "insertion-denaturation" DNA perturbations characteristic of N-acetoxy-acetylaminofluorene adduct formation (127). This type of DNA perturbation is only observed when the bridging nitrogen is substituted with an acetyl group.

Kadlubar *et al* suggested that enzymatically catalyzed imidazole ring opening of dG-C8 adducts may occur *in vivo* (48). These ring-opened derivatives could then act as intermediates in DNA excision processes. Partial repair could lead to apurinic sites, or ring opened guanine residues if the ANP moiety was cleaved.

III. EXPERIMENTAL.

III.1 Materials.

HPLC grade methanol, acetonitrile, isopropanol, and hexane were purchased from Caledon Laboratories Ltd. (Georgetown, Ont.). HPLC grade water was prepared by passing distilled water through a Milli-Q (Millipore Corp., Bedford, MA) water purification system. Chloroform, DMF, diethyl ether, DMSO, n-butanol, acetic anhydride were of reagent grade and were purchased from BDH Chemicals (Toronto, Ont.). Fuming nitric acid was purchased from J.T.Baker Chemical Co. (Jackson, TN). Technical grade 95% ethanol was purchased from Commercial Alcohols Ltd. (Toronto, Ont.)

Pyrene, m-chloroperbenzoic acid, histidine, biotin, CT-DNA, 2'-deoxyribonucleosides and all enzymes used in the enzymatic hydrolysis of DNA were purchased from Sigma Chemical Co. (St. Louis, MO). Sulphur, sodium hydroxide, cadmium chloride, sodium ascorbate, and all buffers were purchased from BDH Chemicals (Toronto, Ont.). $Na_2S \cdot 9H_2O$ was purchased from Mallinkroft Chemicals (Paris, Kentucky,). Pt_2O_5 and 10% Pd on charcoal was purchased from Aldrich Chemical Co. (Milwaukee, Wis).

Preparative chromatography was performed on Aluminum oxide 90, neutral, 70-230 mesh, and Kieselgel 60 230-430 mesh silica gel purchased from E.M. Merk (Darmstadt, Germany) or silica gel, 60-120 mesh, purchased from BDH Chemicals (Toronto, Ont.).

III.2 Instrumentation

III.2.1 General Instrumentation.

pH measurements were performed on a Sargeant Welsh NX pH meter equipped with a combination pH electrode. The pH meter was calibrated with Colour Key BDH standard pH 4.0, 7.0 and 10.0 buffers.

Tritium radioactivity was determined by mixing samples with Amersham ACS aqueous counting scintillant in 12 mL plastic scintillation vials. Vials were counted for radioactivity in a Beckman LS9000 liquid scintillation system (Irvine CA) to an uncertainty of 5% to 15%.

III.2.2 HPLC, TLC, and Electrophoresis.

RPLC and NPLC were performed using Spectra Physics 8000, Spectra Physics 8700 (Santa Clara, CA), and Beckman 110A (Fullerton, CA) solvent delivery systems with UV monitoring of the eluent at 254 nm using Beckman 153 or Beckman 160 UV detectors. A Spectra Physics 770 detector was used for variable wavelength monitoring of the eluent. An HP-1090 liquid chromatograph equipped with a HP-85 computer for data acquisition and a diode array detector for simultaneous wavelength monitoring and UV-VIS spectra acquisition (Palo Alto, CA). Unless stated, fixed 10 or 20 μL loop/valve injectors were used for all sample injections.

The eluent was monitored for fluorescence by a Kratos FS950 Fluoromat fluorescence detector (Westwood, NJ) equipped with a 344 nm to 375 nm band pass excitation filter and 418 nm cutoff emission filter. Fractions were collected in an ISCO 10 model 328 fraction collector (Instrument Specialties Co. Lincoln, Neb.).

The following columns were used and will be referred to as such in the text:

Reverse Phase Columns

A Hibar Licrosorb RP-18, 10 μm, 250 mm x 4.6 mm

   (E. Merk, Darmstadt, F.R. Germany)

B Altex Ultrasphere ODS, 5 μm, 250 mm x 4.6 mm

   (BDH Chemicals, Toronto, Ont.)

C Alltech Licrosorb RP-18, 10 μm, 250 mm x 4 mm

   (Alltech Assoc., Deerfield, NJ)

D Hibar Licrosorb RP-18, 5 μm, 250 mm x 4 mm

E Hibar Licrosorb RP-18, 5 μm, 125 mm x 4 mm

F Partisil ODS-2, Magnum 9, 10 μm, 500 mm x 9 mm

   (Whatman, Inc., Clifton, NJ).

G Vydac C-18, 10 μm, 250 mm x 4 mm

   (The Separations Group, Hesperia, CA)

Normal Phase Columns

G Altex cyano, 5 μm, 250 mm x 4.6 mm

H Altex cyano, 5 μm, 250 mm x 10 mm

Thin layer chromatography (TLC) was performed on Merck silica gel 60 F254 pre-coated plastic sheets 0.2 mm in thickness. Compounds were visualized by their fluorescence after irradiation with a model UVGL-Mineralight UV lamp.

Electrophoresis of plasmid DNA was carried out using agarose gel (10 cm x 20 cm) prepared according to the method of Maniatis et al (128).

Stock solutions of plasmid DNA (0.12 nmole phosphate/μL), 1.8-ANP <u>23</u>

(0.018 nmole/μL) and 1,8-DAP <u>23</u> (0.012 nmole/μL) were freshly prepared in

phosphate buffer (10 mM, pH 7). Aliquots of each solution (10 μL) and a

mixture of 0.25% bromphenol blue and 40% (w/v) sucrose (5 μL) were added

to each well. Electrophoresis for 16 hours occurred at 25mV and maximum

amperage.

II.2.3 UV-Visible, ESR, and NMR Spectroscopy

UV-VIS spectra were acquired on a Perkin Elmer Lamda 9, HP-8451

(Palo Alto CA), and Beckman 253 UV-VIS spectrometers. Fluorescence

spectra were acquired on a Perkin Elmer LS-5 spectrofluorimeter with a

398 nm cutoff filter. Circular dichroism (CD) spectra were acquired on

an AVIV spectropolarimeter (Palo Alto,CA). CD spectra were acquired by

scanning from 600nm to 300nm and then from 300nm to 200nm acquiring data

every nm with a 1.5 nm bandwidth. All spectra were acquired in 1 cm

cells at room temperature.

Electron spin resonance (ESR) spectra of aqueous samples in

capillary tubes were obtained on a Bruker ER-100D electron spin resonance

spectrometer using a T_m-4103 cavity. Microwave frequency was 9.46 GHz at

14.5 dB with field modulation frequency of 100KHz at 10 G$_{pp}$. Magnetic

field was set at 3368G midrange and scanned 100G in 50 sec.

Proton nuclear magnetic resonance (NMR) spectra were obtained at

500 MHz on a Bruker AM-500 and at 250 MHz on a Bruker WM-250. 400 MHz

spectra were acquired on a Bruker AM-400 at the Regional NMR Facility,

University of Guelph, Guelph Ont. NMR absorbances are reported in parts

per million (ppm), and coupling constants are reported in Hz (1/sec).

Spectra were obtained in methanol-d$_4$ or DMSO-d$_6$ as solvents. Methanol and DMSO were used as internal references with trimethylsilane (TMS) as 0 ppm.

III.2.4 Mass Spectrometry.

Mass spectrometry on both derivatized and non-derivatized compounds were performed by Dr. Quilliam, Mr. F. Ramelan, Mr. T.S. Kapron, and Dr. R. Smith of the McMaster University Regional Mass Spectroscopy Centre, Hamilton, Ontario.

III.2.4.1 Field Desorption Mass Spectrometry

Field Desorption (FD) spectra were acquired by Dr. M. Quilliam (McMaster University) on a Varian CH5D mass spectrometer (University college, Cardiff, Wales) equipped with a Varian SS 100 data system. Conditions used for spectra acquisition were:

Emitter: Benzonitrile activated; tungsten

Source: combined FD/Field ionization/EI

Source Temperature: 80°C

Emitter Current: 23 mA.

Acetone was used for tuning and spectra were acquired by dipping the emitter in a solution of the analyte (1-5 mg/mL) in DMF.

III.2.4.2 Fast Atom Bombardment and LC-FAB Mass Spectrometry.

The conditions for LC FAB-MS are described in Table 15. An HP-1090 HPLC solvent delivery system, VG belt interface, and VGZAB-E mass spectrometer were used in the analyses. The sample was dissolved in acetonitrile and 20 μL of the solution was injected into the HP-1090. No glycerol or other FAB matrix was added to the eluting solvent. Glycerol was used for the initial tuning and calibration.

Probe FAB analyses were performed using the MS condition described in Table 15 except mass scanning was from 1000 to 50 amu at 3 seconds/decade. Glycerol was used for initial tuning and mass calibration. Sample were prepared at approximately 1μg/μL in DMF. 1-2 μL of stock solution was mixed with 2-4 μL of FAB matrix and 2-4 μL of the resulting solution was loaded onto the probe.

III.2.4.3 Probe DEI and DEI MS.

Typical conditions for the DEI and DCI MS analyses of silylated derivatives described in Table 16. Reaction conditions for silylation of adducts 46, 47 and 48 are described in III.5.5. 1-2μL of sample in DMF (0.1-1 μg/μL) was loaded onto the filament of the DCI probe, and the probe was inserted into the source. After derivatization reaction by-products were allowed to volatilize, current was applied to the filament and spectral acquisition begun.

Table 15: Conditions for FAB and LC-FAB MS

Mass Spectrometer

Ionization mode: FAB
FAB gun: Xe gas at 8 kV
Source Temperature: 180°C
Accelerating Voltage: 4kV
Scan function:Exponential Scan, 700 to 174 amu, 3 sec/decade
Resolution: 2500 (10% valley)

Interface

Belt Speed: 2 cm /min
Sample Heater: 7 (dial setting)
Solvent Evaporator: 6 (dial setting)

RPLC

Column: Ultrasphere ODS-2, 250X4.4 mm, 5μm
Mobile Phase: 80/20 acetonitrile/water, isocratic
Flow Rate: 1 mL/min

Table 16: Conditions for DEI and DCI MS

Ionization mode: DCI

Source Temperature: 200°C

Accelerating Voltage: 4 kV

Source Pressure: 3×10^{-6} torr

Scan function: Exponential Scan, 1200 to 60 amu
                3 sec/decade

Resolution: 2500 (10% valley)

Probe Filament Heating Rate: 2 (dial setting)

III.3 Synthesis of 1-NP 7 and Disubstituted Pyrenes

This section describes syntheses of the disubstituted pyrenes as described in II.2. The columns used in the RPLC and NPLC analyses of intermediates are described in III.2. All spectroscopic and chromatographic data are tabulated in Appendix B. Unless stated, each intermediate was used as starting material for the next step without further purification. This was necessary because most of the intermediates were unstable or biologically very hazardous. Syntheses were carried out in a laboratory designed for working with biologically hazardous compounds. Further detailed characterization was carried out by co-workers.

III.3.1 Nitration of Pyrene.

This procedure is a modification of that of Streitweiser et al (91). To acetic anhydride (90 mL) cooled in ice water was added cautiously with stirring, fuming nitric acid (90% HNO_3, 10 mL). Caution: unmoderated large scale reactions have been observed to become very warm and erupt from the reaction vessel. To a solution of pyrene (480 mg, 2.37 mMole) in acetic anhydride (72 mL) cooled in ice water, was added dropwise with stirring, the above nitrating reagent (104 mL, 100 equivalents). The reaction mixture turned yellow upon addition of the nitration reagent, and soon a yellow precipitate separated from the solution. After 15 minutes the reaction mixture was filtered. The mother liquor was decomposed with ice water and the yellow filtrate was treated with an equal volume of water (200 mL). The two phase mixture in a flask was placed in a water or ice water bath and stirred for 1 hour.

The collected yellow product was washed with water to afford 283 mg of crude dinitropyrene isomer mixture (62 % yield). NPLC analysis of this product (Column G, IPA/Hexane, 10/90, 2 mL/minute) showed that it contained 1,3-DNP 8, 1,6-DNP 9, 1,8-DNP 10 and 1-NP 7. There was no evidence of unreacted pyrene.

Semi-preparative NPLC (Column H, 95:5 hexane:IPA, 4 mL/min) was successful in separating all four components of the nitration mixture. The poor solubility of the DNP isomer mixture in the mobile phase limited the use of this method to small scale preparations only.

An attempt was made to extract 1,3-DNP 8 from a mixture of the three DNP isomers on a preparative scale using the method of Kaplan et al (100). Four portions of the DNP isomer mixture (4 x 500 mg) were stirred for 14 hours in acetonitrile (4 x 400 mL). The solutions were filtered and the collected supernatant was evaporated under reduced pressure to afford a total of 490 mg of acetonitrile soluble residue (17% yield). The 1,3-DNP content in the starting DNP isomer mixture and acetonitrile soluble residue were analysed by NPLC (Column G, 5/95, IPA/hexane, 2 mL/min).

III.3.2 Reduction of DNPs 8-10 to DAPs 38, 39, and 23.

To yellow needles of dinitropyrene mixture (472 mg, 1.62 mmole) slurried in methanol (200 mL) was added Pt(IV)O$_5$ or 10% Pd on charcoal (50 mg). The heterogeneous solution was blanketed with hydrogen and stirred for 15 hours. TLC analysis (Kiesel gel 60F silica gel, ethyl acetate/DCM, 10/90) of the green, highly fluorescent solution showed that

it contained 1-AP 30, 1,3-DAP 38, 1,6-DAP 39, and 1,8-DAP 23
(R_fs: 0.88, 0.60, 0.41, 0.30 respectively). There was no evidence of
unreduced dinitropyrenes.

III.3.3 Preparative Flash Chromatographic Separation of DAPs 38, 39 and

23.

The methanol solution of DAP isomers described above was filtered
to remove catalyst, water deactivated flash silica (5 gm Kieselgel 60,
230-400 mesh) was added and the methanol was evaporated. This silica was
slurried in 10 mL hexane and applied to the top of a column (1" x 11") of
flash silica (Kieselgel 60, 230-400 mesh). The flash silica was packed
in a section of copper tubing (1" x 12") equipped with stainless steel
end fittings. This column was constructed to withstand the high pressures
generated by the high flow rates (93 mL/min). Glass wool was packed on
top of the added silica and the top fitting was tightly secured. The DAP
isomers were eluted (ethyl acetate/DCM, 10/90, 93 mL/minute) and 20 mL
fractions collected for TLC analysis. (TLC conditions as in III.3.2).
After 20 min the eluent appeared clear, colourless and free of
fluorescent material.

III.3.4 Attempts to Oxidize DAPs 38, 39 and 23 to ANPs 32, 33 and 22.

Attempts to oxidize 1,6-DAP 39 and 1,8-DAP 23 to 1,6-ANP 33 and
1,8-ANP 22 with 6 mole equivalents of MCPBA were not successful.
Oxidation of these starting materials resulted in a mixture of products
in various oxidation states.

The oxidation of 1,3-DAP <u>38</u> resulted in production of 1-nitroso-3-aminopyrene a derivative intermediate in oxidation state between 1,3-DAP <u>38</u> and 1,3-ANP <u>32</u>. To 1,3-DAP (115 mg, .49 mmole) in DCM (145 mL) was added MCPBA (500 mg, 2.9 mmole, 6 equivalents). The solution was blanketed with nitrogen, stirred for 12 hours and excess MCPBA removed in the normal fashion. Evaporation of the DCM afforded a violet residue (85 mg) of 1,3-NOAP which was pure by NPLC (Column G, 95/5 IPA/hexane, 2 ml/min).

II.3.5 Oxidation of DAPs <u>38</u>, <u>39</u> and <u>23</u> to NONPs <u>40</u>, <u>41</u>, <u>21</u>, and

   DNPs <u>8-10</u>.

This procedure is a modification of the procedure of Robinson *et al* (129). Optimal oxidizing conditions were determined using a mixture of the DAP isomers. Excess MCPBA, and dilute reaction conditions were used to prevent azo dimer formation.

The concentration of DAP isomer in each of the pooled fractions was estimated on the basis of 100% recovery of each DAP after flash chromatography. To each pooled fraction (175-250 mL) was added at least 20 equivalents MCPBA. The solution immediately turned deep brown in colour. After stirring for 15 hours, excess MCPBA was removed from the reaction mixture by extracting with 3 x 500 mL 0.1 N $NaHSO_3$, 3 x 500 mL 0.1 N $NaHCO_3$, and 3 x 500 mL water. The organic layer was evaporated affording an orange residue. The residue was dissolved in a minimal volume of DCM and eluted on a silica column (2 x 12 cm, 100% DCM). NPLC analysis of the fast moving yellow band demonstrated it contained DNP and NONP, typically in a 4:1 ratio.

III.3.6   Polysulphide Reduction of DNPs and NONPs to ANPs.

This procedure is a modification of that of Porter *et al* (94). The conditions used by Porter were varied to determine optimal conditions for maximal reduction of DNP isomer mixture and minimum side product production. This procedure was used for the reduction of DNP isomer mixtures produced by the direct nitration of pyrene, and DNP/NONP isomer mixtures produced by the oxidation of the corresponding DAP isomers. Each starting material could be fully reduced to the ANP isomer mixture or corresponding ANP isomer respectively.

To water (16 mL) was added with stirring, $Na_2S \bullet 9 \, H_2O$ (8 gm) and powdered sulphur (4 gm). The solution was stirred for 30 minutes or until the straw yellow colour of polysulphide appeared. In a typical experiment, a 200 mL three necked flask, equipped with septa on the side arms, was charged with a DNP or DNP/NONP mixture (100 mg, 0.350 mmole), absolute ethanol (35 mL), chloroform (35 mL) and was gently refluxed with stirring for 25 minutes under a nitrogen atmosphere. Polysulphide solution (3 mL), and 0.1 N sodium hydroxide (3 mL) were introduced simultaneously through the septa with glass syringes. The yellow solution immediately turned a deep red colour. The progress of the reduction was followed by NPLC (Column G, 5/95, IPA/hexane, 2mL/min) or by TLC (100% DCM). After 15 minutes, additional polysulphide solution (2mL) was added and the reaction was allowed to proceed for one hour.

The red solution was cooled to room temperature, filtered, and partitioned between buffer (200 mL, 0.25 mM phosphate, pH 8) and DCM (200 mL). This solution was stirred vigorously with a cadmium chloride

solution (0.1 N, 200 mL) and the heterogeneous mixture was filtered to remove precipitated cadmium sulphide. The DCM was evaporated under reduced pressure and the residue subjected to repeated dissolution in DCM, and filtration, until no white sulphur precipitate was observed upon dissolution of residue. Five gm of silica gel (BDH, 60-120 mesh) were added and the DCM evaporated under reduced pressure. This silica was slurried in 10 mL hexane, applied to the top of a silica gel column (BDH, 60-120 mesh, 2 cm x 18 cm) and eluted with DCM. A fast eluting yellow fraction contained residual DNP and soluble sulphur species while a later eluting red fraction contained ANP. Typical yields ranged from 62 mg (0.23 mmole, 66%) to 70 mg (0.26 mmole, 77%).

III.3.7   Oxidation of ANPs 32,33 and 22 to NONPs 40,41 and 26.

In a typical experiment, to DCM (5mL) was added either pure ANP isomer, or a mixture of ANP isomers (50mg, 0.202 mmole) and DCM (0.50 mL) containing MCPBA (68 mg, 0.404 mmole, 2 equivalents). The red ANP solution immediately turned orange and a precipitate formed. The mixture was gently heated in a water bath (50 °C) for one minute, 3 gm of water-deactivated silica gel (BDH, 60-120 mesh) was added and the solvent evaporated under reduced pressure. This silica was slurried in hexane (7 mL), applied to the top of a silica gel column (BDH, 60-120 mesh, 2 cm x 11 cm), and eluted with DCM. Two fractions were collected, a fast running orange fraction containing only NONP, and a slower moving red fraction containing unreacted ANP. Unreacted ANP was oxidized and

chromatographed as described above. NONP containing fractions from the two separations were combined. Typical yield of NONP was 0.130 mmole (65% yield).

III.3.8   Reduction of NONPs 40,41 and 26 to HANPs 34, 35 and 27.

Reduction of the NONPs 40,41 and 26 to the corresponding HANPs 34, 35, and 27 was not performed until *in vitro* reaction of the HANPs with CT-DNA was to take place. Typically, 5 equivalents of ascorbate in DMF (5 mL) was added to a stirred orange solution of NONP (1 equivalent) in DMF (5 mL). The solution immediately turned red in colour.

III.3.9   Nitration of [^{3}H]-Pyrene

Tritiated pyrene (38 Ci/mmole, 10 mCi/mL in methanol) was custom synthesized by Amersham Corp., Oakville, Ont. [^{3}H]-pyrene (38 mCi, 1 mmole) in ethanol (3.8 mL) was evaporated in a test tube under a stream of nitrogen. The residue was dissolved in acetic anhydride (300 μL) and nitrating reagent (300 μL) was added. After two minutes an orange precipitate appeared. After five minutes the reaction was slowly quenched with 1% sulphuric acid (600 μL) and stirred in an ice-water bath for 45 minutes. The resulting solution was partitioned twice between ethyl acetate (2 mL) and 4 N NaOH (1.5 mL). The ethyl acetate layers were combined and evaporated under a stream of nitrogen.

The crude residue contained both mono and dinitrated pyrene, as well as unreacted pyrene as determined by NPLC. The clean up of this crude residue consisted of a crude RPLC separation (Column A, 80/20 acetonitrile/water, 2 mL/min) obtaining a crude pyrene/1-NP 7 fraction

(1.6 to 2.2 min) and a crude DNP fraction (2.4 to 3.5 min). The three tritiated DNP isomers were then separated and isolated by NPLC (Column H, 95/5 hexane/IPA, 4 mL/min). UV-VIS spectra of fractions containing tritiated DNP isomers were acquired and aliquots (25 μL) counted for tritium. Typical activities were 14-18 Ci/mmole for [^{3}H]-1-NP 7, and 2 to 6 Ci/mmole for the [^{3}H]- DNPs 8-10.

III.4 Metabolism of 1-NP 7 and 1,8-DNP 10 by *S.typhimurium TA98*.

A solution of Davis Mingioli salts was prepared by dissolving in water (1 L), K_2HPO_4 (28 gm), KH_2PO_4 (8gm), $(NH_2)_2SO_4$ (4 gm), trisodium citrate (1 gm) and $MgSO_4$ (400 mg). A minimal media was produced by diluting the Davis Mingioli salts (200 mL) with water (600 mL).

S.typhimurium strain TA98 was obtained from Dr. H. Rosenkranz, Case Western Reserve University, Cleveland OH. Bacteria were grown in minimal media Davis Mingiola salts (400 mL), plus 10 mM biotin (5 mL), 10 mM histidine (25 mL), and 40% w/v glucose (2 mL) for 12 hours at 37 °C. After 12 hours the cultures were diluted 2:1 with fresh media and the bacteria were allowed to grow until they were in log phase (2-2.5 hour). For metabolism studies, typically a 100 mL aliquot of bacterial culture was then treated with either tritium labelled or unlabelled 1-NP 7, or DNPs 8-10.

To recover metabolites from the medium, the cells were spun down (3000 rpm, 15 min) and the resulting supernatant was extracted with DCM (2 x 100 mL). The DCM was evaporated and the residue was analyzed by RPLC. If tritium labelled starting material was used, the cell pellet was saved for DNA binding and adduct characterization studies.

III.5   Disubstituted Pyrene-DNA Adduct Formation, Isolation, and

Derivatization of Adducts 46,47 and 48.

This section describes the conditions used for the *in vivo*

modification of DNA in *S.typhimurium* TA98NR by [^{3}H]-1,8-DNP 10 or *in*

vitro modification of CT-DNA by HANPs 34,35 and 27. The enzymatic

hydrolysis of these modified DNAs and the RPLC purification of the DNA

adducts and the conditions for the silylation of the HANP-2'-dG adducts

46,47 and 48 are also described.

III.5.1   *In Vivo* [^{3}H]-1,8-DNP-DNA Adduct Formation and Isolation

S.typhimurium strain TA98NR was obtained from Dr. H. Rosenkranz,

Case Western Reserve University, Cleveland OH. A bacterial culture

(200 mL) of *S.typhimurium* TA98 was grown and incubated with [^{3}H]-1,8-DNP

as described in III.4. The cells were centrifuged (15 min, 3000 rpm) and

the cell pellet was washed twice in buffer (40 mM phosphate, pH 7) and

EDTA (25 mM). To the suspension (5 mL), was added protease (5 mg), 10%

w/v SDS (3 mL) and the mixture was incubated with shaking for 2 hours at

37 °C. Ribonuclease (10 mg) was added and the clarified cell lysate was

incubated for a further 30 minutes at 37 °C. The cell lysate was dialysed

against several changes of TRIS buffer (20 mmole, pH 7.2) for 6 hours.

The DNA concentration of the non dialysable fraction fraction was

determined by measuring its UV absorbance at 260 nm (ϵ_{260}

phosphate=6600). An aliquot (200 μL) was counted for tritium

radioactivity by liquid scintillation counting to determine the extent of

covalently bound tritium.

III.5.2   *In Vitro* Reaction of HANPs <u>34,35</u> and <u>27</u> with CT-DNA.

The procedure for reaction of HANPS <u>34,35</u> and <u>27</u> was a modification of that of Howard *et al* (50). An aqueous solution of CT-DNA was prepared by slowly stirring CT-DNA (250 mg) in citrate buffer (250 mL, pH 5), for 14 hours in a sterile screw capped bottle (500 mL). To this viscous DNA solution were added with stirring, DMF (112 mL), and a freshly prepared solution of HANP (35 mg, 0.13 mmole) in DMF (5mL). The HANP solution was generated by the ascorbate reduction of a the corresponding NONP isomer as described in III.3.8. The surface of the reaction mixture was blanketed with nitrogen and allowed to react for twelve to sixteen hours in the dark.

Water saturated phenol was prepared by warming phenol (400 gm) in a screw capped plastic bottle until liquified. Water (200 mL) was added, the mixture was stirred and the layers allowed to separate. Aliquots of the CT-DNA/HANP reaction mixture (30 mL) and water saturated phenol (20 mL) were placed in a 50 mL conical screw capped centrifuge tube, agitated to ensure thorough mixing and centrifuged at 2000 rpm to separate the layers. The lower phenol layer was removed with a 10 mL pipette and discarded. The process was repeated until no more colour was extracted into the phenol layer. The upper aqueous layers were combined, cooled to room temperature and extracted with diethyl ether (3 x 150 mL) in a 500 mL separatory funnel to remove phenol. This afforded a faintly orange coloured solution of modified-DNA. Residual diethyl ether was removed under reduced pressure and the remaining modified-DNA solution

was dialysed against several changes of TRIS buffer (2 L, 20 mM, pH 7) or

phosphate buffer (2 L, 20 mM, pH 7). The non-dialysable pink fraction

contained modified DNA which was hydrolysed to nucleosides.

III.5.3   Enzymatic Hydrolysis of Modified DNA.

The method of Martin *et al* was for the enzymatic hydrolyses of

modified DNA (105). Briefly, a solution of modified DNA (1 mg/mL) was

hydrolysed over a period of twelve to fifteen hours at neutral pH.

DNAse I was added to a concentration of 0.1 mg/mL and incubated at 37°C

for 3 hours. UV-VIS spectra of the modified-DNA solution were obtained

before and after treatment with DNAse I. Nuclease P_1 was then added to a

concentration of 20 μg/mL, alkaline phosphatase was added to 0.5 unit/mL

and acid phosphatase was added to 0.3 unit/mL. The solution was then

blanketed with nitrogen and incubated at 37°C for 12 to 16 hours. The

extent of enzymatic hydrolysis was followed by RPLC (Column C, 80/20

methanol/water, 1 mL/min isocratic).

The hydrolysate of DNA which had been modified *in vivo* with

[^{3}H]-1,8-DNP 10 was not subjected to further purification. The

hydrolysate from DNA which was modified *in vitro* was subjected to further

purification in order to partially separate the adducts 46 ,47 and 48

from unmodified nucleosides.

III.5.4   Isolation of HANP-Nucleoside Adducts 46,47 and 48 from CT-DNA
           Hydrolysates.

Water saturated n-butanol was prepared by adding water (30mL) to

n-butanol (100 mL). The mixture was shaken vigorously and the layers

were allowed to separate. To DNA hydrolysate (25 mL) in a 50 mL plastic

screw capped centrifuge tube was added water saturated n-butanol (10 mL).

The heterogeneous mixture was shaken and centrifuged (2000 rpm, 15 min)

to separate the layers. The lower orange coloured n-butanol layer was

removed and the process was repeated twice.

The n-butanol was evaporated and the residue was dissolved in 3:1

n-butanol:DMSO (1.5 mL). An aliquot (0.5 mL-1 mL) was loaded on the

column (50/50 methanol water, 4 mL/min). After the signal from the

unmodified nucleosides appeared and then returned to baseline, the mobile

phase was changed (80% methanol, 6 mL/min). The adduct, which appeared

as a sharp peak, 4.2 min after the appearance of the methanol solvent front

was collected, and rechromatographed until it was pure by RPLC.

III.5.5   Silylation of 2'-dG 20 and Adducts 46-48 for
           DEI and DCI Mass Spectrometry.

An aliquot of a solution of adducts 46-48 (prepared as described

above) or 2'-dG 20 in dry silylation grade DMF (Pierce Chemical Co.) were

diluted with fresh DMF to make a stock solution of concentration

1.25 μg/μL. To a dry, 1 mL Reacti Vial (Pierce Chemical Co.) was added

80 μL of stock solution (100 μg analyte) and 20 μL BSTFA or MSTBMS

(Pierce Chemical Co.). Derivatization was allowed to take place

overnight at room temperature. MS analysis of the TMS derivatives was

then performed immediately because of their instability. The TBDMS

derivatives were stable for up to six months. However, long term

reaction resulted in increased formation of tetra- and pentakis- TBDMs

derivatives.

IV.   FUTURE WORK

There are many biological and chemical areas of study of the DNPs and nitro-PAH that require further investigation. The investigation of the reductive and oxidative metabolism of nitro-PAH, their DNA-adduct formation, the noncovalent interaction of their metabolites with DNA, and the determination if certain areas of DNA preferentially bind nitro-PAH, will aid in the further understanding of the biological activity of the nitro-PAH.   Furthermore, developing new syntheses of disubstituted PAH as well as investigating analytical techniques such as LC-MS, will aid in the study of metabolism and DNA adduct formation of the nitro-PAH.

IV.1 Metabolism and DNA Adduct Formation.

In this study only preliminary work was done on the relative degrees of covalent DNA binding of 1,8-DNP 10 versus 1-NP 7 in *S.typhimurium* TA98. This was undertaken in an attempt to explain the large difference in the mutagenicity of 1,8-DNP 10 and 1-NP 7. The DNA binding of these compounds and others such as 1,3-DNP 8, 1,6-DNP 9 in a variety of *in vivo* systems should be further investigated. These studies may aid in correlating DNA binding and mutagenic or carcinogenic activity of these compounds.

One of the aims of this study, as described in I.5, was to study the metabolism of all three DNP isomers by *S.typhimurium* test strains. Although this work focuses mainly on the metabolism of 1,8-DNP 10,

Initial studies showed that the metabolism of 1,3-DNP 8, and 1,6-DNP 9

occurred in a similar fashion. Further studies should be undertaken to

fully characterize the metabolites of these other DNP isomers.

In addition, because of time constraints, the RPLC characterization

of only the *in vivo* 1,8-DNP adduct, was undertaken. The tritium labelled

1,3-DNP and 1,6-DNP DNA *in vivo* adducts were not prepared, isolated and

compared to the *in vitro* adducts produced by reaction of 1,3-HANP 34 and

1,6-HANP 35 and CT-DNA. Although it was assumed that 1,3-DNP 8 and

1,6-DNP 9 would form analogous adducts as the *in vivo* 1,8-DNP adduct,

this should be confirmed.

The number of nitro-PAH that have now been detected in

environmental samples is steadily growing. Although the bacterial

metabolism of some of these compounds has been studied, comparison of

metabolism of these compounds with the DNPs may be interesting.

Investigation of the metabolites produced, their relative abundances, and

the time course of their rate of production may useful. Of special

interest is the oxidative metabolism of these compounds by mammalian cell

systems. Metabolites such as epoxides, diolepoxides, and quinones, which

are the result of oxidative metabolism, may also prove to mutagenic.

Although the bacterial metabolism of the DNPs 8-10 have been

thoroughly investigated by co-workers and other investigators, minor

metabolites which are intermediate in oxidation states between the major

intermediates may be yet be shown to be of biological importance. These

metabolites, such as 1-nitroso-8-aminopyrene, or 1-N-hydroxylamino-

8-aminopyrene may useful in studies of nitroreductase substrate

specificity. The N-hydroxy substituted pyrenes may prove useful in the study of structure activity relationships of these direct acting DNA arylating agents.

IV.2 Synthesis

The major difficulty in the synthesis of pure isomers of the DNPs 8-10 for use in metabolism studies lies not in the actual synthesis of the dinitrated species but in their purification. The majority of published procedures report that the standard method of producing pure isomers is to synthesize a crude mixture of the DNPs 8-10 by the nitration of pyrene, followed by a time consuming preparative scale chromatographic separation of the isomers. This process generates a great deal of biologically hazardous waste and is time consuming because of the low solubility of the DNPs 8-10.

One technique would be to separate 1,3-DNP 8 from the DNPs 9 and 10. Although initial attempts at solvent extraction of 1,3-DNP 8 from a mixture of the DNP isomers with acetonitrile were only partially successful, this method shows promise and should be further investigated. The remaining mixture of 1,6-DNP 9 and 1,8-DNP 10 could be reduced to mixture of the corresponding ANP isomers via the Zinin reduction procedure and the resulting 1,6-ANP 33 and 1,8-ANP 22 separated by preparative alumina chromatography. The advantage of this procedure is that the chromatographic separation of 1,6-ANP and 1,8-ANP is facilitated by their relative high solubility in the eluting mobile phase. The separated ANP isomers could then be oxidized to the DNP isomers with an excess of MCPBA.

Another route to the pure DNP isomers would take advantage of the kinetics of the Zinin reduction procedure. By altering reaction conditions, it may be possible to reduce 1,6-DNP 9 and 1,8-DNP 10 selectively at rate different than 1,3-DNP 8. This could result in a mixture of 1,3-DNP 8 and 1,6-ANP 23 and 1,8-ANP 22. The ANP derivatives could again be separated and oxidized to the DNP derivative as described above. Another advantage of these two methods is that the ANP derivatives are very useful starting points for the synthesis of other metabolites such as HANP and NONP derivatives because they are intermediate in oxidation state.

IV.3 Liquid Chromatography-Mass Spectrometry (LC-MS).

The development of novel mass spectrometric techniques for the analyses of both metabolites and DNA adducts of the nitro-pyrenes and other nitro-PAH is of great interest. In this respect the technique of combined LC-MS has the greatest potential.

LC-MS would be very useful for the direct analyses of extracts of culture media for the screening of metabolites. By combining RPLC separation and MS analysis in one step, the opportunities for losses and degradation of unstable metabolites or adducts would be greatly lessened. The new technique of thermospray may be especially useful. In addition, because of the greater sensitivity and selectivity of MS, as compared to UV-VIS detection, lower levels of analyte may be detected.

The use of TBDMS and other sterically crowded trialkyl silyl derivatives of DNA adducts has great potential. These derivatives are quite stable under RPLC conditions and would therefore be quite amenable

to analysis by LC-MS. The advantage of using these stable silylated derivatives is the wealth of MS fragmentation information that is obtained and the much greater sensitivity available with EIMS.

IV.4 Non-covalent Interaction of DNP Metabolites with DNA.

One interesting aspect of this study was the interaction of DNP metabolites and CT-DNA. The observed changes in their UV-VIS spectra and the induced CD spectra are still unexplained. As these phenomena may aid explaining the differences in the biological activity of 1-NP 7 and the DNPS 8-10 further studies should be undertaken. One method of interpreting these observations may be to determine if substitution at different sites on the pyrene nucleus affects the observed spectral changes. By elucidating the nature of the interaction of these compounds with DNA, insight may be gained into the mechanism of biological activity of the DNPs.

IV.5 Questions regarding C8-2'-dG Adduct Formation.

There are still many questions yet to be answered regarding C8-2'-dG adduct formation. Although only one major adduct was characterized, initial results using ^{32}P labelled adducts indicate that there may other adducts present at lower levels. These adducts should also be characterized as they may also play a role in the biological activity of the DNPs 8-10.

There are certain fundamental questions that should be resolved regarding DNP-DNA adduct formation in *S.typhimurium*. Is the C-8-2'dG adduct produced only in specific regions of DNA, or is it

scattered randomly throughout the entire DNA?   Also, if the adduct is only present in certain regions, are there local structural peculiarities that are responsible for the preferential binding?   Investigations by co-workers are presently being carried out to answer these questions.

V. CONCLUSION.

The main purposes of this study were to examine the metabolism of the DNPs 8-10 in bacterial test strains, and to isolate and characterize the DNA adduct(s) which were the result of binding of reactive metabolites to DNA. Most of the research aims set out in I.5 were met.

Supplemented with investigations by co-workers, the metabolic pathway of 1,8-DNP in *S.typhimurium* TA98 was elucidated. This was aided by the use of tritium labelled 1,8-DNP 10. The nitro groups in 1,8-DNP 10 were shown to undergo stepwise reduction and acetylation to a number of metabolites, such as 1,8-ANP 22, and 1,8-AcAAP 24. Initial studies indicated that 1,3-DNP 8 and 1,6-DNP 9 were metabolized in similar fashion.

Many of the metabolites of the DNPs 8-10, both postulated and confirmed, were synthesized and tested for mutagenicity in various *S.typhimurium* test strains. Based on the results of the mutagenicity studies, the reactive species postulated to bind to DNA was either the N-hydroxyamino-nitropyrene or its N-acetoxy derivative. As the latter was postulated to be difficult to synthesize because of its instability, the N-hydoxlyamino-nitropyrenes derivatives were prepared by the reduction of the analogous nitroso-nitropyrenes derivatives.

The major obstacle to the characterization the DNP-DNA adduct produced in *vivo* was that large quantities were needed for spectroscopic characterization. To overcome this problem, the *in vitro* adducts formed

163

by the reaction of 1,3-,1,6- and 1,8-HANP and CT-DNA were produced and isolated from enzymatic DNA hydrolyses by a combination of solvent extraction, and semi-preparative RPLC. Then, tritium labelled 1,8-DNP-DNA adduct, which was produced *in vivo*, was shown to have identical chromatographic behaviour to the *in vitro* DNA adduct.

A wide variety of spectroscopic techniques were used to characterize the *in vitro* adducts. Analysis by RPLC revealed that there was only one major adduct and that this compound was susceptible to both acid and base decomposition. UV-VIS spectroscopy of the adducts indicated that substitution on the pyrene nucleus had occurred through the exocyclic amino group. NMR spectroscopy of the 1,8-adduct 48 and the 1,6-adduct 47 disclosed that only one exocyclic amino-nitropyrene proton was present. Based on this evidence the adducts were tentatively postulated to be the result of bond formation between the exocyclic $N^{1''}$ of a amino-nitropyrene nucleus and C-8 of 2'-dG 20.

The acid decomposition product was postulated to be the deribosylated species. The base decompostion product was postulated to be the C-8/N-9 imidazole ring opened product. These findings were based on chromatographic and UV-VIS spectroscopic results.

MS characterization of these adducts presented formidable problems. The highly hydrogen bonded nature of these compounds required that "soft" ionization, combined LC-MS techniques and derivatization be employed. Fast atom bombardment (FAB) and combined LC-FABMS revealed only low intensity molecular ions and provided little structural information. The combination of trimethylsilyl and *tert*-butyldimethylsilyl derivatization and analysis by desorption electron ionization probe revealed a pattern

of fragments rich in structural information. The success of the TBDMS
derivatives was of special interest because of their potential for use in
combined LC-MS techniques.

Finally, the interaction between selected metabolites of the
DNPs 8-10 and CT-DNA was investigated. The structural similarity between
ANP and DAP derivatives and known DNA intercalators suggests that
non-covalent interaction between these DNP metabolites and DNA could take
place. UV-VIS and CD spectroscopic studies indicated that a strong
interaction was taking place.

VI. APPENDICES

Appendix A. Spectral and Chromatographic Data for di-substituted

pyrenes.

Appendix A consists of Tables 17-21 and is a compilation of UV-VIS,
fluorescence, mass spectrometric and TLC and HPLC chromatographic data for
the disubstituted pyrenes described in Section III.3. Further
characterization, including detailed NMR characterization was carried out
by co-workers.

The following columns were used and and will be referred to as such
in the text:

Reverse Phase Columns

A   Hibar Licrosorb RP-18, 10 μm, 250 mm x 4.6 mm

   (E. Merk, Darmstadt, F.R. Germany)

B   Altex Ultrasphere ODS, 5 μm, 250 mm x 4.6 mm

   (BDH Chemicals, Toronto, Ont.)

C   Alltech Licrosorb RP-18, 10 μm, 250 mm x 4 mm

   (Alltech Assoc., Deerfield, NJ)

D   Hibar Licrosorb RP-18, 5 μm, 250 mm x 4 mm

E   Hibar Licrosorb RP-18, 5 μm, 125 mm x 4 mm

F   Partisil ODS-2, Magnum 9, 10 μm, 500 mm x 9 mm

   (Whatman, Inc., Clifton, NJ).

166

G Vydac C-18, 10 μm, 250 mm x 4 mm

   (The Separations Group, Hesperia, CA)

Normal Phase Columns

G Altex cyano, 5 μm, 250 mm x 4.6 mm

H Altex cyano, 5 μm, 250 mm x 10 mm

Table 17: Chromatographic and Spectral Data for DNPS 8-10

Spectroscopic Data:

	1,3-DNP 8	1,6-DNP 9	1,8-DNP 10
MS[a]		m/z (relative intensity)	
	292 (72)	292 (100)	292 (100)
	262 (14)	262 (16)	262 (16)
	246 (4)	246 (18)	246 (18)
	232 (6)	232 (13)	232 (19)
	216 (18)	216 (30)	216 (36)
	200 (100)	200 (84)	200 (92)

UV-VIS   Absorbance Maxima in nm (extinction coeffecient)

Solvent			
78/22 acetonitrile/water	419	412	399
	288	372	288
	234	282	230
		230	
DMSO	421 (11252)		390 (8300)
	292 (8591)		290 (6900)

Chromatographic Data:

	1,3-DNP	1,6-DNP	1,8-DNP
TLC[b]		r.f.	
Solvent			
60/40 DCM/hexane	.75	.84	.78

HPLC   k'

	1,3-DNP	1,6-DNP	1,8-DNP
RP Column C[c]	3.3	3.2	3.3
RP Column C[d]	4.4	4.0	4.4
RP Column G[e]	5.9	5.5	5.5
NP Column H[f]	2.1	2.5	2.9
NP Column I[g]	1.9	2.0	2.5

----

[a] EI spectra, samples introduced via solids probe.
[b] TLC on chromatography on Merk silica gel 60 F254
[c] 80/20 acetonitrile/water, 2 mL/min
[d] 70/30 acetonitrile/water, 1 mL/min
[e] 60/40 acetonitrile/water to 100% acetonitrile in 20 min, 1 mL/min
[f] 95/5 hexane/isopropanol, 4 mL/min
[g] 95/5 hexane/isopropanol, 6 mL/min

Table 18: Chromatographic and Spectral Data for NONPs 40, 41, and 26.

Spectroscopic Data:

	1,3-NONP 40	1,6-NONP 41	1,8-NONP 26
MS[a]		m/z (relative intensity)	
	276 (70)	276 (84)	276 (75)
	246 (60)	246 (59)	246 (57)
	232 (6)	232 (5)	232 (31)
	216 (25)	216 (30)	216 (71)
	200 (100)	200(100)	200 (100)

- -

UV-VIS   Absorbance Maxima in nm   (extinction coeffecient)

Solvent			
82/18 acetonitrile/water	440	445	446
	232	398	232
		290	
		234	
Methanol			440 (1560)
			390 (1160)
			292 (1040)
DMSO	436 (12892)	442 (11894)	

Chromatographic Data:

HPLC

		k'	
Column			
NP Column H[c]	1.7	1.8	2.1
RP Column F[d]			14
RP Column G[e]	7.2	7.1	7.2

----

a   EI spectra, samples introduced via solids probe.
b   TLC on chromatography on Merk silica gel 60 F254
c   95/5 hexane/isopropanol, 4 mL/min
d   80/20 acetonitrile/water, 4 mL/min
e   60/20 acetonitrile to 100% acetonitrile in 20 min, 1 mL/min.

Table 19: Chromatographic and Spectral Data for HANPs 34, 35 and 37

....

Spectroscopic Data:

....

	1,3-HANP	1,6-HANP	1,8-HANP
MS[a]		m/z (relative intensity)	
			278 (2)
			262 (28)
			248 (4)
			232 (100)
			216 (27)

....

UV-VIS	Absorbance Maxima in nm		
Solvent			
70/30 acetonitrile/water	444-	457	464
	292	308	382
	230	230	298
			230

....

....

Chromatographic Data:

....

HPLC

		k'	
RP Column C[b]	3.1	3.0	2.9

....

a RPLC-MS of ascorbate reduction of 1,8-NONP 26
b 60/40 acetonitrile/water to 100% acetonitrile in 20 min, 1 mL/min.

Table 20: Chromatographic and Spectral Data for ANPs 32, 33, and 22

Spectroscopic Data:

	1,3-ANP 32	1,6-ANP 33	1,8-ANP 22
MS[a]	m/z (relative intensity)		
	262 (100)	262 (100)	262 (100)
	232 (20)	232 (43)	232 (27)
	216 (89)	216 (74)	216 (82)

UV-VIS	Absorbance Maxima in nm (extinction coeffecient)		
Solvent			
72/28 acetonitrile/water	466	488	498
	294	314	398
	244	256	300
		230	232
Methanol	464 (8029)	484 (10343)	494 (8115)

Chromatographic Data:

TLC[b]	1,3-ANP 32	1,6-ANP 33	1,8-ANP 22
Solvent		r.f	
DCM	.47	.58	.42

HPLC		k'	
RP column G[c]	6.71	6.5	6.25
RP Column A[d]	3.3	3.0	3.1
RP Column B[e]		3.2	3.4
NP Column H[f]	7.7	9.8	11.4

----

[a] EI spectra, samples introduced via solids probe.
[b] TLC on chromatography on Merk silica gel 60 F254
[c] 60/40 acetonitrile/water to 100% acetonitrile in 20 min, 1 mL/min
[d] 80/20 acetonitrile/water, 1 mL/min
[e] 80/20 acetonitrile/water, 2 mL/min
[f] 95/5 hexane/isopropanol, 4 mL/min

Table 21: Chromatographic and Spectral Data for DAPs 38, 39, and 23.

Spectroscopic Data:

	1,3-DAP 38	1,6-DAP 39	1,8-DAP 23

MS[a]

	m/z (relative intensity)		
	232 (100)	232 (100)	232 (100)
			218 (12)

UV-VIS   Absorbance Maxima in nm (extinction coeffecient)

Solvent	1,3-DAP	1,6-DAP	1,8-DAP
Acetonitrile			290 (12,500)
			390 (12,160
Methanol	404	396	398 (13,130)
	344	286	362
	238	232	282 (13,540)
			232 (25940)

Fluorescence Emission Maximum
(excitation at 280 nm)   nm

Solvent			
Methanol			447

Chromatographic Data:

	1,3-DAP	1,6-DAP	1,8-DAP

TLC[b]

Solvent		r.f.	
90/10 ethyl acetate/DCM	.41	.6	.30

HPLC

		k'	
RP Column C[c]			10.3
RP Column E[d]			2.6

----

a   EI spectra, samples introduced via solids probe.
b   TLC on chromatography on Merk silica gel 60 F254
c   20/80 methanol water to 100% methanol in 15 min, 1 mL/min
d   70/30 methnol/water, 1 mL/min

Appendix B. Listing of m/z and mass spectra of TBDMS and TMS
derivatives of adducts 46-48.

Appendix B consists of Tables 22-25 and is a listing of m/z for
TBDMS derivatives of the adducts 46-48 and the TMS derivative of
1,8-adduct 48. The mass spectra of the TBDMS derivatives of the 1,3- and
1,6- adducts 46 and 47 are illustrated in Figures 48 and 49. MS
conditions are described in III.2.4.3. The mass spectra of the TBDMS and
TMS derivatives of the 1,8-adduct 48 are illustrated in Figures 44 and 45
(Section II.4).

DEI Spectra   Page

Figure 48: DEI mass spectrum of TBDMS derivatives of the
1,3-adduct 46.

Table 22: Listing of m/z for the TBDMS derivative of
the 1,3 adduct 46.

m/z	%base	m/z	%base	m/z	%base
61.99	0.8	76.85	0.0	96.58	0.0
62.99	1.2	77.00	24.6	96.80	0.0
63.50	0.0	77.49	0.0	97.07	19.4
63.87	0.0	77.51	0.0	97.49	0.0
63.93	3.5 F	78.00	2.6	97.52	0.0
64.00	0.8 F	78.53	0.0	97.93	0.0
64.51	0.1	79.02	6.7	98.03	1.9 F
65.01	2.8	79.49	0.0	98.08	2.4 F
65.50	0.0	80.03	2.9	98.49	0.0
66.01	1.9	80.50	0.1	98.53	0.0
66.50	0.1	80.70	0.0	99.03	3.5 F
66.66	0.0	80.81	0.0	99.09	3.0 F
66.89	0.0	80.87	0.0	99.51	0.1
67.03	15.2	81.01	12.6 F	99.90	0.0
67.49	0.0	81.05	11.1 F	100.02	3.6
67.54	0.0	81.12	0.0	100.51	0.2
67.91	0.1	81.46	0.0	101.01	2.9
68.03	12.9	81.50	0.2	101.51	0.3
68.49	0.0	81.90	0.0	102.01	1.5
68.50	0.0	82.01	1.6 F	102.52	0.2
68.89	0.0	82.05	2.9 F	103.01	2.3
68.97	6.3 F	82.50	0.1	103.51	0.0
69.04	15.2 F	83.05	8.2	104.02	1.2
69.11	0.0	83.51	0.0	104.31	0.0
69.50	0.0	83.93	0.9 F	104.34	0.0
70.04	5.2	84.05	2.0 F	104.53	0.0
70.51	0.1	84.52	0.0	104.64	0.0
70.56	0.0	84.54	0.0	104.90	0.0
71.01	1.6 F	84.90	0.0	105.00	2.9 F
71.06	8.1 F	85.02	1.8 F	105.04	3.5 F
71.51	0.0	85.08	2.9 F	105.51	0.1
71.92	0.0	85.53	0.0	106.03	1.1
72.03	3.7	85.92	0.6 F	106.50	0.2
72.34	0.0	86.02	0.9 F	107.05	4.5
72.51	0.0	86.07	0.8 F	107.51	0.4
72.52	0.0	86.49	0.0	108.04	1.8
72.56	0.0	87.02	1.1	108.51	0.2
72.69	0.0	87.50	0.2	109.06	3.7
72.79	0.0	87.66	0.0	109.51	0.0
73.02	100.0 0	88.01	1.6	110.04	1.2
73.18	0.0	88.51	0.1	110.50	0.0
73.23	0.0	89.02	11.1	111.00	1.5 F
73.47	0.0	89.50	0.0	111.08	2.1 F
73.49	0.0	89.53	0.0	111.50	0.0
74.02	10.5	89.93	0.0	111.81	0.0
74.49	0.0	90.02	1.3	112.07	1.9
74.67	0.0	90.52	0.0	112.51	0.1
74.73	0.0	90.89	0.0	113.08	4.3
74.80	0.0	91.03	8.1	113.47	0.0
75.00	100.0 0	91.92	0.0	113.51	0.1
75.20	0.0	92.03	2.6	113.93	0.0
75.50	0.0	92.51	0.0	114.04	1.5 F
76.01	13.2	92.89	0.0	114.11	0.4 F
76.50	0.1	92.97	2.7 F	114.51	0.1
76.57	0.0	93.04	8.8 F	115.05	14.8
		93.51	0.4	115.51	0.1
		94.04	2.7	115.87	0.0
		94.29	0.0	115.89	0.0
		94.51	0.4	116.02	5.2
		94.96	1.1 F	116.52	0.2
		95.05	7.6 F	116.58	0.0
		95.51	0.1	116.75	0.0
		95.98	1.3 F	116.79	0.0
		96.06	2.5 F	117.01	19.9
		96.48	0.2	117.52	0.0
		96.52	0.0	118.02	2.8

m/z	%base	m/z	%base	m/z	%base
118.50	0.0	140.53	0.1	164.55	0.0
118.91	0.0	140.89	0.0	165.05	1.3
119.04	4.2	141.04	1.1	165.54	0.0
119.51	0.0	141.52	0.1	166.06	0.6
120.04	1.3	142.03	1.0	167.02	3.8
120.51	0.1	142.52	0.0	167.50	0.0
120.54	0.0	143.03	2.8	167.55	0.0
120.99	1.6 F	143.52	0.0	167.89	0.0
121.07	4.0 F	143.56	0.0	168.05	0.7
121.51	0.2	144.03	1.1	168.57	0.0
121.57	0.0	144.50	0.0	169.03	1.0 F
122.05	1.1	144.83	0.0	169.16	0.5 F
122.52	0.0	145.05	2.5	169.55	0.1
122.87	0.0	145.52	0.0	170.06	0.7
123.06	2.1	146.05	0.8	170.53	0.0
123.49	0.0	146.54	0.1	170.79	0.0
123.53	0.0	147.03	13.4	171.05	5.9
124.05	0.7	147.55	0.1	171.25	0.0
124.51	0.0	147.89	0.0	171.56	0.2
125.05	0.9	148.04	2.4	172.05	1.4
125.46	0.0	148.50	0.0	172.40	0.0
125.51	0.1	148.56	0.0	172.56	0.1
126.02	1.2	148.66	0.0	172.87	0.0
126.46	0.0	149.00	14.8	173.06	1.6
126.54	0.2	149.50	0.0	173.53	0.0
126.83	0.0	150.02	2.3	174.06	1.1
126.89	0.0	150.53	0.0	174.59	0.0
127.02	2.9	151.00	3.3 F	175.07	1.8
127.52	0.1	151.09	1.1 F	175.58	0.1
128.03	1.3	151.52	0.0	176.08	2.0
128.52	0.1	151.87	0.0	176.50	0.0
128.73	0.0	152.04	1.3	177.02	1.4 F
128.77	0.0	152.55	0.0	177.12	1.0 F
129.01	26.3	153.01	0.9 F	177.54	0.0
129.51	0.1	153.11	0.8 F	178.06	0.8
129.88	0.0	153.52	0.0	178.42	0.0
130.02	4.3	154.05	0.9	178.56	0.1
130.81	0.0	154.49	0.0	179.05	1.2
131.02	10.0	154.56	0.1	179.52	0.0
131.51	0.1	154.70	0.0	179.55	0.0
131.56	0.0	155.01	19.3 F	180.05	0.8
131.88	0.0	155.14	0.8 F	181.06	0.6
131.90	0.0	155.55	0.1	181.91	0.0
132.04	2.8	156.02	3.3	182.05	0.6
132.53	0.1	156.49	0.0	182.63	0.0
133.00	3.4 F	156.53	0.0	183.05	1.0
133.07	2.3 F	157.03	2.3	183.57	0.0
133.52	0.1	157.52	0.1	184.02	1.6
134.04	3.2	157.61	0.0	184.52	0.0
134.51	0.0	158.04	0.9	184.87	0.0
134.82	0.0	158.53	0.0	185.07	2.7
135.04	3.1	159.05	1.7	185.53	0.0
135.53	0.0	159.52	0.0	186.06	0.9
136.06	1.7	159.91	0.0	186.56	0.1
136.47	0.0	160.06	1.0	187.07	3.6
136.51	0.0	160.53	0.0	188.07	1.0
136.82	0.0	161.06	1.0	188.87	0.0
137.06	1.0	161.55	0.0	189.07	2.7
137.54	0.0	161.79	0.0	190.07	0.9
138.06	0.5	162.06	1.1	190.51	0.0
138.54	0.0	162.51	0.0	190.58	0.0
139.05	0.6	163.06	1.0	191.06	2.0
139.52	0.1	163.55	0.0	192.06	0.8
139.89	0.0	163.90	0.0	193.05	1.3
139.91	0.0	164.06	0.8	193.57	0.1
140.03	0.9	164.51	0.0	193.81	0.0

m/z	%base	m/z	%base	m/z	%base
194.07	0.6	231.83	0.0	283.11	0.9
194.55	10 0.	232.07	4.4	284.13	0.6
195.06	0.6	232.87	0.0	284.79	0.0
196.07	0 4	233.08	2.1	285.14	1.6
196.60	0.0	234.09	0.8	286.12	0.7
197.07	2.1	234 50	0.0	286 59	0.0
197.58	0.1	235.10	1.6	288 74	0.0
198.06	0.6	236.10	0.6	287.11	13.4
198.55	0.0	237.09	0.5	287 74	0.0
198.60	0.0	237 59	0.0	288 11	3.5
199.07	1.7	238.09	0.4	288 85	0.0
200.06	0.7	239 11	1.7	289 12	1.7
201.06	1.0	240.09	0.6	289 54	0.0
202.06	1.3	241.11	1.8	290 12	0.6
202.59	0.0	241 31	0.0	291 14	0.8
203.06	1.2	241 63	0.0	292.17	2.1
204.04	1.3 F	242.07	2.3	293.15	0.9
204.14	0.8 F	242.53	0.0	294.14	0.3
204.58	0.1	243.04	1.4 F	295.12	0.8
205.07	1.1	243.14	1.0 F	296 12	0.4
205.61	0.0	244.10	0.9	296.82	0.0
206.07	1.1	245.10	0.8	296 86	0.0
206.50	0.0	246.11	0.7	297.15	0.8
206.55	0 0	246.50	0.0	298.13	0.7
206.81	0.0	247.11	1.0	299.16	1.6
207.01	7.0	248.11	0.8	300.15	0.6
207.60	0.0	249.10	1.6	300.88	0.0
208.03	1.7	250.12	2.6	301.15	0.9
208.70	0.0	251.10	1.1	302.14	0.5
209.04	1.2	252.10	0.6	303.13	0.5
210.07	0.4	253.10	1.0	304.15	0.4
210.53	0.0	254.08	0.4	305.16	2.6
211.07	1.5	254.51	0.0	306.16	1.1
211.79	0.0	255.12	1.2	307.14	0.6
212.08	2.0	256.12	0.5	308.13	0.3
212.59	0.0	256.64	0:0	309.14	1.6
213.08	2.2	257.10	1.2	309 90	0.0
214.05	2.1	257.88	0.0	310.14	0.8
214.51	0.0	258.07	2.2	310.69	0.0
214.55	0.0	259.09	1.1	311.19	2.8
215.08	1.2	260.11	0.5	312.17	0.9
216.07	1.4	261.11	1.3	313.21	25.5
216.36	0.0	261.83	0.0	313.40	0.0
216.89	0.0	262.07	1.3	314.20	6.9
217.07	2.0	263.10	1.0	315.18	2.1
217.54	0.0	264.12	0.6	316.15	0.5
218.08	0.8	265.10	0.9	317.14	0.4
219.10	0.9	266.10	0.6	318.15	0.4
220.09	0.6	266.60	0.0	318.70	0.0
221.07	2.4	267.09	0.6	319.15	0.5
222.08	0.8	268.08	0.5	319.90	0.0
222.54	0.0	269.11	0.9	320.17	0.6
222.84	0.0	270.09	0.8	321.16	0.8
222.89	0.0	271.12	0.8	322.15	0.4
223.06	0.9	272.11	0.5	322.36	0.0
224.08	0.5	273.10	0.6	323.17	0.5
225.09	0.8	274.11	0.4	324.14	0.3
225.65	0.0	275.12	0.5	325.19	2.3
226.08	0.5	276.12	0.5	325.86	0.0
226.85	0.0	277.12	0.5	326.18	0.8
227.08	1.6	277.63	0.0	327.22	7.4
228.08	0.8	278.14	1.6	327.61	0.0
229.09	1.1	279.12	1.9	328.22	2.1
230.08	0.9	280.13	0.5	329.17	1.2
230.83	0.0	281.06	2.0	330.15	0.6
231.09	2.1	282.07	0 7	330.95	0.0

m/z	%base	m/z	%base	m/z	%base
331.16	0.6	380.90	0.0	438.22	0.3
332.14	0.5	381.25	1.2	439.21	0.4
333.18	0.8	382.23	0.5	440.23	0.2
334.18	0.4	382.85	0.0	441.25	0.6
335.20	3.2	383.13	2.4 F	442.00	0.0
336.19	1.0	383.30	2.6 F	442.25	0.3
337.22	24.7	384.23	0.9	442.83	0.0
337.67	0.0	384.87	0.0	443.27	1.4
337.78	0.0	385.17	0.8	444.27	0.9
338.22	6.7	386.18	0.4	444.92	0.0
339.24	46.3	387.19	2.8	445.25	0.4
339.74	0.0	388.19	1.5	446.22	0.1
340.23	12.4 F	389.20	0.5	447.22	0.3
341.25	100.0 F0	390.22	0.4	448.20	0.1
342.26	38.1 F	391.20	0.3	449.20	0.2
342.53	0.0	392.24	0.7	449.51	0.0
342.78	0.0	393.22	0.5	450.20	0.2
343.25	10.4	394.21	0.3	451.24	0.4
343.63	0.0	395.18	0.4	452.23	0.2
344.23	1.6	396.19	0.3	453.25	0.4
345.16	0.6	397.22	0.6	454.25	0.2
346.16	0.3	398.26	0.7	455.24	0.2
347.18	0.5	399.22	0.7	456.22	0.2
348.19	0.5	399.59	0.0	457.25	0.4
349.20	1.1	400.18	0.7	458.24	0.2
350.18	0.4	401.17	1.6	459.19	0.2
350.93	0.0	402.18	0.9	459.93	0.0
351.20	1.9	403.19	0.5	460.20	0.2
351.81	0.0	403.88	0.0	461.18	0.2
352.19	0.8	404.20	0.3	461.97	0.0
353.20	1.2	405.23	0.3	462.22	0.1
354.20	0.6	406.23	0.4	462.89	0.0
355.18	1.6	406.94	0.0	463.25	0.1
356.17	0.5	407.23	0.3	463.90	0.0
357.19	5.9	408.24	0.4	464.21	0.1
358.18	1.7	408.62	0.0	465.26	0.5
359.18	1.9	409.22	2.9	466.26	0.2
359.36	0.0	410.23	1.2	466.94	0.0
360.18	0.8	411.21	0.7	467.27	0.6
360.41	0.0	412.20	0.3	468.19	0.3
361.21	0.8	413.23	0.5	469.26	0.6
362.20	0.5	414.20	0.5	470.25	0.3
363.20	0.4	415.24	1.6	471.28	0.4
363.52	0.0	416.24	0.6	472.25	0.2
364.20	0.4	417.21	0.3	473.24	0.1
365.19	0.6	417.98	0.0	474.20	0.1
366.20	0.6	418.22	0.2	475.17	0.1
366.90	0.0	419.20	0.3	476.22	0.2
367.21	1.9	420.21	0.2	477.20	0.1
368.22	0.9	421.20	0.2	478.21	0.2
369.22	1.5	422.23	0.2	479.21	0.2
369.67	0.0	423.24	2.0	480.23	0.1
370.22	0.6	424.24	1.1	480.48	0.0
371.17	1.3	425.24	0.7	480.76	0.0
371.93	0.0	426.24	0.4	481.21	0.4
372.16	0.7	427.24	0.5	482.29	0.9
373.18	0.8	428.23	0.4	483.28	0.7
373.38	0.0	429.20	0.7	484.27	0.2
373.74	0.0	430.18	0.5	485.26	0.2
374.20	0.5	431.18	0.3	485.73	0.0
375.22	0.4	432.19	0.2	486.24	0.1
376.21	0.3	433.20	0.2	487.24	0.2
377.21	0.4	434.22	0.2	488.03	0.0
378.23	0.4	435.22	0.2	488.25	0.1
379.23	0.8	436.22	0.2	489.17	0.1
380.22	0.5	437.20	0.2	490.19	0.1

m/z	%base	m/z	%base	m/z	%base
491.23	0.1	549.17	0.0	601.23	0.1
492.22	0.1	549.38	0.0	602.31	0.0
493.22	0.1	550.31	0.1	603.23	0.1
494.21	0.2	551.29	0.1	604.28	0.0
495.21	0.2	551.99	0.0	605.20	0.0
496.22	0.2	552.24	0.2	606.23	0.1
496.49	0.0	552.91	0.0	607.23	0.1
497.24	0.2	553.20	0.2	608.19	0.1
498.26	0.1	554.28	0.1	608.91	0.0
499.24	0.1	555.31	0.1	609.21	0.2
500.25	0.1	556.32	0.2	610.21	0.1
501.22	0.2	557.30	0.1	611.25	0.1
502.19	0.1	558.29	0.1	612.22	0.1
503.13	0.2	559.27	0.1	613.25	0.1
504.17	0.1	560.21	0.0	614.27	0.0
505.17	0.1	561.26	0.1	615.19	0.0
506.23	0.1	562.25	0.0	615.33	0.1
507.22	0.1	563.24	0.1	616.15	0.0
508.23	0.1	564.21	0.1	617.25	0.0
509.26	0.1	565.23	0.0	618.29	0.0
510.22	0.1	565.73	0.0	619.16	0.0
511.27	0.1	566.20	0.0	619.36	0.0
512.25	0.1	567.23	0.1	620.22	0.1
513.25	0.1	568.25	0.1	621.24	0.1
514.24	0.1	568.44	0.0	622.29	0.1
515.24	0.1	569.29	0.1	622.95	0.0
516.22	0.1	570.26	0.1	623.29	0.1
517.25	0.0	571.27	0.1	624.22	0.1
518.23	0.1	572.23	0.1	625.22	0.1
519.26	0.1	573.30	0.0	626.22	0.1
520.24	0.1	574.27	0.1	627.18	0.0
520.94	0.0	575.29	0.1	628.21	0.0
521.04	0.0	576.25	0.0	628.35	0.0
521.31	0.1	577.25	0.1	629.32	0.1
522.33	0.2	578.26	0.1	630.32	0.1
523.29	0.2	578.72	0.0	631.31	0.0
524.28	0.2	579.31	0.0	632.31	0.0
525.18	1.0	580.22	0.1	633.23	0.1
526.18	0.4	581.26	0.2	634.27	0.0
527.19	0.1	581.66	0.0	635.25	0.0
528.23	0.1	582.16	0.7	636.25	0.0
528.68	0.0	583.19	0.3	637.26	0.1
529.23	0.1	584.20	0.1	638.21	0.1
530.32	0.0	585.23	0.1	639.18	0.7
531.28	0.1	586.21	0.0	640.19	0.4
531.92	0.0	586.41	0.0	641.22	0.2
532.24	0.4	587.24	0.1	642.23	0.1
533.23	0.2	587.88	0.0	643.21	0.0
534.24	0.1	588.26	0.0	644.26	0.1
535.16	0.1	589.17	0.1	645.24	0.1
536.26	0.1	590.21	0.1	646.35	0.0
537.30	0.2	590.51	0.0	647.08	0.0
538.32	0.2	591.23	0.1	647.28	0.1
539.26	0.2	592.21	0.1	648.24	0.0
540.26	0.1	592.93	0.0	649.25	0.0
541.24	0.1	593.23	0.1	650.25	0.1
542.24	0.0	594.23	0.1	651.28	0.0
543.22	0.1	594.70	0.0	651.94	0.0
543.47	0.0	594.86	0.0	652.33	0.0
544.27	0.0	595.31	0.1	653.18	0.0
545.26	0.1	595.91	0.0	653.40	0.0
546.22	0.1	596.34	0.9	654.23	0.0
546.95	0.0	597.34	0.4	655.15	0.0
547.06	0.0	598.31	0.2	655.24	0.0
547.30	0.1	599.23	0.1	655.44	0.0
548.28	0.1	600.25	0.0	656.28	0.1

m/z	%base	m/z	%base	m/z	%base
657.25	0.0	707.34	0.0	763.33	0.0
658.31	0.0	708.35	0.1	763.65	0.0
659.25	0.0	709.33	0.1	764.40	0.1
660.26	0.1	710.35	0.1	765.33	0.1
660.46	0.0	711.32	0.0	766.40	0.1
661.30	0.0	712.22	0.0	767.32	0.0
662.40	0.0	712.51	0.0	768.32	0.0
663.13	0.0	713.35	0.1	769.34	0.0
663.36	0.0	714.34	0.0	770.22	0.0
664.04	0.0	715.35	0.0	770.48	0.0
664.33	0.1	716.39	0.0	771.26	0.0
665.07	0.0	717.35	0.0	771.49	0.0
665.34	0.0	718.46	0.0	772.34	0.0
666.28	0.1	719.34	0.0	773.10	0.0
667.27	0.1	720.33	0.0	773.26	0.0
668.33	0.0	721.25	0.0	773.51	0.0
668.59	0.0	721.51	0.0	774.43	0.0
669.37	0.1	722.31	0.0	776.45	0.0
670.40	0.1	723.37	0.0	777.33	0.0
671.29	0.1	724.27	0.0	777.55	0.0
672.25	0.1	724.46	0.0	778.37	0.0
672.90	0.0	725.12	0.0	779.37	0.0
673.26	0.0	725.34	0.1	780.32	0.1
674.29	0.0	726.34	0.0	781.30	0.0
674.89	0.0	727.35	0.0	781.51	0.0
675.35	0.0	728.42	0.0	782.18	0.0
676.33	0.0	729.32	0.0	782.41	0.0
677.39	0.0	730.35	0.1	783.32	0.0
678.38	0.0	731.30	0.0	783.57	0.0
679.32	0.0	731.47	0.0	784.41	0.0
680.30	0.0	732.28	0.0	785.37	0.0
681.28	0.0	733.55	0.0	787.46	0.0
681.51	0.0	734.36	0.0	788.43	0.0
682.27	0.1	735.34	0.0	790.37	0.0
683.25	0.0	736.41	0.0	791.40	0.0
683.46	0.0	737.36	0.0	793.26	0.0
684.18	0.0	738.09	0.0	793.46	0.0
684.45	0.1	738.33	0.0	794.35	0.2
685.19	0.0	739.29	0.2	794.97	0.0
685.39	0.0	740.31	0.1	795.36	0.2
686.16	0.0	741.32	0.1	796.36	0.1
686.38	0.0	742.30	0.0	797.34	0.0
686.51	0.0	743.31	0.0	798.32	0.0
687.43	0.0	743.52	0.0	800.39	0.0
688.29	0.0	744.45	0.1	802.36	0.0
689.33	0.0	745.36	0.0	804.20	0.0
689.52	0.0	746.30	0.0	804.43	0.0
690.27	0.0	747.28	0.0	805.45	0.0
691.28	0.0	749.29	0.0	806.47	0.0
692.28	0.0	750.28	0.0	807.43	0.0
693.41	0.0	750.44	0.0	808.37	0.1
694.38	0.0	751.36	0.0	809.39	0.0
695.32	0.0	751.52	0.0	810.42	0.0
696.28	0.0	752.39	0.0	810.67	0.0
697.36	0.0	753.30	0.0	811.39	0.0
698.12	0.0	754.35	0.0	812.35	0.1
698.29	0.0	754.69	0.0	813.36	0.1
699.33	0.1	755.31	0.0	814.25	0.0
700.10	0.0	756.47	0.0	814.44	0.0
700.37	0.1	757.35	0.0	815.38	0.0
701.34	0.0	758.47	0.0	816.53	0.0
702.28	0.0	760.33	0.0	817.44	0.0
703.28	0.0	760.43	0.0	817.98	0.0
704.29	0.1	761.33	0.0	818.36	0.0
705.31	0.0	761.58	0.0	819.32	0.0
706.29	0.0	762.22	0.0	820.55	0.0

m/z	%base	m/z	%base	m/z	%base
821.46	0.0	886.35	0.0	955.48	0.2
822.46	0.0	887.58	0.0	956.49	0.1
823.43	0.0	888.36	0.0	957.55	0.0
823.66	0.0	890.51	0.0	958.59	0.0
824.31	0.0	891.52	0.0	959.44	0.0
824.52	0.0	892.47	0.0	961.40	0.0
826.37	0.0	893.50	0.0	961.62	0.0
827.54	0.0	894.07	0.0	962.61	0.0
828.29	0.0	894.42	0.0	963.48	0 0
829.52	0.0	895.44	0.0	964.53	0.0
832.51	0.0	895.61	0.0	965.55	0.0
833.46	0.0	896.48	0.0	966.56	0.0
834.45	0.0	897.33	0.0	967.47	0.0
835.20	0.0	897.56	0.0	967.70	0.0
835.59	0.0	898 36	0.0	968.47	0.1
836.47	0.0	899.41	0.0	969 17	0.0
837.37	0.0	900.38	0.0	969 49	0.1
838.39	0.0	901.45	0.0	970.45	0.1
839.43	0.1	902.50	0.0	971 52	0.0
840.42	0.1	903.47	0.0	973.54	0.0
841.11	0.0	904.43	0.0	976 36	0.0
841.43	0.1	905.47	0 0	977.78	0.0
842.25	0.0	906.47	0.0	979.48	0.0
842.50	0.0	907 48	0 0	980 48	0.0
843.43	0.0	908.48	0.0	981 47	0.0
844.37	0.0	911.43	0.0	982.48	0.0
845.30	0.0	913.58	0.0	983.45	0.9
845.58	0.0	915.49	0.0	984.45	0.8
847.52	0.0	916.63	0.0	985.47	0.4
848.45	0.0	918.40	0.0	986.48	0.2
848.66	0.0	919.25	0.0	987.42	0.0
849.29	0.0	920.36	0.0	988.47	0.0
850.39	0.0	920.52	0.0	990.53	0.0
851.33	0.0	921.35	0 0	991.37	0.0
852.48	0 0	922.57	0.0	992.72	0.0
853.45	0.0	923.45	0.0	994.46	0.0
854.43	0.1	924.40	0.0	994.59	0.0
855.47	0.1	925.44	0.0	995.24	0.0
856.47	0.0	926.35	0.2	995.65	0.0
859.26	0.0	927.36	0.1	996.65	0.0
860.38	0.0	928.44	0.1	997.42	0.0
861.42	0.0	929.40	0.0	998.50	0.0
863.19	0.0	930.37	0.0	998.83	0.0
863.33	0.0	931.42	0.0	999.41	0.1
864.47	0.0	933.69	0.0	1,000.46	0.0
865.46	0.0	934.41	0.0	1,001.47	0.1
866.50	0.0	935.40	0.0	1,002.47	0.0
867.31	0.0	937.30	0.0	1,003.66	0.0
867.52	0.0	938.46	0.0	1,007.65	0.0
868.42	0.0	939.39	0.0	1,008.56	0.0
869.39	0.4	940.50	0.0	1,009.34	0.0
870.42	0.3	941.37	0.0	1,011.48	0.0
871.41	0.1	941.68	0.0	1,013.42	0.0
872.37	0.0	942.35	0.0	1,014.58	0.0
873.45	0.0	943.41	0.0	1,015.52	0.0
875.58	0.0	943.67	0.0	1,016.41	0.0
876.53	0.0	944.53	0.0	1,018.52	0.0
877.26	0.0	945.29	0.0	1,020.48	0.0
877.67	0.0	946.48	0.0	1,021.52	0.0
879.45	0.0	947.36	0.0	1,023.57	0.0
880.53	0.0	948.52	0.0	1,026.55	0.0
881.08	0.0	949.47	0.0	1,027.77	0.0
882.97	0.0	951.47	0.0	1,028.56	0.0
883.51	0.0	952.47	0.0	1,029.40	0.0
883.74	0.0	953.48	0.2	1,029.56	0.0
884.34	0.0	954.47	0.2	1,030.63	0.0

m/z	%base	m/z	%base
1032.78	0.0	1141.52	0.0
1033.60	0.0	1142.64	0.0
1034.45	0.0	1147.67	0.0
1035.05	0.0	1149.55	0.0
1035.51	0.0		
1036.47	0.0		
1037.47	0.0		
1040.57	0.0		
1041.59	0.0		
1043.44	0.0		
1044.63	0.0		
1045.98	0.0		
1047.51	0.0		
1048.65	0.0		
1050.54	0.0		
1051.55	0.0		
1053.53	0.0		
1053.69	0.0		
1054.54	0.0		
1056.68	0.0		
1057.66	0.0		
1058.49	0.0		
1059.65	0.0		
1059.91	0.0		
1060.44	0.0		
1060.78	0.0		
1065.68	0.0		
1066.65	0.0		
1067.69	0.0		
1069.63	0.0		
1070.61	0.0		
1071.59	0.0		
1072.57	0.0		
1074.84	0.0		
1075.61	0.0		
1076.41	0.0		
1076.64	0.0		
1076.87	0.0		
1077.44	0.0		
1083.46	0.0		
1083.66	0.0		
1084.61	0.0		
1085.62	0.0		
1086.57	0.0		
1087.57	0.0		
1090.34	0.0		
1091.15	0.0		
1091.60	0.0		
1093.48	0.0		
1094.49	0.0		
1097.61	0.0		
1098.36	0.0		
1101.43	0.0		
1101.68	0.0		
1110.60	0.0		
1111.81	0.0		
1113.52	0.1		
1114.53	0.0		
1115.50	0.0		
1116.72	0.0		
1119.55	0.0		
1120.60	0.0		
1128.89	0.0		
1129.47	0.0		
1132.73	0.0		
1136.74	0.0		
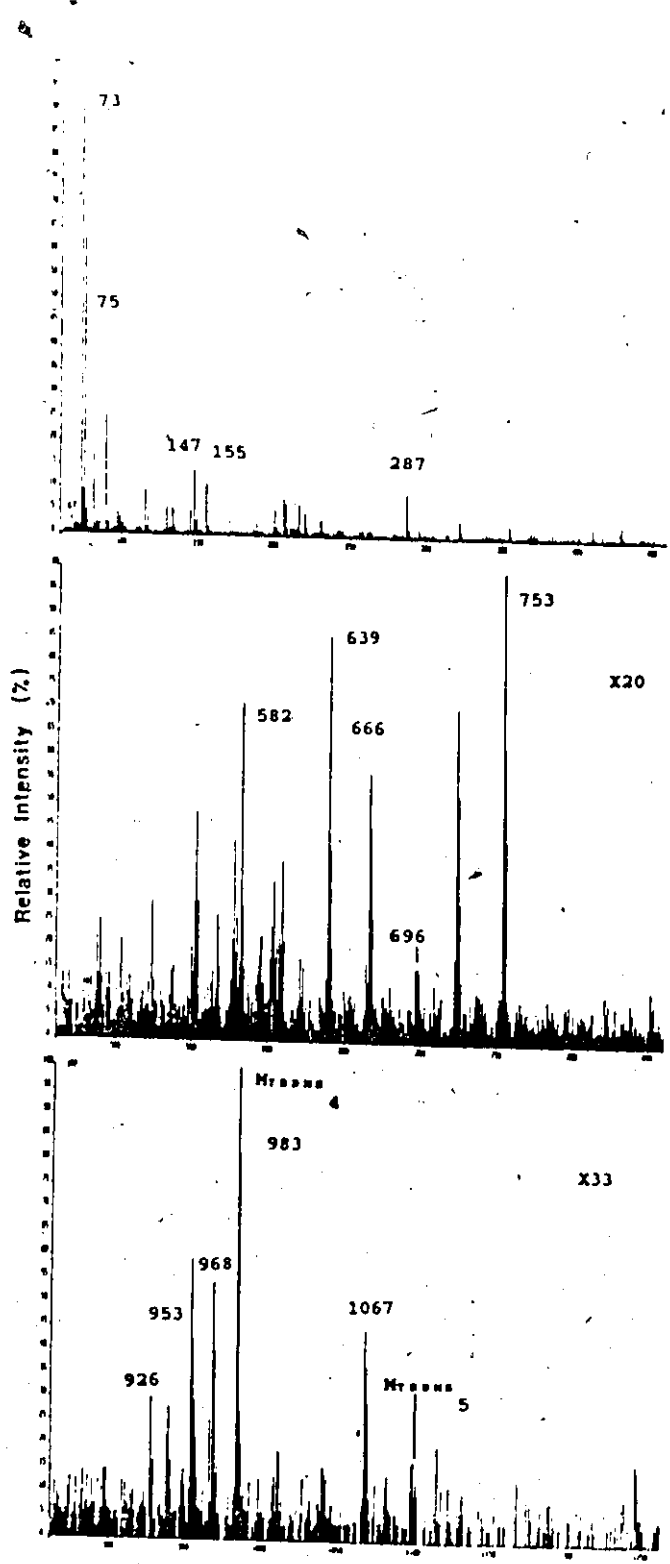
Figure 49: DEI mass spectrum of TBDMS derivatives of the
1,6-adduct 47.

Table 23: Listing of m/z for the TBDMS derivative of the 1,6-adduct 47.

m/z	%base	m/z	%base	m/z	%base
61.99	0.6	105.04	1.8	162.08	0.5
63.00	0.8	106.04	0.5	163.07	0.9
63.94	0.8	107.06	1.8	163.97	0.2
64.00	0.6	107.53	0.3	164.07	0.6
65.02	1.6	108.03	0.5	165.08	0.9
65.91	0.2	108.53	0.3	166.05	0.6
66.02	0.8	109.07	2.5	166.16	0.4
66.51	0.2	110.06	1.0	167.05	0.7
67.04	4.4	111.05	1.8	168.06	0.8
68.04	1.7	112.06	1.0	168.16	0.2
69.04	6.8	113.07	1.4	169.07	0.7
69.97	0.2	114.05	0.4	170.05	0.5
70.05	1.8	114.55	0.2	170.17	0.2
71.06	4.3	115.07	9.6	171.08	3.2
72.04	1.4	116.04	1.4	172.08	0.6
73.03	100.0	117.03	4.2	173.08	1.2
74.03	9.3	118.04	0.7	174.07	0.7
75.01	66.1	119.03	1.6	175.07	1.8
76.01	5.0	120.05	0.4	176.07	0.6
77.01	15.7	121.05	1.6	177.06	1.0
78.02	1.1	122.06	0.6	178.07	0.4
79.02	1.7	123.08	1.2	179.08	0.9
80.04	1.0	124.06	0.4	180.06	0.5
81.02	17.7 F	125.07	0.8	180.15	0.3
81.06	5.0 F	126.05	0.6	181.04	0.7
81.51	0.3	127.05	1.5	182.07	0.5
82.05	1.8	128.05	0.9	183.07	1.3
83.06	4.3	129.03	6.0	183.50	0.2
84.05	2.1	130.04	1.0	184.06	0.5
85.06	2.8	131.03	3.2	184.17	0.2
86.04	0.5	132.06	1.3	185.09	0.9
87.02	1.0	132.54	0.2	186.09	0.4
88.02	0.9	133.02	5.7	187.09	1.6
88.52	0.3	134.06	1.9	188.07	0.9
89.03	25.6	135.05	1.5	189.08	2.6
90.03	2.4	136.06	0.8	190.07	0.9
91.04	3.6	137.07	0.8	191.06	1.2
92.04	0.7	138.02	0.3	192.06	0.8
93.03	2.6	138.10	0.6	193.04	1.5
93.51	0.6	139.07	0.7	193.58	0.2
94.04	0.9	140.08	0.3	194.08	0.4
94.52	0.6	141.05	0.9	194.97	0.2
95.06	3.9	141.14	0.2	195.07	0.6
96.05	1.3	142.05	0.7	195.17	0.2
97.07	4.8	143.05	1.4	196.05	0.2
98.06	3.4	144.05	0.6	196.17	0.2
99.04	3.9	144.53	0.2	197.09	1.5
100.02	2.2	145.08	5.2	198.08	0.4
100.11	0.2	146.07	0.9	199.09	0.7
100.52	0.3	147.05	14.9	200.06	1.9
101.03	3.5	148.06	2.9	201.06	5.6
101.52	0.3	149.04	3.7	202.07	2.8
102.03	1.4	150.04	1.0	203.08	1.8
103.02	2.2	151.05	1.9	204.09	1.1
		152.07	0.8	205.07	1.1
		153.08	1.0	206.09	0.7
		154.04	0.3	207.03	8.0
		155.04	11.4	207.57	0.3
		156.04	1.9	208.05	6.9
		156.16	0.2	209.05	1.9
		157.05	1.8	210.06	0.7
		158.05	0.7	211.11	2.0
		159.08	1.6	212.10	1.9
		160.08	0.5	213.11	1.8
		161.08	1.1	214.07	2.6
				215.10	1.8

m/z	%base	m/z	%base	m/z	%base
215.56	0.4	271.63	0.2	333.20	0.5
216.09	2.2	272.10	0.6	334.17	0.6
217.08	7.1	273.12	0.9	335.20	0.8
218.09	1.6	274.12	1.0	336.21	0.4
218.95	0.2	275.15	0.8	337.20	1.4
219.10	1.0	276.13	0.5	338.21	0.7
219.24	0.2	277.13	0.4	339.24	1.8
220.08	0.8	278.13	0.6	340.19	0.6
220.20	0.2	279.10	1.0	341.18	1.3
220.64	0.2	280.15	1.6	342.19	0.6
221.09	4.9	281.07	3.5	343.18	1.0
222.10	2.0	282.09	1.4	344.17	0.7
222.57	0.2	283.09	1.3	345.17	0.7
223.09	1.2	284.12	0.8	346.16	0.4
224.08	0.5	285.17	1.3	347.17	0.8
225.11	0.8	286.14	0.4	348.21	1.0
226.09	0.8	287.15	9.5	349.22	1.0
227.09	1.3	288.12	2.1	350.18	0.7
228.08	1.0	288.29	0.2	351.21	0.8
229.10	1.4	289.14	1.7	352.17	0.4
230.09	1.2	290.14	0.7	353.23	0.8
231.11	3.7	291.16	0.5	354.23	0.5
232.09	3.6	291.61	0.2	355.14	3.0
233.11	1.4	292.14	0.7	356.13	1.2
234.10	1.1	293.16	0.8	357.17	0.6
234.63	0.2	294.13	0.3	358.15	0.3
235.11	1.0	295.12	2.3	358.32	0.2
236.17	2.0	296.14	1.1	359.16	0.4
237.17	0.5	297.16	0.7	360.16	0.5
238.07	0.4	298.13	0.8	361.21	0.8
238.18	0.2	299.17	1.1	361.67	0.2
239.16	1.3	300.12	0.7	362.19	0.5
240.11	0.5	301.16	1.1	363.21	0.5
241.13	1.1	302.17	0.5	364.21	0.7
242.10	1.7	303.16	0.6	365.22	0.8
243.11	1.7	304.14	0.6	366.20	0.4
244.12	1.4	305.18	0.8	367.25	1.1
245.11	1.6	306.16	0.5	368.30	1.1
246.11	0.8	307.16	0.7	369.21	2.2
247.14	0.7	308.15	0.4	370.18	0.9
248.11	0.3	309.18	0.4	371.19	1.9
249.14	1.1	310.16	0.5	372.17	1.0
250.13	0.6	311.21	1.4	373.20	1.6
251.13	0.6	312.18	0.4	374.20	0.7
252.08	0.8	313.24	3.0	375.18	0.6
252.24	0.2	314.21	1.3	376.14	0.5
253.13	0.6	315.16	1.4	376.27	0.2
254.13	0.6	316.15	0.7	377.19	0.5
255.14	0.6	317.17	0.4	378.20	0.6
256.12	1.5	318.20	0.4	379.23	0.3
257.13	1.2	319.14	0.5	380.25	0.6
258.09	2.1	320.15	0.6	381.26	0.9
259.12	1.4	320.42	0.2	382.24	0.5
260.14	0.5	321.16	0.8	383.21	1.8
261.14	1.8	322.15	4.0	384.25	0.4
262.17	1.3	323.15	1.6	385.18	1.1
263.13	2.3	324.16	0.8	386.20	0.5
264.17	1.4	325.19	0.6	387.17	0.3
265.17	1.2	326.15	0.5	388.19	0.4
266.13	0.5	327.14	0.8	389.21	0.5
267.11	0.8	328.11	0.4	390.29	0.3
268.11	0.7	328.29	0.2	391.23	0.7
268.26	0.2	329.17	0.9	392.22	0.4
269.11	0.9	330.16	0.5	393.23	0.8
270.11	0.6	331.19	0.5	394.24	0.6
271.14	0.7	332.20	0.4	395.27	0.6

m/z	%base	m/z	%base	m/z	%base
396.30	0 7	458.22	0.5	518.26	0.3
397.25	1 6	459 26	0 4	519.32	0.4
397.75	0 2	460.26	0.4	520.33	0.4
398.25	0 4	461.24	0.4	521.35	0.7
399 23	0.5	462.24	0 2	522.36	0.3
400 17	1.0	463 24	0.4	523.40	1.6
401 18	1 1	464.20	0.6	524.38	0.7
402.21	0 5	465 27	0.7	525.22	0.4
403 21	0.5	466 25	0.5	526.26	0 5
404 19	0.3	467.33	0.4	527.26	0.4
405.23	0 4	468 18	0.4	528.25	0.3
406.22	0.5	468.45	0.2	529.30	0.5
407.23	0.7	469.30	0.8	529.53	0.2
408 25	0 4	470.26	0.4	530.24	0.4
409 27	0.7	471.31	0.5	531.23	0.4
410 31	2 5	472.20	0.2	531.45	0.2
411 27	1.0	473.30	0.4	532.26	0.5
412 25	0.6	474.23	0.4	533.31	0.3
413 23	0.7	475.20	0.4	534.35	0.5
414 11	0.2	476 20	0.2	535.39	0.5
414.25	0 4	477 29	0.4	536.30	0.8
415 15	0.5	478.24	0.5	537.37	0.8
416.22	0.4	479.29	0.4	538.26	0.4
417.17	1.4	480.34	0.3	538.50	0.2
418.20	0.4	480.84	0.2	539.32	0.4
419.19	0.5	481.29	0.6	540.27	0.3
420.21	0.7	482.17	0.2	541.32	0.4
421.23	0 9	482.39	0.4	542.36	0.4
422.24	0.6	483.30	0.7	543.27	0.3
423.23	0.8	484.27	0.3	544.25	0.4
424.26	0.7	485.24	0.4	544.40	0.2
425.28	0.6	486.27	0.5	545.30	0.4
426.25	0.6	486.91	0.2	546.29	0.3
427.21	0.7	487.28	1.2	547.31	0.5
428.20	0.3	488.29	0.7	548.36	0.5
429.14	2.1	489.24	1.4	549.40	1.1
430.15	3.2	490.21	0.7	550.41	0.8
431.18	1.2	491.21	0.4	551.41	1.6
432.18	0.6	491 43	0.3	552.31	2.6
433.16	0.5	492.30	0.6	553.30	1.6
433.35	0.2	493.31	0.7	554.27	0.5
434.25	0.6	494.29	0.6	555.28	0.2
435.21	0.5	495.33	0.7	556.31	0.4
436.24	0.7	496.29	0.4	557.29	0.3
437.27	0.4	497.26	0.2	558.28	0.5
437.74	0.2	498.27	0.4	559.32	0.4
438.23	0.4	499.23	0.2	560.32	0.6
439.28	0.5	500.26	0.6	561.32	0.4
440.21	0.3	501.27	0.4	562.34	0.7
441.25	0.4	502.24	0.4	563.38	0.8
442.19	0.9	503.18	1.2	564.36	0 4
443.22	1 1	504.21	0.5	565 42	0.6
444 19	1.1	505.28	0.5	566.28	1 4
445 19	0.7	506.28	0.4	567.23	0 8
446.18	0.6	506.48	0.2	568.23	0.4
447.21	0.9	507.27	0.7	569.20	0.3
448.24	0.7	508.34	0.5	571.30	0.5
449.28	0.6	509.33	0.7	572.34	0.4
450.28	0.4	510.26	0.5	573.36	0 3
451.28	1.1	511.30	0.4	574.39	0.4
452.21	0.6	512.27	0.2	575.44	0.7
453.29	0.4	513.28	0.5	576.46	1.2
454.21	0.3	514.28	0.5	577.45	2.3
455.28	0.6	515.28	0.3	578.44	1.0
456.25	0.3	516.28	0.5	579.44	1.4
457.24	0.4	517.30	0.5	580.40	0.6

m/z	%base	m/z	%base	m/z	%base
581.34	0.9	633.27	0.2	693.39	0.4
582.22	3.9	634.33	0.5	694.42	0.3
583.22	1.6	635.36	0.4	695.35	0.2
584.21	0.8	636.30	0.4	696.35	0.8
585.28	0.3	637.11	0.2	697.33	0.9
586.25	0.3	637.34	0.3	697.61	0.2
587.35	0.7	638.29	0.7	698.35	0.8
587.89	0.5	639.24	4.7	699.41	0.4
588.32	0.3	640.26	2.2	700.36	0.4
588.96	0.2	641.28	1.1	701.36	0.3
589.39	0.4	642.30	0.5	702.38	0.4
590.26	0.5	643.36	0.4	703.41	0.2
590.51	0.2	644.35	0.4	704.42	0.2
591.37	0.3	645.36	0.2	705.44	0.4
592.29	0.6	646.40	0.4	706.45	0.4
592.57	0.2	646.94	0.2	707.42	0.2
593.32	0.8	647.38	0.3	708.41	0.7
594.32	1.0	648.34	0.3	709.39	0.4
595.34	1.2	649.37	0.6	710.36	0.4
596.34	0.7	650.39	0.5	711.43	0.5
596.87	0.2	651.30	0.4	712.35	0.4
597.36	0.7	652.33	0.5	712.58	0.2
598.31	0.4	653.32	0.5	713.38	0.5
599.42	0.5	654.36	0.5	715.42	0.2
600.43	0.5	655.35	0.4	716.38	0.2
601.41	0.9	656.37	0.5	717.32	0.3
602.47	1.3	657.26	0.2	719.29	0.2
603.47	1.8	657.42	0.2	719.53	0.2
604.13	0.2	658.31	0.3	720.41	0.2
604.49	0.9	659.40	0.2	721.37	0.2
605.47	1.1	660.39	0.2	722.41	1.0
606.40	0.5	661.48	0.2	723.41	3.8
607.34	1.2	662.28	0.3	724.41	2.8
608.28	1.1	662.58	0.3	725.41	1.6
608.54	0.2	663.35	0.3	726.39	0.7
609.28	2.1	663.68	0.2	727.40	0.2
610.31	1.1	664.34	0.9	728.44	0.4
611.31	0.3	665.37	0.7	729.38	0.4
612.08	0.2	666.38	3.1	730.37	0.4
612.36	0.2	667.36	2.5	731.18	0.2
613.28	0.5	668.36	1.4	731.54	0.2
614.26	0.2	669.38	0.5	732.44	0.5
615.15	0.3	670.38	0.4	733.42	0.3
615.41	0.4	671.37	0.5	734.46	0.3
616.30	0.4	672.38	0.3	735.35	0.5
617.26	0.4	673.41	0.2	736.42	0.6
617.49	0.2	674.35	0.2	737.44	0.6
617.94	0.2	675.45	0.5	738.41	0.5
618.28	0.3	676.44	0.5	739.43	0.4
618.55	0.2	677.46	0.4	740.47	0.5
619.40	0.4	678.41	0.5	741.48	0.3
620.33	0.5	679.29	0.4	742.41	0.4
621.28	1.0	679.58	0.2	743.35	0.3
621.55	0.2	680.37	0.7	743.62	0.2
622.27	0.5	681.35	0.4	746.39	0.2
623.30	0.9	682.35	0.3	747.46	0.2
624.29	0.3	683.36	0.3	749.43	0.3
625.32	0.4	684.37	0.2	750.44	0.5
626.45	0.2	685.31	0.2	751.41	0.5
627.29	0.3	685.52	0.2	752.36	0.5
628.31	0.5	686.46	0.4	753.39	5.4
629.37	0.3	687.35	0.3	753.72	0.2
630.32	0.2	688.38	0.3	754.38	3.4
630.54	0.2	689.44	0.2	755.38	2.3
631.28	0.3	691.34	0.4	756.48	0.5
632.31	0.2	692.44	0.4	757.39	0.4

m/z	%base	m/z	%base	m/z	%base
757.73	0.2	823.47	0.5	895.49	0.2
758.43	0.3	824.52	0.3	896.52	0.4
759.41	0.3	826.49	0.2	897.49	0.4
761.57	0.2	827.60	0.2	898.50	0.2
762.43	0.3	828.56	0.5	899.32	0.2
763.37	0.4	830.53	0.3	899.67	0.2
764.42	0.3	831.53	0.2	900.46	0.2
765.42	0.5	832.56	0.3	901.56	0.2
766.47	0.4	833.50	0.3	903.37	0.2
767.43	0.3	834.59	0.3	904.43	0.2
768.42	0.3	835.56	0.2	905.51	0.2
769.41	0.4	836.44	0.2	908.52	0.4
769.62	0.2	837.38	0.2	909.53	0.2
770.57	0.3	837.63	0.2	910.55	0.3
771.52	0.2	838.47	0.5	911.48	0.2
772.49	0.2	839.54	0.4	912.56	0.2
773.43	0.2	841.57	0.3	913.52	0.2
774.45	0.3	842.59	0.2	914.43	0.3
775.52	0.2	843.60	0.2	914.66	0.2
776.44	0.2	844.63	0.2	915.64	0.3
777.50	0.3	845.56	0.2	916.69	0.2
778.39	0.2	847.59	0.2	918.51	0.2
779.40	0.2	849.52	0.2	919.58	0.2
780.48	0.4	850.53	0.2	920.50	0.2
781.36	0.3	851.47	0.6	921.51	0.2
782.40	0.2	852.50	0.4	922.54	0.3
783.41	0.5	853.55	0.5	923.47	0.2
784.45	0.4	854.48	0.2	924.47	0.2
785.49	0.3	855.43	0.3	924.67	0.2
786.49	0.4	856.47	0.2	926.43	0.9
787.45	0.3	857.53	0.3	927.46	0.5
788.51	0.2	857.74	0.2	928.39	0.5
789.51	0.2	858.61	0.2	930.59	0.2
790.44	0.3	860.52	0.2	932.46	0.2
792.55	0.2	862.50	0.2	933.41	0.2
793.58	0.2	864.57	0.3	935.47	0.2
794.38	0.4	865.63	0.2	937.54	0.6
795.48	0.4	866.56	0.3	938.53	0.8
796.45	0.4	867.55	0.2	939.58	0.5
797.46	0.5	868.47	0.2	940.51	0.3
798.47	0.2	868.79	0.2	941.69	0.2
799.48	0.2	869.40	0.2	942.54	0.2
800.48	0.4	871.55	0.2	943.56	0.2
801.50	0.2	872.60	0.2	944.56	0.2
802.62	0.2	873.60	0.3	946.45	0.2
803.44	0.3	874.58	0.4	947.59	0.4
803.75	0.2	877.52	0.2	948.50	0.4
804.38	0.3	877.72	0.2	949.56	0.3
804.66	0.2	878.52	0.4	950.66	0.2
805.52	0.4	880.57	0.2	952.49	0.3
806.43	0.3	881.56	0.3	953.53	1.7
807.50	0.3	882.74	0.4	954.51	1.2
808.47	0.3	883.49	0.2	955.53	0.8
809.48	0.2	884.41	0.2	956.56	0.6
810.44	0.3	884.65	0.2	957.53	0.4
811.49	0.3	885.56	0.4	958.53	0.2
812.43	0.4	886.43	0.2	959.57	0.2
813.45	0.4	886.68	0.2	960.59	0.2
815.51	0.2	887.59	0.2	961.59	0.3
816.52	0.2	888.55	0.4	963.67	0.2
817.49	0.2	889.60	0.2	965.61	0.7
818.43	0.2	890.45	0.2	966.67	0.2
819.40	0.3	892.51	0.4	967.54	1.6
820.56	0.2	893.59	0.2	968.53	1.2
821.46	0.6	894.38	0.2	969.58	0.4
822.46	0.4	894.63	0.3	970.58	0.5

m/z	%base	m/z	%base
971 64	0.2	1097.56	0 3
972.65	0 2	1098.68	0 5
978.53	0 3	1099.63	0 3
981 67	0 2	1100.67	0 4
982 57	0 3	1101.60	0 3
983.50	2 9	1107.64	0.2
984 52	2.4	1111.73	0 2
985.54	0 8	1113.46	0.2
986 59	0 6	1114.66	0.6
987 54	0 3	1115.95	0 2
986 63	0 3	1117.83	0 3
989 57	0 2	1122.75	0.3
989.94	0 2	1128.75	0 2
990 64	0 2	1130.67	0 2
991 63	0 2	1131.74	0 3
992 58	0 4	1132.86	0 2
996.62	0 2	1142.88	0.2
998.54	0 4	1144.88	0.2
999.60	0 2	1152.56	0.2
1000 83	0 2	1166.82	0.2
1002.78	0.2	1167.65	0.4
1007.57	0.3	1173.87	0.3
1008.61	0.4	1175.91	0.2
1009.67	0.2	1176.86	0.2
1010.53	0.5	1182.69	0.2
1011.54	0 5	1184.96	0.2
1012.65	0.2	1187 90	0.2
1013.59	0.3	1188.83	0.3
1019.55	0.2	1190.77	0.2
1020.45	0.2	1201.05	0.2
1022.03	0.2	1201.96	0 1
1023.55	0.2	1204.88	0.2
1026.70	0.2	1206.84	0.2
1027.59	0.4	1208.56	0 1
1031.70	0.2	1209.98	0.2
1032.53	0.3	1212.88	0.1
1032.82	0.2	1214.68	0.2
1035.62	0.2	1215.83	0 1
1037.78	0 2	1217.80	0.2
1038.73	0.2	1218.67	0 1
1039.62	0.2	1227.77	0 1
1040.55	0 5	1230.68	0 1
1041.62	0 4	1233.13	0 1
1042.62	0.4	1234.99	0 1
1043.60	0.2	1236.95	0.2
1045.53	0.2	1238.70	0.3
1046.59	0.2	1240.93	0 1
1050.57	0.2	1243.71	0 1
1052.56	0.2	1243.94	0 1
1065.99	0.2	1245.95	0.5
1066.57	0.3	1246.93	0 5
1067.68	1.3	1247.88	0.2
1068.66	1.1	1248.89	0.2
1069.67	0.8	1249.78	0 1
1070.63	0 3		
1073.77	0.2		
1074.82	0.4		
1078.65	0.2		
1080.69	0.2		
1081.70	0.3		
1082.63	0.4		
1083.67	0.2		
1084.66	0.2		
1085.64	0.2		
1087.73	0.2		
1088.70	0.2		

Table 24: Listing of m/z for the TBDMS derivative of
the 1,8-adduct <u>48</u>.

m/z	%base	m/z	%base	m/z	%base
62 01	0 4	107.54	0 1	171.61	0.2
63 01	0 6	108.06	0 2	172.10	0 8
63.96	1 0	109 08	0 5	173 09	1.1
64 02	0 1	110.08	0 2	174.09	0 3
64.97	0.1	111 04	4 1	175.09	0.7
65 04	0 7	112.07	0.6	176.08	0.3
66.03	1 3	113 07	1 2	177 07	0.4
66 53	0 2	114.07	0.3	178.09	0.2
67.05	1 3	115 09	15 6	179.09	0.4
68.04	0.6	116.08	1.7	180.08	0.2
69.00	1 9 F	117.05	3.4	181.10	0.2
69.07	2 8 F	118.05	0.4	182.09	0.2
70.06	1 0	119.07	2 0	183:10	0.2
71.07	1 7	120.06	0 4	184.08	0.2
72.05	1.6	121.04	1.5	185.10	0.4
73.05	100.0	122.05	0.2	186.10	0.4
74.05	7 9	123.08	0.3	187.11	0.6
75.03	98 8	124.08	0.2	188.11	0.2
76.03	8.3	125.06	0.9	189.12	3.7
77.03	19.6	126.06	0 4	190.12	0.8
78.03	1.5	127.06	2.2	191.09	0.6
79.03	1.0	128.07	0.6	192.10	0.2
80.05	0.4	129.05	7.8	193.07	0.4
81.04	42.9	130.06	1.0	194.06	0.4
82.05	3.1	131.05	2.0	195.08	0.2
83.07	1.2	132.09	2.6	196.09	0.1
83.96	0.6	133.04	5.7	197.11	2.5
84.07	0.4	134.08	2.2	198.11	0.5
85.06	1.0	135.06	3.1	199.11	0.5
86.02	0.5	136.08	0.6	200.10	0.2
87.04	0.6	137.08	0.3	201.10	0.4
88.03	0.6	139.07	0.4	202.10	0.3
89.05	39.0	140.08	0.1	203.10	0.4
90.05	3 4	141.05	2.0	204.10	0.2
91.05	2.4	142.06	0.5	205.11	0.5
92.06	0.3	143.06	1.1	206.11	0.2
93.03	1.3	144.06	0.4	207.05	2.8
93.53	0.1	145.10	2.9	208.06	0.6
94.05	0.4	146.09	0.4	209.07	0.4
94.54	0.1	147.07	22.4	211.12	1.6
95.06	0.9	148.07	3.5	212.13	4.9
96.04	0.7	149.05	4.8	213.14	1.6
96.51	0.1	150.05	0.8	214.11	0.4
97.08	1.4	151.06	1.1	215.12	0.3
98.06	0.4	152.06	0.5	216.11	0.4
99.06	1.6	153 07	0.4	217.12	0.6
100.04	3.6	154.07	0.3	218.12	0.2
100.54	0.1	155.06	30.7	219.14	0.4
101.05	3.0	156.06	4.9	220.14	0.1
102.04	0.6	157.07	2 0	221.11	1.2
103.03	4.6	158.07	0.3	222.11	0.3
104.04	0.6	159.09	0.5	223.10	0.4
105.05	0.8	160.09	0.1	224.12	0.1
106.06	0.2	161.09	0.2	225.13	0.2
		162.09	0 1	226.11	0.1
		163.07	1 2	227.13	0.2
		164.09	0.2	228.14	0.1
		165.09	0.4	229.12	0.4
		166.10	0.2	230.11	0.2
		167.06	0.8	231.14	2.8
		168.07	0.2	232.13	0.9
		169.09	0.3	233.14	0.6
		170.09	0.2	234.14	0.1
		171.10	4.5	235.13	0.2

m/z	%base	m/z	%base	m/z	%base
236.13	0.1	396.22	0.1	307.18	0.1
237.15	0.3	397.28	0.2	309.20	3.5
238.13	0.1	399.27	0.2	310.20	1.0
239.18	0.7	401.21	0.7	311.23	0.4
240.14	0.2	402.22	0.3	312.21	0.1
241.14	0.2	403.20	0.1	313.27	1.1
242.11	0.4	409.29	3.3	314.22	0.3
243.13	0.2	410.29	1.1	315.21	0.1
244.14	0.1	411.28	0.5	323.16	0.1
245.15	0.2	412.27	0.1	325.19	0.1
246.16	0.1	413.27	0.1	327.20	0.2
247.16	0.3	415.23	0.1	328.21	0.1
249.15	0.3	417.23	0.2	329.20	0.6
250.14	0.1	423.30	1.6	330.20	0.2
251.14	0.2	424.31	0.9	331.23	0.1
252.13	0.1	425.29	0.3	333.23	0.1
253.14	0.1	427.31	0.2	335.26	0.5
255.18	0.1	429.24	0.4	336.25	0.2
256.18	0.1	430.25	0.2	337.26	0.4
257.16	0.9	431.25	0.1	338.24	0.2
258.13	0.4	438.21	0.1	339.28	0.8
259.15	0.3	439.28	0.2	340.26	0.2
261.16	0.6	441.27	0.1	341.31	5.1
262.13	0.3	443.35	0.5	342.31	1.3
263.15	0.4	444.32	0.9	343.26	0.4
264.15	0.1	445.33	0.4	344.16	0.3
265.14	0.3	446.29	0.1	345.19	0.1
266.13	0.1	450.18	0.1	347.23	0.2
267.14	0.2	451.31	0.3	349.26	0.5
268.11	0.1	452.25	0.1	350.25	0.2
269.13	0.2	453.28	0.2	351.25	0.4
270.12	0.2	455.35	0.1	352.25	0.2
271.12	0.2	457.29	0.1	353.25	0.3
272.13	0.1	458.32	0.2	354.23	0.1
273.16	0.2	465.34	0.4	355.20	0.4
274.14	0.1	466.30	0.1	356.19	0.2
275.17	0.2	467.33	0.4	357.25	4.3
276.15	0.1	468.21	0.4	358.26	1.3
279.16	0.4	469.31	0.3	359.25	0.5
280.15	0.1	470.30	0.1	360.23	0.2
281.09	0.9	471.35	0.1	361.21	0.2
282.10	0.3	487.30	0.1	363.21	0.1
283.13	0.2	489.23	0.1	365.23	0.1
284.15	0.1	494.22	0.1	367.26	0.3
285.20	0.3	495.24	0.2	368.28	0.1
286.19	0.1	496.26	0.1	369.27	0.4
287.17	27.4	524.31	0.2	370.23	0.2
288.17	6.3	525.22	1.4	371.22	0.3
289.17	2.8	526.21	0.5	372.20	0.1
290.18	0.6	527.25	0.2	373.22	0.2
291.17	0.2	537.35	0.1	374.23	0.1
293.17	0.2	538.37	0.1	377.26	0.2
295.15	0.5	539.34	0.1	379.26	0.1
296.20	0.2	541.26	0.2	381.27	0.2
297.17	0.3	552.26	0.3	383.24	0.4
298.16	0.2	553.30	0.2	384.23	0.1
299.19	0.2	566.25	0.1	385.21	0.2
300.19	0.1	580.24	0.2	386.22	0.1
301.22	0.3	581.31	0.2	387.25	5.7
302.19	0.1	582.22	2.7	388.26	2.0
303.18	0.5	583.22	1.2	389.26	0.6
304.18	0.2	584.22	0.5	390.26	0.1
305.21	0.4	585.22	0.1	391.24	0.1
306.20	0.1	589.23	0.1	395.23	0.2

m/z	%base	m/z	%base	m/z	%base
591.27	0.1	672.36	0.0	774.47	0.0
595.38	0.1	673.35	0.0	780.43	0.0
596.42	1.0	674.22	0.0	787.42	0.0
597.42	0.5	676.33	0.0	788.40	0.0
598.43	0.2	676.57	0.0	794.40	0.1
600.24	0.0	677.40	0.0	795.41	0.1
600.42	0.0	678.30	0.0	796.37	0.0
601.40	0.0	679.45	0.0	797.40	0.0
602.26	0.0	680.28	0.0	802.39	0.0
602.53	0.0	681.36	0.0	803.36	0.0
603.27	0.0	682.37	0.0	805.34	0.1
604.17	0.0	683.41	0.0	806.38	0.0
606.22	0.0	684.35	0.0	808.48	0.0
607.25	0.1	685.35	0.0	811.38	0.1
608.25	0.1	687.33	0.1	812.40	0.1
609.28	0.4	688.39	0.1	813.39	0.1
610.29	0.2	689.28	0.1	816.48	0.0
611.27	0.1	690.43	0.0	832.49	0.0
612.31	0.0	691.36	0.1	832.61	0.0
616.39	0.0	693.57	0.0	833.53	0.0
619.36	0.0	694.32	0.0	835.58	0.0
620.31	0.0	696.43	0.0	837.45	0.0
621.28	0.1	697.28	0.0	838.44	0.0
622.28	0.1	699.37	0.1	839.47	0.1
623.28	0.1	700.36	0.0	840.51	0.0
624.26	0.2	701.39	0.0	842.47	0.0
625.24	0.1	702.39	0.0	843.47	0.0
626.29	0.0	703.41	0.1	844.44	0.1
627.38	0.0	704.37	0.0	851.48	0.1
629.25	0.0	705.39	0.1	852.49	0.0
630.19	0.0	707.31	0.0	853.52	0.1
633.31	0.0	709.40	0.0	854.47	0.1
634.29	0.0	711.36	0.0	855.37	0.0
636.31	0.0	711.51	0.0	855.49	0.0
637.33	0.0	712.40	0.0	856.45	0.0
638.25	0.3	713.35	0.0	859.47	0.1
639.26	3.0	714.47	0.0	860.51	0.0
640.26	1.6	715.27	0.0	861.54	0.0
641.27	0.5	722.39	0.0	862.50	0.0
642.27	0.2	723.41	0.0	863.47	0.0
643.29	0.0	724.38	0.0	867.60	0.0
644.33	0.0	725.42	0.0	868.47	0.0
646.28	0.0	726.42	0.0	869.48	0.4
647.27	0.0	729.40	0.1	870.50	0.3
647.36	0.0	730.42	0.0	871.48	0.1
648.30	0.1	735.47	0.0	872.53	0.1
649.36	0.0	737.43	0.0	873.47	0.0
650.32	0.0	738.39	0.0	874.58	0.0
652.29	0.0	739.37	0.1	883.48	0.0
652.37	0.0	740.37	0.1	884.45	0.0
653.30	0.1	740.57	0.0	885.47	0.0
654.29	0.1	741.51	0.0	894.42	0.0
655.33	0.0	743.37	0.0	896.48	0.1
656.32	0.0	743.58	0.0	897.46	0.0
657.33	0.0	745.36	0.0	898.50	0.0
657.43	0.0	748.41	0.0	899.49	0.0
664.37	0.0	751.43	0.0		
665.30	0.0	754.45	0.1		
666.37	0.1	755.48	0.0		
667.37	0.1	759.47	0.0		
670.51	0.0	763.41	0.0		
671.37	0.0	764.47	0.0		
671.52	0.0	770.50	0.1		

m/z	%base	m/z	%base
908.50	0.0	981.50	0.0
911.54	0.0	982.53	0.0
924.43	0.0	983.53	3.1
925.45	0.0	984.53	2.4
926.42	0.4	985.53	1.5
927.43	0.4	986.54	0.6
928.42	0.2	987.54	0.2
929.44	0.1	988.52	0.1
930.43	0.0	989.53	0.0
933.43	0.0	998.54	0.0
938.48	0.0	999.57	0.0
939.55	0.0	1000.43	0.0
942.34	0.0	1001.66	0.0
943.39	0.0	1002.70	0.0
950.57	0.0	1008.58	0.0
951.59	0.0	1010.51	0.0
952.54	0.0	1030.74	0.0
953.55	0.4	1031.52	0.0
954.56	0.3	1032.63	0.0
955.55	0.2	1033.67	0.0
956.59	0.1	1057.57	0.0
957.63	0.0	1066.56	0.0
958.61	0.0	1068.70	0.0
965.59	0.0	1069.65	0.0
966.64	0.0	1082.70	0.0
967.56	0.1	1083.67	0.1
968.53	0.2	1085.59	0.0
969.53	0.1	1147.75	0.0
970.53	0.1	1164.81	0.0
971.52	0.0		
973.50	0.0		

Table 25: Listing of m/z for the TMS derivative of
the 1,8-adduct <u>48</u>.

m/z	%base	m/z	%base	m/z	%base
61.0	1.7	81.6	0.0	106.1	0.5
61.1	0.7	82.0	0.0	106.2	0.1
62.0	0.2	82.1	1.9	106.6	0.0
62.1	0.1	82.1	0.3	107.1	0.9
63.0	1.6	83.0	0.0	107.2	0.2
63.0	1.0	83.1	2.8	107.6	0.1
63.1	0.1	83.2	0.5	108.1	1.0
64.0	0.4	84.0	2.4	108.2	0.1
64.0	0.3	84.1	2.0	108.6	0.2
65.0	1.4	84.1	0.3	108.6	0.0
65.1	0.4	85.1	1.7	109.1	1.5
65.1	0.1	85.2	0.3	109.2	0.3
65.6	0.0	86.0	1.6	110.1	1.3
66.0	0.0	86.1	1.4	110.2	0.2
66.1	2.9	87.1	0.9	111.1	1.8
66.1	0.1	87.1	0.1	111.2	0.2
66.6	0.3	88.0	0.5	112.1	1.3
66.6	0.0	88.1	0.1	112.2	0.2
67.1	1.6	89.1	3.2	113.1	3.0
67.1	0.8	89.1	0.2	113.2	0.5
68.0	0.1	90.1	0.6	113.6	0.1
68.1	1.4	90.1	0.1	114.1	0.9
68.1	0.6	91.1	2.1	114.2	0.1
69.0	1.2	91.1	0.5	114.6	0.0
69.1	6.9	92.1	0.7	115.1	1.8
69.1	1.0	92.1	0.2	115.2	0.3
70.1	2.0	93.0	16.1	115.6	0.1
70.1	1.0	93.1	2.6	115.6	0.0
71.1	4.1	93.2	0.3	116.1	2.7
71.2	0.7	93.6	0.0	116.2	0.4
72.1	4.5	94.1	1.4	116.6	0.0
72.1	0.4	94.1	0.4	116.7	0.0
73.0	0.0	94.6	0.1	117.1	7.7
73.1	100.0	94.6	0.0	117.2	1.1
73.1	7.5	95.0	6.0	118.1	1.3
74.0	0.0	95.1	2.8	118.2	0.2
74.1	8.7	95.2	0.4	119.1	1.8
74.1	0.7	96.1	1.3	119.2	0.3
75.1	67.7	96.1	0.2	120.1	2.1
75.1	4.9	96.5	0.0	120.2	0.1
76.1	5.7	96.6	0.0	120.6	0.0
76.1	0.5	97.1	2.1	121.1	1.0
77.1	13.3	97.2	0.4	121.2	0.2
77.1	1.5	98.1	1.7	121.6	0.0
77.6	0.1	98.2	0.3	122.1	0.7
78.0	1.3	99.1	2.4	123.1	1.3
78.1	0.2	99.2	0.3	124.1	0.6
78.6	0.0	99.6	0.0	124.2	0.1
79.1	1.2	100.1	5.0	125.1	1.8
79.1	0.2	100.1	0.4	125.2	0.2
80.1	1.9	100.6	0.1	126.1	1.0
80.1	0.1	101.1	5.9	126.2	0.1
80.9	0.0	101.1	0.4	127.1	2.5
81.1	15.4	101.6	0.0	127.2	0.2
		102.1	1.2	127.6	0.0
		102.1	0.1	128.1	1.1
		102.9	0.0	128.6	0.0
		103.1	17.9	129.1	8.0
		103.1	1.1	129.2	1.0
		104.1	2.3	130.1	1.9
		104.1	0.2	130.2	0.3
		105.1	1.9	131.1	4.1
		105.1	0.3		

m/z	%base	m/z	%base	m/z	%base
131 2	0 4	161 2	0 2	199 3	0 1
132 1	3 2	162 2	0 5	200.2	1 3
132 2	0 5	163.1	0 7	201 2	1 6
133.1	4 9	164 2	0 4	201 3	0 2
134.1	1 1	165 1	0 5	202.2	1 6
135 1	1.0	165.2	0 1	203 2	0 9
135 2	0.2	166.1	0 5	203 3	0 2
136.2	1 0	166.2	0.1	204.2	2 4
136.6	0.0	167.1	2 1	204.3	0 4
137.1	1.0	168 1	0.7	205.2	1 6
137.2	0 1	168.2	0 1	205.3	0 2
138.2	0 6	169.1	17.7	206 2	0.8
139.1	0 5	169.2	1 1	207.1	6 3
139.2	0 1	170 1	25 4	208 2	1 7
140.1	0 8	170.2	1 3	209 2	1.4
140.2	0 1	171.1	8 0	210 2	0 7
141.1	1 4	171.2	0 4	211.2	0 8
141.2	0 2	171.7	0 0	212.2	0 8
142.1	1 6	172.1	2 4	213.2	1 1
142.2	0 2	172.2	0 2	214.2	1 9
143.1	3 7	173.1	2 2	215.2	1 8
143.2	0 3	173.2	0 3	216.2	1 8
144.1	1 6	174.1	1 1	217.2	8 3
144.2	0 2	174.2	0 1	218.2	2 4
144.6	0 0	175.1	0 9	219.2	1 6
145.1	4 4	175.2	0 1	220.2	0 6
145.2	0 6	176.1	0 5	221.2	2 5
146.1	1 7	177.2	0 9	222.2	0 9
146.2	0 2	178.2	0 5	223.2	2 2
146.7	0 0	179.1	0 8	224.2	0 9
146.8	0 0	179.2	0 1	225.2	1 5
147.1	42.5	180.2	0 5	226.2	1 0
147.2	1 9	180.2	0 1	227.2	1 8
147.6	0 0	181.2	0 7	228.2	1 3
148.1	7 0	182.2	0 5	229.2	1 3
148.2	0 3	182.2	0 1	230.2	1 6
149.1	11 0	183.2	0 8	231.2	1 7
149.6	0 0	183.3	0 1	232.2	1 8
149.7	0 0	184.2	0 7	233.2	1 0
150.1	1 4	184.3	0 1	234.2	0 8
150.2	0 2	185.2	1 1	235.2	0 7
151.1	1 1	185.2	0 2	236.2	0 7
151.2	0 2	186.1	0 8	237.2	0 7
152.1	0 7	186.2	0 1	238.2	0 6
152.2	0 1	187.2	1 7	239.2	4 5
153.1	0 7	187.2	0 2	240.2	1 4
153.2	0 1	188.1	1 2	241.2	1 3
154.1	0 6	188.2	0 1	242.2	1 6
154.2	0 1	189.1	2 2	243.2	1 8
154.9	0 0	189.2	0 3	244.2	1 0
155.1	15 4	190.2	1 0	245.2	1 7
155.2	0 9	191.2	5 5	246.2	0 9
156.1	3 6	192.2	1 5	247.2	0 9
156.2	0 3	193.1	1 5	248.2	0 6
157.1	5 1	194.2	0 6	249.2	0 6
157.2	0 4	195.1	0 8	250.2	0 6
158.1	1 5	195.2	0 1	251.2	0 7
158.2	0 1	196.2	0 8	252.2	0 7
159.1	1 5	196.3	0 1	253.2	0 8
159.2	0 2	197.2	0 9	254.2	0 6
160.1	0 6	197.3	0 1	255.2	1 4
160.2	0 1	198.2	0 9	256.2	0 7
161.1	0 9	199.2	1 1	257.2	1 3

m/z	%base	m/z	%base	m/z	%base
258.2	1 3	321.2	0.5	385 3	0.6
259 2	1 3	322.2	0.4	386.3	0.5
260 2	1 1	323 2	0.5	386 8	0.0
261 2	1 0	324.2	0.4	387 3	5 4
262.2	1 0	325.3	0.9	388 3	2 0
263 2	0.8	326.3	0.6	389.3	0.7
264.2	0 5	327.3	1.2	390 3	0.5
265 2	1 2	328 3	0.8	391 3	0.4
266 2	0 6	329.3	1.0	392 3	0.3
267.2	1 8	330.2	0.6	393.3	0.4
268.2	0 9	331.2	0.7	394.3	0.3
269.2	1 2	332.2	0.6	395 3	0.5
270.2	0.7	333.2	0.5	396 3	0.3
271.2	1.0	334.2	1.4	397 3	0.6
272.2	0.8	335.2	0.9	398.3	0.4
273.2	0.7	336.2	0.5	399.3	0.5
274.2	0.5	337.3	0.5	400.3	0.4
275.2	0.6	338.3	0.4	401.3	0.4
276.2	0.5	339.3	1.1	402.3	2.7
277.2	0.5	340.3	0.6	403.3	1.1
278 2	0.5	341.3	1.0	404.3	0.4
279.2	1.3	342.3	0.5	405.3	0.3
280.2	1.1	343.3	0.7	406.3	0.3
281.2	1.9	344.3	0.5	407.3	0.3
282.2	0.9	345.3	0.5	407.7	0.0
283.2	1.0	346.3	0.4	408.3	0.3
284.2	0.6	347.3	0.4	409.3	0.4
285.3	1.4	348.3	0.4	410.4	0.4
286.2	0.8	349.3	0.4	411.4	0.5
287.2	0.8	350.3	0.4	412.3	0.7
288.2	1.2	351.3	0.9	413.3	0.5
289.2	1.0	352.3	0.7	414.3	0.4
290.2	0.6	353.3	0.6	415.3	0.4
291.2	0.6	354.3	0.6	416.3	0.3
292.2	0.5	355.2	1.1	417.3	0.3
293.2	0.6	356.3	0.6	418.3	0.3
294.2	0.6	357.3	1.9	419.3	0.3
295.2	1.7	358.3	0.7	420.3	0.4
296.2	0.8	359.2	2.0	421.3	0.4
297.2	0.8	360.2	0.8	422.3	0.3
298.2	0.6	361.3	1.7	423.3	0.4
299.2	1.4	362.3	0.8	424.3	0 4
300.2	0.7	363.3	0.6	425.4	0.6
301.2	0.6	364.3	0.4	426.4	0 4
302.2	0.5	365.3	0.5	427.3	0 4
303.2	0.5	366.3	0.6	428 3	0.4
304.2	0.6	367.3	0.8	429 3	0 6
305.2	0.7	368.3	0.7	430.3	0.4
306.2	0.5	369.3	1.0	431 3	0 3
307.2	0.6	370.3	0.5	432.3	0 3
308.2	0.5	371.3	0.7	433.3	0.2
309.2	0.8	372.3	0.9	434.3	0.3
310.2	0.5	373.3	0.5	435.3	0 4
311.3	0.9	374.3	0.4	436.3	0 4
312.2	0.6	375.3	0.4	437.3	0 8
313.3	2.4	376.3	0.3	438 3	0.5
314.3	0.9	377.3	0.4	439.4	0.5
315.2	0.7	378.3	0.4	440.4	0.7
316.2	0.5	379.3	0.5	441.4	0.5
317.2	1.1	380.3	0.4	442.3	0.3
318.2	0.7	381.3	0.5	443.4	0.4
319.2	0.7	382.3	0.4	444.3	0.4
320.2	0.5	383.3	0.6	445.3	0.3
		384.3	0.4		

197

m/z	%base	m/z	%base	m/z	%base
446.3	0.3	504.3	0.2	567.4	0.2
447.3	0.3	505.3	0.2	568.4	0.3
448.3	0.3	506.4	0.2	569.3	0.9
448.5	0.0	507.3	0.4	570.4	0.6
449.3	0.3	508.3	0.5	571.4	0.4
450.3	0.5	509.4	0.7	572.4	0.3
451.3	0.6	510.4	0.6	573.4	0.8
452.3	0.4	511.4	0.6	574.4	0.4
453.3	0.4	512.4	0.8	575.4	0.3
453.6	0.1	513.4	0.5	576.4	0.2
454.3	0.3	514.4	0.3	577.5	0.2
454.6	0.0	515.4	0.2	578.5	0.1
455.4	0.4	516.3	0.6	579.5	0.2
456.4	0.3	517.4	0.4	580.4	0.2
457.4	0.3	518.4	0.3	581.4	0.4
458.3	0.3	519.4	0.2	582.4	0.4
458.6	0.1	520.4	0.2	583.4	0.3
459.4	0.3	521.4	0.3	584.4	0.3
460.3	0.3	522.4	0.4	585.4	0.3
461.3	0.2	523.4	0.5	586.4	0.3
462.3	0.2	524.4	0.5	587.4	0.2
463.3	0.2	525.3	0.9	588.4	0.9
464.3	0.3	526.4	0.5	589.4	0.5
465.3	0.4	527.4	0.4	590.4	0.2
466.3	0.4	528.4	0.2	591.4	0.2
467.4	0.6	529.4	0.2	592.3	0.2
468.3	0.4	530.4	0.2	593.4	0.2
468.6	0.1	531.4	0.2	594.4	0.3
469.4	0.4	532.4	0.1	595.4	0.3
470.4	0.2	533.4	0.2	596.4	0.3
471.4	0.4	534.4	0.2	597.4	0.3
472.3	0.3	535.4	0.2	598.4	0.3
472.6	0.0	535.7	0.0	599.4	0.2
473.4	0.2	536.4	0.2	600.4	0.2
474.3	0.2	537.4	0.4	601.4	0.2
475.3	0.2	538.4	0.6	602.4	0.2
476.3	0.2	539.4	1.2	603.5	0.1
477.3	0.2	540.3	2.5	604.4	0.1
478.4	0.2	541.3	1.2	605.4	0.1
479.4	0.3	542.4	0.5	606.4	0.1
480.4	0.2	543.4	0.3	607.4	0.1
481.4	0.3	544.4	0.2	608.4	0.1
482.4	0.4	545.4	0.1	609.4	0.2
483.3	1.5	546.4	0.1	610.4	0.3
484.3	0.7	547.4	0.2	611.4	0.3
485.3	0.3	548.4	0.2	612.4	0.4
485.6	0.0	549.5	0.2	613.4	0.3
486.4	0.2	550.5	0.3	614.4	0.2
487.4	0.2	551.5	0.4	615.4	0.2
488.4	0.1	552.4	0.3	616.4	0.1
489.3	0.2	553.4	0.1	617.4	0.1
490.3	0.2	554.1	1.7	618.4	0.1
491.3	0.2	554.4	0.5	619.4	0.1
492.3	0.3	555.3	25.1	620.4	0.3
493.4	0.3	556.3	11.0	621.4	0.2
494.4	0.3	557.3	4.2	622.4	0.1
495.4	0.4	558.3	1.1	623.4	0.2
496.4	0.4	559.4	0.4	624.4	0.2
497.4	2.3	560.4	0.1	625.4	0.2
498.4	0.9	561.4	0.1	626.4	0.5
499.4	0.5	562.4	0.2	627.4	3.2
500.4	0.3	563.4	0.2	628.4	1.7
501.3	0.3	564.4	0.2	629.4	1.0
502.3	0.2	565.4	0.2	630.4	0.3
503.3	0.3	566.4	0.3	631.3	0.2

m/z	%base	m/z	%base	m/z	%base
632.4	0.1	697.4	0.1	761.5	0.0
633.4	0.1	698.4	0.1	762.5	0.0
634.4	0.1	699.4	0.1	763.4	0.0
635.4	0.1	700.4	0.1	764.5	0.0
636.3	0.2	701.4	0.1	765.5	0.0
637.4	0.2	702.4	0.0	766.5	0.0
638.4	0.1	703.4	0.0	767.5	0.0
639.4	0.1	704.4	0.0	768.5	0.0
640.4	0.1	705.4	0.0	769.5	0.0
641.4	0.2	706.4	0.0	770.5	0.1
642.4	0.2	707.4	0.0	771.5	0.0
643.4	0.4	708.4	0.1	772.5	0.0
644.4	0.3	709.4	0.1	773.4	0.0
645.3	0.2	710.4	0.1	774.6	0.0
646.4	0.1	711.4	0.1	775.4	0.0
647.4	0.1	712.4	0.1	776.4	0.0
648.4	0.1	713.4	0.1	777.5	0.0
649.4	0.1	714.4	0.1	778.4	0.0
650.4	0.1	715.4	0.1	779.5	0.0
651.4	0.1	716.4	0.1	780.5	0.0
652.4	0.1	717.4	0.1	781.5	0.0
653.4	0.1	718.4	0.0	782.4	0.0
654.4	0.2	719.4	0.0	783.4	0.0
655.4	0.1	720.4	0.0	784.4	0.1
656.4	0.1	721.5	0.0	785.4	0.2
657.4	0.1	722.5	0.0	786.4	0.1
658.4	0.1	723.5	0.1	787.4	0.1
659.4	0.1	724.4	0.1	788.4	0.1
660.4	0.0	725.4	0.2	789.5	0.0
661.4	0.1	726.4	0.1	790.5	0.0
662.4	0.1	727.4	0.2	791.5	0.0
663.4	0.1	728.4	0.1	792.5	0.0
664.4	0.1	729.4	0.1	793.5	0.0
665.4	0.1	730.4	0.1	794.6	0.0
666.4	0.1	731.4	0.1	795.4	0.0
667.4	0.1	732.4	0.1	796.6	0.0
668.4	0.1	733.4	0.0	797.5	0.0
669.4	0.1	734.4	0.0	798.5	0.1
670.4	0.1	735.4	0.0	799.5	0.2
671.4	0.1	736.4	0.1	800.4	1.0
672.4	0.1	737.4	0.0	801.4	0.6
673.4	0.1	738.4	0.1	802.5	0.3
674.4	0.1	739.5	0.0	803.4	0.1
675.4	0.1	740.4	0.0	804.5	0.0
676.4	0.1	741.4	0.1	805.4	0.0
677.5	0.1	742.4	0.1	806.5	0.0
678.4	0.1	743.4	0.2	808.5	0.0
679.4	0.1	744.4	0.2	809.5	0.0
680.4	0.1	745.4	0.1	810.5	0.0
681.4	0.1	746.4	0.0	811.5	0.0
682.4	0.1	747.4	0.0	812.5	0.0
683.4	0.2	748.4	0.0	813.4	0.1
684.4	0.1	749.5	0.0	814.4	0.0
685.4	0.1	750.4	0.0	815.4	5.2
686.4	0.1	751.6	0.0	816.4	3.5
687.4	0.1	752.5	0.0	817.4	1.8
688.4	0.1	753.5	0.0	818.0	0.2
689.4	0.1	754.5	0.0	818.6	0.7
690.4	0.0	755.4	0.0	819.2	0.0
691.5	0.0	756.5	0.0	820.4	0.1
692.4	0.1	757.5	0.1	821.3	0.0
693.4	0.1	758.4	0.1	823.4	0.0
694.4	0.1	759.5	0.0	824.5	0.0
695.4	0.1	760.4	0.0	825.5	0.0
696.4	0.1				

VII. REFERENCES

1. R. Johnstone and J. Miller, Occupational Diseases and Individual Medicine, p.3, W.B. Saunders Co., Phil., PA, (1961).

2. Polynuclear Aromatic Hydrocarbons: Chemistry, Metabolism and Carcinogenicity, R. Freudenthal and P. Jones, Eds., Raven Press, NY, (1976).

3. M.Lee, M. Novoty and K. Bartle, Analytical Chemistry of PAHs, p. 26, Academic Press, NY, (1981).

4. J. Schiller, Anal. Chem., 49, 2292, (1977).

5. R. Jones, M. Guerir and B. Clark, Anal. Chem., 49, 1766, (1981).

6. D. Sheutzle, F. Lee and T. Prater, Int. J. Environ. Anal. Chem., 9, 93, (1981).

7. E. Schnick, G. Bachlechner, K. Varmuza and H. Klus, Fres. Z. Anal. Chem., 322, 213, (1985).

8. J. Butler and P. Crosley, Atmos. Environ., 15, 91, (19881).

9. M. Katz, T. Sakuma and A. Ho, Environ. Sci,. Technol., 12, 909, (1978).

10. K. Bartle, M. Lee and A. Wise, Chem. Soc. Rev. 10, 113, (1981).

11. A. Bjorseth, Anal. Chim. Acta., 94, 21, (1977).

12. G. Deachenko, Environ. Sci. Technol., 13, 329, (1979).

13. T. Panalaks, J. Environ. Sci. Heal. A, 11, 399, (1976).

14. M. Blumer, W. Blum and T. Reich, Environ. Sci. Technol. 11, 1083.

15. Carcinogenesis: A Comprehensive Survey, Vol. 3, P. Jones and R. Freudenthal, Eds.; Raven Press, NY, (1978).

16. <u>Principles of Drug Action</u>, A. Goldstein, L, Arnow and S. Kaplan, Eds., p. 681, J. Wiley and Son, NY, (1974).

17. R. Cartwright, Environ. Heal. Perspec., <u>49</u>, 13, (1983).

18. R. Beauchamp, CRC Rev. in Toxicol., <u>11</u>, 33, (1982).

19. G. Brown and D. Carr, Fed. Proc., <u>33</u>, 1387, (1974).

20. G. Lofroth, E. Hefner, L. Alfheim and M. Moller, Science, <u>209</u>, 1037, (1980).

21. H. Rosenkranz, E. McCoy, D. Sanders, M. Butler, D. Kiriazids and R. Mermelstein, Science, <u>209</u>, 1039, (1980).

22. D. Levin, W. Barnes and E. Klekowski, Mutat. Res., <u>63</u>, 1, (1979).

23. B. Simmons, J. Natl. Cancer. I., <u>62</u>, 893, (1979).

24. H. Tokiwa and Y. Ohnishi, CRC Rev. in Toxicol., <u>17</u>, 27, (1986).

25. H. Rosenkranz, Mutat. Res., <u>140</u>, 1, (1984).

26. C. Crisp and G. Fisher, Mutat. Res., <u>76</u>, 51, (1980).

27. W. Dehren, N. Pitz and R. Tomingas, Cancer Lett., <u>4</u>, 5, (1977).

28. T. Gibson, Mutat. Res., <u>122</u>, 155, (1983).

29. H. Tokiwa, R. Nakagawa, K. Morita and Y. Onishi, Mutat. Res., <u>85</u>, 195, (1981).

30. J. Pitts, K. Van Cauwenberghe, D, Grosjean, J. Schmidt, D, Fritz, W. Belser, G. Knudson and P. Hynds, Science, <u>202</u>, 515, (1979).

31. B. Ames, J. McCann and E. Yamasaki, Mutat. Res., <u>31</u>, 347, (1975).

32. H. Rosenkranz and R. Mermelstein, Mutat. Res., <u>114</u>, 217, (1983).

33. J.Cole, C. Arlett, J. Lowe and B. Bridges, Mutat. Res., <u>93</u>, 213, (1983).

34. M. Nakayasu, H. Sakamoto, K.Wakabuyashi, M. Sugamura, M. Terada and H. Rosenkranz, Carcinogenesis, <u>3</u>, 917, (1982).

35. J. Natchman and S. Wolff, Environ. Mutagenesis, 4, 1, (1982).

36. N. Danford, P. Wilcox and J. Parry, Mutat. Res., 105, 349, (1982).

37. M.Moeller and S. Thorgeirsson, Mutat. Res., 151, 137, (1985).

38 H. Ohgaki, C. Negishi, K. Wakabayashi, K. Kusama, S. Sato, and T. Sugamura., Carcinogenesis, 5, 583, (1984).

39. S. Takayamo, T. Ishikawa, H. Nakajima and S.Sato, Japn. J. Cancer Res., 76, 457, (1985).

40. K. Motohisha and C. Nagata, Chem-Biol. Interact., 3, 459, (1987).

41. W. Bard and P. Brookes, Cancer Res., 33, 3278, (1973).

42. D. Bryant, D. McCalla, M. Leeksma and P. Laneuville, Can. J. Microbiol., 27, 81, (1981).

43. H. Rosenkranz and L. Poirier, J. Natl. Canc. I., 62, 873, (1979).

44. F. Messier, C. Lu, P. Andrews, B. McCarry, M. Quilliam and D. McCalla, Carcinogenesis, 2, 1007, (1981).

45. E. Rosenkranz, E. McCoy, R. Mermelstein and H. Rosenkranz, Carcinogenesis, 3, 121, (1982).

46. E. Miller and J. Miller, Cancer, 47, 2327, (1981).

48. F. Kadulbar, L. Unruh, F. Beland, K. Straub amd F. Evans, Carcinogenesis, 1, 139, (1980).

49. F. Kadlubar, J. Miller and E. Miller, Cancer Res., 38, 3628, (1978).

50. P. Howard, R. Heflich, F. Evans and F. Beland, Cancer Res., 43, 2052, (1983).

51. T. Flammang, J. Westra, F. Kadlubar and F. Beland, Carcinogenesis, 6, 251, (1985).

52. R. Heflich, E. Fifer, Z. Djuric and F.Beland, Environ. Health Persp., 62, 135, (1985).

53. A. Vergee and G. Whitemore, Cancer Res., $\underline{43}$, 78, (1983).

54. J-K. Lin, B. Schmall, I. Scharpe, I. Miura, J. Miller and E. Miller, Cancer Res., $\underline{35}$, 832, (1975).

55. J-K. Lin, J. Miller and E. Miller, Cancer Res., $\underline{35}$, 844, (1975).

56. R. Gupta, M. Reddy and K. Randerath, Carcinogenesis, $\underline{3}$, 1081, (1982).

57. Y. Yamazoe, R. Roth and F. Kadlubar, Carcinogenesis, $\underline{7}$, 179-182, (1986).

58. R. Franz, H-R. Schulter and H-G. Neumann, Chem-Biol. Interact., $\underline{59}$, 281, (1986).

59. F. Beland, D. Tulis, F. Kadlubar, K. Straub and F. Evans, Chem-Biol. Interact., $\underline{31}$, 1, (1980).

60. R. Moschel, M. Piggtt, N. Costantino and A. Dipple, Carcinogenesis, $\underline{4}$, 1201, (1083).

61. L. van Houte, J.Bokma, J. Lutgerink, J. Westra, J. Retil, R. van Grondelle and J. Blok, Carcinogenesis, $\underline{8}$, 759, (1987).

62. A. Gaagliano, N. Geactinov, V. Ibanez, R. Harvey and H. Lee, Carcinogenesis, $\underline{3}$, 969, (1982).

63. R. Benn and H. Gunther, Angew. Chem., $\underline{22}$, 350, (1983).

64. D. Krapp, Handbook of Analytical Derivatization Reactions; J. Wiley and Sons, (1979).

65. C. Cooper, O. Ribeiro, P. Farmer, A. Hewer, C. Walsh, K. Pal, P. Grover and P. Sims, Chem. Biol. Interact., $\underline{32}$, 209, (1980).

66. N. Scribner, J. Scribner, D. Smith, K. Schram and J. McCloskey, Chem-Biol. Interact., $\underline{26}$, 27, (1979).

67. B. Gaugler, H. Neumann, N. Scribnera and J. Scribner, Chem-Biol. Interact., 27, 335, (1979).

68. M. Quilliam, J. Tempelton and J. Westmore, Steroids, 29, 613, (1977).

69. A. Burlingame, K. Straub and T. Baille, Mass Spectrom. Reviews, 2, 331, (1983).

70. M. Vestal, Mass Spectrom. Reviews, 2, 447, (1983).

71. G. Wood, Mass Spectrom. Reviews, 1, 63, (1982).

72. D. Williams, C. Bradley, G. Bojesen, S. Santikarn and L. Taylor, J. Am. Chem. Soc., 103, 5700, (1981).

73. J. Eagles, C. Javanoud and R. Self, Biomed. Environ. Mass Spec., 11, 431, (1984).

74. Y. Tondeur, M. Shorter, M. Gustafson and R. Fandey, Biomed. Environ. Mass Spec. 11, 622, (1984).

75. J. Gower, Biomed. Environ. Mass. Spec. 12, 191, (1985).

76. M. Baldwin and F. McLafferty, Org. Mass Spectrom., 7, 1353, (1973).

77. J. Thenot, J. Nowlin, D. Carrol, F. Montgomery and E. Horning, Anal. Chem., 51, 1101, (1979).

78. R. Cotter, Anal. Chem., 51, 317, (1979).

79. M. Ohashi, K. Tsujimoto and A. Yasuda, Chem. Lett., 439, (1976).

80. A. Bruins, Anal. Chem. 52, 605, (1980).

81. C. Edmonds, J. McCloskey and V. Edmonds, Biomed. Environ. Mass Spectrom. 10, 237, (1983).

82. D. Games and E. Lewis, Biomed. Environ. Mass Spectrom., 7, 433, (1983).

83. K. Levsen, K. Schafer and P. Dobberstein, Biomed. Environ. Mass Spectrom., 11, 308, (1984).

84. M. Quilliam, K. Ogilivie and J. Westmore, Org. Mass Spectrom. 16, 129, (1981).

85. J. Stroh, J. Look, R. Milberg, L. Brayton, T.Kihara, Z. Huang, K. Rinehart and I. Lewis, Anal. Chem., 57, 985, (1985).

86. D. Watson, G. Taylor and S. Murray, Biomed. Mass Spectrom. 13, 65, (1986).

87. Personal communication, L. Davies, Department of Biochemistry, McMaster University, Hamilton, Ontario.

88. R. Mermelstein, D. Kiriazides, M. Butler, E. McCoy and H. Rosenkranz, Mutat. Res., 89, 187, (1981).

89. E. McCoy, M. Anders and H. Rosenkranz, Mutat. Res., 121, 17, (1983).

90. E. Fifer, R.H. Heflich, Z. Djuric, P. Howard and F. Beland, Carcinogenisis, 7, 65, 1986.

91. A. Streitweiser and R. Fahey, J. Org. Chem., 27, 2352, (1962).

93. J.Porter, Org. Synthesis, 20, 455, (1973).

94. F. Cotton and G. Wilknson, Advanced Inorganic Chemistry A Comphrehensive Text, 2nd ed., p. 529, Interscience Publishers, NY, (1973).

95. G. Klopman, D. Tonnucci, M. Holloway and H. Rosenkranz, Mutat. Res., 126, 139, (1984).

96. A. Tallec, Ann. Chim., 3, 155, (1968).

97. A. Tallec, Ann. Chim., 3, 347, (1968).

98   R. Heflich, P. Howard and F. Beland, Mutat. Res., 149, 25, (1985).

99. S. Bodin, P. Ruchle, R. Roth, G. Bosh, L. Bosh, G. Opperman and J. Saugier, in: <u>Proceedings of the 7th International Symposium on PAH</u>, pg. 135, Batelle Press, Columbus, OH, (1982).

100. S. Kaplan, Org. Magn. Resonance, <u>15</u>, 197, (1981).

101. <u>Handbook of Polycyclic Aromatic Hydrocarbons</u>, p.323, A. Bjorseth, Ed., Marcel Decker Inc., NY, (1983).

102. Personal communication, J. Fulton, Department of Chemistry, McMaster University, HAmilton, Ontario.

103. M-S. Tang and M. Lieberman, Carcinogenesis, <u>4</u>, 1001, (1982).

104. R. Fourney, P. O'Brien and W. Davidson, Carcinogenesis, <u>7</u>, 1535, (1986).

105. C. Martin, F. Beland R. Roth and F. Kadlubar, Cancer Res. <u>42</u>, 2678, (1982).

106. K.Kuo, R.McCune, C. Gerkle, R. Midgett and M. Erlich, Nucleic Acids Res., <u>8</u>, 4763, (1980).

107. E. Kriek and J. Westra, Carcinogenesis, <u>1</u>, 459, (1980).

108. E. Kriek, J. Westra, V. Juhl and E. Miller, Biochem., <u>6</u>, 177, (1970).

109. G. Hansen and B. Munson, Anal. Chem., <u>50</u>, 1130, (1978).

110. G. Daves, Acc. Chem. Res., <u>12</u>, 359, (1979).

111. D. Carroll, I. Dzidic, M. Horning, F. Montgomery, J. Nowlin, R. Stilwell, J-P. Thenot and E. Horning, Anal. Chem., <u>51</u>, 1858, (1979).

112. M. Quilliam, K. Ogilvie, K. Sadana, J. Westmore, Org. Mass Spectrom., <u>15</u>, 207, (1980).

113. M. Quilliam and J. Yaraskavitch, J. Liq. Chromatog., <u>8</u>, 449, (2985).

114. <u>Pierce Chemical Company, 1986-1987 Handbook</u>, p. 186, Pierce Chemical Co., Rockford, Ill. (1986).

115. M. Quilliam, F. Messier, P. D'Agistino, B. McCarry and M. Lant, Spectroscopy: An Int. J., <u>3</u>, 33, (1984).

116. G. Hartman, W. Behr, K-A. Beissner, K. Hanikel and A. Sipple, Angew. Chim., Int. Ed., <u>7</u>, 693, (1968).

117. <u>Principles of Nucleic Acid Structure</u>, p. 371, W. Saegner, ed., Springer-Verlag Inc., N.Y., (1983)

118. <u>Exciton Coupling in Organic Stereochemistry</u>, p. 4, N. Harada and K. Nakanishi, eds., University Books, NY, (1983),

119. Personal communication, K. Nakanishi, Department of Chemistry, Columbia University,

120. D. Fornasiero and T. Kurucsev, J. Phys. Chem., <u>85</u>, 613, (1981).

121. M. Kaneko and C. Nageto, Chem-Biol. Interact., <u>3</u>, 459, (1971).

122. C. Zammer, B. Puschendorf, H. Grunicke, P. Chandra and H. Venner, Eur. J. Biochem.,<u>21</u>, 269, (1971).

123. G. Fasman, B. Shauffhausen, L. Goldsmith and A. Adler, Biochem., <u>9</u>, 2814, (1970).

124. S. Mong, D. Eubanks, A. Prestayko and S. Crooks, Biochem., <u>21</u>, 3174, (1982).

125. R. Fournet, P. O'Brien and W. Davidson, Carcinogenesis, <u>7</u>, 1535, (1986).

126. H. Rosenkranz, E. McCoy, M Frierson and G. Klopman, Eviron. Mutagen., <u>7</u>, 645, (1985).

127. R. Fuchs and M. Duane, Biochem., <u>13</u>, 4435, (1974).

128. T. Maniatis, E. Fritsch and J. Sambrook, <u>Molecular Cloning, A</u> <u>Laboratory Manual</u>, p. 150, Cold Spring Harbour, Clod Spring Harbour, NY, (1983).

129. C. Robinson, L. Milewich and P. Hofer, J. Org. Chem., <u>31</u>, 524, (1966).